

GI_Forum - Special Issue

12th International Symposium on Digital Earth



Table of Content

Special Edition:

12th International Symposium on Digital Earth: Digital Earth for Sustainable Societies

Thomas Blaschke - Josef Strobl - Julia Wegmayr (Eds.)

Cuizhen Wang – Inthuorn Sasanakul – Herrick Brown
sUAS Remote Sensing for Closed-canopy Tree Inventory on Earthen Dams
Page 5 - 12
DOI: 10.1553/giscience2021_01_s5

Malini Krishnan – Rajan Krishnan Sundara
Generation of Spatial Profiles & Mapping of Volcanic Ash Distribution
Page 13 - 23
DOI: 10.1553/giscience2021_01_s13

Alexander Ariza – Hannah Kemper – Gerhard Kemper
Integration of Ground Truth Data via Cloud Computing for Enhanced Burn Severity Mapping – An Example from Honduras
Page 24 - 32
DOI: 10.1553/giscience2021_01_s24

Mattia Marconcini – Annekatriin Metz – Marconcini – Thomas Esch – Noel Gorelick
Understanding Current Trends in Global Urbanisation - The World Settlement Footprint Suite
Page 33 - 38
DOI: 10.1553/giscience2021_01_s33

Sepideh Tavakkoli Piralilou – Hejar Shahabi – Robert Pazur
Automatic Landslide detection using Bi-Temporal Sentinel 2 Imagery
Page 39 - 45
DOI: 10.1553/giscience2021_01_s39

Zahra Dabiri – Daniel Hölbling – Lorena Abad – Snævarr Guðmundsson
Comparing the Applicability of Sentinel-1 and Sentinel-2 for Mapping the Evolution of Ice-marginal Lakes in Southeast Iceland
Page 46 - 52
DOI: 10.1553/giscience2021_01_s46

Martin Sudmanns – Hannah Augustin – Lucas van der Meer – Christian Werner – Andrea Baraldi – Dirk Tiede
One GUI to Rule Them All: Accessing Multiple Semantic EO Data Cubes in One Graphical User Interface
Page 53 - 59
DOI: 10.1553/giscience2021_01_s53

Tobias Kugler – Lorenz Wendt
Evaluation of Digital Elevation Models Derived from Multi-Date Satellite Stereo Imagery for Urban Areas
Page 60 - 67
DOI: 10.1553/giscience2021_01_s60

Martin Werner
Spatially Supervised Text Mining for Social Media Cleaning and Preprocessing
Page 68 - 75
DOI: 10.1553/giscience2021_01_s68

Nicole Hein – Jörg Blankenbach
Evaluation of a NoSQL Database for Storing Big Geospatial Raster Data
Page 76 - 84
DOI: 10.1553/giscience2021_01_s76

Monika Kuffer – Sabine Vanhuyse – Stefanos Georganos – Jon Wang
Meeting User Requirements for Mapping and Characterizing Deprived Urban Areas in Support of Pro-Poor Policies
Page 85 - 93
DOI: 10.1553/giscience2021_01_s85

Tahira Ullah – Sven Lautenbach – Alexander Zipf
Deriving Indicators for Points of Interest and Analyzing Mixed Activities in Urban Areas
Page 94 - 103
DOI: 10.1553/giscience2021_01_s94

Filippo Iodice – Federica D’Acunto – Lorenzo Bigagli
Mapping Nitrogen from Satellite Data to Improve Soil Quality - A Worked Example
Page 104 - 111
DOI: 10.1553/giscience2021_01_s104

Sheng Zhang – Yong Xue – Xiran Zhou
Dynamic Workflow Engine of Atmospheric Big Remote Sensing Data Processing Powered by Heterogenous Platform for High Performance Computing
Page 112 - 119
DOI: 10.1553/giscience2021_01_s112

Manuela Hirschmugl – Carina Sobe – Lorenzo Traverso – David Cifuentes – Alfonso Calera – Cosette Khawaja – Marco Colangeli
Energy from Biomass: Assessing Sustainability by Geoinformation Technology
Page 120 - 129
DOI: 10.1553/giscience2021_01_s120

Matti Möttöus – Matthias Dees – Heikki Astola – Stanisław Dałek – Eelis Halme – Tuomas Häme – Monika Krzyżanowska – Annikki Mäkelä – Gheorghe Marin – Francesco Minunno – Gero Pawlowski – Juho Penttilä – Jussi Rasinmäki
A Methodology for Implementing a Digital Twin of the Earth’s Forests to Match the Requirements of Different User Groups
Page 130 - 136
DOI: 10.1553/giscience2021_01_s130

Tuomas Häme – Laura Sirro – Matthias Dees – Annikki Mäkelä – Juho Penttilä – Gheorghe Marin – Margarida Tomé
Energy from Biomass: Assessing Sustainability by Geoinformation Technology
Page 137 - 142
DOI: 10.1553/giscience2021_01_s137

Filippo Iodice – Federica D’Acunto – Lorenzo Bigagli
Monitoring Land Degradation from Space
Page 143 - 149
DOI: 10.1553/giscience2021_01_s143

Iskar Jasmani Waluyo Moreno – José García Hernández – Agustín Bolóm Gómez – Julio Cesar García
Using Open-Source Data and Software to Analyse Land-Use Changes and Deforestation in Marqués de Comillas, Chiapa, Mexico (Work in Progress)
Page 150 - 157
DOI: 10.1553/giscience2021_01_s150

Gulnara Nyussupova – Gaukhar Aidarkhanova – Madiyar Kadylbekov – Laura Kenespayeva – Roza Kelinbayeva – Bazaraly Kozhakhmetov
Nationalization of Indicators for Sustainable Development Goals in the Republic of Kazakhstan through Geoinformation Technologies
Page 158 - 168
DOI: 10.1553/giscience2021_01_s158

Alessandro Scandiffio
Mapping Flooded Paddy-Rice Fields in the Landscape between Turin and Milan: A GIS-Based
Method for Detecting Scenic Routes for Experiential Tourism
Page 169 - 178
DOI: 10.1553/giscience2021_01_s169

Alberto Vavassori – Carlo Andrea Biraghi – Gorica Bratic – Daniela Carrion – Giorgio Zamboni –
Maria Antonia Brovelli
Citizen Science Tools for Lake Monitoring in the Framework of the United Nations Sustainable
Development Goals: The Project SIMILE
Page 179 - 186
DOI: 10.1553/giscience2021_01_s179

Henry Martin – Daniel Reck – Martin Raubal
Using Information and Communication Technologies to Facilitate Mobility Behaviour Change and
Enable Mobility as a Service
Page 187 - 193
DOI: 10.1553/giscience2021_01_s187

Martin Loidl – Ursula Witzmann-Müller
Observing Cyclists' Mobility Patterns for better Decisions
Page 194 - 200
DOI: 10.1553/giscience2021_01_s194

Andreas Braun
Extraction of Dwellings of Displaced Persons from VHR Radar Imagery – A Review on Current
Challenges and Future Perspectives
Page 201 - 208
DOI: 10.1553/giscience2021_01_s201

Stefan Lang – Lorenz Wendt – Dirk Tiede – Yunya Gao – Vanessa Streifender – Hira Zafar –
Adebawale Adebayo – Gina Schwendemann – Peter Jeremias
Multi-Feature Sample Database for Enhancing Deep Learning Tasks in Operational Humanitarian
Applications
Page 209 - 219
DOI: 10.1553/giscience2021_01_s209

Getachew Workineh Gella – Lorenz Wendt – Stefan Lang – Andreas Braun – Dirk Tiede – Barbara
Hofer – Yunya Gao – Barbara Riedler – Ahmad Alobaidi – Gina Marciela Schwendemann
Testing Transferability of Deep-Learning-Based Dwelling Extraction in Refugee Camps
Page 220 - 227
DOI: 10.1553/giscience2021_01_s220

Yunya Gao – Stefan Lang – Dirk Tiede – Lorenz Wendt – Getachew Workineh Gella
Suggestions on the Selection of Satellite Imagery for Future Remote Sensing-Based Humanitarian
Applications
Page 228 - 236
DOI: 10.1553/giscience2021_01_s228

Editorial

Digital Earth for Sustainable Societies.

Digital Earth is a global initiative aimed at harnessing the world's data and information resources to describe and digitally represent our planet, and to monitor, measure and forecast natural and human activities on earth. Digital Earth is the name referring to a concept by former US vice president Al Gore, describing a virtual representation of the Earth connected to the world's digital knowledge. In his remarkable 1998 speech, Gore described a digital future where children - indeed all the world's citizens – could interact with a computer-generated three-dimensional spinning virtual globe and access vast amounts of scientific and cultural information to help them understand the Earth and human activities.

We have come a long way since 1998, mostly along an evolutionary trajectory. More recently, though, we experienced serious disruption potentially generating a strong impulse accelerating digital transformation in general. Making the best possible use of this disruptive impulse, 'surfing' it towards a broader acceptance of integrating real with virtual worlds for the benefit of humankind and its sustainable livelihoods is the challenge, and the opportunity we are facing right now.

The University of Salzburg and its Department of Geoinformatics – Z_GIS host the 12th International Symposium on Digital Earth (ISDE12) from 06-08 July 2021. The Covid-19 pandemic required various changes to the organizers. In fact, the Covid-19 pandemic fostered the digital transition and made 'dashboards' popular to mass internet users. Surely, the underlying methods and technologies – broadly speaking: Earth Observation, GIS/Geoinformatics, positioning (GNSS) and location services – had come a long way, from technical wizardry to the ubiquitous use by the masses.

It is now safe to say – almost 23 years after Al Gore's visionary speech - that the creation of the digital society is on its way through technological development, theoretical and empirical scientific research and increasingly inclusive and seamless technology.

Talking about Digital Earth: do we consider this simply a new name for established concepts around Geoinformatics? We aim far beyond that. Anything starting with 'Geo' tends to be put into a little box together with disciplines with a long and different track record. Digital transformation of our societies, economies and all the processes driving them requires a much broader approach. It requires location, though, to connect all the relevant elements and actors. Digital Earth therefore establishes fundamental geospatial concepts all across, serving as a strong transversal approach to future-proofing an information-driven world.

ISDE12 therefore links a broad range of research areas. We are pleased to present work by researchers who actively contribute to the creation of the Digital Earth society. Next to classic research papers we created a category "Best practice papers for Sustainable Development Goals" and can now publish the 28 best papers that underwent a rigorous blind review.

The symposium hosted prominent keynote speakers who addressed the main conference topic and encouraged further discussion. Ryosuke Shibasaki, Martin Visbeck, Huadong Guo, Martin

Raubal, Karl Steinitz, Nadine Alameh, Barbara Ryan, Lawrie Jordan, Yana Gevorgyan in the plenary sessions and another key note speakers in the sub-events shared their insights into new developments in the field, and by doing so inspiring new research and cooperative initiatives.

We truly thank our partner organisations who significantly helped to make this symposium possible, particularly the Austrian Academy of Sciences – ÖAW, the State of Salzburg with its ITG – Innovations- und Technologietransfer GmbH and all industry and media partners!

Neither the symposium nor this publication would have been possible without the help of many people working in the background. We are deeply indebted to all those who contributed to the conference and supported us as editors through their work, effort, time and, above all, patience. We would like to mention the authors who underwent a rigorous review process resulting in high quality publications. We particularly thank Julia Wegmayr (University of Salzburg) who provided invaluable assistance with her competent handling of general conference affairs (from contribution registration to public relations).

We do hope that the symposium gives a wide picture of current developments in Digital Earth, that the ideas presented here encourage further research, and thus foster development of powerful methods and tools as well as effective strategies for sustainable societies.

Josef Strobl, Thomas Blaschke and Julia Wegmayr

sUAS Remote Sensing for Closed-canopy Tree Inventory on Earthen Dams

Cuizhen Wang¹, Inthuorn Sasanakul¹ and Herrick Brown¹

¹University of South Carolina, USA

Abstract

More than half of the U.S. dams are privately owned and experienced the overgrowth of trees. There is a need to improve dam inspection and maintenance in a timely manner. Small Unmanned Aircraft Systems (sUAS) have been increasingly utilized for near-surface landscape mapping and reconnaissance. This study tests an sUAS protocol of closed-canopy tree survey on earthen dams. A DJI Matrice 100 flight was launched on September 22, 2020. The orthoimage and 3D point cloud are extracted, and the canopy height model is built. Treetops and crowns are delineated using an integrated watershed segmentation and image segmentation procedure. The results include a tree survey inventory that contains the locations, tree heights and crowns of 284 trees growing on the downslope of the dam. Given the flight flexibility and fine 3D details acquired from inexpensive drones, sUAS has a high potential for assessing tree overgrowth toward remediation solutions of earthen dams.

Keywords: sUAS remote sensing, watershed segmentation, 3D tree inventory, earth observation

1 Introduction

Dams provide beneficial functions such as flood control in our living environment. Of the 90,000 dams listed in the U.S. National Inventory of Dams, 65% are privately owned earthen dams, ageing and lacking maintenance (NID 2018), raising serious concerns about their hydraulic stability against extreme weather events. Trees growing on dams, for example, have been recognized as an attributor to dam erosion. Tree roots loosen the soil mass and create root cavities that may lead to seepage failure (FEMA 2005). Remediation varies depending on the size, health, and location of trees growing on the dam. Knowing the location and structural information of trees helps to understand the stability and potential remediation of a dam. However, earthen dams are generally small in size. Conventional remote sensing, even the high-resolution satellite imagery freely accessible via web platforms such as Google Earth, could not reach the resolution needed for a detailed tree survey on these dams.

Defined as *Personal Remote Sensing* (Jensen 2017), small Unmanned Aircraft Systems (sUAS), or drones, have been increasingly utilized for timely near-surface observations. Recent technological advancements have equipped drones with an improved capacity of payload,

sensors and flight time to accomplish various field missions. With highly overlapped images taken from a drone flying above the canopy, the 3D landscape can be obtained (Dong et al. 2020). It makes the sUAS imaging superior to the 2D satellite/airborne remote sensing. The low-cost sUAS may also outcompete LiDAR on affordability, accessibility and operational efficiency in the vertical dimension.

This study aims to test the feasibility of sUAS for 3D canopy reconstruction and tree survey on earthen dams experiencing an overgrowth of trees. It indicates the potential of sUAS remote sensing in dam inspection. With the rapid development of sUAS technology, it may be operationally deployed for improved observations of land properties to assist societal decision making.

2 Materials and Methods

2.1 Study site and data sets

An earthen dam, the Sweet Bay Pond Dam in downtown Columbia, South Carolina, is selected as the study site. It is 180 meters long and is a state-regulated C1 dam, i.e., with high hazard potentials in loss of life or severe damage to infrastructure (FEMA 2005). As shown in the fall-season picture (Fig.1), dense trees grow into closed-canopy woodland on the downslope of the dam. Along with tree overgrowth, signs of seepage erosion on the downslope were spotted during our field survey. The most common tree is black gum (*Nyssa sylvatica*) that is leaf-off and shows a light grey tone in the figure. Another dominant tree is tulip poplar (*Liriodendron tulipifera*), which is still green but starts to show its fall colour. Loblolly pine (*Pinus taeda*) remains dark green.



Figure 1: An oblique view of Sweet Bay Pond Dam in Columbia, SC. Photo was taken with a DJI Mavic Pro on October 26, 2019.

The sUAS data was collected on September 22, 2020, using DJI Matrice 100 (M100) assembled with a 5-band MicaSense RedEdge-M sensor: blue, green, red, red edge, and near-infrared (NIR). The flight was made around noon on a sunny day at a flight height of 90m above ground. The images were taken at an 85% endlap and 80% sidelap. Ground control points (GCPs) was collected with a survey-grade GNSS Base+Rover unit. Forty-two trees were surveyed, and tree heights were measured. Also used in the study is the U.S. Geological Survey (USGS) LiDAR point cloud product collected in 2010 at 1.4m footprint and 18cm vertical accuracy.

2.2 Approaches

The sUAS images are calibrated in the Pix4DMapper package. Relying on the Structure from Motion (SfM) technique (Westoby et al. 2012), the 3D perception of the landscape is resolved, enabling the extraction of orthoimage and point cloud. The orthoimage is resampled to 5cm pixel size. With the 3D mass points from the point cloud, the Digital Surface Model (DSM) is created that represents the top elevation above ground. The Digital Terrain Model (DTM) is the elevation of the bare earth surface. Since sUAS point cloud is based on photogrammetry, it only contains a single z value at a given (x,y) location. Therefore, the DTM is not available in vegetated areas where the camera cannot view the ground.

Here we propose to integrate the airborne LiDAR with sUAS point clouds to create the DTM. LiDAR allows multiple returns at a single location owing to the strong penetration capacity of laser signals. Ground returns in LiDAR product are extracted, which fairly represent the terrain on the bare earth. For sUAS point cloud, point returns on open ground (no shrubs or forbs) such as dam crest are also extracted. Both sources of ground returns are merged to build the DTM product. Our previous study compared their ground returns on a bare dam, confirming that the sUAS-extracted elevation is comparable to LiDAR elevation (Morgan et al. 2020). Therefore, geo-matching of the two sources is not performed.

The DTM and DSM raster layers are resampled to 20cm cell size. The Canopy Height Model (CHM) is simply calculated as $(DSM - DTM)$, which represents the height of all cells above ground (Mielcarek et al. 2018). Only pixels with $CHM > 10m$ are considered as tree canopy. The topmost point of an individual tree (treetop) in the CHM is identified using a Variable-sized Window Filter (Popescu and Wynne 2004). It identifies the local maxima with a height-dependent crown searching window. A circular searching window is used in this study, and the extracted local maxima represent treetops of individual trees.

Two approaches are adopted to extract tree crowns. A Marker-Controlled Watershed Segmentation approach (Meyer and Beucher 1990) is first applied. Assuming a tree crown follows the mathematical morphology of an inversed watershed, the approach divides the CHM into multiple segments or tree crowns. This procedure works fine in delineating standalone trees against the ground. However, poor performance has been commonly observed in closed-canopy when tree crowns overlap each other. The dam in this study has an overgrowth of trees, which often grow in closed canopy at a similar height. The CHM-based watershed segmentation could not effectively delineate these overlaid crowns. The orthoimage is then used to leverage the deficiency. The RedEdge-M image depicts the spectral variation of trees in the visible-NIR region. Adjacent pixels with similar spectral and textural features

are grouped into segments using the Mean Shift approach, a nonparametric classifier to delineate clusters with complex shapes from multimodal feature space (Comaniciu and Meer 2002).

Tree crowns are thus extracted by intersecting the watershed segments and image segments. The colour information on the orthoimage allows breaking large watersheds while the height-based morphological feature breaks large image classes. Finally, the extracted tree height is compared with field measurements for accuracy assessment. Two commonly applied evaluation metrics are used: the root mean square error (RMSE) and the mean absolute error (MAE).

3 Results and Discussion

3.1 Orthoimage and point cloud

Fig.2 displays the sUAS orthoimage overlaid with the point cloud. The flight date is in early fall. As shown in the orthoimage, trees are still green but start to show signs of fall colour (e.g. the darker tone of black gum trees). The point cloud is visually continuous due to its highly dense points at cm-level spacing. An average density of 70 points/m² reveals more structural details of the tree canopy than the 0.5 points/m² USGS LiDAR product. The study site has an elevation range of 47.5-79.06m above sea level. Dam crest and open areas have lower elevation with a blueish tone. For trees in the woodland, taller ones stand out in a reddish tone. The large gaps in the top right of the figure represent data missing from calibration errors of sUAS images.

3.2 Digital terrains and canopy height

The sUAS point cloud on the dam crest and open areas are extracted after removing all points that have apparent vertical structures. The LiDAR ground returns have a much lower density, but there are enough ground points under the tree canopy. The integrated ground points from both sources are used to create the DTM. The grid size is set to 20cm to compensate for the two data sources. With densely distributed sUAS point cloud, canopy height is extracted in high details. Fig.3a demonstrates the 3D profile of a pine tree in which all points align to make up its crown's shape. The treetop is easily measured at the height of 27.66m. In the canopy height map (Fig.3b), trees grow into a closed canopy. Taller trees

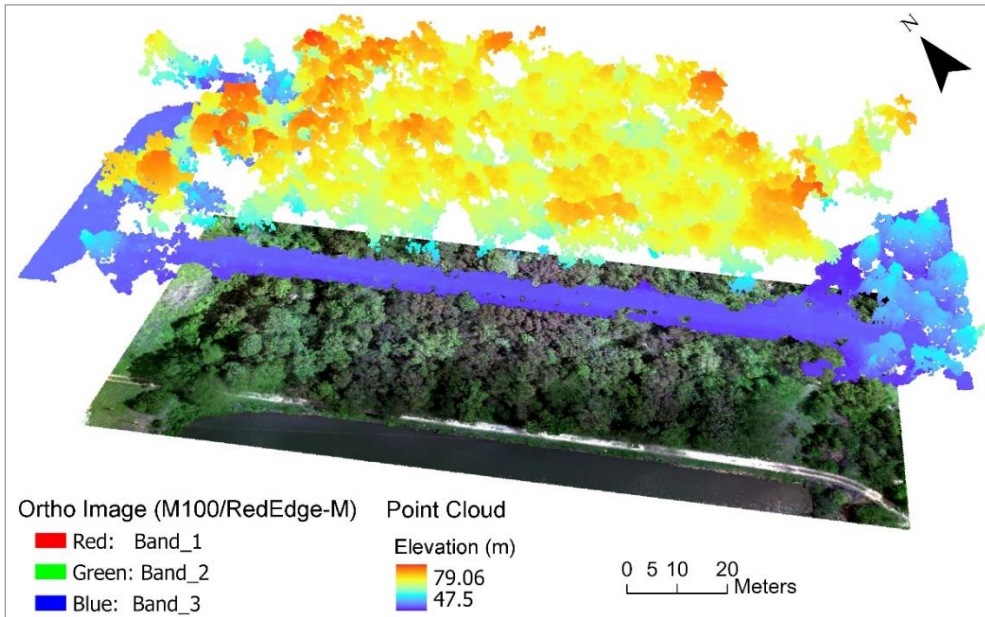


Figure 2: The sUAS-extracted orthoimage and point cloud.

stand out as individual clumps in a dark green tone. Similarly, the TIN noises in the southwest end of the mission area reflect image calibration errors.

3.3 Treetop and crown delineation

The CHM allows the delineation of treetops and crowns from the continuous canopy cover. A treetop is a point with the local maximum of CHM that represents the topmost point of a tree. One tree is assumed to have one treetop point. A total of 286 crowns are extracted (Fig.4). A treetop point is associated with a watershed segment but not necessarily the image segment.

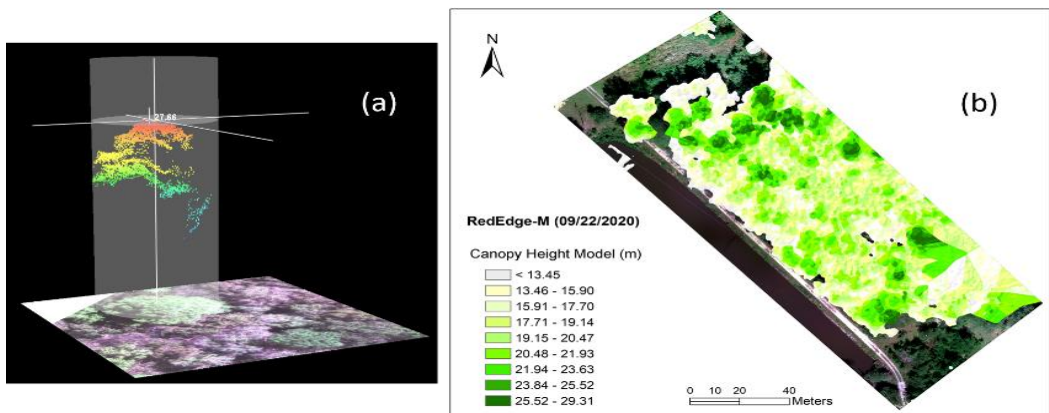


Figure 3 Example 3D profile of a pine tree (a) and the CHM map (b).

Therefore, some tree crowns do not have their treetops marked. For trees with relatively standalone crowns, for example, those at the northwest entrance, circular-shaped tree crowns are identified. Inside the woodland, trees turn to grow together in a close canopy; therefore, tree crowns become irregularly shaped and inter-connected.

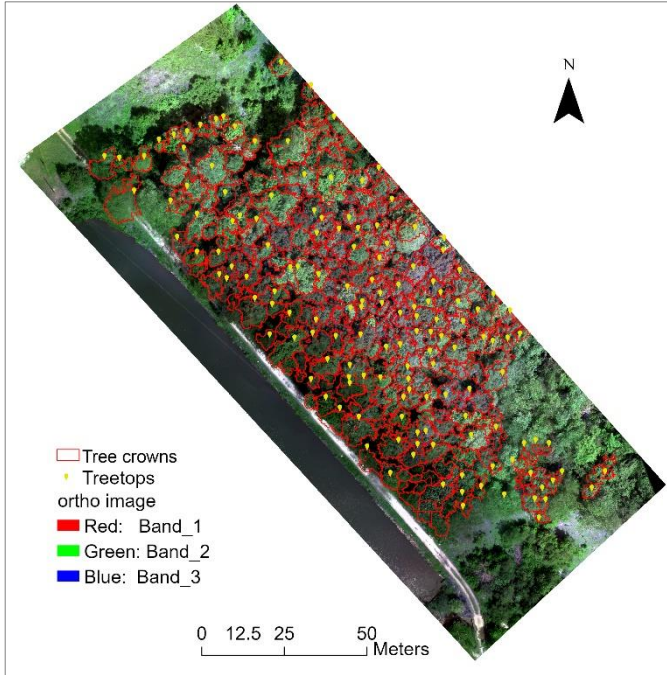


Figure 4 The extracted tree crowns and treetops.

With 27 randomly selected points on the flat dam crest, the average sUAS-extracted elevation is 3.59cm higher than the LiDAR-recorded elevation, indicating that the sUAS point cloud has decent vertical accuracies. Of the 42 field-measured trees, the sUAS-extracted tree height has a linear agreement with field records ($r = 0.517$, $p < 0.001$). However, the sUAS results have an omnidirectional overestimation, with the MAE and RMSE values 6.59m and 7.37m, respectively.

The overestimation of tree height may partially come from the imperfect field measurements using Nikon Forestry Pro. In the ideal circumstance of flat terrain and open areas, the laser rangefinder can reach a 1.0m accuracy. At our study site, trees grow in a dam downslope that is lower than the crest. Due to dense tree covers, tree height can only be measured by the surveyor standing at the crest. Its readings are inevitably lower when assuming a flat ground of the woodland. The tree base is also easily biased by a dense understory canopy. A more rigid field experiment will be conducted in the future for an improved validation process.

Integrating orthoimage and point cloud enables the 3D imaging that considers both colour and height information in canopy reconstruction. It is superior to conventional remote sensing due to the much finer spatial details. We can launch flexible sUAS missions to collect data over

the interested area at desired dates. In this sense, sUAS serves as user-controlled remote sensing or “*personal remote sensing*” as defined in current literature. Despite these technical and operational advances, image calibration errors are a common drawback for sUAS missions over dense forests. Our M100/RedEdge-M has a net weight of 2,663g, and the mission has a calibration rate of 92% at a 90m flight altitude. Uncalibrated images result in data missing. Another challenge of the low-cost sUAS for 3D tree survey in closed-canopy is the need for bare earth surface because sUAS point cloud only records the elevation of the top canopy. Nowadays, the LiDAR data products have been popularly available, which provide a reliable source of ground elevation for sUAS deployment.

Overall, this study demonstrates the high potential of sUAS in quantitative tree survey in dense forests. Owing to its fine spatial details, time efficiency and flexibility in data acquisition, sUAS remote sensing could bridge traditional remote sensing and intensive *in-situ* field experiments in monitoring our ever-changing environment. Earth observation for social well-being is an essential aspect of the Digital Earth information system. As the 3D imaging for dam inspection showcased in this study, sUAS may provide improved Earth observations for our society.

4 Conclusion

This study tests the feasibility of sUAS for 3D tree survey of closed-canopy woodland. With the reconstructed 3D canopy from sUAS orthoimage and point cloud, treetops are extracted using a local maxima approach. Tree crowns are delineated by an integrated approach of watershed segmentation and image segmentation. A tree survey inventory is established that includes a total of 284 trees with records of the location, height, and crown size. A comparison of elevation on the dam crest shows that the M100 point cloud has decent vertical accuracy against LiDAR (<5cm). The sUAS-extracted tree height indicates an overestimation of 6-7 meters, although it may partially attribute to imperfect field measurements. Image calibration error in dense woodland remains an issue for drone deployment, which needs further investigation of flight configuration for more stable sUAS missions. Nevertheless, the study indicates that sUAS could become an efficient tool of 3D tree surveys for engineers to assess the impact of tree overgrowth on dam performance. With high-resolution satellite imagery readily available, 3D imaging from sUAS offers consumer-oriented updating of our living environment to assist societal decision making.

Acknowledgment

This work was supported by the ASPIRE-II Program from the Office of the Vice President for Research, University of South Carolina. We are grateful to Mr. Robert Livingston who granted our access to his dam property. The work could not be done without his support.

Reference

- Comaniciu, D., & Meer, P. (2002). Mean shift: a robust approach toward feature space analysis. *IEEE Transactions on Pattern Analysis and Machine Intelligence*, 24:603-619.
- Federal Emergency Management Agency (FEMA) (2005). *Technical manual for dam owners: impacts of plants on earthen dams*, FEMA Document 534. Retrieved from <https://www.fema.gov/media-library-data/20130726-1446-20490-2338/fema-534.pdf>.
- Dong, X., Zhang, Z., Yu, Y., Tian, Q., & Zhu, X. (2020). Extraction of information about individual trees from high-spatial-resolution UAV-acquired images of an orchard. *Remote Sensing*, 12,133, doi:10.3390/rs12010133.
- Jensen, J.R. (2017). *Drone Aerial Photography and Videography: Data collection and image interpretation* (e-book).
- Mielcarek, M., Stereńczak, K. & Khosravipour, A. (2018). Testing and evaluating different LiDAR-derived canopy height model generation methods for tree height estimation. *Int. J. Appl. Earth Observation and Geoinformation*, 71:132–143.
- Morgan, G., Hodgson, M.E. & Wang, C. (2020). Using sUAS-derived point cloud to supplement LiDAR returns for improved canopy height model on earthen dams. *Papers in Applied Geography*, 6(1):436-448.
- National Inventory of Dams (NID) (2018). *The 2018 National Inventory of Dams*. Retrieved from <http://nid.usace.army.mil>.
- Popescu, S.C. & Wynne, R.H. (2004). Seeing the trees in the forest. *Photogrammetric Engineering & Remote Sensing*, 70(5):589-604.
- Westoby, M.J., Brasington, J. Glasser, N.F., Hambrey, M.J. & Reynolds, J.M. (2012). Structure-from-Motion' photogrammetry: a low-cost, effective tool for geoscience applications. *Geomorphology*, 179:300-314.

Generation of Spatial Profiles & Mapping of Volcanic Ash Distribution

Malini Krishnan¹ and Rajan Krishnan Sundara¹

¹International Institute of Information Technology, India

Abstract

Defining spatial distribution of airborne volcanic ash in the neighbourhood of an erupting volcano is a synoptic scale problem, severely impacting lives and livelihoods. Robust algorithms are needed to model such complex phenomenon from sparse field data. This study investigated optimal modelling of the spatial dispersion of ash using Empirical Bayesian Kriging (EBK): a geostatistical, probabilistic algorithm. Both distance and ash temperature values of samples from the 2010 Icelandic eruption were spatially correlated using semivariograms to generate prediction and error surfaces. Results showed that block averages were 90% accurate as validated against NCEP NWP model data. The work supports the utility of EBK in datasets where spatial autocorrelation is not significant. Furthermore, the results could help generate risk maps to delineate safety zones for aircrafts.

Keywords: volcanic ash, kriging, geostatistics, spatial analysis

1 Introduction

Waldo Tobler's First Law of Geography, states "Everything is related to everything else, but near things are more related than distant things." This law provides the foundation of the fundamental concepts in spatial dependence and spatial autocorrelation, and is utilized specifically in spatial interpolation techniques. Spatial autocorrelation (Zhu et al., 2019) is a key concept that is used to analyse the degree of dependency among observations (samples) in a given geographic space. Distance between neighbours, lengths of shared borders, and orientation are just some of the measurements used in conjunction, when modelling a given field, to estimate the unknowns.

When given a random spatial field with unbounded variation causing high or low spatial autocorrelation, it is necessary to analyse how the choice of the geostatistical method can accurately model the variable of interest. This paper will investigate the appropriateness of the spatial interpolation technique Kriging, in particularly for clustered, heteroskedastic datasets.

In addition, the generation of highly accurate prediction estimates, even in severe weather scenarios over synoptic scales: embracing a pure spatial analysis approach can be a powerful method to supplement grid-based models. Deterministic techniques, in general do not model uncertainties accurately. Therefore, stochastic geostatistical methods are needed to model even

small-scale spatial variances. To demonstrate and evaluate this, we have chosen a variant of Kriging named Empirical Bayesian Kriging (EBK), and applied it in this study.

Kriging is primarily a spatial algorithm. When spatiotemporal data must be analysed, usually the datasets are either grouped or split based on temporal criteria, to apply kriging, or to study the patterns (van Stein et al., 2020 and Krivoruchko et al., 2020). In this investigation, we chose four main data clusters spatially disjoint in both 2D and 3D (Altitude wise), as well as temporally (across four days). While performing kriging, the assumption was to treat the input data (May 16th, 17th and 18th) samples as pure spatial data. However, the temperature prediction and error estimate outputs have been rigorously evaluated against the available fourth day's test data (May 14th), which in reality, was also spatially and temporally disjoint from the input dataset. A process has been defined on how to customize spatiotemporal data sampled in transects, and appearing spatially random to be redefined as a spatially clustered dataset. Meaning, a technique like EBK, which was primarily designed purely for transect samples, can still be applied in other spatiotemporal contexts. Therefore, the site under study can be modelled as accurately as possible.

2 Study Site

The 2010 eruption of an Icelandic volcano, called Eyjafjallajokull, was selected for this study. The ash was dispersed across the European airspace for several days. Facility for Airborne Atmospheric Measurements (FAAM) aircrafts were flown in-sync with satellite overpasses for multiple days, near potentially hazardous ash laden regions to collect a variety of scientific data. British Atmospheric Data Centre (BADC, 2013) released a subset of the weather data for research purposes.

The data collected by the BOMEM Michelson interferometer over four days (May 14, May16, May 17, May 18) was chosen for this study, and depicted in the Minimum Bounding Region (MBR) created, including the vent location as shown in the Figure 1. While the field sampling durations extended several hours, a small portion of the recorded temperature data considered to be from an ash-significant regions was prepared. The processing involved mapping the attribute data against the flight path information by referring to the discussions made amongst the scientific crew on board the sorties.



Figure 1: Map showing the MBR with Data Locations w.r.t. Volcanic Vent over Europe

For the 4 days of flight data, 16th, 17th and 18th were used as input, while 14th data was considered as test dataset for evaluating the accuracy of estimations. The MBR encompasses around 5 lakh square Kilometers of area. The temperature distribution across those days were compared and plotted in Figure 2.

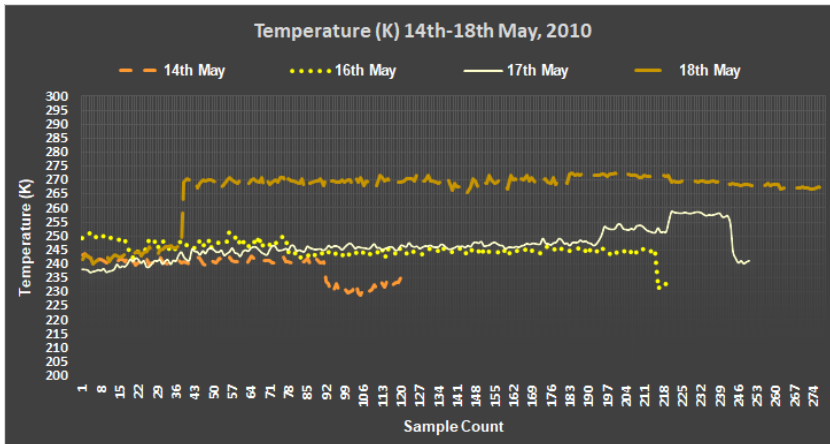


Figure 2: Temperature Distribution Plot of Data Samples

2.1 Validation Dataset

An Ash Dispersal Forecast and Civil Aviation Workshop [9] was conducted post eruption to benchmark dispersion models based on ash & weather data from the Hekla eruption in 2000. Ash concentration contour maps were generated at different flight levels.

While all the operative models were tested and compared based on properties of ash, our paper focuses on temperature variable as a proxy to model the ash dispersion. The NCEP/NCAR (National Centre for Environmental Prediction/National Centre for Atmospheric Research) reanalysis climate/weather dataset from the USA used in the workshop was therefore chosen for validation. Data for each day was downloaded from the repository (NCEP/NCAR 20th Century Reanalysis Weather Data Repository, 2016) according to the pressure altitude of the flight routes, and time duration (set to European Projection configuration).

The initial step was to understand the temperature profiles simulated by Numerical Weather Prediction (NWP) models such as NCEP, theoretically, over continental and oceanic Europe for the same period and region of interest. Daily composites for the period between May 14-May18 were compared annually from 2008-2011, minimum and maximum temperature values predicted at 350/400/700/800 mb Pressure Altitudes it was observed that there were no variations in temperature greater than 8K in total. Contrastingly, May 17th 2010 samples (collected by flight) revealed a variation of up to 22K at very short spatial scales. Furthermore, up to a 27K drop in air temperature was observed on May 17th when compared against the usual Environment Lapse Rate (ELR) (expected at 700 mb).

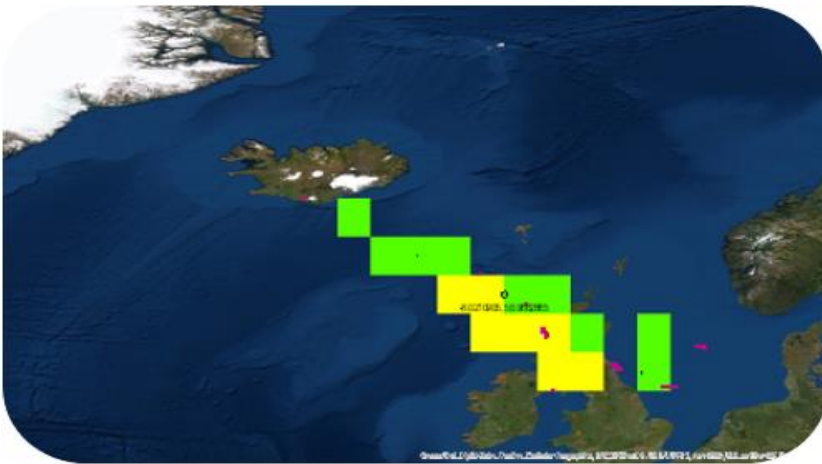


Figure 3: Map showing Overlay of Grids of NCEP Rasters from May 14th to May 18th 2010

Figure 3 clearly shows that coarse grid sizes used in NWP models do not accurately represent the state of the atmosphere even during large volcanic eruptions in any given region. The average temperature of the overlay created from using rasters of each day was $\sim 253\text{K}$. This paper (Threnbert et al., 1988) describes the interpolation approach used in NCEP models, and, discusses the limitations arising in accuracy of model outputs in the context of large geographic regions.

3 Methodology – Kriging

Linear regression techniques can produce good estimates of global mean, but are not very effective in modelling the observed small-scale variations accurately. Consequently, a robust spatial interpolation technique, based on stochastic geostatistical theory, called Kriging, originally drafted for mining industry, is cross-applied on air temperature data sampled from the affected region, at various altitudes to interpolate values at unknown locations. Kriging or Gaussian Process is a weighted average technique that assigns higher weights on nearby observations, based on the distance and direction characteristics.

The process involves, the generation of a semivariogram, which expresses the rate of change of regionalized variable w.r.t. different distance bands. By interpreting the sampled data as the result of a random process, kriging builds a methodological basis to provide a scope for estimating the spatial inference of quantities in unobserved locations. Kriging is also useful in quantifying uncertainty associated with the estimator since the sample values are expected to be correlated between themselves owing to their locational proximity. Using Linear Mixed Model framework in a Bayesian context, clusters are modelled using EBK. This method calculates, structured drift, spatial variations and errors separately. EBK produces surface outputs for prediction by fitting different transitive functions.

4 Empirical Bayesian Kriging

EBK implemented in ArcGIS software (Gribov et al., 2020 and Krivoruchko et al., 2019) effectively represents the stochastic spatial process locally as non-stationary random field, where the parameters vary across space. Local models are built by simulating multiple theoretical semivariograms, created by sub setting the input data to apply the REML (Restricted Maximum Likelihood Estimation) method.

In EBK, the Bayesian framework estimates only prior distributions using observed marginal distributions. The estimates were predicted by considering temperature concentrations as a response variable; while location variables, derived from flight data, were used as predictors. EBK model is calculated by:

$$\gamma(h) = \text{Nugget} + b|h|^\alpha \quad (1)$$

γ is the semivariance, b is the positive slope; α is the power between 0.25-1.75, Nugget which has a positive value.

4.1 Block Grade – Prediction and Error Estimates

To compare the NCEP temperature averages (measured in Kelvin) with the prediction estimates of kriging, 1x1 degree grids were created. EBK block averages, shown in Figure 4, reveal a narrow range of global temperature estimates: ranging between 241K to 251K. The global mean is ~243K, around 10K less than NCEP average.

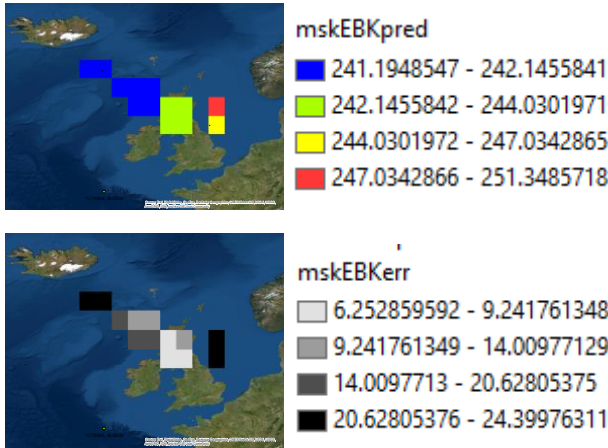


Figure 4: Maps showing Block Grade EBK – Prediction Estimates (above) & Error Estimates (below)

5 Verification & Validation

The interpolated values were verified and validated using the methods below.

5.1 Verification

Error Analysis

While the Root Mean Square (RMS) value is desired to be as low as possible for any interpolation algorithm: a special metric to assess Kriging efficiency is RMS-Standardized, which is expected to be close to 1. EBK had an RMS of 2.596989 and RMSS of 0.938776. RMS values close to zero indicates that the estimates are unbiased. EBK met the criteria with high accuracy (0.018348).

EBK Profile Analysis

Although the correlation between the distances and temperature is low ($R^2 = 0.294$), due to the clustered distribution of the samples, EBK profile (figure 5) reveals a steady decrease in temperature as the distance from the vent gradually increases, as observed in the sampled inputs for the MBR.

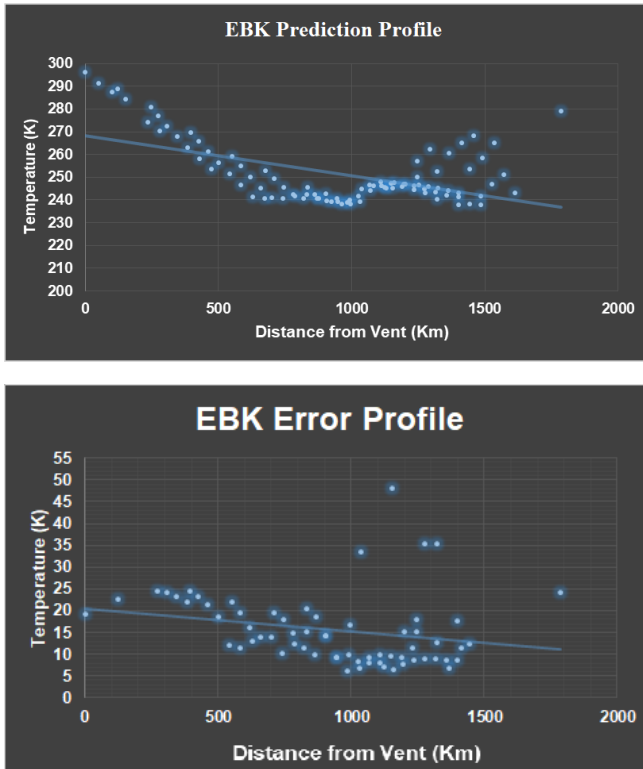


Figure 5: Plot of Temperature Prediction vs Distance Profile (above) and Error Profile (below)

The errors are also not highly correlated with distance, however, are higher in magnitude as the distance from the vent increases.

5.2 Validation

EBK vs NCEP - Profile Analysis

As shown in Figure 6, when EBK averages were validated against the NCEP NWP model values for the same duration in the area of interest, a consistent deviation of 10K was observed. However, the small-scale spatial variations were also accurately estimated using the EBK method with a maximum deviation of ~12K.

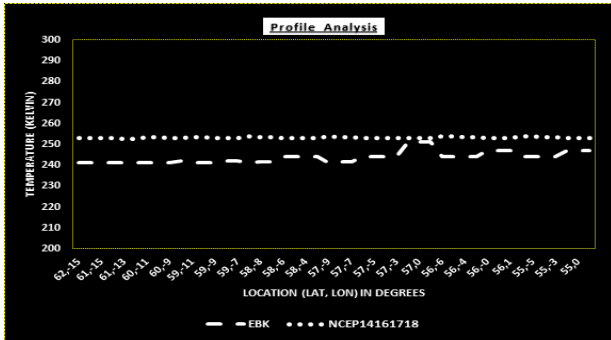


Figure 6: Plot Validating EBK Prediction Profile against NCEP Profile

Figure 7 shows the non-parametric probability density estimation for NCEP and EBK block averages. While EBK estimates had a Standard Deviation of $\sim 3K$, NCEP measured at $\sim 0.57K$.

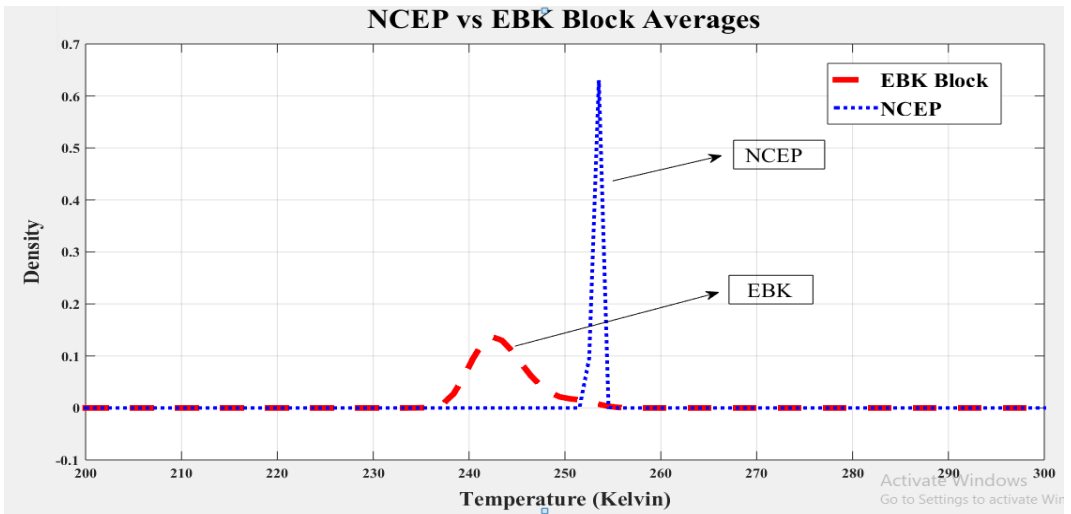


Figure 7: Plot of Probability Density Estimates - EBK Prediction vs NCEP

Against Test Data – 14th May 2010

Out of the four days of samples, three (16th, 17th, 18th May) were used to interpolate data, while one (14th May) was used as test data to validate the predicted results. Figure 8 compares the flight data on May 14th against the kriged output, using 16th/17th/18th data for the same location. Spatially, these test samples were located almost at the centre of the Minimum Bounding Region, and were equidistant from each day's cluster, and the vent. Although altitude information was not used for kriging, The test dataset was from the highest altitude (8000 meter) and hence all values were below 250K. The test dataset had just 122 samples in comparison to the 200+ each from the other 3 datasets, making ideal to be used for

verification. Altitude into validation scope solely aided in comparing kriged estimates against NCEP data at specific pressure bands

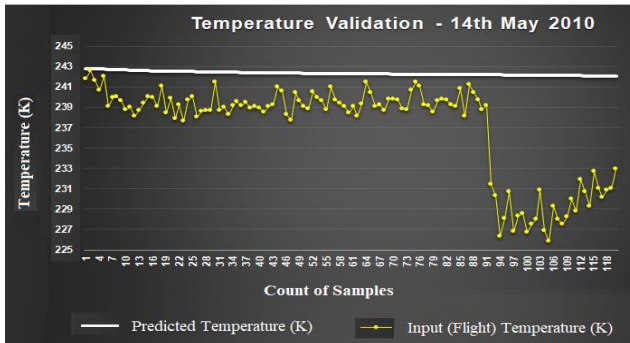


Figure 8: Plot showing Validation of Kriged Temperature Estimates Against May 14th Flight Temperature Samples

The global prediction estimates of EBK using point kriging method had a range spanning approximately 70K. On average, an overestimation error of less than 8K was observed when tested against 14th May 2010 (test data). Thus, the error is within 10% threshold for EBK prediction estimates.

Local Estimates

Prediction and error estimates were grouped into intervals of 5K to compare the input data against the kriged outputs for each day. The comparative visualization in Figure 9 reveals the degree of unbiasedness (<1K global error in locations where each day’s temperature data is available). The map below (figure 9) compares the variations observed for input data against the predicted data, where samples from the 14th May were located. This clearly shows EBK is an acceptable exact interpolator for variance.

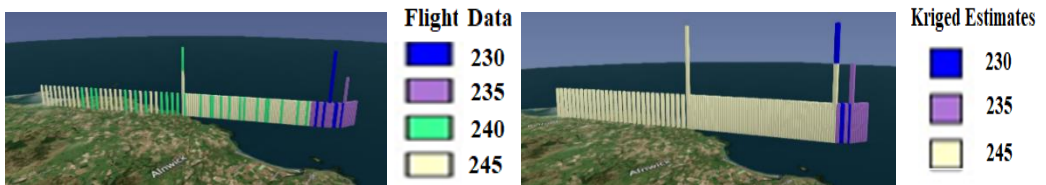


Figure 9: Maps Showing Temperature Variations - Flight Samples against Kriged Estimates on May 14th

6 Results – Discussion

For a three hour forecast of normal weather, the measure of success for prediction of temperatures is defined by UK Met Office (2021) to be within $\pm 2^{\circ}$ C 92% of the time it is reported. The smallest size of the grid cell achieved for this study site with kriging was 4x2/2x4

units. The error range for this zone was found to be between 0K-2K. With EBK, the defined success rate was achieved for a spatial resolution as low as 2km x 4km.

In the aerospace industry, this roughly translates the detection of potential ash laden field as early 20 seconds ahead of time by jet aircrafts in cruising altitude with high airspeeds and wind speed conditions. This methodology is highly suited to augment onboard severe weather alert systems, despite its probabilistic origins and simulation scope. The study can also help to define guidelines for sample data collection during future eruptions to assess the safety of an airspace.

7 Mapping Risk Zones

Given a potential use case in the aviation industry, we try to generate Go/No-Go Zones using the point prediction map produced using EBK by comparing against NCEP values. The NCEP has a narrow temperature range of 251.4K-253.9. Figure 10 shows regions with same range of observations highlighted in green (~247K to ~254K). Areas with gradual

Areas with gradual variations in orange reveal EBK underestimations/overestimations against NCEP ($\pm 25K$), while regions with red depict significant overestimations in comparison against NCEP ($\sim +40K$).

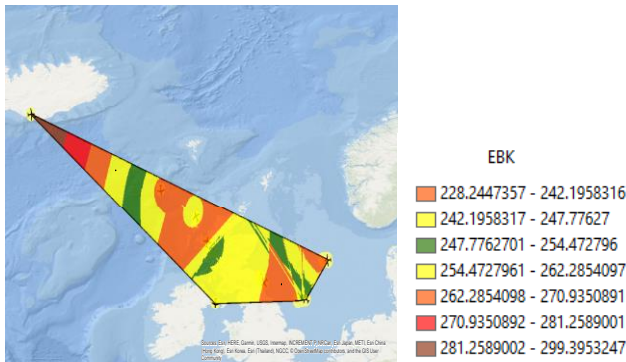


Figure 10: Map Showing Risk Zones Categorized As Go/No-Go Regions

Irrespective of the significant global variations in the input temperature across days, the EBK risk map reflects integration of unbiased global averages and small-scale variations, wherever adequate data is available.

8 Conclusion

In summary, it is observed that the EBK not only produces estimates of block mean with up to 90% accuracy closer to NWP averages, but also models small-scale spatial variances better than NWP models, even at coarser spatial resolutions. In addition, it is also evident that when EBK is applied as a punctual kriging method, it can produce unbiased averages even for

spatially clustered, heteroskedastic datasets. Hence, even in nonstationary datasets with absence of significant spatial autocorrelation, EBK can be used to assess the likelihood of volcanic ash concentration exceeding a defined threshold at a given place, so that risk to aviation operations can be determined.

The method involved partitioning the whole dataset into small subsets to model each partition, and then by combining all outputs to predict at unknown locations using a distance metric in a Bayesian framework. The Kriging technique, though originally conceived, designed, and implemented for Gaussian world with higher emphasis on Spatial Autocorrelation, is well suited for ash dispersion modelling. In addition, for smaller datasets, we established that EBK is an appropriate method to model the simultaneous existence of spatial autocorrelation and spatial heterogeneity at different degrees. These are typically observed in events that obey Pareto conditions, and can therefore be used to generate accurate maps for airborne volcanic ash dispersion.

References

- Thakur, M., Samanta, B., & Chakravarty, D. (2018). A non-stationary geostatistical approach to multigaussian kriging for local reserve estimation, *Stochastic Environmental Research and Risk Assessment*, 32(8), 2381–2404. <https://doi.org/10.1007/s00477-018-1533-1>.
- Krivoruchko K. & Gribov A. (2014). Pragmatic Bayesian kriging for non-stationary and moderately non- Gaussian data, *Mathematics of Planet Earth: Proceedings of the 15th Annual Conference of the International Association for Mathematical Geosciences: Lecture Notes in Earth System Sciences, Springer, pp.61-61*. https://doi.org/10.1007/978-3-642-32408-6_15.
- Zhu R, Janowicz K, & Mai G. (2019). Making direction a first-class citizen of Tobler's first law of geography. *Transaction in GIS*, 23:398–416. <https://doi.org/10.1002/tgis.12550>
- Airborne volcanic ash temperature data and flight logs collected of May 2010, using the BAe-146-301 Atmospheric Research Aircraft [ARA], flown by Directflight Ltd & FAAM (NERC & Met Office) obtained via, British Atmospheric Data Center (BADC) repositories. [Accessed on 30 July 2013].
- UK Met Office, Global accuracy at a local level, <https://www.metoffice.gov.uk/about-us/what/accuracy-and-trust/how-accurate-are-our-public-forecasts>. [Accessed on 30 January 2021].
- Trenberth & Olson, (1988). The Twentieth Century Reanalysis Project 3. <https://rmets.onlinelibrary.wiley.com/doi/pdf/10.1002/qj.776>
- Gribov A & Krivoruchko, (2020). Empirical Bayesian kriging implementation and usage. *Science of the Total Environment*, 20;722:137290. <https://doi.org/10.1016/j.scitotenv.2020.137290>.
- Konstantin Krivoruchko & Alexander Gribov, (2019), Evaluation of empirical Bayesian kriging, *Spatial Statistics*, 100368,ISSN:2211-6753. <https://doi.org/10.1016/j.spasta.2019.100368>
- Bonadonna, C., Folch, A., Loughlin, S. et al (2012). Future developments in modelling and monitoring of volcanic ash clouds: outcomes from the first IAVCEI-WMO workshop on Ash Dispersal Forecast and Civil Aviation. *Bull Volcanol* 74, 1–10. <https://doi.org/10.1007/s00445-011-0508-6>
- Bas van Stein, Hao Wang et al (2020). Cluster-based Kriging approximation algorithms for complexity reduction, *Applied Intelligence*, 50:778–791 <https://doi.org/10.1007/s10489-019-01549-7>
- Konstantin Krivoruchko & Jorge Mateu, (2020), COVID-19 Epidemic Data Modeling in Space-Time Using Innovation, Diffusion Kriging.
- NCEP/NCAR 20th Century Reanalysis Weather Data Repository- <https://www.esrl.noaa.gov/psd/cgi-bin/data/composites/plot20thc.day.v2.pl> [Accessed on 21 April 2016]

Integration of Ground Truth Data via Cloud Computing for Enhanced Burn Severity Mapping – An Example from Honduras

Alexander Ariza¹, Hannah Kemper² and Gerhard Kemper²

¹UN Spider Bonn, Germany

²GGS GmbH Speyer, Germany

Abstract

Until now, most severity products are generated from a reclassification of dNBR index ranges. In this study, we focused on an automated global burn severity mapping approach. Using the catalogue of satellite imagery and the high-performance computing power of GoogleEarthEngine we propose an automated pipeline to generate severity maps of burned areas at a medium scale of 30 and 10m from the time series of Landsat and Sentinel2 images. Landsat-8 images available during 2020 and the dNBR spectral index were used to calculate the severity level of each pixel using a calibration model and linear regression adjustments, which were taken in the field from the CBI index in an app developed for field capture. A calibration approach was carried out to give the severity level of the final burned areas after several carefully designed logic filters on the normalized burn rate (NBR). This script focuses on the fires that occurred in Honduras in 2020. The regression model found a similar spatial distribution and strong correlation between the areas analyzed in the field and those generated from the dNBR. The preliminary global validation showed that the overall accuracy reached 53.85%. However, the adjustments through the correlation models improved the results, yielding an R^2 of 0.93 for the quadratic model, 0.79 for the Exponential model and 0.72 for the linear model.

Keywords: burn severity, Composite Burn Index (CBI), GEE, disaster management, regression models

1 Introduction

Accurately mapping burned areas is essential for quantifying carbon budgets (Chuvieco et al., 2018; Padilla et al., 2015) and for analyzing the relationship between vegetation and climate. It is needed to assess the impacts of fire as a land management tool and quantify trends and patterns in fire occurrence, among other relevant applications. Digital image processing aiming to map fire activities has been applied to a variety of images from sensors of various spatial, temporal, and spectral resolutions (Alonso-Canas and Chuvieco, 2015; Chuvieco et al., 2018). Considering the computational power of Google Earth Engine (GEE) it is a powerful tool to enhance image preprocessing and algorithm application to big datasets. Common datasets used for image classification, burn severity detection or change detection in GEE are Landsat (Long

et al., 2019), MODIS or Sentinel-1 radar imagery. Analyses experienced a major improvement using (semi-)automatic image classification and thus are based on a greater database of thousands of images. Implementing new algorithms from Machine Learning for image classification and damage detection, big steps towards an automated burn severity workflow have been taken (Parks et al., 2018). Nevertheless, all these remote sensing data workflows show difficulties in integrating ground truth data to validate the created results. One of the major shortcomings in remote sensing image processing is that several common techniques use validation with reference images (Parks et al., 2018). Further, it is crucial to integrate ground truth data from the field into the methodology. This is enabled considering the power of Citizen Science and modern web applications like EpiCollect, which allows bi-directional communication between workers in the field and the image repository of their project (Ananensen et al., 2019). Regarding the applicability of EpiCollect in the field of Geosciences and Remote Sensing, the advantages of real-time ground truth data for validation of computed results are apparent (Hoffmann et al., 2016).

2 Area of Study

The Central Forest Corridor region is located in the centre of Honduras. It has a size of 186,525 ha and is delimited to safeguard water-producing areas of 13 municipalities.

3 Methodology

In this study, the limits of the severity map were defined by the spatial extent of the Central American fires in spring 2020. The resolution of the severity products was 30 and 10 m. The severity mapping of the burned area through GEE is described in Figure 1.

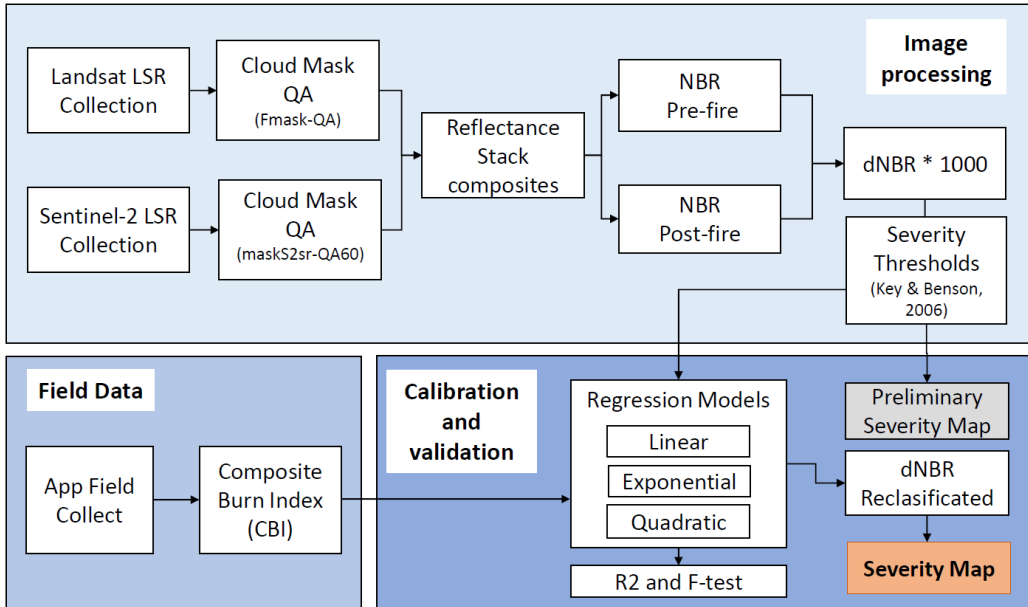


Figure 1: Workflow from image processing (chapter 3.1), field data (chapter 3.2) and model calibration and validation (chapter 3.3)

As shown in Figure 1, the pipeline consisted mainly of three steps: model training, per-pixel processing and modelling of the burned area.

3.1 Datasets and Image processing

We produced fire severity metrics for the study area in GEE based on the Landsat 8 and Sentinel 2 Surface Reflectance. The data has been corrected atmospherically using the Land Surface Reflectance Code (LaSRC)¹, which uses the quality assurance (QA) layers, which are produced during the atmospheric correction process, to estimate the amount of high aerosol that impact the derived surface reflectance. The clouds were masked using FMask (Zhu & Woodcock, 2014) as well as a per-pixel saturation mask in Landsat images, and the maskS2sr function based on the Sentinel 2 band 'QA60' the correction was concluded.

In this phase, we generate Landsat and Sentinel composites for the cloudless dates before the fire (from 06 to 30 March) and after the fire (from 15 to 17 April) using a pixel-based approach within the GEE platform, and then we reduce pixel unmasking in the reflectance stack composite using pre-and post-fire "mosaic". Then, we calculated spectral transformations in order to enhance the discrimination of changes in the land surface. In this study, we calculated two

¹<https://www.usgs.gov/media/files/landsat-8-collection-1-land-surface-reflectance-code-product-guide>

spectral transformations, the Normalized Burn Ratio (Formula 1), which contrasts the difference in reflectance between the NIR and the SWIR-2 (Short Wave Infrared), and the temporal index version dNBR (Formula 2) (Miller et al., 2007). We calculated spectral transformations in order to enhance the discrimination of changes in the land surface.

$$NBR = \left(\frac{NIR - SWIR}{NIR + SWIR} \right)$$

Formula 1: Normalized Burn Ratio

$$dNBR = (NBR_{prefire} - NBR_{postfire}) \times 1000$$

Formula 2: Differential Normalized Burn Ratio

The dNBR shows the best contrast between healthy photosynthetic vegetation and burnt vegetation. This index, similarly to NDVI, has values between -1 and 1, but it was multiplied by 1000 in order to manage the data type (integer) better, to follow the convention established by Key and Benson (2006). Therefore, higher values above 100 dNBR are set as the "burnout" threshold. In the same way, the dNBR can be used to assess the severity of burns, as areas with higher dNBR values indicate more serious damage. In contrast areas with negative dNBR values may show higher vegetation productivity. dNBR can be classified according to the ranges of severity of burns. The thresholds of severity levels used in this study were those proposed by the United States Geological Survey (USGS), in this case, the class marks of the unburned to high ranges of the Key and Benson (2006) classification were used. These dNBR thresholds thus establish the respective fire severity classes (Table 1).

Table 1: Thresholds of severity levels from dNBR index

Severity Level	dNBR Range (scaled by 10^3)	dNBR Range (not scaled)
Enhanced Regrowth, high (post-fire)	-500 to -251	-0.500 to -0.251
Enhanced Regrowth, low (post-fire)	-250 to -101	-0.250 to -0.101
Unburned	-100 to +99	-0.100 to +0.99
Low Severity	+100 to +269	+0.100 to +0.269
Moderate-low Severity	+270 to +439	+0.270 to +0.439
Moderate-high Severity	+440 to +659	+0.440 to +0.659
High Severity	+660 to +1300	+0.660 to +1.300

3.2 Field data

The field data represents the composite burn index (CBI) (Key and Benson, 2006), which rates factors such as surface fuel consumption, soil char, vegetation mortality, and scorching of trees. CBI is rated on a continuous scale from zero to three, with CBI = 0 reflecting no change and CBI = 3 reflecting the highest degree of fire-induced ecological change.

The field data were collected using EpiCollect, a tool developed in 2009 by the Imperial College London research group, which allows taking and sending georeferenced information from phones to a central website. The information there is analyzed graphically and filtered according to the variables, using Google Maps/Earth. The stored data can be downloaded and viewed directly on the phone in Google Maps. The tool to capture field data is available here: (<https://five.epicollect.net/project/cbi>).

3.3 Severity calibration model

We aimed to determine whether our GEE based methodology (the calibration by regression models via CBI method) produced Landsat-based fire severity datasets with equivalent or higher validation statistics than severity datasets produced using one pre-fire and one post-fire scene (i.e., the standard approach since these metrics were introduced).

This calibration has two components, first the result of the dNBR index classified into five severity intervals (Carl and Key, 2006), and second the CBI field index which relies on 13 field-plots covering the research area, with a homogenean distribution per every severity class. Of the 13 field-based CBI plots, 23% are considered not burnt, (CBI=0), low severity (CBI <1.0) 23%, moderate-low severity (CBI 1.0 and <1.5) 8 %, moderate-high severity (CBI 1.5 and <2.0) 23 %, and 23% are high severity (CBI >2.0).

(Figure 2).

After, we evaluated the global accuracy of preliminary classification through the confusion matrix. Subsequently, the dNBR values were adjusted through regression analysis by three different models (linear, exponential and quadratic), evaluated through an ANOVA test in order to determine how well each model fits the field data. Using the SPSS tool, a variety of goodness-of-fit statistics are presented, using the value of R squared (R^2), and the statistic F. Finally, we extracted GEE-derived dNBR, values based on spatial analysis and then applied linear regression through statistic reducer function "ee.Reducer.linearRegression", to evaluate the performance of each severity metric. Specifically, we quantified the correspondence of each severity metric (the dependent variable) to CBI (the independent variable) as the coefficient of determination, which is the R^2 of a linear regression between predicted and observed severity values.

We conducted this analysis for the fire study area and reported R^2 values. We then conducted a parallel analysis but used dNBR reclassify derived severity mapping. This parallel analysis allows a comparison of severity datasets produced using one pre-fire and one post-fire image (e.g., CBI-derived metrics) with the calibration by regression approach as with GEE.

4 Results and Analysis

Using GEE, we were able to produce dNBR quickly, and CBI including composite burned index on (specifically to calibration by regression method) for the 13 fields-plots analyzed; fire averaged about 237,40 hectares (Figure 2).

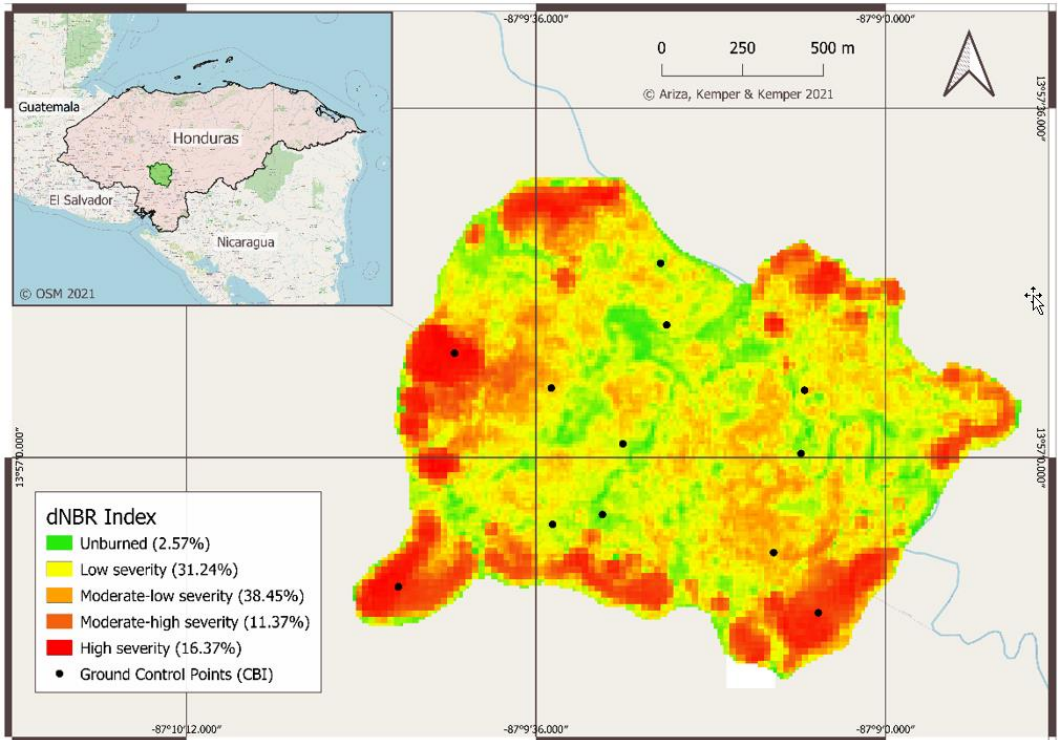


Figure 2: Severity mapping and location of the 13 CBI included in the calibration of the differential normalized burn ratio (dNBR). Tegucigalpa, Honduras

The entire process took approximately one minute, though this is a rough estimate that depends on the size and available resources shared with other users (Gorelick et al., 2017). Nonetheless, the processing time is quick with fairly low investment in terms of human labour.

The confusion matrix results showed the outcome of the preliminary classifier dNBR, with an overall accuracy of 53,8%. However, as can be seen in Table 2, the regression analysis results of R^2 , the value of the F test, and its significance value for each of the three models are presented. Although the linear regression model presents a moderate value of R^2 (0.87), its significance value F is the highest (83.58), while the quadratic model with the highest value of R^2 (0.93) presents a significance value of F minor (79.37), all models with a significance of 0.000, less than 0.05 which allows concluding that there is a significant relationship between the variables (dNBR and CBI), is much stronger in the linear and quadratic model.

Table 2: Regression Analysis Results of dNBR as dependent variable and CBI as an independent variable

Model Equation	Model summary					Parameter Estimates	
	R ²	F	df1	df2	Sig	b1	b2
Linear	0.874	83.579	1	12	.000	332.757	139.751
Quadratic	0.935	79.376	2	11	.000	-7.299	
Exponential	0.729	32.218	1	12	.000	2.932	

The correspondence between CBI and each severity metric for 13 plots covering fire was evaluated simultaneously using the regression models; the adjust was consistently higher for the GEE-derived severity high and moderate class as compared to the unburned class (Figure 3).

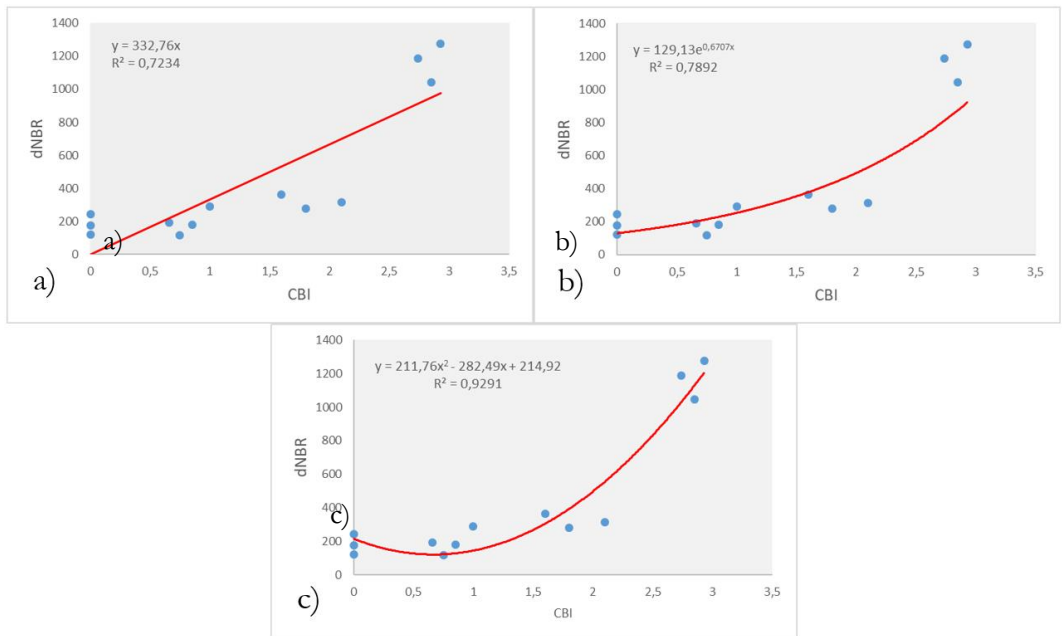


Figure 3: Regression models showing the correlation of CBI control points with dNBR. a) linear R²= 0.87; b) exponential R²=0.79; c) quadratic R² = 0.93

In general terms, the linear and quadratic models improve the fit of the severity mapping through the dNBR. Furthermore, the inclusion of the CBI increased the correspondence to field severity measure for the fire. In this case, all terms in the linear, exponential and quadratic regressions for severity metric were statistically significant ($p < 0.05$).

5 Conclusions

This paper presented a practical and efficient methodology for producing one Landsat 8 and Sentinel 2 based fire severity metric: dNBR and specifically the calibration by regression CBI method. This method relies on Google Earth Engine and provides expanded potential in terms of fire severity monitoring and research in regions outside of Honduras that does not have a dedicated program for mapping fire severity. We aimed to evaluate differences between the GEE-based calibration by a regression of the CBI method approach to the standard approach in which one pre-fire and post-fire Landsat scene is used to produce severity datasets through the thresholds of severity levels from dNBR index. The inclusion of the CBI provided additional improvements in the class severity Thresholds definitions for fire severity mapping on GEE. This provides further evidence that the inclusion of the field data should be considered when multiple fires are of interest (Parks et al., 2018). In conclusion, the application of the different regression models (Linear, Quadratic and Exponential) under the test of general significance (F) is greater than their level of significance, which allows us to conclude that the application of the regression model (Linear and Quadratic) provides a better fit of the severity obtained by the CBI than the dNBR-only intercept model.

Acknowledgement

Juan Carlos Villagran de Leon, programme officer head of UN-SPIDER Programme United Nations Office for Outer Space Affairs (UNOOSA); and Dáryl Medina Reyes from Forest Conservation Institute of Honduras (ICF).

References

- Aanensen, D.; Huntley D.; Feil,E.; al-Own, F.; Spratt, B. 2009. EpiCollect: Linking Smartphones to Web Applications for Epidemiology, Ecology and Community Data Collection. *PLoS ONE* 4(9): e6968. doi:10.1371/journal.pone.0006968
- Alonso-Canas, Itziar, and Emilio Chuvieco. 2015. Global burned area mapping from ENVISAT-MERIS and MODIS active fire data. *Remote Sensing of Environment*.
https://doi.org/10.1016/j.rse.2015.03.011.
- Chuvieco, Emilio, Joshua Lizundia-Loiola, Maria Lucrecia Pettinari, Ruben Ramo, Marc Padilla, Kevin Tansey, Florent Mouillot, et al. 2018. Generation and analysis of a new global burned area product based on MODIS 250 m reflectance bands and thermal anomalies. *Earth System Science Data*.
https://doi.org/10.5194/essd-10-2015-2018.
- Gorelick, Noel, Matt Hancher, Mike Dixon, Simon Ilyushchenko, David Thau, and Rebecca Moore. 2017. Google Earth Engine: Planetary-scale geospatial analysis for everyone. *Remote Sensing of Environment*. https://doi.org/10.1016/j.rse.2017.06.031.
- Hoffmann, G. P., Borelli, R. M., I. J., Schmidt Nanni, A. (2018): “O uso de geotecnologias livres: QGIS e EpiCollect no levantamento de dados em geociências”, *GeoFocus (Artículos)*, nº 21, p. 39-55. ISSN: 1578-5157 http://dx.doi.org/10.21138/GF.504
- Key, C.H., Benson, N.C. 2006. Landscape Assessment (LA). In: Lutes, D.C., Keane, R.E., Caratti, J.F., Key, C.H., Benson, N.C., Sutherland, S., & Gangi, L.J. (eds). *FIREMON: Fire effects monitoring*

- and inventory system. USDA Forest Service, Rocky Mountain Research Station. Gen. Tech. Rep. RMRS-GTR-164-CD, 1-55.
- Long, T., Zhang, Z., He, G.; Jiao, W.; Tang, C.; Wu, B.; Zhang, X.; Guizhou, W.; Yin, R. 2019. 30 m Resolution Global Annual Burned Area Mapping Based on Landsat Images and Google Earth Engine. *Remote Sensing*. doi:10.3390/rs11050489
- Miller, Jay D., Eric E. Knapp, Carl H. Key, Carl N. Skinner, Clint J. Isbell, R. Max Creasy, and Joseph W. Sherlock. 2009. Calibration and validation of the relative differenced Normalized Burn Ratio (RdNBR) to three measures of fire severity in the Sierra Nevada and Klamath Mountains, California, USA. *Remote Sensing of Environment*. <https://doi.org/10.1016/j.rse.2008.11.009>.
- Padilla, Marc, Stephen V. Stehman, Ruben Ramo, Dante Corti, Stijn Hantson, Patricia Oliva, Itziar Alonso-Canas, et al. 2015. Comparing the accuracies of remote sensing global burned area products using stratified random sampling and estimation. *Remote Sensing of Environment*. <https://doi.org/10.1016/j.rse.2015.01.005>.
- Parks, Sean A.; Holsinger, Lisa M.; Voss, Morgan A.; Loehman, Rachel A.; Robinson, Nathaniel P. 2018. "Mean Composite Fire Severity Metrics Computed with Google Earth Engine Offer Improved Accuracy and Expanded Mapping Potential" *Remote Sens.* 10, no. 6: 879. <https://doi.org/10.3390/rs10060879>
- Zhu, Zhe, and Curtis E. Woodcock. 2014. Automated cloud, cloud shadow, and snow detection in multitemporal Landsat data: An algorithm designed specifically for monitoring land cover change. *Remote Sensing of Environment*. <https://doi.org/10.1016/j.rse.2014.06.012>.

Understanding Current Trends in Global Urbanisation - The World Settlement Footprint Suite

Mattia Marconcini¹, Annekatriin Metz- Marconcini¹, Thomas Esch¹ and Noel Gorelick²

¹German Aerospace Center (DLR), Wessling, Germany

²Google Switzerland, Zurich, Switzerland

Abstract

To improve the understanding of current trends in global urbanisation, we have launched the World Settlement Footprint (WSF) suite, a collection of novel datasets aimed at providing accurate, reliable and frequent information on the location and extent of human settlements, as well as on their morphology and built-up density. In this paper, we present three of its products (i.e., the WSF-Evolution, WSF2019 and WSF3D), which are expected to become an asset for national statistical offices, local authorities, academia, civil society, private sector, geospatial information community, as well as international organisations involved in the implementation of the Sustainable Development Goal 11 of the United Nations and the New Urban Agenda.

Keywords: global urbanisation, settlement extent, settlement growth, building height, world settlement footprint

1 Introduction

The Sustainable Development Goal (SDG) 11 of the United Nations (UN) aims at renewing and planning human settlements in a way that offers opportunities for all, including access to essential services, transportation, green public spaces, housing and energy, while reducing the impact on the environment and the use of the resources. In this context, accurate, reliable and frequent information is needed on the location and extent of human settlements and their morphology and built-up density. To this purpose, the increasing availability of Big Earth data (as from satellite observations) and related analytics tools (e.g., Artificial Intelligence) has recently opened unprecedented opportunities. However, in the last few years, this has led to the generation of several global layers, primarily focusing only on delineating the actual settlement extent, sometimes with low quality.

To overcome this limitation, the German Aerospace Center (DLR) in collaboration with the European Space Agency (ESA) and the Google Earth Engine team has been generating the World Settlement Footprint (WSF) suite, an unprecedented collection of global datasets aimed at advancing the understanding of urbanization at the planetary scale. In this framework, the first layer to be completed and released open-and-free has been the WSF2015, a 10m

resolution binary mask outlining the 2015 global settlement extent derived by jointly exploiting multitemporal optical Landsat-8 and radar Sentinel-1 (S1) imagery (Marconcini et al., 2020). This will be soon followed by other three products, namely

- 1) The WSF-Evolution, which outlines the global settlement growth at 30m resolution on a yearly basis from 1985 to 2015;
- 2) the WSF2019, which outlines the 2019 global settlement extent at 10m resolution; and
- 3) the WSF3D, which estimates the average height of built-up areas globally at 90m resolution.

In the following, an overview is presented of these three layers, which are expected to become an asset for a variety of end users in the framework of several thematic applications, helping to support the achievement of SDG11, as well as the New Urban Agenda.

2 The WSF-Evolution

To effectively foster the sustainable development of human settlements, information on their actual extent is relevant but not sufficient. Indeed, for characterising ongoing trends, a proper understanding of past growth is also necessary. In this framework, a few global layers already exist; nevertheless, they are available for a limited number of time steps and mostly exhibit quite poor quality (as by simple visual comparison versus historical Google Earth imagery). To overcome this drawback, we have implemented a novel iterative approach that - given the lack of suitable archived high-resolution radar imagery - effectively outlines the past settlement extent based on Landsat data alone, acquired globally from late 1984 at 30m resolution.

Initially, we extract - out of all available corresponding Landsat scenes - the minimum, maximum, mean and standard deviation over time per pixel of different spectral indices for each year in the past. These include the normalised difference vegetation index - NDVI, the normalised difference built-up index - NDBI and the modified normalised difference water index - MNDWI. Next, starting from 2015 by using the WSF2015 as reference, we iteratively extract settlement and non-settlement training samples for the year t by: i) adaptively thresholding the corresponding temporal mean NDVI, NDBI and MNDWI; and ii) employing morphological filtering to the settlement mask generated for the year $t+1$. Supervised Random Forest classification is finally applied over the sole pixels marked as settlement at time $t+1$. It is worth noting that, in this way, we cannot address the cases where settlement shrinking occurs; nevertheless, this is a considerably minor phenomenon compared to the ongoing global urbanisation, and it is mainly confined locally.

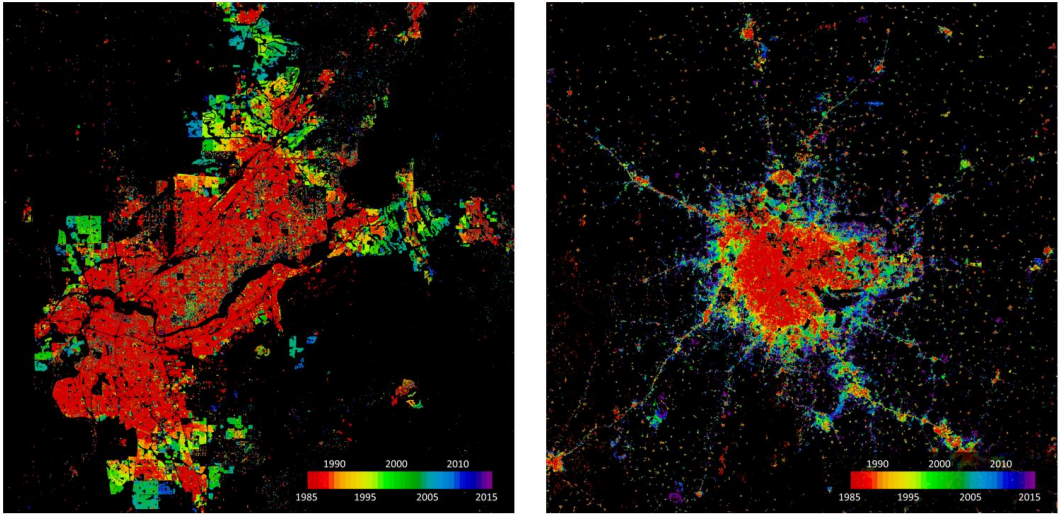


Figure 1: Samples of the 30m spatial resolution WSF-Evolution layer for Sacramento, USA (left) and Bangalore, India (right).

After an extensive test phase, the implemented approach has been eventually employed for generating the WSF-Evolution, i.e. a dataset outlining the global settlement extent at 30m spatial resolution on a yearly basis from 1985 to 2015. Specifically, the entire classification process has been performed on the Google Earth Engine (GEE) platform (Gorelick et al., 2017). Figure 1 shows two samples of the WSF-Evolution for Sacramento (USA) and Bangalore (India), covering an area of $\sim 60 \times 60 \text{ km}$ and $\sim 80 \times 80 \text{ km}$, respectively. To quantitatively assess the accuracy of the dataset, similarly to the case of the WSF2015, an extensive campaign based on crowdsourcing photointerpretation of very high-resolution airborne and satellite Google Earth imagery is currently undergoing. In particular, for the years 1990, 1995, 2000, 2005, 2010 and 2015, $\sim 180 \text{ K}$ reference cells of $30 \times 30 \text{ m}$ size distributed over 100 sites worldwide are being labelled, thus summing up to overall $\sim 1 \text{ M}$ samples.

3 The WSF2019

The advent of Sentinel-2 (S2) in 2015 has marked a milestone in Earth observation. Here, the higher number of spectral bands and higher spatial resolution (i.e., 10-20m) with respect to Landsat data, along with the 5-day revisit time since March 2018, have enabled unprecedented possibilities for monitoring urbanisation. Accordingly, to outline the current global settlement extent, we have implemented a new approach that jointly exploits multitemporal S1 and S2 imagery. Under the hypothesis that settlements generally show a more stable behaviour with respect to all other information classes, temporal statistics are calculated for both S1- and S2-based indices. In particular, a comprehensive analysis has been performed by exploiting a number of reference building outlines to identify a suitable and robust subset, which ultimately resulted in 31 temporal features, including 6 from S1 and 25 from S2. Among others, these include minimum, maximum, mean or standard deviation overtime per pixel of: i) the original

radar backscattering in the case of S1, and ii) different spectral indices of S2. As with the WSF2015 and WSF-Evolution, training points for the settlement and non-settlement class are then generated by thresholding specific features (i.e., overall 16 out of the 31 above). In particular, thresholds vary depending on the 30 climate types of the well-established Köppen Geiger scheme (Peel et al., 2007). These have been determined by statistically analysing the distribution of the chosen 16 features within the areas marked as a settlement in the WSF2015. Finally, binary Random Forest classification is applied and a dedicated post-processing is performed to mask out roads by combining the corresponding OpenStreetMap (OSM) layer (OpenStreetMap contributors, 2020) and the novel dataset predicting roads missing from OSM recently published by Facebook (Facebook development team, 2020).



Figure 2: Samples of the 10m spatial resolution WSF2019 layer (in pink) superimposed to Google Earth reference imagery for the cities of Havana, Cuba (left) and Sana'a, Yemen (right).

The method has been tested on a number of study sites throughout the different climate regions and, after assessing its effectiveness (by extensive qualitative comparison against reference Google Earth and Bing Maps imagery), it has been ultimately employed to generate the WSF2019, a novel 10m resolution mask outlining the global settlement extent for the year 2019. Figure 2 reports two samples of the final product of Havana (Cuba) and Sana'a (Yemen), both covering an area of $\sim 10 \times 10$ km. Also in this case, the whole processing has been performed in the GEE environment, and a dedicated crowd-sourcing-based validation exercise is about to be completed, where ~ 700 K reference labels are being collected based on 2019 VHR imagery available from Google Earth.

4 The WSF3D

Besides a proper delineation of the extent of human settlements, precise information on the

building heights is of key importance for better estimating the distribution of the resident population, energy consumption, greenhouse gas emissions, and urban heat island effects or material stock allocation. In this framework, so far, no layer exists, providing a 3D map of the built-up areas globally. To overcome this limitation, we have designed a dedicated methodology, which allows estimating the built-up height by jointly exploiting: the 12m resolution TanDEM-X digital elevation model (TDX-DEM) generated out of TerraSAR-X and TanDEM-X 2012 imagery (Zink et al., 2014), the corresponding 3m resolution original amplitude imagery (TDX-AMP), the WSF2015, as well as S2 and OSM data. In particular, the corresponding workflow consists of three modules. All areas marked as non-settlement in the WSF2015 are excluded a priori from the analysis.

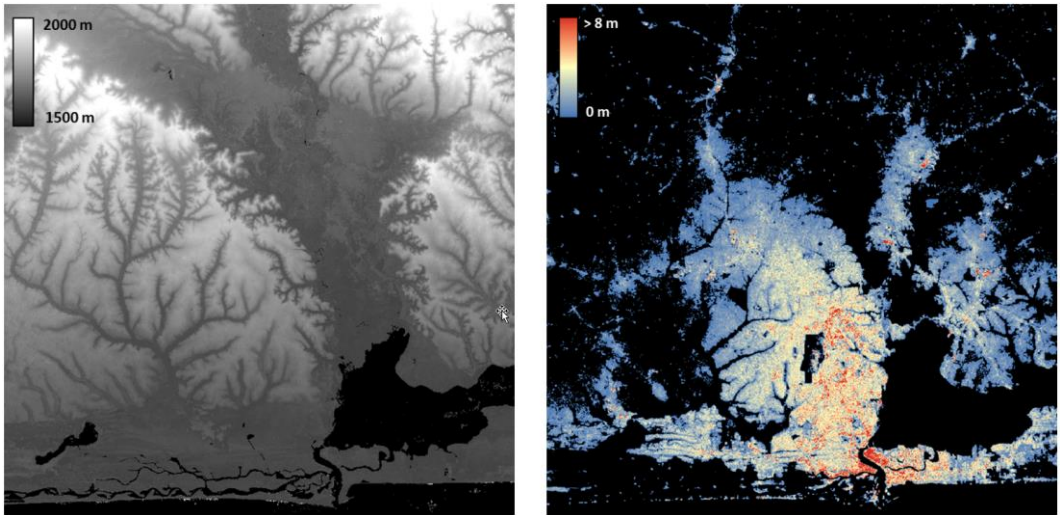


Figure 3: Lagos (Nigeria) – (left) 12m spatial resolution TanDEM-X DEM (TDX-DEM); (right) Sample of the 90m spatial resolution WSF3D average built-up height (BUH) layer.

The first module is dedicated to identifying local vertical edges in the TDX-DEM, whose mean value in a defined 90x90m grid is used for estimating the average building height (BH). Specifically, the generalisation to 90m proved effective in compensating for the effects of building layover. Next, the second module generates a 12m resolution building mask by combining TDX-AMP, OSM and S2 data. Wherever available, building outlines from OSM are used; elsewhere, the TDX-AMP is employed for estimating the location and extent of buildings (Esch et al., 2011). Here, to exclude vertical structures like trees or high hedges present in the built-up environment, a vegetation mask derived from the analysis of the S2 temporal maximum NDVI is also applied. The resulting mask is then used for computing the building fraction (BF) within each cell of the 90m grid above. In the last module, BH and BF are finally merged for estimating the average built-up height (BUH) per 90m cell.

The method has been recently applied globally for generating the WSF3D dataset. In particular, this includes the final BUH, BF and the average built-up volume obtained by multiplying the BUH with the area of the reference 90m cell (i.e., $\sim 8100\text{m}^2$ at the equator). As

an example, Figure 3 depicts for an area of $\sim 70 \times 70 \text{ km}$, including Lagos (Nigeria), both the available TDX-DEM and the corresponding WSF3D BUH. Two parallel exercises are currently aiming to assess the quality of the layer: On the one hand, detailed reference building height information is being gathered for 15 globally distributed regions. On the other hand, the height of more than 150K buildings is being labelled (in terms of the number of floors) by photo-interpretation of Mapillary panorama imagery.

5 Conclusion and Outlook

In this paper, we introduced the WSF-Evolution, WSF2019 and WSF3D layers as part of the WSF suite, aiming to support a comprehensive characterisation of human settlements globally. The three datasets demonstrated particularly accurate and reliable, as confirmed by the highly positive feedback from a number of champion users, who have been yet granted preliminary access to them, namely the World Bank, Asian Development Bank, UN-HABITAT, and International Committee of the Red Cross to cite some. Among others, they proved to be a key resource for analysing urbanisation in developing countries (where often no or poor information is available), supporting the assessment of different SDG 11 indicators, as well as estimating flood exposure or predicting COVID-19 contagion risk. Upon completion of the corresponding quantitative validation activities (expected by mid-2021), all of them are envisaged to be released open and free to the public through multiple resources, including the ESA Urban Thematic Exploitation Platform (U-TEP) and the Geoservice of the Earth Observation Center (EOC) of DLR. As next steps, we already plan: i) to update the WSF-Evolution layer, by using the WSF2019 as a reference and targeting the period 1985-2019; ii) to go beyond the settlement/non-settlement categorisation by generating the WSF2019-Imperviousness, which aims to estimate the settlement per cent soil sealing globally.

References

- Esch, T., Zeidler, J., Palacios-Lopez, D., Marconcini, M., Roth, A., Mönks, M., Leutner, B., Brzoska, E., Metz-Marconcini, A., Bachofer, F., Loekken, & S., Dech, S. (2020). Towards a Large-scale 3D Modelling of the Built Environment - Joint Analysis of TanDEM-X, Sentinel-2 and Open Street Map Data. *Remote Sens.* 12, 2391. doi.org/10.3390/rs12152391.
- Facebook development team (2020): Map with AI. mapwith.ai (07.02.2021).
- Gorelick, N., Hancher, M., Dixon, M., Ilyushchenko, S., Thau, D., & Moore, R. (2017). Google Earth Engine: Planetary-scale geospatial analysis for everyone. *Remote Sens. Environ.*, 202.
- Marconcini, M., Metz-Marconcini, A., Üreyen, S., Palacios-Lopez, D., Hanke, W., Bachofer, F., Zeidler, J., Esch, T., Gorelick, N., Kakarla, A., & Strano, E. (2020). Outlining Where Humans Live – The World Settlements Footprint 2015. *Scientific Data* 7(242). doi.org/10.1038/s41597-020-00580-5.
- OpenStreetMap contributors (2020). Planet dump retrieved from <https://planet.osm.org> (07.02.2021)
- Peel, M. C., Finlayson, B. L., & McMahon, T. A. (2007). Updated world map of the Köppen-Geiger climate classification. *Hydrol. Earth Syst. Sci.* 11, 1633–1644.
- Zink, M., Bachmann, M., Brautigam, B., Fritz, T., Hajnsek, I., Moreira, A., Wessel, B., & Krieger, G. (2014). TanDEM-X: The new global DEM takes shape. *IEEE Trans. Geosci. Remote Sens.* 2, 8–23.

Automatic Landslide Detection Using Bi-Temporal Sentinel 2 Imagery

Sepideh Tavakkoli Piralilou¹, Hejar Shahabi^{2,3} and Robert Pazur^{2,4}

¹University of Salzburg, Austria

²Slovak Academy of Sciences, Slovakia

³University of Tabriz, Iran

⁴Swiss Federal Institute for Forest, Snow and Landscape Research WSL, Switzerland

Abstract

Landslide inventory data sets are required for any landslide susceptibility mapping and prediction approaches. However, generating accurate landslide inventory data sets depends on applied methods and quality of input data, for example spatial resolution for satellite imagery. Therefore, the accuracy and availability of inventories vary in different studies. This study evaluated a strategy of sudden landslide identification product (SLIP) for landslide detection using Bi-Temporal Sentinel 2 Imagery and ALOS Digital Elevation Model (DEM). The resulting landslide detection map was then compared with an improved version of SLIP based on a fuzzy overlay. The resulting probability map was classified into three classes using the natural breaks method; the third class with the highest probability was extracted as the final map. The accuracy assessment stage demonstrated that using the improved version increased the accuracy by 16% compared to the SLIP method.

Keywords: earth observation, sudden landslide identification product (SLIP), Sentinel 2

1 Introduction

Landslides are the most dangerous and unpredictable natural hazards that usually result in severe destructions, damaging natural resources, and loss of human life and property (Hölbling et al., 2015). They occur in different types, frequencies, and intensities worldwide (Ngo et al., 2020 and Ghorbanzadeh et al., 2019A). Seeking suitable solutions to prevent and mitigate its calamitous consequences is, therefore, a high priority for society. Recent advances in remote sensing, increasing availability of Earth observation data, and progress in semi-automated and automated techniques enable the monitoring and analysis of large areas. In this regard, many machine learning (ML) methods and procedures have been developed and applied for landslide inventory mapping from different satellite imageries (Ghorbanzadeh et al., 2019B and Ghorbanzadeh et al., 2020). The ML methods are categorized into two main groups of supervised and unsupervised techniques (Mou et al., 2017). In supervised methods and model selection, the training dataset plays a vital role in mapping landslides, and the performance and accuracy of the model have a strong correlation with the quantity and quality of training data

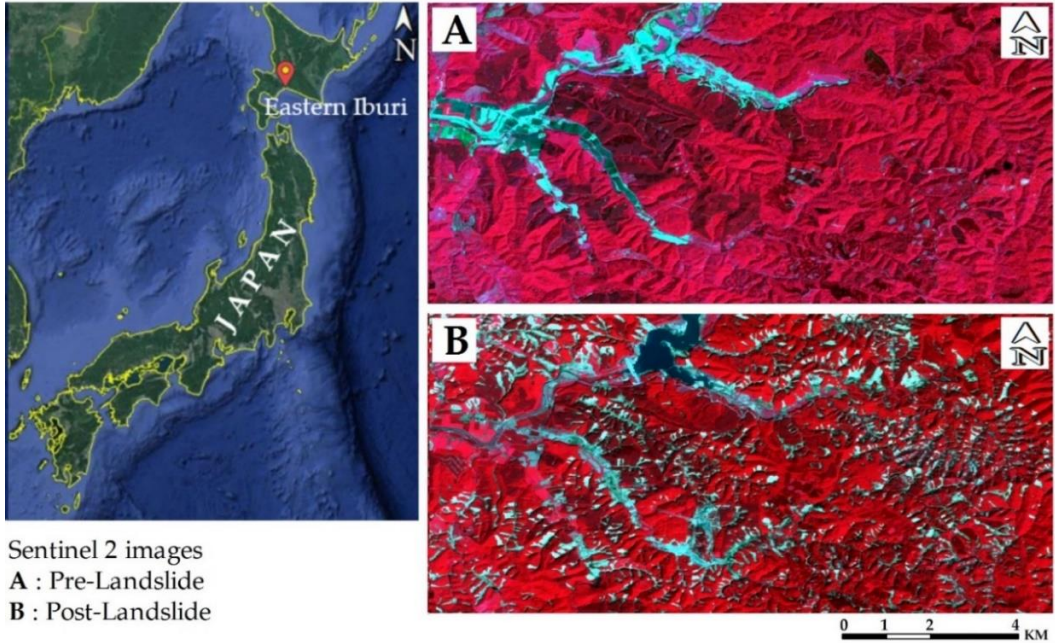
(Ghorbanzadeh et al., 2020 and Hölbling 2012). In the unsupervised methods, pixels that share similar spectral characteristics are grouped as a cluster, and the similarity threshold is usually defined by the user (Tran et al., 2019). The standard unsupervised methods are K-means clustering or Interactive self-organization data analysis (ISODATA) (Karami et al., 2015 and Abburu et al., 2015). Although they are easy to apply and do not require any labelled data for classification and clustering data, their resulting classification accuracy is usually lower than supervised approaches.

For the case of bi-temporal images, some techniques, including image differencing, normalized difference vegetation index (NDVI), change vector analysis (CVA), spectral features variance, and image rationing has been applied for land surface change detection and landslide detection in particular (Vázquez-Jiménez et al., 2018, Ramos-Bernal et al., 2018 and Solano-Correa et al., 2018). In these techniques, mapping land surface changes or deformation caused by landslide phenomena is more achievable, but selecting the optimal thresholds to classify or separate change from no-change is still a challenge (Panuju et al., 2020).

In this study, we followed a sudden landslide identification product (SLIP) strategy to overcome the thresholding issue for landslide detection using bi-temporal images. SLIP combines multiple related spectral channels from bi-temporal images to estimate landscape changes. In this regard, we examined image indices such as red change (Fayne et al., 2019) and modified normalized multiband drought index (mNMDI) and fuzzy overlay to automatically detect and classify landslides without introducing any thresholds to data.

2 Study area

The chosen study area for this investigation is Eastern Iburi, which is in Hokkaido, Japan (see figure 1). On September 6th, 2018, an earthquake struck Eastern Iburi with a magnitude of 6.6 (Mw), resulting in the deaths of 41 people; 36 of the victims were perished by landslides (Yamagishi et al., 2018). Nearly 5600 landslides, primarily shallow, were caused by the earthquake equal to an area of 46.3 km². However, the main reason for such a copious number of landslides was that the day before the earthquake, typhoon Jebi brought torrential rainfalls into the region, making the area highly susceptible to landslides (Osanai et al., 219). A landslide inventory map in this region is generated by the Geographical Survey Institute (GSI) of Japan. It is used as a perfect reference map to evaluate the accuracy of our method in landslide detection. More details on the landslide inventory map are available in Zhang et al., 2019.



Sentinel 2 images
A : Pre-Landslide
B : Post-Landslide

Figure 1: The location of our case study area of Eastern Iburi in Hokkaido, Japan. Pre and post landslide Sentinel-2 images are presented by the band combination 8-4-3 (NIR, Red, Green).

3 Data and methodology

In this study, Sentinel 2A images were acquired for dates before and after the landslide event. Based on the SLIP method, we used a stack of five images that had cloud cover less than 10% for both the pre-landslide image and post-landslide image. Before using these datasets for landslide mapping, Sen2Cor (Main-Knorn et al., 2017) plugin, which is available for SNAP software, was used to apply atmospheric corrections. Besides, since the slope is an essential factor in detecting landslides (Ghorbanzadeh et al., 2019B), we used 12-meter ALOS Digital Elevation Model to generate a slope layer used with satellite images. Sentinel 2A images include 13 bands with a spatial resolution ranging from 10 to 60 meters. Furthermore, all images and slope layers were resampled to 10-meter resolution in QGIS software for further analysis.

3.1 Sudden Landslide Identification Product (SLIP)

The research methodology established based on a change detection algorithm called SLIP proposed by Fayne, et al. (2019) utilizes Landsat-8 multispectral images and elevation data from the Shuttle Radar Topography Mission to detect landslides. In SLIP there are two crucial indices called Red Change and Normalized Multiband Drought Index (NMDI) that directly impact detecting landslides. The former index calculates the ratio of changes in Red bands (655 nm) in pre and post landslide images, expressed as equation 1, to map soil exposure. The

latter index is mainly used for measuring drought and flood conditions. It is sensitive to soil moisture and vegetation [15], making it an ideal tool to evaluate and map soil moisture changes. NMDI (Equation 2) is firstly created for MODIS multispectral data, but its performance was reported insufficient for landslide detection tasks; the authors modified (Equation 3 to be applicable) on Landsat-8 data for landslide detection. For Red change index, areas with more than a 40% increase in red reflectance were labelled as one and areas below the threshold were marked as zero. Also, mNMDI was calculated for pre and post landslide images and then using Spectral Characteristics Viewer from the U.S. Geological Survey mNMDI maps converted to binary maps with soil moisture one and without soil moisture zero. By subtracting post and pre-binary mNMDI maps, a change detection map with values -1, 0, and 1 is created, and then all values less than one are labelled as zero.

$$\text{Red Change} = \frac{(\text{R655 post} - \text{R655 pre})}{\text{R655 pre}} * 100 \quad (1)$$

$$\text{NMDI} = \frac{(\text{R 860nm} - (\text{R 1640nm} - \text{R 2130nm}))}{(\text{R 860nm} + (\text{R 1640nm} - \text{R 2130nm}))} \quad (2)$$

$$\text{mNMDI} = \frac{(\text{R 860nm} - \text{R 2200nm})}{(\text{R 860nm} + \text{R 2200nm})} \quad (3)$$

Moreover, the slope is another essential factor that authors used for mapping landslides. In SLIP, the slope is reclassified between zero and three based on the susceptibility to landslide; the higher susceptibility, the higher value, and vice versa. The remaining areas with values close to three show a high probability of being landslide, and values less than two indicate no landslide. The selection of thresholds and reclassification in the SLIP case study was based on the study site's topographical and physical characteristics.

3.2 Improved Sudden Landslide Identification Product (ISLIP)

In this section, we introduce ISLIP as an enhanced version of SLIP for landslide detection. In SLIP, the Landsat-8 multispectral data is used, while in ISLIP, we use Sentinel-2 images bands that have a similar wavelength as Landsat-8 bands for indices such as Red Change and mNMDI. However, in SLIP, the Red Change index can have infinite values, but in our method, we standardized it (Equation 4) between 0 and 1. Furthermore, we calculated mNMDI using the similar Sentinel 2 bands, and in our case, the values ranged between -1 and 1. The slope layer also was fuzzified between zero and one based on the vulnerability of landslide in our study area. To transform all layers into the same scale, we first subtracted pre-landslide mNMDI from post-landslide mNMDI, then fuzzified simply using linear fuzzy membership in QGIS, values close to 1 allocated higher membership and vice versa.

$$\text{Modified Red Change} = \frac{(\text{R665 post} - \text{R665 pre})}{(\text{R665 post} + \text{R665 pre})} \quad (4)$$

To detect landslides without introducing any thresholds, “AND” fuzzy overlay operators were used to combining all three layers, and then using the natural break clustering method, overlay map clustered into three classes.

4 Results

Represented in figure 2 are the resulting red change, pre and post landslide mNMDI indices, and mNMDI change map. According to the red change map (figure 2A), where landslides occurred, high positive values indicate changes from vegetation to bare soil due to landslide. For negative values, it shows the transformation from more minor moisturized areas to areas with high moisture like vegetation or water bodies. Moreover, in the pre-landslide mNMDI map (figure 2C), areas covered with dense vegetation show higher values, while low and negative values represent farms, bare lands, and dry soils. However, in the post-landslide mNMDI map (figure 2B), due to landslides and high soil exposure, the spatial distribution of values close to zero became frequent. Finally, in the change detection map (figure 2D), areas with more changes are associated with high positive values, and it is due to the subtraction of pre-landslide mNMDI from the post-landslide mNMDI map. Finally, the resulting map of applying the “AND” fuzzy operator on all three fuzzified inputs (Red Change, mNMDI change map, and slope) shows the probability of being a landslide ranges between zero and one; the higher values, the higher probability of being landslide. The output map is clustered into three classes, and the third class with the highest landslide probability was able to identify landslides with high accuracy. To compare our result with the SLIP method, we also mapped landslides using the SLIP method based on the procedure mentioned in [15], and pixels with values higher than 2.4 were selected as landslides.

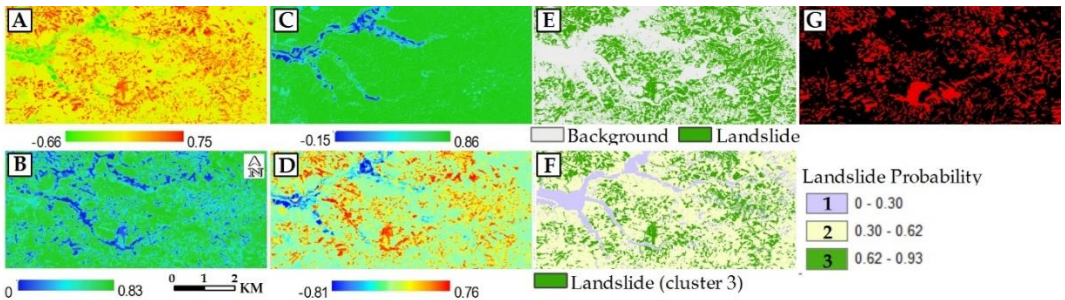


Figure 2: Spectral indices generated from Sentinel 2 images. Maps stand for (A) Red Change, (B) pre-landslide mNMDI, (C) post-landslide mNMDI, (D) mNMDI change map, (E) detected landslides (using SLIP), (F) detected landslides (using ISLIP), and (G) inventory map. Also, Maps from A to D are non-fuzzified layers and presented to indicate the indices change before and after landslide events.

5 Accuracy assessment and discussion

The resulting maps of areas detected as landslides were compared with the ground truth landslide inventory to calculate the precision accuracy assessment metric. The precision metric indicates the proportion of regions, which are correctly detected as landslide areas. Quantitative accuracy assessment using the landslide inventory map (figure 2, G) showed that ISLIP method could see landslides with an accuracy of 72%, while the SLIP method was 58% accurate. Therefore, the ISLIP has a better performance in landslide detection. One of the

factors that helped us achieve higher accuracy compared to the SLIP method is the higher spatial resolution of Sentinel-2A images.

The ISLIP algorithm shows how freely available Sentinel 2A images can be used for automated and landslide detection. However, the applied algorithms' transferability on the other regions is still considered a limitation of this study. The algorithms map changes on the surface within areas with high slopes. Thus, the slope factor played an important role in identifying the landslides, and the wrong fuzzification of the slope factor can result in a systematic bias in detecting landslides. Also, these algorithms may not be demonstrating the same accuracy for the landslides that covered by vegetation after the event.

6 Conclusions

The applied SLIP and ISLIP could automatically detect landslides to reduce the amount of time needed to analyze satellite imagery manually. This algorithm examined a large area and could show an acceptable accuracy compared to the current supervised classification models, which can be considered a practical approach in landslide research.

References

- Hölbling, D., et al. *Object-based landslide mapping on satellite images from different sensors*. in *EGU General Assembly Conference Abstracts*. 2015.
- Ngo, P.T.T., et al., *Evaluation of deep learning algorithms for national scale landslide susceptibility mapping of Iran*. *Geoscience Frontiers*, 2020. **12**(2): p. 505-519.
- Ghorbanzadeh, O. and T. Blaschke. *Optimizing Sample Patches Selection of CNN to Improve the mIOU on Landslide Detection*. in *GISTAM*. 2019.
- Ghorbanzadeh, O., et al., *Evaluation of Different Machine Learning Methods and Deep-Learning Convolutional Neural Networks for Landslide Detection*. *Remote Sensing*, 2019. **11**(2): p. 196.
- Ghorbanzadeh, O., et al., *Landslide Mapping Using Two Main Deep-Learning Convolution Neural Network (CNN) Streams Combined by the Dempster—Shafer (DS) model*. *IEEE Journal of Selected Topics in Applied Earth Observations and Remote Sensing*, 2020.
- Mou, L., P. Ghamisi, and X.X. Zhu, *Unsupervised spectral–spatial feature learning via deep residual Conv–Deconv network for hyperspectral image classification*. *IEEE Transactions on Geoscience and Remote Sensing*, 2017. **56**(1): p. 391-406.
- Hölbling, D., et al., *A semi-automated object-based approach for landslide detection validated by persistent scatterer interferometry measures and landslide inventories*. *Remote Sensing*, 2012. **4**(5): p. 1310-1336.
- Tran, C.J., et al., *Unsupervised Classification for Landslide Detection from Airborne Laser Scanning*. *Geosciences*, 2019. **9**(5): p. 221.
- Karami, A., et al., *Gully erosion mapping using object-based and pixel-based image classification methods*. *Environmental & Engineering Geoscience*, 2015. **21**(2): p. 101-110.
- Abburu, S. and S.B. Golla, *Satellite image classification methods and techniques: A review*. *International journal of computer applications*, 2015. **119**(8).
- Vázquez-Jiménez, R., et al., *Thresholding algorithm optimization for change detection to satellite imagery*, in *Colorimetry Image Processing*. 2018, InTech.
- Ramos-Bernal, R.N., et al., *Evaluation of unsupervised change detection methods applied to landslide inventory mapping using ASTER imagery*. *Remote Sensing*, 2018. **10**(12): p. 1987.
- Solano-Correa, Y.T., F. Bovolo, and L. Bruzzone, *An approach for unsupervised change detection in multitemporal VHR images acquired by different multispectral sensors*. *Remote Sensing*, 2018. **10**(4): p. 533.
- Panuju, D.R., D.J. Paull, and A.L. Griffin, *Change Detection Techniques Based on Multispectral Images for Investigating Land Cover Dynamics*. *Remote Sensing*, 2020. **12**(11): p. 1781.
- Fayne, J.V., et al., *Automated Satellite-Based Landslide Identification Product for Nepal*. *Earth Interactions*, 2019. **23**(3): p. 1-21.
- Yamagishi, H. and F. Yamazaki, *Landslides by the 2018 Hokkaido Iburi-Tobu Earthquake on September 6*. *Landslides*, 2018. **15**(12): p. 2521-2524.
- Osanai, N., et al., *Characteristics of landslides caused by the 2018 Hokkaido Eastern Iburi Earthquake*. *Landslides*, 2019. **16**(8): p. 1517-1528.
- Zhang, S., et al., *Characteristics of landslides triggered by the 2018 Hokkaido Eastern Iburi earthquake, Northern Japan*. *Landslides*, 2019. **16**(9): p. 1691-1708.
- Main-Knorn, M., et al. *Sen2Cor for sentinel-2*. in *Image and Signal Processing for Remote Sensing XXIII*. 2017. International Society for Optics and Photonics.

Comparing the Applicability of Sentinel-1 and Sentinel-2 for Mapping the Evolution of Ice-marginal Lakes in Southeast Iceland

Zahra Dabiri¹, Daniel Hölbling¹, Lorena Abad¹ and Snævarr Guðmundsson²

¹University of Salzburg, Austria

²South East Iceland Nature Research Center, Iceland

Abstract

Monitoring ice-marginal lakes is important for glaciological and geomorphological studies, as well as hazard and risk assessment. Sentinel-1 synthetic aperture radar (SAR) and Sentinel-2 optical data opened a new era for multi-temporal analysis and studying geomorphological changes. The purpose of this study is to compare the applicability of Sentinel-1 and Sentinel-2 data for mapping the changes in ice-marginal lake areas at the southern margin of the Vatnajökull ice cap, southeast Iceland, between 2016 and 2020. We semi-automatically mapped the ice-marginal lakes with object-based image analysis (OBIA) and based on image time series using 1) the polarization products derived from Sentinel-1 data, and 2) the spectral information of Sentinel-2 data, and compared the results. Our results show that Sentinel-1 performed better regarding the detection of the number of ice-marginal lakes, whereas Sentinel-2 performed better regarding lake delineation. Moreover, we discuss the applicability of optical and SAR data for mapping and monitoring the evolution of ice-marginal lakes.

Keywords: Sentinel-1, Sentinel-2, ice-marginal lake, object-based image analysis, Iceland

1 Introduction

Monitoring of ice-marginal (or proglacial) lakes is important for glaciological and geomorphological studies, as well as hazard and risk assessment. Ice-marginal lake development is a result of deglaciation, where changes in the lake area and appearance are visible consequences of climate change (Dell, Carr, Phillips, & Russell, 2019; Shugar et al., 2020). In recent years, freely available Copernicus data, including Sentinel-1 C-band Synthetic Aperture Radar (SAR) data and Sentinel-2 optical data, opened a new era for multi-temporal monitoring and analysing, for example, changes in lake ice (Tom et al., 2020) or glacial lakes (Wangchuk & Bolch, 2020). SAR data has a nearly all-weather imaging capability that facilitates the monitoring of ice-marginal lakes, especially in areas where frequent cloud cover limits the availability of optical imagery. However, the potential of SAR data for mapping ice-marginal lakes needs to be further exploited. Usually, mapping of the glacial geomorphology is largely

done by manual techniques, while (semi-)automated mapping approaches are still relatively rare (Robb, Willis, Arnold, & Gudmundsson, 2015). Object-based image analysis (OBIA) provides a set of suitable tools for semi-automated delineation and classification of geomorphological phenomena (Hölbling et al., 2017). It has been used for mapping various glacial and geomorphological features, for example, glaciers (Robson, Hölbling, Nuth, Strozz, & Dahl, 2016), rock glaciers (Robson et al., 2020), supraglacial lakes (Mitrkari, Arora, & Tiwari, 2017), drumlins (Eisank, Smith, & Hillier, 2014), and landslides (Hölbling et al., 2012). The purpose of this study is to compare the applicability of Sentinel-1 and Sentinel-2 data for multi-temporal analysis of yearly changes in the ice-marginal lake area between 2016 and 2020 using OBIA.

2 Materials and Methods

2.1 Study Area

We focused on ice-marginal lakes at the southern margin of the Vatnajökull ice cap in southeast Iceland, which have shown a constant evolution over the last years (Guðmundsson et al., 2019), in particular the ice-marginal lakes of the outlet glaciers Breiðamerkurjökull and Fjallsjökull, i.e. Jökulsárlón, Breiðárlón, and Fjallsárlón (Figure 1).

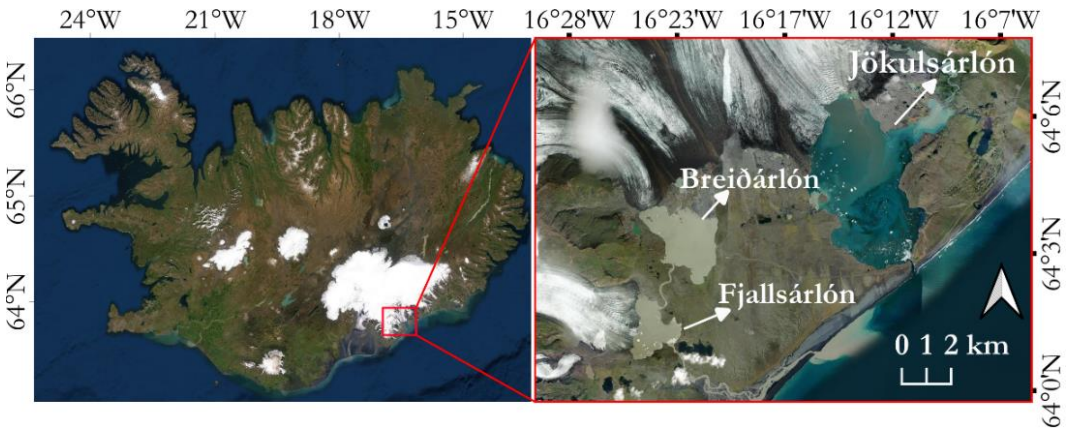


Figure 1: The study area located in southeastern Iceland (left), and the location of the Jökulsárlón, Breiðárlón, and Fjallsárlón ice-marginal lakes. Background images © ESRI.

2.2 Data and Data Preparation

We used multi-temporal Sentinel-1 and Sentinel-2 data from 2016 to 2020 (Table 1) and considered only summer images (one for each year) to avoid snow-cover on the ground. To facilitate comparability of the mapping results, we selected Sentinel-1 and Sentinel-2 images from the same or, when not possible, from similar acquisition dates per year. We selected Sentinel-1 Interferometric Wide Swath Level-1 Ground Range Detected georeferenced imagery with 10 m spatial resolution, with Vertical-Horizontal (VH) and Vertical-Vertical (VV)

polarisations from the ascending orbit (track 145). The Sentinel-2 top of atmosphere reflectance images were selected based on the visibility of lakes, using the Google Earth Engine (GEE) platform.

Table 1: Acquisition dates of Sentinel-1 and Sentinel-2 data used in this study.

Sentinel-1 data	2016/06/06	2017/06/18	2018/06/01	2019/06/21	2020/06/15
Sentinel-2 data	2016/06/06	2017/06/18	2018/06/01	2019/06/23	2020/06/17

The pre-processing of the Sentinel-1 data included updating the orbit state vectors using the Sentinel precise orbit file provided by the European Space Agency (ESA) (Filipponi, 2019), and data calibration by calculating the backscatter coefficient (i.e. sigma nought) so that the pixel values represent the SAR backscatter of the reflecting surface. We applied the Range Doppler Terrain Correction operator available in the Sentinel Application Platform (SNAP) to correct the topographical variations of the scenes using the freely available Global Earth Topography And Sea Surface Elevation at 30 arc-second resolution (GETASSE30) digital elevation model (DEM). We converted sigma values from linear units to decibel (dB).

2.3 Object-based Image Analysis

The OBIA classification was performed on Sentinel-1 and Sentinel-2 data separately using eCognition (Trimble) software. First, we applied the multiresolution segmentation (MRS) algorithm to create homogenous image objects. Then the lakes were semi-automatically classified based on spectral and spatial information.

Sentinel-1 Data

First, we created three new layers: namely a mean ($VH+VV/2$), and two ratios (VV/VH and VH/VV , respectively). We then applied the MRS with a Scale Parameter (SP) set to 50, and the homogeneity criteria, i.e. shape and compactness were set to 0.1. The “mean” layer was used for the classification of the water bodies, by applying a classification threshold of < -19 dB for the backscatter coefficient. The classified water objects were merged and then assigned to the class "lake", considering the size of the merged polygons.

Sentinel-2 Data

First, we calculated the normalised difference vegetation index (NDVI), the normalised difference water index (NDWI), the normalised difference snow index (NDSI), as well as a brightness layer based on the mean reflectance of the visible spectral bands. Next, we applied the MRS using the spectral bands, the NDVI, NDWI, and NDSI indices, and the brightness layer with an SP of 500, and the shape and compactness criteria were set to 0.3 and 0.4, respectively. However, after visually assessing the segmentation results, we adapted the settings for 2018 (SP: 800, shape and compactness criteria: 0.5 and 0.4, respectively) to better delineate the lakes. We used the $NDWI \geq 0.3$ to classify water areas and the NDVI layer and size criteria for classification refinement.

2.4 Validation

We used reference data from Guðmundsson et al. (2019), which was created by digitizing the ice-marginal lakes on pan-sharpened Landsat imagery (15 m) from 2018/05/28 for validation of the lake area delineation and the number of detected lakes (cf. section 3.2). Due to the absence of complete reference data, we assessed the accuracy of the OBIA classification results only for the year 2018.

3 Results

3.1 Object-based Image Analysis Classification Results

The OBIA classification results based on Sentinel-1 and Sentinel-2 are shown in Figure 2. We were able to classify all three major ice-marginal lakes and several small lakes semi-automatically. Visual inspection of the results using Sentinel-1 and Sentinel-2 data shows no major errors.

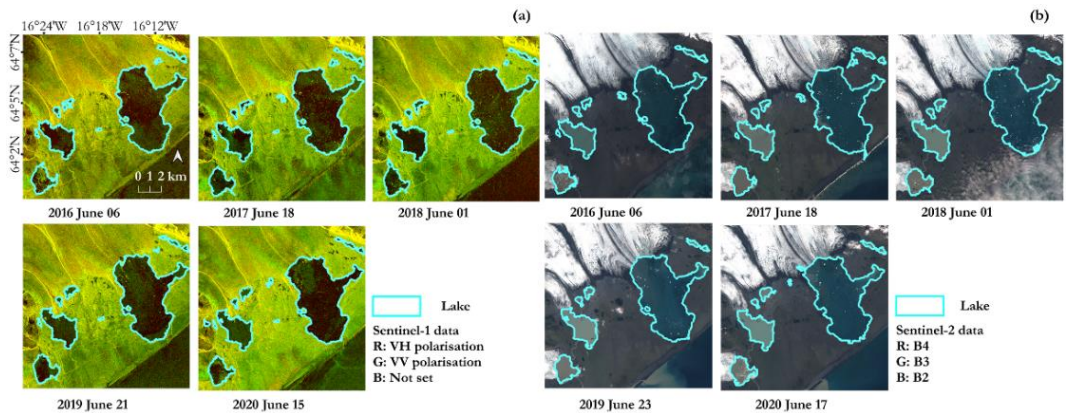


Figure 2: The OBIA classification of the ice-marginal lakes (cyan colour) using (a) the multi-temporal Sentinel-1 data, and (b) the multi-temporal Sentinel-2 data.

3.2 Validation Results

The reference data contained fourteen ice-marginal lakes, ten of which were identified using Sentinel-1, and six were identified using Sentinel-2. Moreover, we used the intersection over union (IoU) metric to compare the semi-automatically derived lake areas of the three main ice-marginal lakes (i.e. Jökulsárlón, Breiðárlón, and Fjallsárlón) to the reference (Table 3).

Table 3: Accuracy assessment of the OBIA classification for Sentinel-1 and -2 (2018/06/01).

		Jökulsárlón	Breiðárlón	Fjallsárlón
Sentinel-1	IoU (%)	84	83	86
Sentinel-2	IoU (%)	94	95	94

The comparison shows that the ice-marginal lakes were accurately identified. In general, the classification based on Sentinel-2 produced better results than the classification based on Sentinel-1, with the best IoU for Breiðarlón (95%). The best classification result using Sentinel-1 data was achieved for Fjallsárlón, with an IoU of 86%. The lake outlines derived from Sentinel-1 and Sentinel-2 for June 2018 as well as the reference data are shown in Figure 3. The lower accuracy using the IoU metric of the Sentinel-1 mapping results can partly be explained by slight shifts in lake position in comparison to the reference layer due to the side-looking geometry of SAR imagery and the usage of the default GETASSE30 DEM for terrain correction in SNAP. The use of a more accurate and higher resolution DEM would likely help to overcome the SAR geometric distortion, however, in this study, we aimed at a fully automatic and transferable SAR pre-processing workflow using SNAP.

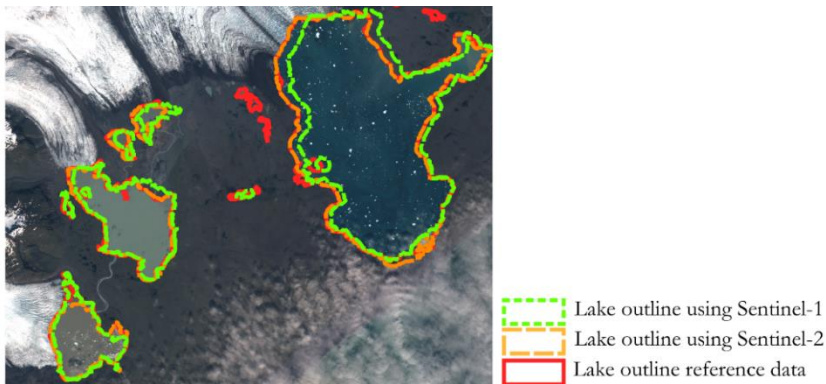


Figure 3: Illustration of the classification results using Sentinel-1 (green), Sentinel-2 (orange), and the reference data (red). Background image: Sentinel-2 image from 2018/06/01.

3.3 Lake Area Change From 2016 to 2020

We compared the change in area per lake as shown in Figure 4. The mapping results using Sentinel-1 show that Jökulsárlón gradually increased from 2016 to 2020, whereas, the mapping results derived from Sentinel-2 show a significant increase from 2016 to 2017, followed by a stable period until 2020. The lake areas of Breiðarlón and Fjallsárlón increased from 2016 to 2018 for both mapping results, followed by a slight decrease revealed by the Sentinel-1 results from 2018 to 2020. Sentinel-2 mapping results show an abrupt decrease from 2018 to 2019 and an increase from 2019 to 2020 for these two lakes. This can partly be explained by the existence of clouds on the Sentinel-2 image from 2019 which partially obscured the shore of the Breiðarlón lake and affected the segmentation and classification. A comparison to the reference data from 2018 shows that, except for the Sentinel-1 result for Breiðarlón, the semi-automated mapping results underestimated the lake area. Potential classification errors might be explained by the existence of ice blocks on the lake surface and by high soil moisture at the lakeshores. Another reason for differences compared to the reference data might be that the reference data was created based on different imagery with coarser spatial resolution.

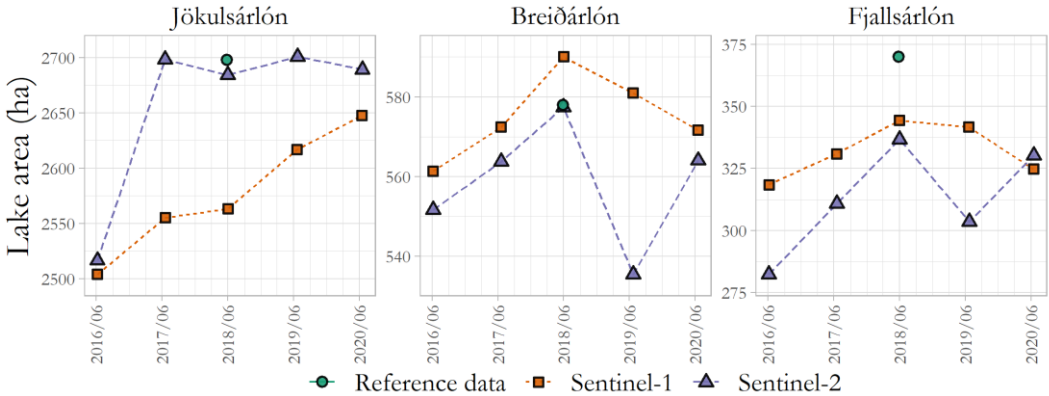


Figure 4: Change in area per lake from 2016 to 2020 for the Sentinel-1 and Sentinel-2 results.

4 Discussion and Conclusions

Sentinel-1 and Sentinel-2 show great potential for multi-temporal monitoring of ice-marginal lakes. These sensors offer high temporal and high spatial resolution data, while Sentinel-1 can be particularly useful for multi-temporal monitoring of ice-marginal lakes, regardless of weather and illumination conditions. We developed a semi-automated OBIA workflow and achieved good accuracy values for both sensors. Guðmundsson et al. (2019) describe that most of the large ice-marginal lakes in front of outlet glaciers at the southern margin of the Vatnajökull ice cap continuously grow, particularly due to recent climate change. However, our mapping results do not show such a trend for Breiðárlón and Fjallsárlón after 2018. Further investigations are needed to confirm this and to assess how classification errors influence these findings. Moreover, a combined analysis of both, Sentinel-1 and Sentinel-2 data, could offer further opportunities for analysing geomorphological changes (Dabiri et al., 2020).

Acknowledgements

This research has been supported by the Austrian Science Fund (FWF) through the Doctoral Collage GIScience (DK W 1237-N23) and the project MORPH (Mapping, monitoring and modelling the spatio-temporal dynamics of land surface morphology; FWF-P29461-N29).

References

- Dabiri, Z., Hölbling, D., Abad, L., Helgason, J. K., Sæmundsson, Þ., & Tiede, D. (2020). Assessment of Landslide-Induced Geomorphological Changes in Hítardalur Valley, Iceland, Using Sentinel-1 and Sentinel-2 Data. *Applied Sciences*, *10*(17), 5848. <https://doi.org/10.3390/app10175848>
- Dell, R., Carr, R., Phillips, E., & Russell, A. J. (2019). Response of glacier flow and structure to proglacial lake development and climate at Fjallsjökull, south-east Iceland. *Journal of Glaciology*, *65*(250), 321–336. <https://doi.org/doi:10.1017/jog.2019.18>
- Eisank, C., Smith, M., & Hillier, J. (2014). Assessment of multiresolution segmentation for delimiting drumlins in digital elevation models. *Geomorphology*, *214*, 452–464. <https://doi.org/10.1016/j.geomorph.2014.02.028>
- Filipponi, F. (2019). Sentinel-1 GRD Preprocessing Workflow. *Proceedings*, *18*(1), 11. <https://doi.org/10.3390/ECRS-3-06201>
- Guðmundsson, S., Björnsson, H., Pálsson, F., Magnússon, E., Sæmundsson, Þ., & Jóhannesson, T. (2019). Terminus lakes on the south side of Vatnajökull ice cap, SE-Iceland. *Jökull*, *69*(April), 1–34. <https://doi.org/10.33799/jokull2019.69.001>
- Hölbling, D., Eisank, C., Albrecht, F., Vecchiotti, F., Friedl, B., Weinke, E., & Kociu, A. (2017). Comparing Manual and Semi-Automated Landslide Mapping Based on Optical Satellite Images from Different Sensors. *Geosciences*, *7*(2), 37. <https://doi.org/10.3390/geosciences7020037>
- Hölbling, D., Füreder, P., Antolini, F., Cigna, F., Casagli, N., & Lang, S. (2012). A Semi-Automated Object-Based Approach for Landslide Detection Validated by Persistent Scatterer Interferometry Measures and Landslide Inventories. *Remote Sensing*, *4*(5), 1310–1336. <https://doi.org/10.3390/rs4051310>
- Mitkari, K. V., Arora, M. K., & Tiwari, R. K. (2017). Extraction of Glacial Lakes in Gangotri Glacier Using Object-Based Image Analysis. *IEEE Journal of Selected Topics in Applied Earth Observations and Remote Sensing*, *10*(12), 5275–5283. <https://doi.org/10.1109/JSTARS.2017.2727506>
- Robb, C., Willis, I., Arnold, N., & Gudmundsson, S. (2015). A semi-automated method for mapping glacial geomorphology tested at Breidamerkurjökull, Iceland. *Remote Sensing of Environment*, *163*, 80–90. <https://doi.org/10.1016/j.rse.2015.03.007>
- Robson, B. A., Bolch, T., MacDonell, S., Hölbling, D., Rastner, P., & Schaffer, N. (2020). Automated detection of rock glaciers using deep learning and object-based image analysis. *Remote Sensing of Environment*, *250*(July), 112033. <https://doi.org/10.1016/j.rse.2020.112033>
- Robson, B. A., Hölbling, D., Nuth, C., Strozzi, T., & Dahl, S. O. (2016). Decadal scale changes in glacier area in the Hohe Tauern national park (Austria) determined by object-based image analysis. *Remote Sensing*, *8*(1), 67. <https://doi.org/https://doi.org/10.3390/rs8010067>
- Shugar, D. H., Burr, A., Haritashya, U. K., Kargel, J. S., Watson, C. S., Kennedy, M. C., ... Strattman, K. (2020). Rapid worldwide growth of glacial lakes since 1990. *Nature Climate Change*, *10*(10), 939–945. <https://doi.org/10.1038/s41558-020-0855-4>
- Tom, M., Aguilar, R., Imhof, P., Leinss, S., Baltsavias, E., & Schindler, K. (2020). Lake Ice Detection from Sentinel-1 SAR with Deep Learning. *ISPRS Annals of Photogrammetry, Remote Sensing and Spatial Information Sciences*, *V-3–2020*(3), 409–416. <https://doi.org/10.5194/isprs-annals-V-3-2020-409-2020>
- Wangchuk, S., & Bolch, T. (2020). Mapping of glacial lakes using Sentinel-1 and Sentinel-2 data and a random forest classifier: Strengths and challenges. *Science of Remote Sensing*, *2*, 100008. <https://doi.org/10.1016/j.srs.2020.100008>

One GUI to Rule Them All: Accessing Multiple Semantic EO Data Cubes in One Graphical User Interface

Martin Sudmanns^{1,2}, Hannah Augustin¹, Lucas van der Meer¹, Christian Werner¹,
Andrea Baraldi³ and Dirk Tiede¹

¹University of Salzburg, Austria

²Spatial Services GmbH, Salzburg, Austria

³Baraldi Consultancy in Remote Sensing (BACRES), Modena, Italy

Abstract

Spatio-temporal analysis capabilities of big Earth observation (EO) data are possible now on various infrastructures, but the transferability and interoperability of analyses remain challenging. This contribution describes an approach for interacting with multiple semantic EO data cubes, where for each observation, at least one nominal (i.e., categorical) interpretation is available and can be queried in the same instance. Our in-house developed Web-based graphical user interface (GUI) provides technical access to multiple semantic EO data cubes, regardless of what infrastructure they are implemented on. It is designed to create semantic models using a graphical language, and an inference engine is able to evaluate these models against existing semantic EO data cubes based on a user's defined area and timespan of interest. Querying on a semantic level allows the transferability of semantic models across EO data cubes. Our contribution shows an approach towards solving this open research gap and discusses relevant challenges such as transferability of semantic models, on-demand instantiation, and federated EO data cubes. We believe that this approach offers new opportunities for improved semantic and syntactic interoperability in EO analyses and is better positioned to allow semantically-enabled queries possible in a federated EO data cube context.

Keywords: Big Earth observation data, interoperability, spatio-temporal querying, semantic EO data cubes

1 Introduction

Infrastructures for accessing and processing big Earth observation (EO) data are becoming increasingly mature and reliable. A prominent example is Google Earth Engine (Gorelick et al., 2017), but especially technologies based on the "data cube" idea, like the Earthserver (Baumann et al., 2016), the Euro Data Cube (<https://eurodatacube.com/>), or implementations of the Open Data Cube (Killough, 2018). Almost all of them employ some sort of spatio-temporal analysis capabilities. There is still no community-agreed definition for EO data cubes, but several works exist to better understand. The data cube manifesto (Baumann, 2017) defines

a data cube as “a massive multi-dimensional array; ‘massive’ entails that we talk about sizes significantly beyond the main memory resources of the server hardware. Data values of the same data type sit at grid points as defined by the d axes of the d-dimensional data cube. Coordinates along these axes allow addressing data values unambiguously.”. These new technological advances offer users access to EO data via spatio-temporal coordinates rather than archive-specific file-based access. New challenges surround how best to allow flexible and transferable analyses, potentially across multiple data cubes and technical infrastructures.

One of the most notable concepts for improving the transferability of analyses and algorithms is to populate EO data cubes with analysis-ready-data (ARD) (Lewis et al., 2018, Dwyer et al., 2018, Giuliani et al., 2017). Imagery calibrated to bottom-of-atmosphere (surface reflectance) together with a set of mandatory and optional quality information (e.g. cloud contamination) is one example of ARD for optical EO data. CEOS defines ARD as “satellite data that have been processed to a minimum set of requirements and organised into a form that allows immediate analysis with a minimum of additional user effort and interoperability both through time and with other datasets” (Lewis et al., 2018). In theory, this allows an algorithm to be executed in different EO data cubes as long as they provide ARD. An example is the Water Observation from Space (WOFS) algorithm (Mueller et al., 2016), which has been successfully applied in the Digital Earth Australia and Digital Earth Africa data cubes.

Challenges in interoperability can be broken down into syntactic and semantic aspects of communication, while transferability is used in the context of robustness to changes of inputs. Syntactic interoperability can be achieved by technical standards for communication between a software client and a server (Schaeffer et al., 2012). Semantic interoperability refers to “the ability of services and systems to exchange data in a meaningful/useful way” (Research Data Alliance 2015). Transferability can refer to many things, but here we refer to the ability of an algorithm or analytical workflow to be used with different sets of input variables, ideally with minimal to no customisation required. These differences include but are not limited to different spatio-temporal areas of interest (e.g. geographic locations, time-spans, spatial extent or shape), different imagery from the same sensor, different sensor data (e.g. resolution, revisit time, spectral and radiometric characteristics), and even different application scenarios.

An approach beyond providing ARD is the semantic EO data cube, which provides additional semantic enrichment and data (Augustin et al., 2019). A semantic EO data cube is defined as “a data cube, where for each observation at least one nominal (i.e., categorical) interpretation is available and can be queried in the same instance”. This allows executing analyses and data combination on a semantic level towards improved semantic interoperability; as long as the interpretation (semantic enrichment) of the data is the same, an algorithm is semantically interoperable and can be transferred across multiple data cubes and multiple sensors. However, such an implementation requires image understanding routines within an expert system (e.g. a factbase storing the facts (data and information), knowledgebase storing rules, inference engine applying the rules to the facts) in which semantic EO data cubes take over the role as factbases (Tiede et. al, 2017, Laurini & Thompson, 1992, p. 641).

The semantic EO data cube is a method mainly developed at the Department of Geoinformatics – Z_GIS; the infrastructure was built around the Sen2Cube.at semantic EO data cube for Austria. The semantically-enabled approach allows semantic querying, facilitated

by our in-house developed Web-based Graphical User Interface (GUI) designed to allow users to switch between semantic EO data cubes of very different locations worldwide. The main purpose of the GUI is to develop, share and execute models based on the same semantic querying language, establishing a growing, common knowledge base.

2 Semantic EO data cubes and GUI-based access

A semantic EO data cube is typically embedded in a larger infrastructure that allows regular updates and semantic enrichment (and potentially automated instantiation of new EO data cubes) and convenient Web-based access directly in the browser with a graphical query language. Semantic models defined in the graphical querying language are translated into data cube queries and evaluated by an inference engine. Additional functionality includes a quick preview of query results, processing metadata (e.g. model, time frame, processing time) and access to query results either as a download or direct integration in other applications as a standardised WMS.

Semantic enrichment refers to interpreted content of EO imagery, i.e., mapping data to an interpretation that represents stable concepts. It is a necessary pre-processing step to create a semantic EO data cube. These interpreted concepts are generally non-ordinal, categorical variables; however, subsets of these variables may be ordinal (e.g., vegetation categorised by increasing greenness or intensity). The relative level of semantic enrichment can vary in terms of complexity and the “symbolic” level of the concepts/variables. The concept of semantic enrichment itself is independent of the technology and can be potentially achieved with other approaches, including any artificial-intelligence-based approach.

The definition of a semantic EO data cube as having at least one interpretation together with every observation requires not only a spatio-temporal data model that considers thematic information layers but also a metadata model. The metadata model must: (1) define the type of semantic enrichment; (2) allow displaying the type of the content in the GUI; and (3) allow automated evaluation of semantic models in the inference engine. To achieve this, we invented a ‘layout’ of a semantic EO data cube to describe the thematic information layers of the semantic EO data cubes. All of the three components are developed generically and consider the layout, thus allowing the creation of different ‘flavors’ of semantic EO data cubes.

Multiple semantic EO data cubes and the knowledgebase containing semantic models are accessible via the same GUI. This means that the GUI serves as a unified access point for multiple semantic EO data cubes (See Figure 1). Users do not need to use different access points for different semantic EO data cubes, while the semantic EO data cubes can even be hosted on different infrastructures.

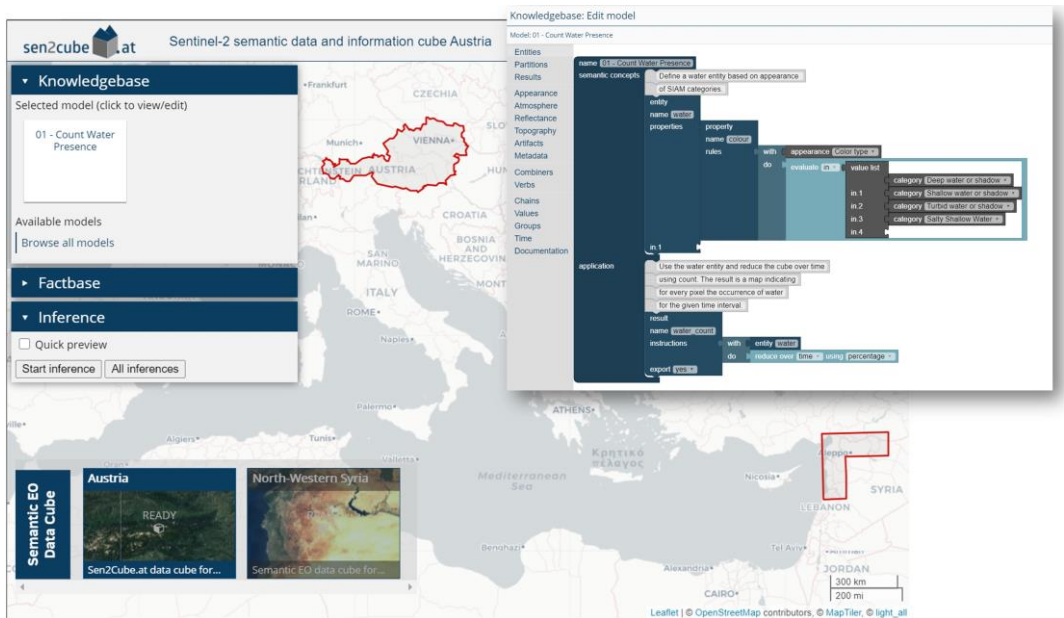


Figure 1: The GUI is designed to provide direct access to different semantic EO data cubes as factbases of the expert system (here: Sen2Cube.at covering Austria and a semantic EO data cube covering the north-western part of Syria). Since the factbases are defined using the same layout, the same semantic models are directly transferable and applicable between the different cubes.

Achieving semantic and syntactic interoperability between two or more semantic EO data cubes requires considering the transferability and re-usability of the semantic models and its dependency on the type of semantic enrichment and additional information (Sudmanns et al., 2018). The formulation of the semantic models is tied to the semantic EO data cube content, and we have identified three cases for achieving interoperability. First, if the layout of the semantic EO data cubes is defined differently, the models are directly transferable without any further adjustments. This is the easiest case in which users can switch between the semantic EO data cubes in the GUI and apply their semantic models. Second, if the layouts are different, it depends on which thematic information layers the models use. Usually, not all interpretation categories are used by a model. Therefore, the first sub-case is that the subset of categories used in a model is available in the layout, even if the rest is different. The second sub-case is that a model uses categories that are not available in the layout of another data cube, resulting in a situation in which the model cannot be evaluated. An example would be that one semantic EO data cube uses a different semantic enrichment or a digital information model, which is not available within an EO data cube at a different geographic location.

In our current setup, two semantic EO data cubes are instantiated and accessible within the Web-based GUI. Although the semantic EO data cube covering Austria is deployed on the EODC GmbH infrastructure and the one covering the north-western part of Syria is deployed on the University of Salzburg infrastructure. The GUI is designed to allow users to switch between them in the selection menu. Users create a model and can apply it to both of them, which is possible since both semantic EO data cubes are instantiated based on the same layout

(Figure 2). Therefore, the first case to achieve semantic and syntactic interoperability is already covered, while the second case with the two sub-cases remains a research gap.

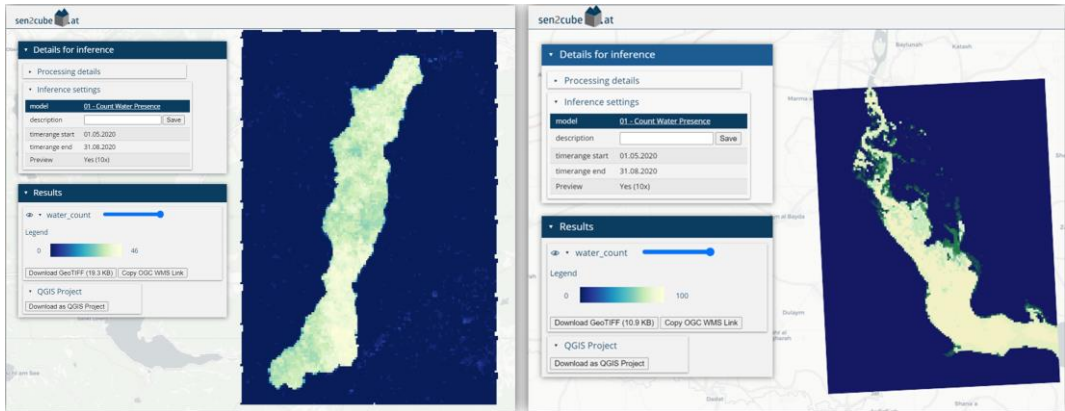


Figure 2: A semantic model can be transferred to multiple semantic EO data cubes and create comparable results. Here: Surface water extraction in Austria (left) and Syria (right) using the same semantic model, bright colours indicate a higher number of water observations in the selected time span.

3 Discussion

The in-house inference engine is programmed not to make any assumptions about the content, i.e., data and information layers of the semantic EO data cube. Every semantic model is evaluated based on the layout that defines the loading and processing of the required datasets.

Compared to accessing an EO data cube containing ARD using a Jupyter-Notebook, our approach creates an additional overhead in the development phase but removes several burdens from the users to create transferable analyses. It is easier to transfer semantic models instead of Jupyter Notebooks because the semantic enrichment and the inference engine abstract loading correct products and datasets from the users. The semantic model definition is separated from the selected AOI or time interval. Since the model creation and application are separated, and the model development approach is free of coding, it can contribute to increasing user uptake and allows the inclusion of new users, e.g., in an educational context, or allows different clients (mobile, desktop,...) to access the same knowledgebase and factbase. Once several semantic EO data cubes are available and accessible in the GUI, users do not need multiple access points or even have to learn different interfaces to conduct analyses on different parts of the world or using different sensors.

The main challenges with this approach are how to exchange models between semantic EO data cubes that have different layouts and how to deal with spatio-temporally dependent models. The key is to identify whether a model uses semantic categories that are a proper subset of the semantic EO data cube against which it will be queried. Further, some semantic models may not be fully independent of the geographic areas that are covered by the semantic EO data cube. This includes the formalisation of temporal sequences of agricultural practices

that may be shifted due to different altitudinal belts or completely different due to the location (e.g. different latitude or hemisphere). Different climate zones or atmospheric conditions may also limit the transferability of some semantic models. A possible solution could be to calculate advanced measurements of fitness-for-use of available imagery and associated semantic EO data cubes or evaluate the spatio-temporal applicability of semantic models.

4 Conclusion and path forward

The concept and implementation of semantic EO data cubes are relatively new, yet they show promising performance and are suitable to be investigated further. They implement an image interpretation strategy such as computer vision to perform semantic enrichment, thus containing EO data together with at least one (categorical) interpretation. This approach allows querying using semantic models that are evaluated by an inference engine. Querying on the semantic level is the next level of abstraction that allows for semantic and syntactic interoperability. However, defining and instantiating semantic EO data cubes and evaluating the transferability of semantic models still requires extensive human expert intervention, similar to other EO based algorithms developed in a specific context.

In this contribution, we show our approach of making multiple semantic EO data cubes technically accessible to users within a single GUI, which is designed to allow users to choose between the single data cubes in a selection menu. A knowledgebase stores semantic models that can be used to query any of the semantic EO data cubes. We also show the challenges that may arise when semantic EO data cubes have different layouts and, therefore, may require different models.

Next investigations and outlook will be aligned along four lines of research with research gaps that have not yet been solved or tackled: (1) extending the layout to describe semantic EO data cubes, thus allowing machine-readable requests about the content and capabilities to allow automated evaluation whether a model is able to be evaluated or not; (2) automating the instantiation of multiple semantic EO data cubes based on a selected layout, their deployment in state-of-the-art cloud infrastructures and accessibility within one GUI; thus, users should not necessarily be concerned with the hosting provider of the semantic EO data cube; (3) enabling a single semantic query to be conducted across multiple semantic EO data cubes, e.g., in a federated context; (4) conducting user studies for testing and evaluating the efficiency of our approach compared to other approaches. These are pre-requisites for the successful implementation of (on-demand) semantic EO data cubes. Once they are operational, additional questions will concern application- and domain-related suitability of semantic models as well as the maintenance of the semantic EO data cubes, e.g. specifying user roles (admin, user, maintainer, ...) to define which user is allowed to submit a semantic query and how much resources will be available and allocated.

References

- Augustin, H., Sudmanns, M., Tiede, D., Lang, S., & Baraldi, A. (2019). Semantic Earth observation data cubes. *Data*, 4(3), 102. <https://www.mdpi.com/2306-5729/4/3/102>
- Baumann, P., Mazzetti, P., Ungar, J., Barbera, R., Barboni, D., Beccati, A., ... & Wagner, S. (2016). Big data analytics for earth sciences: The EarthServer approach. *International Journal of Digital Earth*, 9(1), 3-29. <https://doi.org/10.1080/17538947.2014.1003106>
- Baumann, P. (2017). Data Cube manifesto. <https://earthserver.eu/tech/datacube-manifesto/The-Datacube-Manifesto.pdf>
- Dwyer, J. L., Roy, D. P., Sauer, B., Jenkerson, C. B., Zhang, H. K., & Lymburner, L. (2018). Analysis ready data: enabling analysis of the Landsat archive. *Remote Sensing*, 10(9), 1363. <https://doi.org/10.3390/rs10091363>
- Giuliani, G., Chatenoux, B., De Bono, A., Rodila, D., Richard, J. P., Allenbach, K., ... & Peduzzi, P. (2017). Building an earth observations data cube: lessons learned from the swiss data cube (sdc) on generating analysis ready data (ard). *Big Earth Data*, 1(1-2), 100-117. <https://doi.org/10.1080/20964471.2017.1398903>
- Gorelick, N., Hancher, M., Dixon, M., Ilyushchenko, S., Thau, D., & Moore, R. (2017). Google Earth Engine: Planetary-scale geospatial analysis for everyone. *Remote sensing of Environment*, 202, 18-27. <https://doi.org/10.1016/j.rse.2017.06.031>
- Killough, B. (2018). Overview of the open data cube initiative. In: IGARSS 2018 IEEE *International Geoscience and Remote Sensing Symposium* (pp. 8629-8632). <https://doi.org/10.1109/IGARSS.2018.8517694>
- Laurini, R., & Thompson, D. (1992). *Fundamentals of spatial information systems* (Vol. 37). Academic press. San Diego.
- Lewis, A., Lacey, J., Mecklenburg, S., Ross, J., Siqueira, A., Killough, B., ... & Hosford, S. (2018). CEOS analysis ready data for Land (CARD4L) overview. In IGARSS 2018 IEEE *International Geoscience and Remote Sensing Symposium* (pp. 7407-7410). <https://doi.org/10.1109/IGARSS.2018.8519255>
- Mueller, N., Lewis, A., Roberts, D., Ring, S., Melrose, R., Sixsmith, J., ... & Ip, A. (2016). Water observations from space: Mapping surface water from 25 years of Landsat imagery across Australia. *Remote Sensing of Environment*, 174, 341-352. <https://doi.org/10.1016/j.rse.2015.11.003>
- Research Data Alliance. (2016). Agrisemantics Working Group. <https://www.rda-alliance.org/group/agrisemantics-wg/case-statement/agrisemantics-working-group>. Accessed March 2021.
- Schaeffer, B., Baranski, B., Foerster, T., & Brauner, J. (2012). A Service-oriented Framework for Real-time and Distributed Geoprocessing. In E. Bocher and M. Neteler (Eds.), *Geospatial Free and Open Source Software in the 21st Century*, Springer Heidelberg. doi:10.1007/978-3-642-10595-1_1
- Sudmanns, M., Tiede, D., Lang, S., & Baraldi, A. (2018). Semantic and syntactic interoperability in online processing of big Earth observation data. *International Journal of Digital Earth*, 11(1), 95-112. <https://doi.org/10.1080/17538947.2017.1332112>
- Tiede, D., Baraldi, A., Sudmanns, M., Belgiu, M., & Lang, S. (2017). Architecture and prototypical implementation of a semantic querying system for big Earth observation image bases. *European journal of remote sensing*, 50(1), 452-463. <https://doi.org/10.1080/22797254.2017.1357432>

Evaluation of Digital Elevation Models Derived from Multi-Date Satellite Stereo Imagery for Urban Areas

Tobias Kugler¹ and Lorenz Wendt¹

¹Paris-Lodron-University of Salzburg, Austria

Abstract

High-resolution digital elevation models of urban areas can support humanitarian organisations in their work; especially the 3D reconstruction of buildings is desirable because it can be used for population estimation and damage analysis after crises and disaster events. In this paper, we test the quality of multi-date DEMs with 15 Pléiades images from Port-au-Prince, Haiti using the automatic stereo pipeline *s2p*. We focus on triplet combinations with images taken from different dates. This study investigates the meta-parameters satellite azimuth and incident angle to understand which recording geometry yields a good result in terms of completeness and accuracy. It is assumed that the closer the multi-date constellation gets to an in-orbit triplet, the better the quality of the DEM.

Keywords: satellite photogrammetry, digital elevation model, multi-date, matching quality indicator

1 Introduction

With the increasing availability of very high-resolution satellite imagery, such as from the Earth observation satellites Pléiades-1A&1B or the WorldView series, it has now become possible to create digital elevation models directly and fully automatically from stereo image pairs (de Franchis, Meinhardt-Llopis, Michel, Morel, & Facciolo, 2014; Gong & Fritsch, 2019; Krishna, Srinivasan, & Srivastava, 2008; Rupnik, Pierrot-Deseilligny, & Delorme, 2018). Thanks to this development, these data and their applications are also becoming interesting for actors outside the classical spectrum. Especially in the humanitarian field, automated derived elevation models yield a wide range of benefits. In this context, elevation models of urban areas are of particular interest, as they can be used for damage analyses of buildings or population estimates. To be able to act appropriately in crisis situations, quickly available data plays a decisive role. Often, however, high-quality in-orbit stereo image pairs are either not available in the archives, or have to be acquired in a time-consuming process (Krauß, D'Angelo, & Wendt, 2019). To address this shortcoming and reduce the reliance on in-orbit stereo pairs, several works have attempted to create DSMs from images with different acquisition times (multi-date), or combining images from different satellites (cross-sensor) (Facciolo, De Franchis, & Meinhardt-Llopis, 2017; Krauß et al., 2019; Ozcanli et al., 2015; Qin, 2019). While these works had access to a tremendous stock of images (up to 200 images per site),

humanitarian organizations do not have the budget to acquire this number of images. For this reason, this study examines a Cost-effective approach by using only three images for the generation of a DEM. It addresses the question of which recording geometry yields the best results given that every chosen image in a triplet was taken at a different date. While other work has shown which parameter constitutes a good stereo pair, this study investigates the constellation of the satellite azimuth and the incident angles within a triplet. It can be assumed that the smaller the deviation of the three recording points from an optimal in-orbit tristereo recording, the better the quality of the calculated DEM. From a set of 15 images, all possible combinations are computed and the satellite azimuth and the incident angle are plotted. To generate the DEM, a multiview stereo method is used, which means that the images are first processed pairwise and then the resulting DEM are merged. Afterwards, the completeness and the accuracy of every fused DEM is computed by comparing it against a fusion of two in-orbit tristereo DEMs. This groundtruth data represents the best possible outcome obtained with optical data. Completeness is defined as a percentage of the valid cells. A cell is counted a valid if the vertical error is less than 1 meter with respect to the ground truth data. Accuracy is the root mean square error of all the calculated cells.

2 Related Works

The quality of the generated DEMs can vary significantly and depends on the respective recording parameters. Various works have shown which parameters result in a good stereo pair. On one hand, the convergence angle plays a decisive role. While Krauß et al. (2019) indicate an optimal angle between 5 and 15 degrees for Pléiades images, Facciolo et al. (2017) report an optimal angle of about 20 degrees for Worldview 3 images. On the other hand, it is obvious that the time difference between the two images is an important factor. The closer the images are to each other, the greater the likelihood that the images will be similar, and therefore more suitable for matching. As the time difference between the images increases, the urban structures on the ground will also have changed due to construction activity, making it difficult for the images to match. The same is true for seasonal influences such as vegetation periods or snow. Nevertheless, Facciolo et al. (2017) report that good results could also be achieved for images with the same DOY. Furthermore, Qin (2019) and Krauß et al. (2019) report that the angle difference also influences the quality. The larger this difference is, the worse is the completeness of the generated DEMs. In addition, sun elevation must be sufficiently large, so that no long shadows are formed, which are difficult to match (Krauß et al. 2019).

3 Data

The data used for this study consists of 15 panchromatic Pléiades acquisitions of Port-au-Prince, Haiti (Figure 1). The images cover an area of roughly 120 km² and were acquired between July 2013 and April 2015 with a ground sample distance (GSD) of 0.7 m. There are 3 triplets and 3 tuples that were taken from the same orbit, respectively. To reduce computing power and save time, one test site has been chosen (Figure 2). The test site has an extent of 400 x 400 meters and is located in a flat terrain with relatively large and rectangular urban structures.



Figure 1: Data coverage in Google Earth



Figure 2: Footprint of the test site (07.2013)

Table1: Overview of available Pléiades images.

short name	acqu. date	satellite azimuth [°]	global incident angle [°]	sun elevation [°]
20130705_001	05.07.2013	234.66	8.43	70.8
20130705_002	05.07.2013	280.17	5.68	70.8
20130705_003	05.07.2013	328.24	8.11	70.8
20130706_001	06.07.2013	128.75	13.55	69.0
20130706_002	06.07.2013	73.34	13.78	68.7
20130706_003	06.07.2013	100.85	12.13	68.8
20141117_001	17.11.2014	243	18.96	50.1
20141117_002	17.11.2014	318.11	17.90	50.0
20141117_003	17.11.2014	274.26	14.90	50.0
20150429_00A	29.04.2015	238.1	6.43	71.9
20150429_00B	29.04.2015	300.62	6.13	71.9

As groundtruth, a composite of two tristereo Pléiades DEMs were taken. It was processed by the CATENA multi-stereo processing chain (Krauß et al., 2019) and consists of the same optical input data this study is using. This groundtruth DEM represents the best possible output of the existing data. By comparing the multi-date tristereo DEMs with the optimum, the deviation of the recording geometry from the optimal recording geometry can be measured.

4 Method

In the first step, the images and their RPC files were cropped to the extent of the test site using the opensource tool "RPC Cropper". The repository can be found on github (https://github.com/carlodef/rpc_cropper). However, the images cannot be cropped directly. Since this tool only accepts image coordinates as input, the geographical coordinates of the test site had to be converted into the image coordinates for each image. Afterwards, all

possible combinations of three images are calculated. Since not all images overlap the test site, only 11 images are available for the area of interest. Combinations with images of the same date or only one day difference are not used when conducting the study. Only those combinations where the images were taken on different days are tested. This results 36 valid image combinations.

After these preparation steps, the DEMs can be generated with the fully automatic pipeline software `s2p`. It allows the processing of three-view stereo datasets by handling the stereo pairs independently and merging the resulting elevation models automatically. No further prior processing of the images is necessary. The only input required is the cropped images and their RPC file. A refinement of the semi-global matching (SGM) algorithm is used to match the images (Facciolo, Franchis, & Meinhardt, 2015). To solve the stereo image rectification problem of pushbroom cameras, `s2p` cuts the images into small tiles. For detailed information about how the `s2p` pipeline works, see (de Franchis et al., 2014). The resolution of the generated DEMs is 1 meter. Of the 36 image combinations, 26 resulted in an output. The remaining combinations yield an error, meaning no elevation model can be calculated.

Finally, the elevation models are aligned to the ground truth data. The co-registration is done with the Open-source tool "demcoreg" (<https://github.com/dshean/demcoreg>) which uses the algorithm outlined by Nuth & Kääb (2011). Since both heights are calculated using the ellipsoid WGS84 and have the same resolution, no prior vertical datum shift or resampling is necessary. Subsequently, a benchmark test of the generated DEMs takes place, carrying out a grid-based comparison of the DEM and the groundtruth dataset regarding completeness and accuracy.

5 Results

Figure 3 shows three generated multi-date DEMs. The images of the triplets span a period of 21 months. The quality of the DEMs varies quite strongly: while DEM A has a completeness of 29.8% and an RMSE of 2.95 meters, DEM C reaches only 14% and an RMSE of 81.53 meters. However, the visual observation as well as the RMSE value of DEM A indicate that significantly more pixels are useful to estimate houses and their heights for humanitarian operations. Figure 4 shows that with a threshold of 2 meters, already more than 40% completeness is achieved. In addition, it can be assumed that with a simple filling hole function this could be increased.

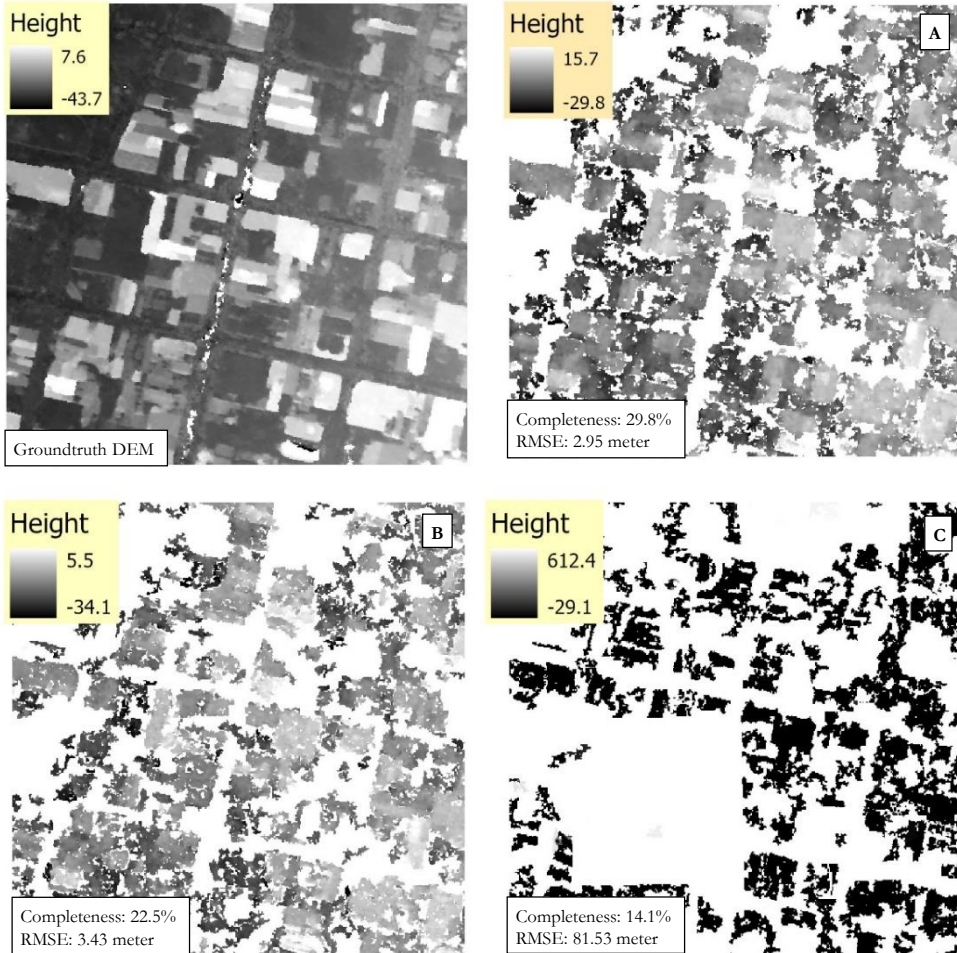


Figure 3: Comparison of three generated multi-date DEM's with ground truth data. Height values are in meter. Image combinations are: A) 20130705_003 - 2141117_003 - 20150429_00A, B) 20130705_002 - 20141117_002 - 20150429_00A, C) 20130705_001 - 20141117_001 - 20150429_00A

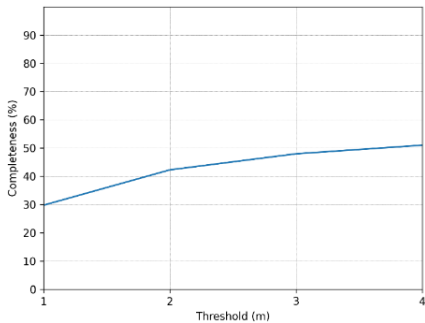


Figure 4: Completeness of DEM A with increasing threshold for valid pixels

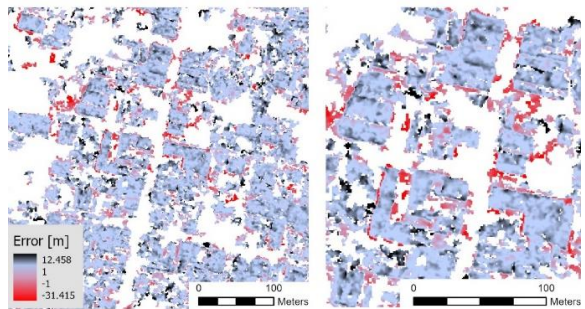


Figure 5: Error Image of DEM A with a zoom in on the right side. Stretched visualization (0.5% Clip)

The error image of DEM A (Figure 5) shows that smaller error values occur mainly within the roof surfaces. High error values, on the other hand, occur along building edges. Streets and spaces in between are hardly matched. Also single buildings are missing completely.

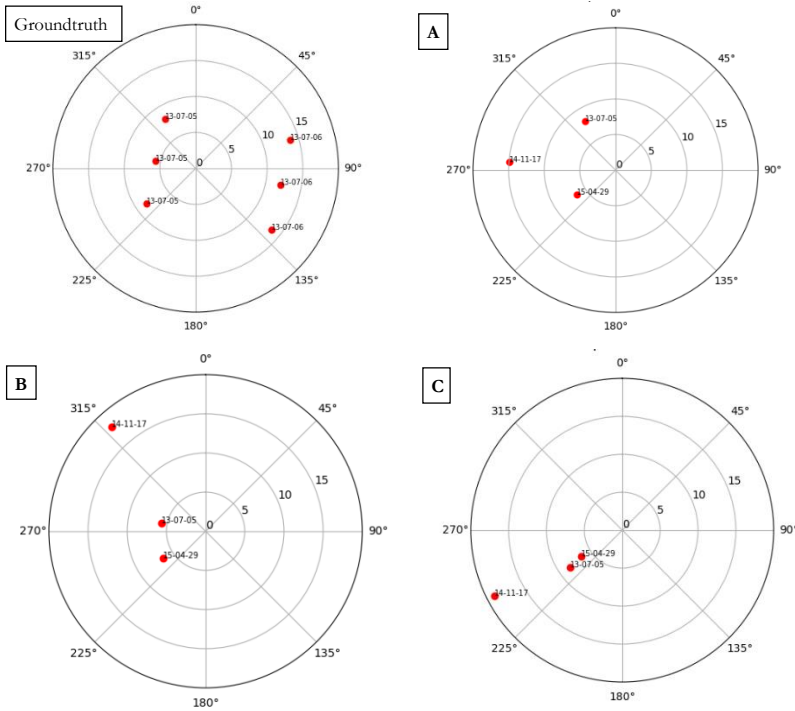


Figure 4: skyplot of the satellite constellation of the 3 DEMs and the ground truth data. The satellite azimuth angle ranges from 0° to 360° and the incident angle from 0° to 20°. Note how the two triplets at ground truth are arranged on a line and look at the scene from two opposite sides, getting optimal coverage.

The different multi-date triplets on the skyplot illustrate that the images of an in-orbit triplet are on one line. To replicate this optimal constellation, one image from 29.04.2015 could be substituted in DEM A and DEM B, while the third image (14-11-17) does not fit. These two DEMs also show better completeness values than DEM C. In contrast, all images of DEM C have a very similar azimuth value, and thus, cannot represent the scene from different angles, leading to poor results.

For the best-achieved result, DEM A, the individual images have an incident angle of 8.1° (20130705_003), 14.9° (20141117_003) and 6.4° (20150429_00A). The time difference is 21 months. The recording positions are arranged so that the target was captured from the front, the centre, and the back. The convergence angle between each pair is within the ideal range of values recommended by Facciolo et al. (2017) and Krauß et al. (2019).

stereo pairs for DEM A	convergence angle
20130705_003-20141117_003	12.0°
20130705_003-20150429_00A	10.3°
20141117_003-20150429_00A	10.4°

6 Discussion and next steps

The achieved completeness values with a selection of only three images are low. Nevertheless, the best results are achieved when the recording geometry of the images simulate an in-orbit recording and capture the target from the front, the centre, and back. A drawback of the method is that the influence of the time difference cannot be determined, since all combinations have the same time span.

Due to the low completeness values, the next step is to check whether single stereo pairs provide better results than triplets. If this is the case, the question arises of how to merge the stereo pairs outside of s2p. One possibility is to take the median for each pixel. Another possibility would be to weight the DEMs using the Convergence Angle, the Coverage, or the Sun Elevation Difference and fill the NoData places of the best DEM with the information of the others.

Finally, it would be interesting to test the quality of the generated DEMs at sites with different urban characteristics to see if an industrial area with large rectangular buildings (harbour area) differs from small-structured cottage settlements on steep slopes (south of Port-au-Prince).

References

- de Franchis, C., Meinhardt-Llopis, E., Michel, J., Morel, J.-M., & Facciolo, G. (2014). An automatic and modular stereo pipeline for pushbroom images. *ISPRS Annals of Photogrammetry, Remote Sensing and Spatial Information Sciences, II-3*, 49–56. <https://doi.org/10.5194/isprsannals-II-3-49-2014>
- Facciolo, G., De Franchis, C., & Meinhardt-Llopis, E. (2017). Automatic 3D Reconstruction from Multi-date Satellite Images. *2017 IEEE Conference on Computer Vision and Pattern Recognition Workshops (CVPRW)*, 1542–1551. Honolulu, HI: IEEE. <https://doi.org/10.1109/CVPRW.2017.198>
- Facciolo, G., Franchis, C. de, & Meinhardt, E. (2015). MGM: A Significantly More Global Matching for Stereovision. *Proceedings of the British Machine Vision Conference 2015*, 90.1-90.12. Swansea: British Machine Vision Association. <https://doi.org/10.5244/C.29.90>
- Gong, K., & Fritsch, D. (2019). DSM Generation from High Resolution Multi-View Stereo Satellite Imagery. *Photogrammetric Engineering & Remote Sensing, 85*(5), 379–387. <https://doi.org/10.14358/PERS.85.5.379>
- Krauß, T., D'Angelo, P., & Wendt, L. (2019). Cross-track satellite stereo for 3D modelling of urban areas. *European Journal of Remote Sensing, 52*(sup2), 89–98. <https://doi.org/10.1080/22797254.2018.1551069>
- Krishna, B. G., Srinivasan, T. P., & Srivastava, P. K. (2008). *Dem generation from high resolution multi-view data product. 4*.
- Nuth, C., & Kääb, A. (2011). Co-registration and bias corrections of satellite elevation data sets for quantifying glacier thickness change. *The Cryosphere, 5*(1), 271–290. <https://doi.org/10.5194/tc-5-271-2011>
- Ozcanli, O. C., Dong, Y., Mundy, J. L., Webb, H., Hammoud, R., & Tom, V. (2015). A comparison of stereo and multiview 3-D reconstruction using cross-sensor satellite imagery. *2015 IEEE Conference on Computer Vision and Pattern Recognition Workshops (CVPRW)*, 17–25. Boston, MA, USA: IEEE. <https://doi.org/10.1109/CVPRW.2015.7301292>
- Qin, R. (2019). A Critical Analysis of Satellite Stereo Pairs for Digital Surface Model Generation and A Matching Quality Prediction Model. *ISPRS Journal of Photogrammetry and Remote Sensing, 154*, 139–150. <https://doi.org/10.1016/j.isprsjprs.2019.06.005>
- Rupnik, E., Pierrot-Deseilligny, M., & Delorme, A. (2018). 3D reconstruction from multi-view VHR-satellite images in MicMac. *ISPRS Journal of Photogrammetry and Remote Sensing, 139*, 201–211. <https://doi.org/10.1016/j.isprsjprs.2018.03.016>

Spatially Supervised Text Mining for Social Media Cleaning and Preprocessing

GI_Forum 2021, Issue 1
Page: 68 - 75
Research Paper
Corresponding Author:
martin.werner@tum.de
DOI: 10.1553/giscience2021_01_s68

Martin Werner¹

¹Technical University of Munich, Germany

Abstract

In this paper, we show a framework for partial bot rejection based on spatially supervised text mining from social media messages. We show qualitative results towards the reduction of known bots and give hints on how this cleaning technique can help us in filling gaps of current signals related to human life on Earth based on social media. The bot rejection framework is based on using a spatial signal for supervising a machine learning model with extreme label noise still being able to reject some of the unwanted components of the social media stream. Furthermore, we comment that such models show significant biases and can, therefore, not be used responsibly without bias analysis and mitigation per application.

Keywords: social media analysis, text mining, data cleaning

1 Introduction

Urbanization is one of the most pressing and challenging megatrends for human life on Earth. As depicted in Figure 1, the rural population has constantly been increasing up to today, but with a slowing effect, it is expected to start decreasing by the mid of the current century. In contrast, the urban population is expected to have at least linear growth in the time such that by 2050 urban areas give a home to more than double as many people as the rural areas (United Nations Department of Economic Affairs, 2018). Moreover, the local dynamics of this development are surprising, if not daunting. For example, it is expected that Delhi, India, will become the largest city by 2030, overtaking Tokyo. In 2018, however, the United Nations report 37.4 million inhabitants for Tokyo and only 28.5 million for Delhi. The expectation formulated for 2030 is that Tokyo will shrink to 36.5 million inhabitants while Delhi will grow to nearly 39 million inhabitants. This is a growth of 11 million inhabitants in 12 years or about one million inhabitants per year. This extreme local variability of the dynamics implies heavy challenges, for example, for the transport system (food, mobility, waste disposal etc.), for the infrastructure (electricity, water, healthcare, police, etc.), and for the environment (e.g., air and water pollution).

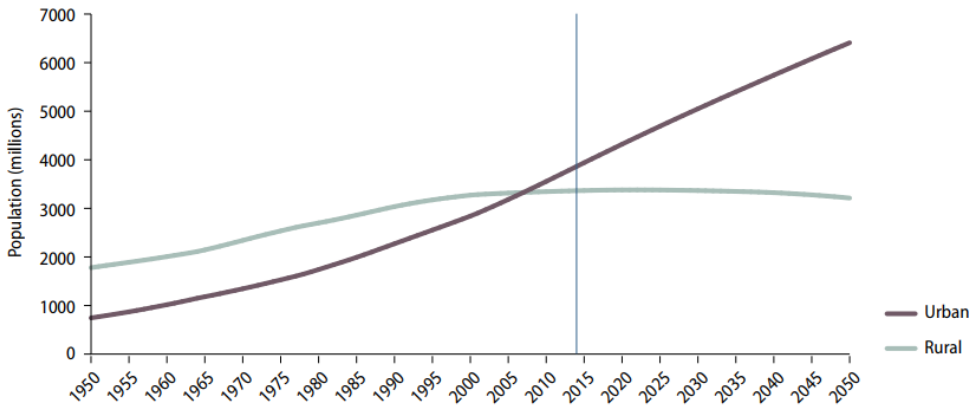


Figure 1: Global Urban Population Compared to Rural Population - 1950 - 2050 as Expected by the United Nations.

The United Nations have established 17 Sustainable Development Goals (SDGs), many of which have strong interaction with the process of urbanization (United Nations, 2019). For example, urbanization is related to zero hunger and no poverty, as the hope for jobs and fleeing from rural poverty is one reason people move into the city. Good health and wellbeing, as well as quality education, are challenged as well because these rely on infrastructures that might be difficult to grow at the needed pace and at the same time motivate people to relocate to the urban areas. Furthermore, clean water and affordable and clean energy is similarly challenging as the energy density needed in megacities is difficult to provide with renewable energies today. The consequences of quick urbanization processes directly challenge sustainable cities and communities, climate action, life on land, and life below water in terms of pollution.

In order to cope with this situation on a global scale, innovative methods of data acquisition and data analysis are needed, which go beyond the current observational capabilities mainly based on remote sensing from space. Because these overhead observation systems do not observe the process of urbanization, but rather the impact of urbanization on morphological structures, while it is comparably easy to see cities grow from a spaceborne platform, it might be difficult to get a reliable signal on the expected minor shrinkage of Tokyo. It is unlikely that this will result in a major change in the morphology. Therefore, we propose and follow a different path of using additional signals with strong anthropogenic components to better understand these dynamics.

One such signal is represented by night light observations as, for example, provided by NASA and NOAA. These images represent the amount of light emitted at night, which correlates with human settlements quite strongly. In addition, the amount of light has been used to estimate census parameters in the United States. The more light is being observed, the higher the population density and the average income (Chen & Nordhaus, 2019). Figure 2a depicts an example of such night light observations. The limitation of these observations is twofold: long integration times are used in order to come up with clear signals, and the resolution remains limited. That is, light gives us kind-of an upper bound to the urban extent as light is among the first persistent signals in settled areas.

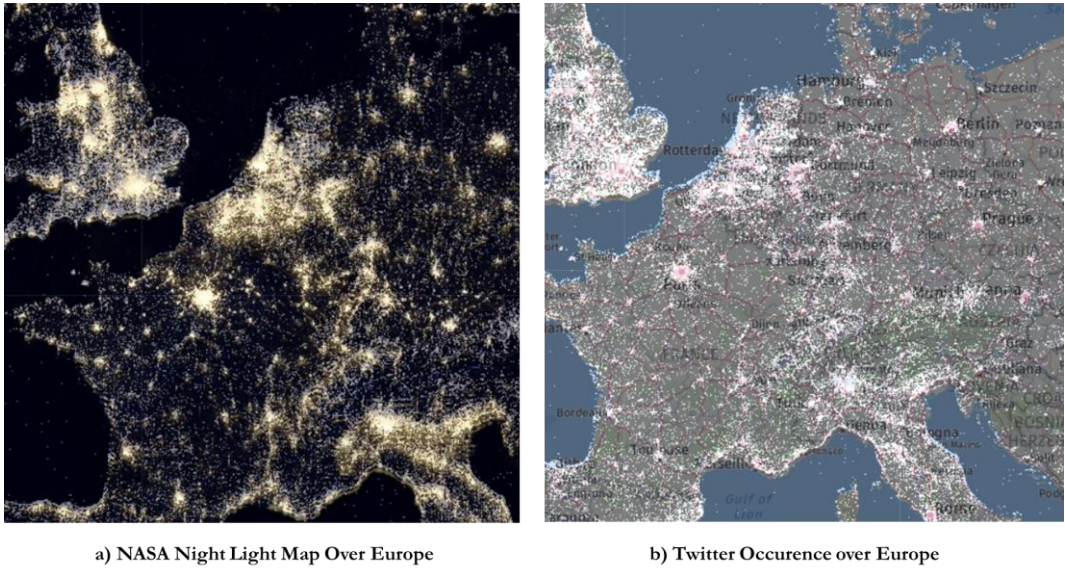


Figure 2: NASA Night Light Imagery and Twitter Occurrence over Europe.

Another promising signal can be extracted from social media depicted in Figure 2b. Social media message frequency also correlates to population density in areas of social network adoption (Li et al., 2013). However, social media is full of special noise patterns induced by a high number of bots sending messages and frequent trends that have a varying spatial resonance ranging from global (#metoo) to very local resonance (e.g., hashtags related to local events). Therefore, long integration times are needed as well, such that the social media data represents a reasonable average behaviour. However, when looking closely at densities, it seems that social media is more focused on city centres and, therefore, a more selective signal compared to night light emission. None of these signals can truthfully represent the sociodemographic indicators of interest, including population density, wealth, and income, but all of them show a slightly different pattern of correlation with these signals of interest. Therefore, we expect a joint observation of all of these signals towards unexpected diverging patterns is a suitable monitoring aid for systematic urbanization analytics.

This paper shows how a spatial knowledge injection method applied to text mining can be used to reduce some unwanted signals from social media, making social media a more reliable signal. In order to clean up the Twitter signal, the aim is to remove components that are just due to bots or automated messaging. In order to detect a component of such bot messages, we apply text mining to the social media messages in order to detect a very spurious pattern of bots, namely, that many bots are not using sensible location information. We learn a bot rejection model based on training it with all precisely geolocated tweets based on whether the location is over land or ocean. While some of these messages over the ocean might originate from shipping, many of these messages are expected to be blurring the patterns of urbanization we want to observe.

2 Methodology

2.1 Datasets

In this study, we use three datasets. The first dataset is the NASA/NOAA Night Light Imagery for 2018. It represents the average light emission in 2018 across the globe in a medium resolution of about 500m per pixel (of course varying across the globe due to the WGS84 projection). This data has been acquired by the Suomi NPP satellite and processed by NASA to account for the moon phase dynamics trying to normalize towards a moon-phase independent representation of the light emission. This dataset comprises 3.73 billion pixels. The second dataset is a sample of all observed social media messages throughout 2018 acquired from the public Twitter stream, representing about one per cent of the total social media messages on this platform. We sampled a set of 220 million precisely geolocated tweets (note that these include bots and retweets due to the specification of the stream API endpoint) and process both the geospatial location and the raw text, including hashtags and punctuation in all observed languages. The third dataset is the dataset representing country boundaries across the world. For this purpose, we take the LSIB 2017 Large Scale International Boundary Polygons Dataset as published by the United States Department of State at the Office of Geographer. It presents 284 countries in 312 features modelled with 2,342,905 points.

2.2 Labeling

In a first step, we label Twitter data from the first three months based on the country dataset in two categories: land and water. As we already expect very high label noise in this dataset as some tweets might be from very good bots or human beings around the ocean, we do not create geospatial buffers around the countries to take care of coastal areas into account. Instead, we rely on the fact that most tweets in the ocean are observed far enough from the nearest country. In order to do this efficiently, we need to rely on a dedicated implementation based on well-performing bulk loaded in-memory R*-trees to speed up point in polygon queries. We rely on HDF5 and boost::geometry for the core operations and modern C++, including OpenMP for parallel processing. We follow a strict property map interface, that is, records that are implicitly linked by their primary key, which is just the row number in the memory block allowing for constant-time access to individual records. With an average Gaming PC (Intel i7, 32 GB RAM), we process the point in polygon join in this way in 8 hours without simplifying geometry. The resulting dataset is heavily imbalanced, with only 5.7 million tweets observed over water. Hence, we then create a class-balanced dataset by sampling alternating between land and water classes such that we gain a temporally ordered sub-dataset with the same numbers of water and land classes and a total of 11 million¹.

¹ Source codes and details of this project and are available at <https://www.bgd.lrg.tum.de/code/2021-landwatersplit>.

2.3 Text Mining

The data mining problem induced by the labelling process is to develop a text mining model that can be applied across many languages, including non-human languages like hex-codes observed for some bots. As explained, we have now a labelled dataset of tweets based on whether it was observed over the ocean or a country. In a second step, we train a skip-gram model with subword information on the tweet text towards detecting the class “water” or “land” (Bojanowski et al., 2016). This model is based on cutting text into small pieces of n consecutive characters, so-called n -grams, and assigning a randomly initialized vector of chosen dimension with each n -gram. Then, we minimize an objective function using a variant of gradient descent which balances two aspects: one loss term pulls vectors associated with textually nearby n -grams (those that appear not farther away than a chosen parameter “context window” in the text) towards each other minimizing their Euclidean distance in the embedding space while a second loss term compares with random non-neighbouring word vectors and pushes the representing vectors away from each other. Word embeddings obtained in this unsupervised way are then used to numerically represent words or sentences (by taking the mean of the words or n -gram tokens). We apply a deep neural network with one softmax layer to directly transform these learnt word embeddings into a classification result for tweets. As expected, the model’s performance is not excellent, as calling for a land/water split from textual data is not plausible. Nevertheless, it gives us an interesting signal regarding the trustworthiness of tweet messages, as we explain in the sequel. More concretely, we train a model with an embedding dimension of 10 and tune parameters for an optimal overall F1-score. Therefore, we train on the first million entries in the balanced sample, use the second million entries to validate hyperparameters, and evaluate over time in slices of one million tweets. Results are depicted in Figure 3. The model reaches a performance of about 0.8 F1-score, keeping in a window of less than 5 per cent around. It is interesting to see that numbers degrade only a neglectable amount over time and stabilize around 0.80 overall F1 quickly. This is a hint that only a small fraction of the model does not generalize over time.

Furthermore, it is nice to see that the precision of the water class is higher instead of the land class. The surprising characteristics of this model are visualized as well in Figure 3 as a ROC curve which shows the behaviour of the false-positive rate as opposed to the true positive rate when changing the threshold parameter τ at which the decision between land and water is made. Depending on the actual application and its demands, a suitable τ can be chosen to trade-off precision and recall.

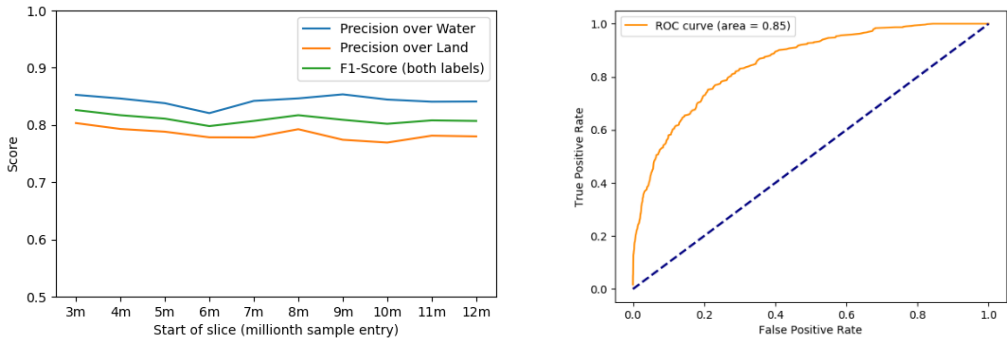


Figure 3: Performance of the classifier over time and in relation to choosing a classification threshold □

3 Results

We apply this model over land and reject tweets that are similar to those observed throughout the oceans. Figure 4 depicts an application of this framework to a one-month data sample taken from the Twitter social network. That is, we trained in the past and take fresh data and classify it into the two classes “ocean” and “land”. This figure is representative of all the one-million slices.

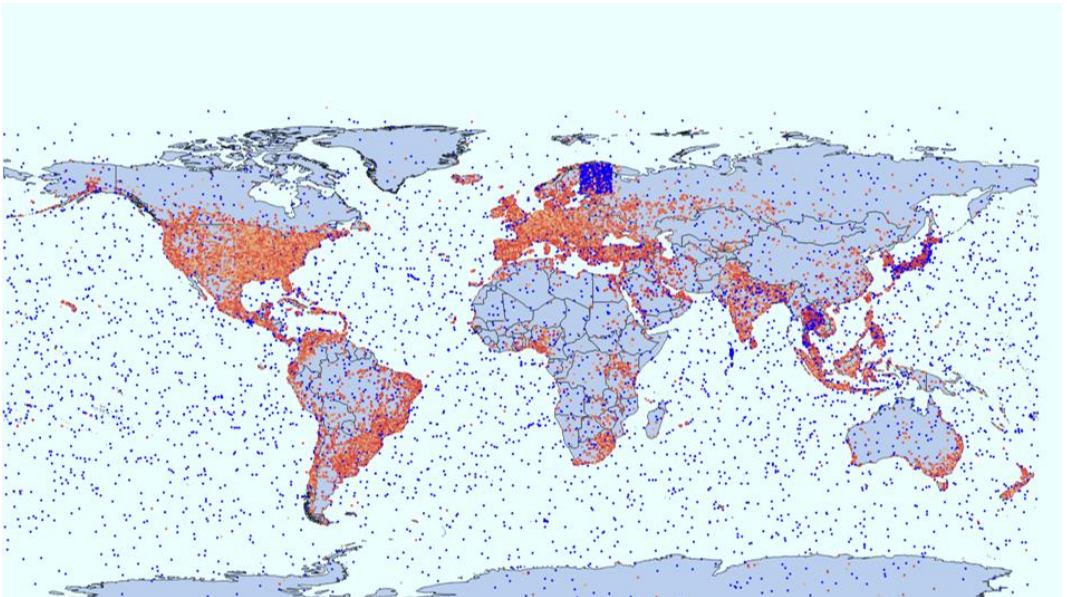


Figure 4: Illustration of Bot Rejection Result on a One-Month Data Sample.

Without knowing exactly, what the model rejects over land, Figure 4 shows the behaviour of the trained model. As one can see, the model predicts low values over the ocean and higher values over land while it predicts surprisingly low values, for example, for the rectangle over Finland, which represents a known bot using fake locations from this rectangle. This illustrates that a spatially semisupervised bot rejection scheme is able to correctly reject some of the fake messages that we observe in social media datasets. At the same time, however, it is easy to see some unwanted results. For example, in Japan and more generally around Asia, we are rejecting many more tweets as in countries with western languages. This is a severe bias, which is easy to explain. Most of the Twitter social network data is communicated in the English language, and non-western languages take only a small fraction of the data. Therefore, the model is overfitted to English (or more generally Western) languages and has problems learning Asian languages from the given sample or because of the pictographic script. Still, with a thorough case by case evaluation, it seems to be viable to apply this model at least in Europe and the United States and it can, for example, enable the detection and analysis of urban structures below the very noisy Finland bot which is difficult without such a scheme.

Further research is needed to assess for each possible social media mining application independently whether such a bot rejection scheme is helpful (increasing correlation) or not (e.g., ethically unsound due to biases) and where to put the threshold on the bot scores. This is a difficult question that needs to be answered in the light of individual applications as it depends on the spatial integration area (how much data is left for further analysis in each analysis unit), the spatial focus (are we interested in the city centres, where social media presents a strong signal or more in the extended urban space and the borders of cities, where social media messages become rare). Furthermore, the rejection scheme puts a tradeoff between preprocessing and data mining in the sense that even if the model was correctly able to reject tweets originating from bots, it would as well reject some messages (false positives) that weaken the spatial signal. Therefore, a selective threshold leads to less data in the following data-mining stage, a weak threshold reduces the impact of the current approach. Finally, one might want to probabilistically calibrate the classifier and use the calibrated scores for upstream processing instead of simple thresholding. This might mitigate some difficulties of setting a threshold but implies a more complex input of weighted messages to the upstream data mining stages.

4 Conclusion

This paper explored how the injection of spatial knowledge into a text mining problem through labelling can help filter streams of location-based social network messages sensibly. We were able to reject the most obvious bot over Finland. We were able to reject the most obvious bot over Finland. This qualitative result is not enough to understand the behaviour of this model. We will emphasise possible applications in future work, especially towards propaganda awareness, social media trend analysis, outlier and event detection, and land cover classification. This is, to the best of our knowledge, the first time that a spatially semisupervised bot detection and rejection model was designed and showed to perform well with an area under curve measure (ROC_AUC) of 0.85. For clarity, we do not claim that this model rejects bots. Any claim towards this direction would ignore that language models like GPT-3 (Brown

et al., 2020) and BERT (Devlin et al., 2018) can generate text in a quality that is nearly indistinguishable from human text and that human beings are often steering bot networks to, for example, disseminate fake news or bots just pick up valid messages for retweets. We claim to be helpful to filter a very specific component of communication samples that overlaps with bots. We envision using this framework of spatial supervision as well beyond social media classification.

We expect that models that allow us to observe and compare anthropogenic signals from a multitude of decoupled sensing systems (social media, light, activity, prosperity, ...) help to put in place global indicators for many of the United Nations Sustainable Development Goals, most importantly, “sustained communities” and “life on land”. However, more research in bias estimation, de-biasing, and more generally in the ethical implications of using social media signals is needed before a wide adoption is encouraged.

References

- Bojanowski, P., Grave, E., Joulin, A., & Mikolov, T. (2016). Enriching word vectors with subword information. *arXiv preprint arXiv:1607.04606*.
- Brown, T. B., Mann, B., Ryder, N., Subbiah, M., Kaplan, J., Dhariwal, P., Neelakantan, A., Shyam, P., Sastry, G., Askell, A., & others. (2020). Language models are few-shot learners. *arXiv preprint arXiv:2005.14165*.
- Chen, X., & Nordhaus, W. D. (2019). VIIRS nighttime lights in the estimation of cross-sectional and time-series GDP. *Remote Sensing*, 11(9), 1057.
- Devlin, J., Chang, M.-W., Lee, K., & Toutanova, K. (2018). Bert: Pre-training of deep bidirectional transformers for language understanding. *arXiv preprint arXiv:1810.04805*.
- Li, L., Goodchild, M. F., & Xu, B. (2013). Spatial, temporal, and socioeconomic patterns in the use of Twitter and Flickr. *Cartography and Geographic Information Science*, 40(2), 61–77.
<https://doi.org/10.1080/15230406.2013.777139>
- United Nations. (2019). *Sustainable Development Goals*. <https://sustainabledevelopment.un.org/>
- United Nations Department of Economic Affairs. (2018). *2018 Revision of World Urbanization Prospects*. <https://population.un.org/wup/>

Evaluation of a NoSQL Database for Storing Big Geospatial Raster Data

Nicole Hein¹ and Jörg Blankenbach¹

¹RWTH Aachen University

Abstract

Database systems capable of efficiently storing geospatial data are widespread. However, recent developments in earth observation systems, remote sensing, mobile mapping, and crowd sourcing lead to large amounts of geospatial mass data that can hardly be handled efficiently with the existing solutions. Especially large geospatial raster data require novel concepts for well-organized data storage.

A concept for storage of large geospatially and temporally referenced image data using the NoSQL graph database system Neo4j as a research subject of the project “RiverView®” is introduced. New strategies and access structures have been developed to ensure the persistence and performant access to image data in Neo4j. These strategies are compared with the up-and download performance of the widespread Rasdaman array database system.

Keywords: geospatial raster database, graph database, big geo data, image database, Neo4j

1 Introduction

Database systems storing spatial-related data (spatial or geodatabase systems) have become standard in the geospatial domain, e.g. as a core component of modern geoinformation systems or distributed spatial data infrastructures. Due to the emergence of novel or further developed geospatial data acquisition methods like mobile mapping systems or multi-sensor earth observation systems, the storage of big geospatial raster data is becoming increasingly important.

This study is part of the research project “RiverView®” and presents an approach for storing of big geospatial raster data within a NoSQL database as well as a benchmark with an existing database system.

2 State of the art and related work

Geodatabase systems are very common in the field of geospatial data management (Bill 2016). Consequently, there are several commercial and free geodatabase systems available like Oracle Spatial and Graph (Oracle Corporation 2021), PostgreSQL/PostGIS (PostgreSQL Global Development Group 2021, PostGIS Project Steering Committee 2021) and MySQL (Oracle Corporations and/or affiliates 2021). Often these storage systems are further developed object-relational databases that have been expanded by specific spatial data types, spatial access structures, and analyses (Yeung & Hall 2007). While in the past, geodatabase systems were mainly applied for storing spatial features as vector data (vector features), more recently, the demand for the efficient storage of spatial raster data has risen. The reason for this development is, in particular, the advent of further developed geospatial data acquisition methods like modern laser-scanning devices, high-resolution digital cameras and novel remote sensing sensors producing large volume raster data sets that require efficient storage (Nebiker 1997). Raster data is represented by (often equidistant) raster cells, which, in the case of raster images, are picture elements and can be stored in implicit structures like matrices or arrays (Nebiker 1997). Brisaboa et al. (2017) described the efficient querying of raster and vector data via k^2 - respectively R-Tree data structures. Database systems for storing image data and its classifications have been developed since the late 1970s, e. g. REDI and GRAIN (Chang et al. 1980), (Tamura et al. 1984). In the 1990s, Peter Baumann developed the first prototype of Rasdaman (Rasta Data Manager) to store multidimensional arrays in a database system, especially for geospatial or space sciences (Baumann 1993), (Baumann et al. 1997). Rasdaman is a middleware working with PostgreSQL and SQLite on a storage basis (Baumann 2018). Since the term Big Data arose (Chalmers et al. 2013) with its different types and particular challenges (Lansley et al. 2019) arises, NoSQL database systems are becoming increasingly popular. In (DeZyre 2019) several reasons are identified for using NoSQL database systems in terms of Big Data because relational database systems are not suitable for the complexity and heterogeneity of upcoming data. Additionally, NoSQL database systems are easily expandable. Since Big Data is complex and contains highly interconnected information, it is represented well as a graph (Miller 2013).

3 Background

The research project RiverView® (FiW 2020) aims at developing a novel approach for the holistic monitoring of medium and small watercourses. The core component of RiverView® is an unmanned surface vehicle (RiverBoat, Fig. 1) equipped with multiple sensors, which allows for autonomous digital water data acquisition with high spatial and temporal resolution. In addition to chemical-physical sensors, an above-water mapping system is installed, containing an omnidirectional multi-camera system consisting of 6 individual cameras, with which georeferenced images (5 MP each) of the water environment can be recorded continuously at high temporal frequency (max. 10 Hz).



Figure 1: RiverBoat



Figure 2: Water body information system

For managing all collected data, a GIS-based water body information system (Fig. 2) was developed. Therefore, efficient and powerful storage capacities due to the heterogeneous and large volume datasets are required. Whilst the scalar and vectorial data (e.g. O₂ level, water temperature) can be inputted directly in a relational geodatabase, image data storage in particular is a major challenge because it has to fulfil the following characteristics:

- 1) (Near) real-time data export
- 2) Scalability / Big Data ability
- 3) Handling heterogeneous data

Pre-existing solutions (e.g. PostgreSQL/PostGIS, Oracle) have been tested for geospatial image storage (Hein & Blankenbach 2017). However, after concluding evaluations, several problems (e. g. no real-time ability, no Big Data ability) were identified.

Hence, a novel concept was developed for storing geospatial raster data based on the NoSQL database system Neo4j. Neo4j (Neo Technology 2018) is a graph database that includes the topological components “node”, “relationship”, “property” and “label” as well as data indexing features to find nodes as basic information item faster in the graph. For geospatial data handling Neo4j provides a spatial library including e. g. spatial search trees (R-Trees) to accelerate read operations on spatial data (Taverner 2019).

4 Raster Data Storage and Indexing

A geospatial raster image is a matrix of picture elements (pixels) consisting of colour and possibly transparency information. In practice, two approaches are commonly pursued for the database-driven storage of geospatial raster images. Either the raster images are stored directly in the database (e. g. by using Binary Large Object (BLOB)) or using an image file format on the hard disk. In both cases, the metadata (e.g. spatial reference, image dimensions and resolution) are stored in the database that enables the deployment of useful access structures to the data.

Database indices are utilised as efficient access structures that have to be optimised, in this case for raster data in different resolutions. For the latter image, pyramids are used to provide the original image in different resolutions (Fig. 3, left).

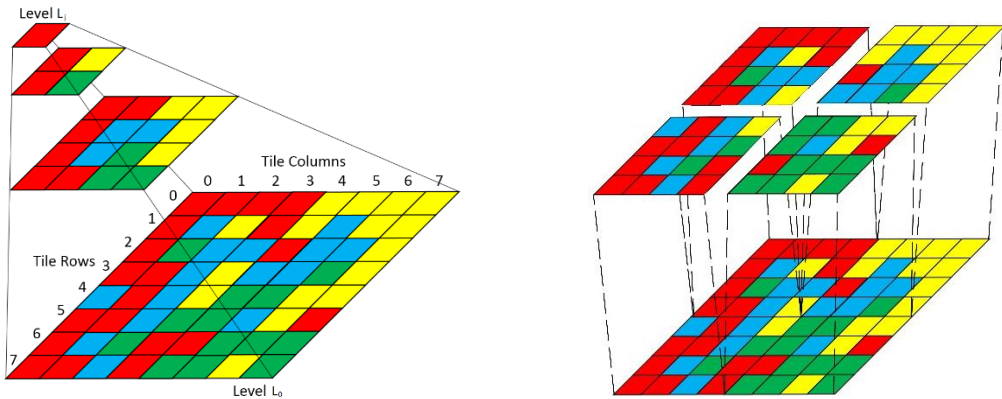


Figure 3: Image pyramid and adapted tiling (Source: Esri 2021)

Another crucial database access structure for raster data is tessellation (Fig. 3, right). For real-time applications, the ability to load only parts of images is necessary, hence, images must be split into delimited parts. Therefore, rectangular blocks are normally applied, which is why this process is also commonly known as tiling. However, in general, different tiling strategies can be used, e.g.:

- 1) **Aligned Tiling:** The Aligned Tiling Strategy (ATS) divides the image data into rectangular tiles with equal height and width (Fig. 4, left top).
- 2) **Random Tiling:** The Random Tiling Strategy (RTS) calculates for each rectangular tile an individual height and width randomly (Fig. 4, left bottom).
- 3) **Region-of-Interest Tiling Strategy (RoITS):** This tiling strategy was explicitly developed for the RiverView application because large parts of the images contain water or sky, which are less relevant to users. Thus, the general idea was to tile only the interesting areas in the image in a more granular way. The RoITS, therefore, identifies points of interest (POI), e.g. by calculating the image feature points using the SIFT (Lowe 2004) algorithm (Fig. 4, right). The more feature points found in an area, the more granular the area of the image is tiled: If a certain amount of points are found in a rectangle, a tile is defined.



Figure 4: ATS (left top), RTS (left bottom) and RoITS (right)

Both, image pyramids and tiling, is then used to create a spatial index, speeding up spatial queries (e.g. query boxes) on the data. In geodatabases, search trees usually represented by graphs are applied and are stored separated from the data itself. A very widespread spatial search tree is an R-Tree (Fig. 5) (Guttman 1984).

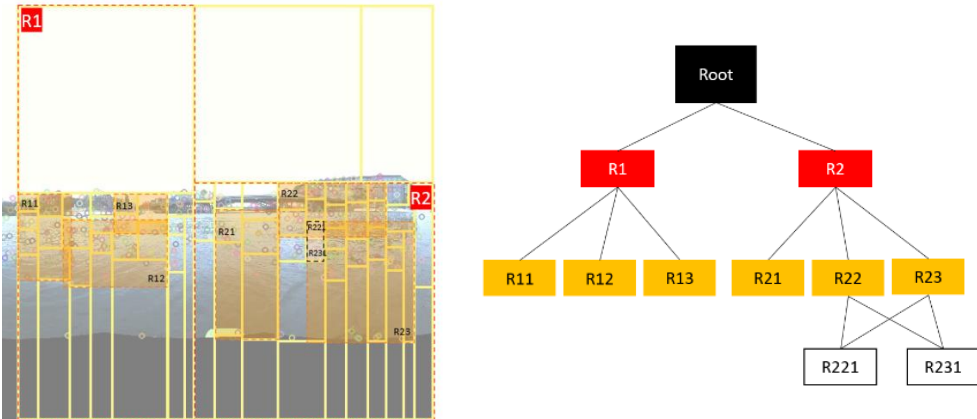


Figure 5: R-Tree on image (right) and R-Tree as graph (left)

5 Implementation

For the implementation of the raster data storage in Neo4j, it had to be decided whether only the metadata and the access structures or also the image data itself should be stored in the database (see section 4). Out of preliminary tests, the storage of binary (raster) data directly in the database is not efficient, which is also confirmed by (Armbruster 2016). Hence, the raster data is stored on hard disk while Neo4j holds the metadata.

Thus, for each image, the following steps were conducted:

- 1) An image pyramid (Gaussian pyramid) is created.
- 2) Each level of the pyramid is tiled using the respective variants ATS, RTS and RoITS.
- 3) A search tree (R-Tree) is created for each pyramid level.
- 4) The tilesets are stored on a hard disk while the metadata, a link of each tile, and the R-Tree is stored into Neo4j.

For the implementation of these four consecutive steps, OpenCV and NumPy were used. Uploading images in Neo4j is done via Python with the extension Neo4j Spatial. In the database, only the extends of the image tiles are stored as polygons and the spatial reference as point positions.

For the subsequent benchmark of our new raster data management concept, the images were imported additionally into Rasdaman, a powerful image database storing multidimensional array data.

6 Evaluation

Whilst data access structures lead to a performance gain at read access, they cause a decrease in performance for write access. Hence, for benchmarking an evaluation between the two databases, Rasdaman and Neo4j, regarding up- and download performance was conducted. Both databases (Neo4j v3.4.9; Rasdaman v9.6) were installed on the same computer with Linux Debian 8 (6GB RAM).

Fig. 6 shows the upload results of the different tiling strategies with varying tiling sizes (480 x 480, 500 x 500, 1000 x 1000) on the abscissa axis and the time in seconds on the ordinate axis. For RoITS at 50 POI, the tiles are 481 x 633 pixels on average. At 100, POI the tiles have an average size of 554 x 805 pixels. RoITS needs the longest time for uploading data – no matter which size of POI is considered. ATS and Rasdaman show a fast upload time.

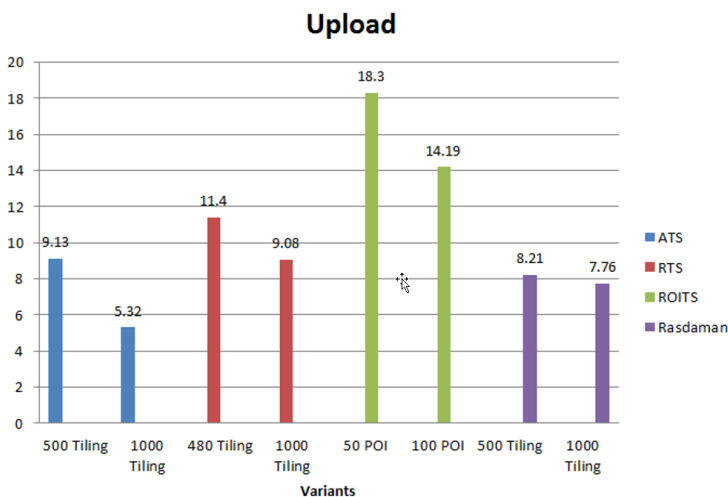


Figure 6: Upload benchmark with comparison to Rasdaman

The download test is triggered by specifying spatial coordinates of a section of the image which is required. Hence, a bounding box (range) query with the geometric function “intersects” is executed in the database. Furthermore, the corresponding tiles within the bounding box are loaded from the database. Fig. 7 depicts the average download time for the resolutions of the pyramid levels 0 to 3 when the entire image (8000 x 4000 pixels) is loaded. It is notable that Rasdaman (both tiling sizes) and ATS (500 x 500 pixels) take the longest time, taking approximately 3 seconds for the download. All strategies vary between 1.15 and 1.62 seconds. Fig. 8 shows the download times in the resolution levels 0 to 3 of the pyramid level with a bounding box of $(x_1, y_1, x_2, y_2) = (3526, 512, 7654, 3709)$. Considering the number of nodes, it can be concluded that the higher the number of generated nodes there is, the more time the download takes (see Table 1, Fig. 7 and Fig. 8).

A similar result to the upload emerges: Rasdaman (both strategies) and ATS with 500 x 500 tiling require the most time. All other strategies require between 0.66 and 0.92 seconds.

Table 1: Number of nodes for strategies

Strategy	Size	Number of nodes
ATS	500 x 500 pixels	13,086
ATS	1000 x 1000 pixels	3,349
RTS	480 x 480 pixels	5,317
RTS	1000 x 1000 pixels	2,520
RoITS	50 POI	6,601
RoITS	100 POI	4,573

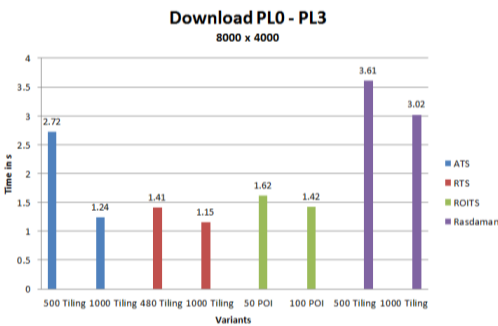


Figure 7: Download benchmark, 8000 x 4000

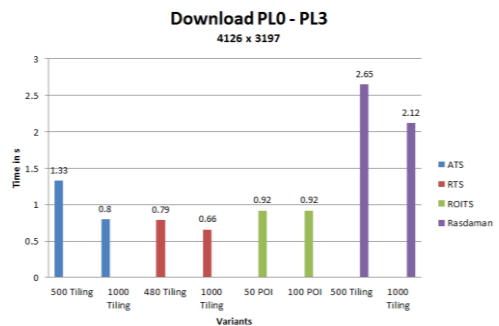


Figure 8: Download benchmark, 4126 x 3197

7 Summary and Conclusion

The collection of large amounts of geospatial image data in the project RiverView® requires efficient data storage. Since existing solutions do not offer an optimal solution, a raster data storage concept based on the NoSQL database system Neo4j was developed and implemented. A crucial aspect is the implementation of data access structures such as image pyramids and tiling. Hence, different tiling strategies were evaluated and benchmarked for up- and download. Based on these benchmarks it is evident that the RTS and RoITS tiling strategies perform best in download. Generally, the strategy implemented depends on the application type. In summary, efficient geospatial raster data management with Neo4j is possible based on the developed strategies and can even be used for real-time applications. It is also conceivable to extend the approach to remote sensing and satellite data sets for write-once-read-many use-cases. In future work, the approach will be further developed to point clouds and also additional evaluations considering other solutions (e.g. Open Data Cube) are planned.

Reference

- Armbruster, S. (2016). Welcome to the Dark Side: Neo4j Worst Practices (& How to Avoid Them). <https://neo4j.com/blog/dark-side-neo4j-worst-practices/>
- Baumann, P. (1993). Language support for Raster Image Manipulation in Databases. *Visualization in Science & Technology*.
- Baumann, P., Furtado, P., Ritsch, R. & Widmann, N. (1997). Anfrageformulierung und Ablage dimensionsbehalteter Daten in Rasdaman. https://doi.org/10.1007/978-3-642-60730-1_17
- Baumann, P. (2018). Rasdaman – Raster data manager. <https://rasdaman.com>
- Bill, R. (2016): Grundlagen der Geo-Informationssysteme. 6. Auflage, Wichmann-/VDE-Verlag, Berlin
- Brisaboa, N., de Bernardo, G., Gutiérrez, G., Luaces, M. R. & Paramá, J. R. (2017), Efficiently Querying Vector and Raster Data. *The Computer Journal*, Volume 60, Issue 9, September 2017, Pages 1395–1413, <https://doi.org/10.1093/comjnl/bxx011>
- Chalmers, S. & Bothorel, P.-C. C. (2013). Big Data – State of the Art. *Report, Télécom Bretagne*.
- Chang, N. S. & Fu, K. S. (1980). A relational database system for images. *Pictorial Information Systems*: Springer Berlin Heidelberg. https://doi.org/10.1007/3-540-09757-0_11
- DeZyre (2019). NoSQL vs SQL – 4 Reasons why NoSQL is better for Big Data applications. <https://tinyurl.com/y2yrmkqn>
- Esri (2021). Tiled Elevation Service. <https://developers.arcgis.com/documentation/tiled-elevation-service/>
- FiW Aachen (2020). RiverView®. <https://www.river-view.de>
- Guttman, A. (1984). R-Trees: A Dynamic Index Structure for Spatial Searching. *Proceedings of the 1984 ACM SIGMOD international conference on Management of data – SIGMOD '84*. <https://doi.org/10.1145/602259.602266>
- Hein, N. & Blankenbach, J. (2017). Vergleich von PostGIS und Rasdaman als Geodatenbank für großvolumige Bilddatenbestände eines mobilen Mappingsystems. In J. Strobel, G. Griesebner, & T. Blaschke (Eds.), *AGIT 3-2017 – Journal für Angewandte Geoinformatik*: Wichmann Verlag. <https://doi.org/10.14627/537633001>
- Lansley, G., de Smith, M., Goodchild, M. & Longley, P. (2019). Big Data and Geospatial Analysis. *Computers and Society*. <https://arxiv.org/abs/1902.06672>

- Lowe, D. (2004). Distinctive Image Features from Scale-Invariant Keypoints. *International Journal of Computer Vision*.
- Miller, J. J. (2013). Graph Database Applications and Concepts with Neo4j.
- Nebiker, S. (1997): Spatial raster data management for geo-information systems – a database perspective. Doctoral thesis, ETH Zurich. <https://doi.org/10.3929/ethz-a-001847022>
- Neo Technology (2018). Neo4j. <https://neo4j.com/>
- NumPy Developers (2018). NumPy. <https://www.numpy.org/>
- Oracle Corporations (2021). Spatial and Graph features in Oracle Database. <https://www.oracle.com/database/technologies/spatialandgraph.html>
- Oracle Corporations and/or affiliates (2021). MySQL. <https://www.mysql.com>
- OpenCV Dev Team (2019). OpenCV. <https://www.opencv.org/>
- Pathak Siddharth, D., Thakur Siddharth, J., Shitole Siddharth, J., Gaikwad, D. P. & Satam Tejas, S. (2014). Implementation of R-Trees for Spatial Image Processing and Cloud Detection., *International Journal of Engineering Research & Technology (IJERT)*. ISSN: 2278-0181
- PostGIS Project Steering Committee (2021). PostGIS. <https://postgis.net/>
- Tamura, H. & Yokoya, N. (1984). Image database systems: A survey. *Pattern Recognition 17-1*. [https://doi.org/10.1016/0031-3203\(84\)90033-5](https://doi.org/10.1016/0031-3203(84)90033-5)
- Taverner, C. (2019). Neo4j Contrib Spatial. <https://neo4j-contrib.github.io/spatial/>
- The PostgreSQL Global Development Group (2021). PostgreSQL. <https://postgresql.org/>
- Yeung A.K.W., Hall G.B. (2007): Spatial Database Systems. The GeoJournal Library, vol 87. Springer, Dordrecht. https://doi.org/10.1007/1-4020-5392-4_4

Meeting User Requirements for Mapping and Characterizing Deprived Urban Areas in Support of Pro-Poor Policies

Monika Kuffer¹, Sabine Vanhuyse², Stefanos Georganos² and Jon Wang¹

¹University of Twente, ITC, The Netherlands

²Université libre de Bruxelles, Belgium

Abstract

Spatial data on Low-and-Middle-Income-Country (LMIC) cities, and deprived areas within cities, are often not readily available in support of local and global information needs. To address this information gap, we propose the systematic semi-automated SLUMAP framework that provides policy-relevant information on deprived urban areas in Sub-Saharan Africa (SSA), based on free open-source software (FOSS). First, we assess user needs for spatial information on deprivation (ranging from local communities to global research and policy support). Second, we show how free or low-cost image datasets can be used for mapping the location of deprived areas at the city scale and providing an overall assessment of their spatial patterns. This is implemented as a grid-based approach using machine learning and assessing the contribution of a large number of spectral and spatial features derived from open or low-cost imagery. Third, we show how higher (spatial and spectral) resolution data can provide a detailed characterization of such areas, with a GEOBIA/machine-learning workflow and deep learning techniques. We illustrate the experiments and results on the city of Nairobi (Kenya) and discuss transferability to SSA cities.

Keywords: slum, earth observation, sustainability, spatial inequalities, machine learning

1 Introduction

Urbanization rates are rising in most Low-and-Middle-Income Countries (LMICs) (UN, 2019). Most of this increase is happening in areas commonly known as slums, informal settlements and areas of inadequate housing, hereafter “deprived urban areas”. In particular, African cities are rapidly growing, while there is an insufficient provision of low-income serviced housing. The urban Sustainable Development Goal 11 (SDG 11) has the “proportion of urban population living in slums, informal settlements or inadequate housing” as its first indicator to measure progress towards sustainability. Unfortunately, data for this indicator is commonly not readily available for supporting local or global monitoring. Existing datasets supporting the SDG 11.1.1 indicator are country-level estimates without a reference to individual cities. Thus, existing data failed to provide insights into the spatial patterns of deprived urban areas and their dynamics within cities. Earth Observation (EO) data has, in principle, the capability to map deprived urban areas (e.g., Wang, Kuffer, Roy, & Pfeffer, 2019), as data archives are

growing and computational power is increasing. However, EO methods fall short in providing scalable, transferable, and low-cost solutions that respond to user needs (Kuffer et al., 2020). Therefore, to date, EO has not been used as an effective tool to provide relevant information to various users on urban development issues, specifically for monitoring deprived urban areas and accounting for the local SDG 11.1.1 indicator. To make appropriate use of the growing amount of EO data and advancements in methods, it is essential first to understand user needs. However, there is a general communication gap between the EO experts and potential users of EO data, hereafter “users”. We observe that the EO community is developing methods that are mostly based on very high resolution (VHR) commercial EO data, often for a small subsection of a city. At the same time, urban development questions typically require an understanding of patterns at the city or regional scale. In addition, resource constraints and understanding of advanced methods is hindering the knowledge transfer from research to users. The paper aims to provide an overview of spatial information needs in deprived urban areas and develop solutions for meeting these needs. Examples from Nairobi (Fig. 1) illustrate recent developments in machine learning and FOSS solutions for developing a systematic semi-automated SLUMAP framework that provides policy-relevant information on deprived urban areas.



Figure 1:
A deprived area in Nairobi
(Photo: Ángela Abascal Imízcoz).

2 Methodology

2.1 Mapping user needs and requirements

The first step towards shortening the gap between existing inconsistent/unavailable datasets and essential geospatial resources in deprived urban areas is to develop an adequate understanding of user needs and requirements at (inter)national and local levels. This was done through the assessment of data requirements by way of an online survey, fortified by additional discussions and workshops that covered diverse users:

- An online survey of users utilizing deprived urban area-related spatial data (N = 112). The survey included different professions and sectors working with ‘slum’ related data, including civil society, government, international and research organizations.

The backgrounds of respondents were GIS, EO and data science (40%), urban planning (28%), social (20%), environmental (9%) and health (4%) professions.

- Interactions with community-based organizations in Nairobi and Lagos, in form of online meetings due to COVID restrictions.
- Workshops (at the World Urban Forum and hybrid local/online workshops in Lagos and Accra), expert discussions with local and national authorities (Kenya and Lagos).

The questions and discussion points included spatial, temporal, contextual information requirements of users as well as requirements about data access, aggregation, uncertainties and ethics/privacy. Two major aspects discussed in the user interactions that are key for routine and accurate production of maps of deprived urban areas at continental scale are highlighted (Fig. 2), namely (i) the need for a low-cost mapping system and (ii) the local data requirements (characterization) for the city and community-level data on deprived urban areas. To show how data can be produced that respond to the user needs, we use the case of Nairobi to explore the potential of several HR and VHR sensors (i.e., Sentinel-1/2, SPOT6/7, WorldView-3 and Google Earth (GE) images) for mapping and characterizing deprived urban areas. The city-scale mapping using Sentinel-1/2 data is responding to the user needs for a low-cost mapping system. This allows for developing a standardized and scalable mapping system and drastically increases scalability and repeatability (routine mapping). The local characterization explores the potential of VHR images to respond to the user needs on urban morphology, environmental/ health aspects (e.g., garbage piles) and automatizing building mapping (in support of local planning needs).

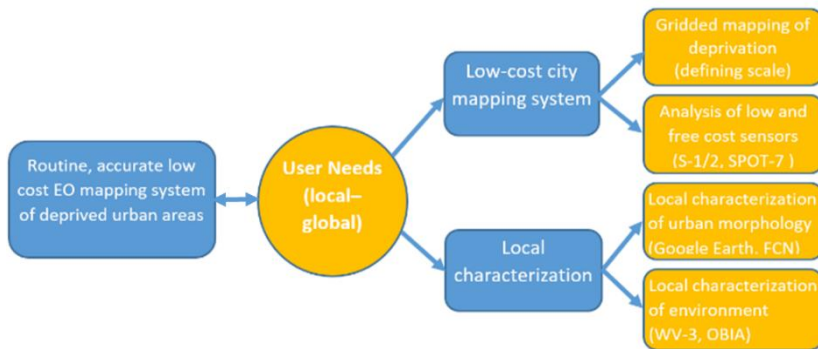


Figure 2: A semi-automated SLUMAP framework.

2.2 Using open vs. low-cost imagery at the city scale

To assess the potential of free-cost Sentinel-1/2 for mapping the morphological deprivation probability at the city scale, we develop a machine learning workflow using FOSS software GRASS GIS in a Jupyter Notebook and R. A grid-based approach is implemented. Gridded mapping has proved successful for mapping slums with VHR GE images (Duque et al., 2017). Besides, it tends to have a high transferability potential, as reflected by the increasing number of available global gridded layers (e.g., WorldPop, GHSL, GUF, etc.), and it responds to privacy concerns (e.g., ‘blurs’ the boundaries). We apply our workflow to an area of interest

covering the city of Nairobi (652 km²). We use Sentinel-1/2 and SPOT7, which is considered low-cost commercial imagery (Fig. 3) and compare the results. Ancillary open global datasets (i.e., SRTM, OSM and a preliminary version of the World Settlement Footprint 2019 – unpublished to date - which is an improvement of the World Settlement Footprint 2015 (Marconcini et al., 2020)) are also included in the experiments. First, a wide set of over 2000 spectral, spatial and ancillary features are extracted. For optical imagery, these features are mainly based on vegetation indices, water or moisture indices, built-up indices, image transforms, texture metrics (e.g., GLCM, Structural Feature Set) and a few metrics calculated on an unsupervised classification (such as the Mean Patch Size). For SAR they are mostly based on intensity, coherence, textures and filtered bands. Ancillary features include geomorphometric features, built-up and street density. Statistics are calculated in 50m x 50m grid cells, and feature selection (using the VSURF - Variable Selection Using Random Forest - algorithm (Genuer, Poggi, & Tuleau-Malot, 2015)) is implemented prior to random forest (RF) classification, for parsimony. The classification scheme includes 8 land-use/land-cover classes: (1) High to mid-density built area, (2) Low density built area, (3) Industry/large structures, (4) Paved ground/Bare ground, (5) Vegetation, (6) Water, (7) Deprived urban areas (typical), and (8) Deprived urban areas (atypical). For our focus classes (7 and 8), a detailed class description is provided in the textbox. For training and testing, 3962 manually labelled samples (i.e., grid cells) representing the dominant class are used. Several feature combinations are assessed, and their respective performances are compared based on accuracy metrics (i.e., precision, recall and F1 score).

Textbox:	Definition of deprived classes:
(7)	Very compact arrangement of low-rise buildings, generally forming 'organic' patterns. No structured street layout, except for a few main streets. Little or no vegetation.
(8)	Arrangement of buildings with a density that varies from compact to mid-dense, and a pattern that is more regular than in class 7.

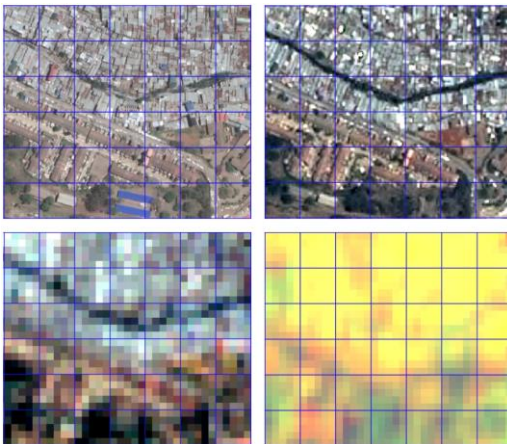


Figure 3:

Interface between deprived and non-deprived urban areas. Top left: GE imagery. Top right: SPOT7 (RGB). Bottom left: S2 (RGB). Bottom right: S1 intensity (VV, VH, VV/VH).

2.3 Local characterization of deprived areas

Next, we investigate the characterization of intra-deprived areas environments (i.e., garbage piles, built-up morphology). First, we make use of VHR superspectral data collected by the WorldView-3 satellite (8 multispectral and 8 SWIR bands) to map the urban environment in

deprived urban areas. State-of-the-art machine learning classifiers and processing methods such as Geographic Object-Based Image Analysis are deployed (Georganos, Grippa, Lennert, et al., 2018; Georganos, Grippa, Vanhuyse, Lennert, Shimoni, & Wolff, 2018). Moreover, we assess the created land cover/ land use (LULC) models for deprived areas. The assessment focuses on maximizing their interpretability and transferability and alleviate the data management and processing burden (Georganos, Grippa, Vanhuyse, Lennert, Shimoni, Kalogirou, et al., 2018). For example, this included defining a suitable grid size that reflects the urban patterns of deprived areas but still allows data aggregation to ease processing. We extract various indicators at a grid level (i.e., 25 meters) derived from the modelled LULC of these regions. For instance, these indicators may be pertinent to open space, building density, or the proportion of garbage piles. The training data on garbage piles were collected in collaboration with local community-based groups in Mathare (a deprived area in Nairobi), a key environmental issue that emerged in interaction with communities. A similar effort is presently ongoing in other communities. Second, we extract building footprints and map the morphological patterns using GE imagery. These morphological patterns allow differentiating deprived urban areas from better-off areas at the city scale. To achieve this, we largely rely on open tools and free data. There are two major steps in this approach: (1) extracting building footprints from GE imagery by using deep learning techniques (modified U-Net architecture) using a global training dataset provided by Wuhan University that containing labelled building footprint (gpcv.whu.edu.cn/data/building_dataset.html), and (2) measuring the morphological configuration of buildings with the open-source tool MOMEPEY (<http://docs.momepy.org/en/stable/>).

3 Results

3.1 User requirements for evidence-based policy-making

The results of the user need assessment (Fig. 4) shows that data on deprived urban areas are not available or accessible for users. In workshops, it was stressed that data, if at all available, are often not usable (e.g., not covering the area of interest) or are too dated. Most data needs relate to routine and up-to-date information about the location of deprived urban areas, building information and more detailed characterisation of their environment.

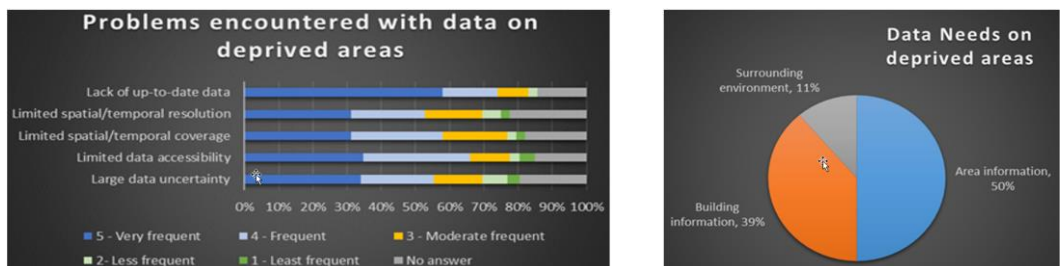


Figure 4: Existing data gaps and data needs on deprived urban areas: assessment of problems encountered by users (left) and user's data needs on deprived areas (right).

3.2 City-scale results

For each of the assessed feature combinations, the original set can be drastically reduced to a small number of important predictors with VSURF. The results of the random forest classifications are validated with an independent test set, focusing on the two deprived urban area classes. The best combination of SPOT7 and ancillary predictors achieves higher accuracy than the best combination of Sentinel1/2 and ancillary predictors (Tab. 1). However, the difference is not as marked as could be expected given the spatial resolution gap. The morphological deprivation probability is computed by summing the class probability of classes 7 and 8 (Fig. 5). Considering that Sentinel images are free datasets with wide temporal availability, they constitute a valuable option for mapping the morphological deprivation probability at the city scale, allowing for frequent updates, as required by users.

Table 1: Accuracy assessment of the best feature combinations involving Sentinel-1 (S1), Sentinel-2 (S2), SPOT7, and ancillary global datasets.

Class	Metric	S2	S2	SPOT7	SPOT7
		S1	S1	Ancillary	Ancillary
Class 7	Precision	0.94	0.96	0.86	0.94
	Recall	0.89	0.89	0.89	0.93
	F1	0.91	0.92	0.87	0.94
Class 8	Precision	0.79	0.84	0.79	0.88
	Recall	0.82	0.89	0.78	0.89
	F1	0.80	0.86	0.79	0.89

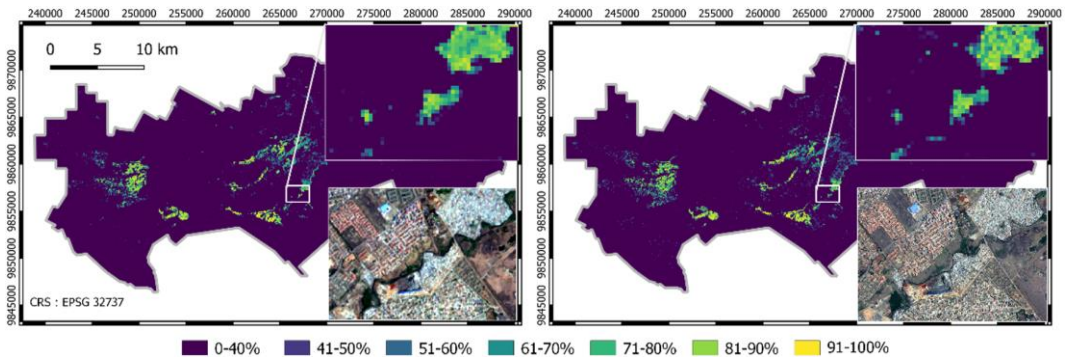


Figure 5: Morphological deprivation probability classes in 50x50m grid cells (Nairobi). Left: S1-S2-Ancillary (with S2 RGB subset). Right: SPOT7-Ancillary (with SPOT7 RGB subset).

3.3 Local characterization based on LULC

Taking as an example Mathare, Nairobi, Fig. 6 illustrates the potential of our modelled LULC for characterizing the local environment in a deprived area. Notably, garbage pile density (Fig. 6.a) is a very important socio-economic and health indicator as it can be associated with disease exposure, water/sanitation and act as a socio-economic proxy for the surrounding neighbourhoods (Engstrom, Hersh, & Newhouse, 2017). The lack of openness (Fig. 6.c) can also be detected. The detection of vehicles (Fig. 6.e) reflects socio-economic activity to a

degree. The RF Out of Bag Overall Accuracy of the map product for Mathare using all valuable WV-3 resources (multispectral + shortwave infrared) surpassed 87%. Finally, these indicators can be extracted in a gridded format (25 m), as illustrated in Fig. 6.g, which maps the spatial distribution of garbage piles across Mathare.

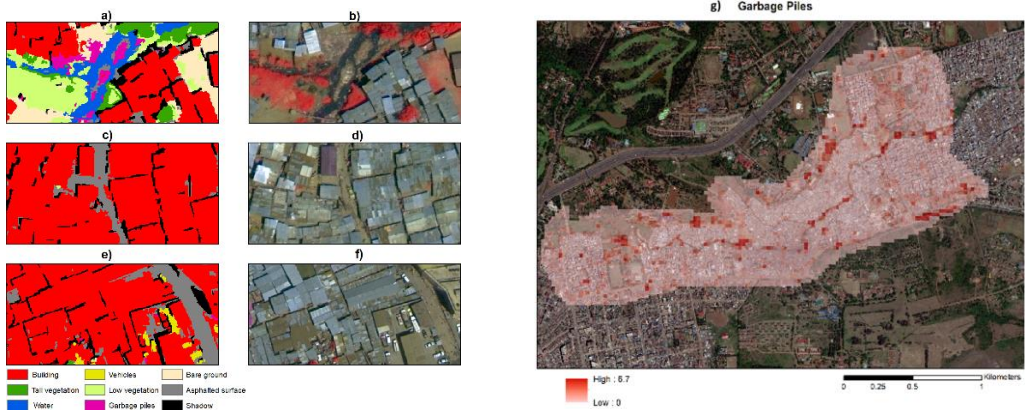


Figure 6: Subsets of mapped LULC in deprived areas in Mathare, Nairobi: a) garbage piles; c) lack of openness; e) detection of vehicles (b,d,f RGB); g) garbage piles density (%) at a 25 meter spatial resolution.

3.4 Local characterization based on building footprints extraction and urban morphology

Fig. 7 shows buildings extracted from different places within the city of Nairobi. Visually, the building configuration exhibits a significant difference especially comparing the building patterns in Fig. 7(b), where building patterns in deprived areas can be quite different from the other places shown in Fig. 7.a, c, d.

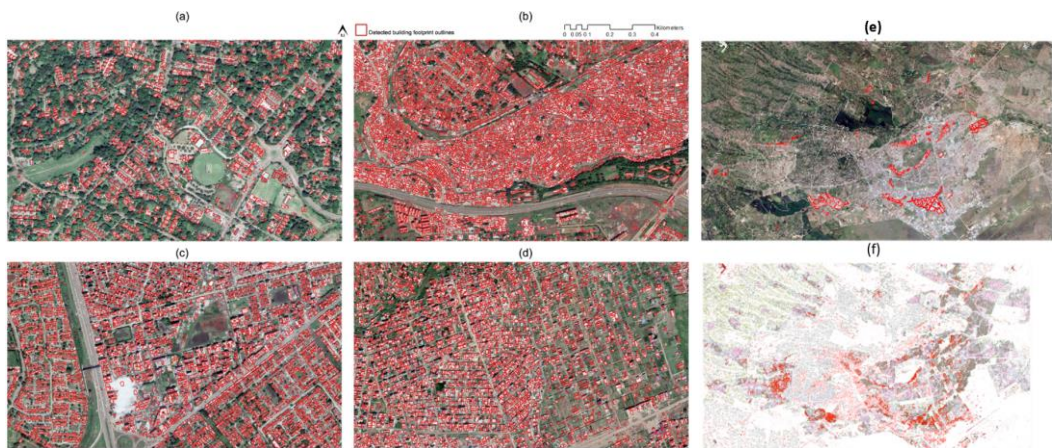


Figure 7: (a-d) Building footprints extracted from different neighbourhoods; (e) manually delineated deprived areas (dated); (f) building clusters based on building morphological metrics (Nairobi).

Once the morphological building patterns are explicitly measured, similar building patterns are classified within the same morphological clusters. The morphological cluster highlighted in red (Fig. 7.f) reflects the distribution of deprivation areas delineated in Fig. 7.e.

4 Conclusions

Deprived areas emerge with the rapid urbanization occurring in LMICs and the insufficient provision of low-cost urban housing. An increasing number of people migrate to cities, with complex drivers such as climate change. Global datasets do not account for these areas, and local data often ignore them. Our results show the capability of the SLUMAP framework that builds upon a FOSS solution to respond to user needs for routine and accurate mapping of deprived urban areas. To protect privacy, exact settlement boundaries are not shown, which could be used against communities (e.g., land tenure conflicts). A fine-scale local characterization makes use of commercial (WV-3) and freely available (GE) VHR data to meet the local needs for detailed environmental characterization, such as garbage piles mapping and morphological characterization of built-up density patterns at local and city scale. The SLUMAP framework is transferable to other SSA cities to provide data allowing for inter-city comparisons.

References

- Duque, J., Patino, J., Betancourt, A., 2017. Exploring the Potential of Machine Learning for Automatic Slum Identification from VHR Imagery. *Remote Sensing* 9, 895. <https://doi.org/10.3390/rs9090895>
- Engstrom, R., Hersh, J. S., & Newhouse, D. L. (2017). *Poverty from space : using high-resolution satellite imagery for estimating economic well-being*. Retrieved from Washington, D.C.: <http://documents.worldbank.org/curated/en/610771513691888412/Poverty-from-space-using-high-resolution-satellite-imagery-for-estimating-economic-well-being>
- Genuer, R., Poggi, J.-M., & Tuleau-Malot, C. (2015). *V\$URF: An R Package for Variable Selection Using Random Forests* Retrieved from
- Georganos, S., Grippa, T., Lennert, M., Vanhuyse, S., Johnson, B. A., & Wolff, E. (2018). Scale Matters: Spatially Partitioned Unsupervised Segmentation Parameter Optimization for Large and Heterogeneous Satellite Images. *Remote Sensing*, 10(9), 1440.
- Georganos, S., Grippa, T., Vanhuyse, S., Lennert, M., Shimoni, M., Kalogirou, S., & Wolff, E. (2018). Less is more: optimizing classification performance through feature selection in a very-high-resolution remote sensing object-based urban application. *GIScience & Remote Sensing*, 55(2), 221-242. doi:10.1080/15481603.2017.1408892
- Georganos, S., Grippa, T., Vanhuyse, S., Lennert, M., Shimoni, M., & Wolff, E. (2018). Very High Resolution Object-Based Land Use–Land Cover Urban Classification Using Extreme Gradient Boosting. *IEEE Geoscience and Remote Sensing Letters*, 15(4), 607-611.
- Kuffer, M., Thomson, D. R., Boo, G., Mahabir, R., Grippa, T., Vanhuyse, S., . . . Kabaria, C. (2020). The Role of Earth Observation in an Integrated Deprived Area Mapping “System” for Low-to-Middle Income Countries. *Remote Sens.*, 12(6), 982.
- Marconcini, M., Metz-Marconcini, A., Üreyen, S., Palacios-Lopez, D., Hanke, W., Bachofer, F., . . . Strano, E. (2020). Outlining where humans live, the World Settlement Footprint 2015. *Scientific Data*, 7(1), 242. doi:10.1038/s41597-020-00580-5
- UN. (2019). *World Urbanization Prospects. The 2018 Revision*. New York, US: United Nations.
- Wang, J., Kuffer, M., Roy, D., & Pfeffer, K. (2019). Deprivation pockets through the lens of convolutional neural networks. *Remote Sens. Environ.*, 234, 111448.

Deriving Indicators for Points of Interest and Analyzing Mixed Activities in Urban Areas

Tahira Ullah¹, Sven Lautenbach² and Alexander Zipf^{1,2}

¹Heidelberg University, Germany

²Heidelberg Institute for Geoinformation Technology GmbH, Germany

Abstract

This paper evaluates indicators to analyse mixed activities, representing a combination of various facilities and services, in urban areas. Although mixed activities play an important role in urban planning projects, measuring them has been problematic due to the lack of appropriate data and measurement approaches. In ecology, there are dozens of potential diversity indices, which have been deployed in recent land use studies to measure mixed activities. However, ecologists have highlighted that these indices are not always expressed in intuitive units. Recognizing the limitation of commonly used diversity indices, Hill numbers, which represent a mathematically unified family of diversity indices, are used. Taking advantage of new data sources such as Points of Interest (POIs) from OpenStreetMap, this study applied Hill numbers on POIs to measure mixed activities at a quarter level in Frankfurt. Results showed that Hill¹ (exponential of Shannon) is an appropriate quantitative measure to describe the diversity of facilities and services by a single numerical value. However, it is difficult to explain which factor, namely evenness or richness, has a stronger impact on the index. To gain a more comprehensive picture of mixed activities we suggest to consider further indicators such as evenness and richness.

Keywords: Diversity Indices, mixed activities, OpenStreetMap, Hill numbers, POIs

1 Introduction

The development of pedestrian-friendly city with a variety of services such as eating, education, healthcare, shopping, and personal services has become an important goal for urban planning, local authorities, families, and economic groups (Manaugh & Kreider, 2013). There is an increasing demand from different parties to estimate the heterogeneity of facilities and services, also known as mixed activities, using an overall diversity indicator (Grant, 2002). Such an indicator could then be used to compare different city quarters, cities, or even different regions.

The measurement and assessment of biological diversity has a long history in ecology (Hill, 1973; Whitaker, 1965). Urban land-use studies have taken advantage of these biological indicators to analyse mixed activities. Two commonly used biodiversity indices that have been used in the context of land-use diversity is the Shannon index which quantifies the degree of mixture among different species (Frank, 1994; Manaugh & Kreider, 2013) and the Simpson's

Index (Ritsema van Eck & Koomen, 2008; Berger et al., 2004). Another promising indicator are Hill numbers, which integrate species richness, Shannon, and Simpson Index into a further class of diversity measures.

In this study, we explore the suitability of Hill numbers to assess the diversity of mixed activities based on Points of Interest (POIs) from OpenStreetMap (OSM). We will examine, how accurately mixed activities at a city quarter level can be measured, using the northern quarters of Frankfurt in Germany as a case study.

2 Study area: Data Source and Data Type

To measure mixed activities in urban areas we use Points of Interest (POI) from OpenStreetMap. OpenStreetMap (OSM) has the objective to create an open, free, digital map of the world through the efforts of volunteers (Goodchild, 2007). In OSM, POIs characterize important locations on a map represented by nodes, ways, or relations.

We obtained POI data for five city quarters in Frankfurt am Main via the Openpoiservice, which is a Web Service within the Openrouteservice infrastructure (Neis & Zipf, 2008). In total 55 categories of facilities were selected including eating, education, healthcare, shopping, and personal services. Indicators were calculated based on the POIs for each of the five city quarters separately.

For the study area, we selected the northern part of Frankfurt am Main due to its heterogeneity regarding mixed activities between the city quarters. Frankfurt am Main is the fifth biggest city in Germany with a population of 747.000 inhabitants (Stadt Frankfurt am Main, 2017). The quarters Eschersheim and Hedderheim comprise of various facilities and services due to their relative proximity to the city Center, whereas Praunheim and Niederursel are quieter quarters. Niederursel contains some of the scientific institutes of the Goethe-University Frankfurt. In Kalbach-Riedberg, one of the largest town-planning projects “Am Riedberg” was build, including residential areas, parks, green spaces, schools, healthcare services, and sports areas (Stadtplanungsamt Frankfurt am Main, 2021).

3 Methodology

Figure 1 provides an overview of the overall methodology. Facilities belong to different categories, which defines the level at which diversity indices are calculated. Since we had to assume that POIs from OSM are not complete and the proposed indices are sample size dependent, standardization was necessary to compare unequally large samples. We used the coverage estimator introduced by Good (1953). It is a measure of sample completeness, giving, in our context, the proportion of the total number of POIs in a quarter that belong to the categories represented in the sample (Chao & Jost, 2006). It describes the sum of the frequencies of the categories sampled, which is 100% when all categories are known (Chao, 2014). To estimate uncertainties, we used a bootstrap method, in which we calculated the Hill number and the coverage for each of the 100 bootstrap samples. Table 1 provides the average coverage of each city quarter and the respective reference sample size.

Table 1: Average coverage of quarters for reference sample n

City quarter	coverage	sample size n
Eschersheim	0.94	69
Heddernheim	0.96	125
Kalbach-Riedberg	0.94	70
Niederursel	0.98	89
Praunheim	0.95	51

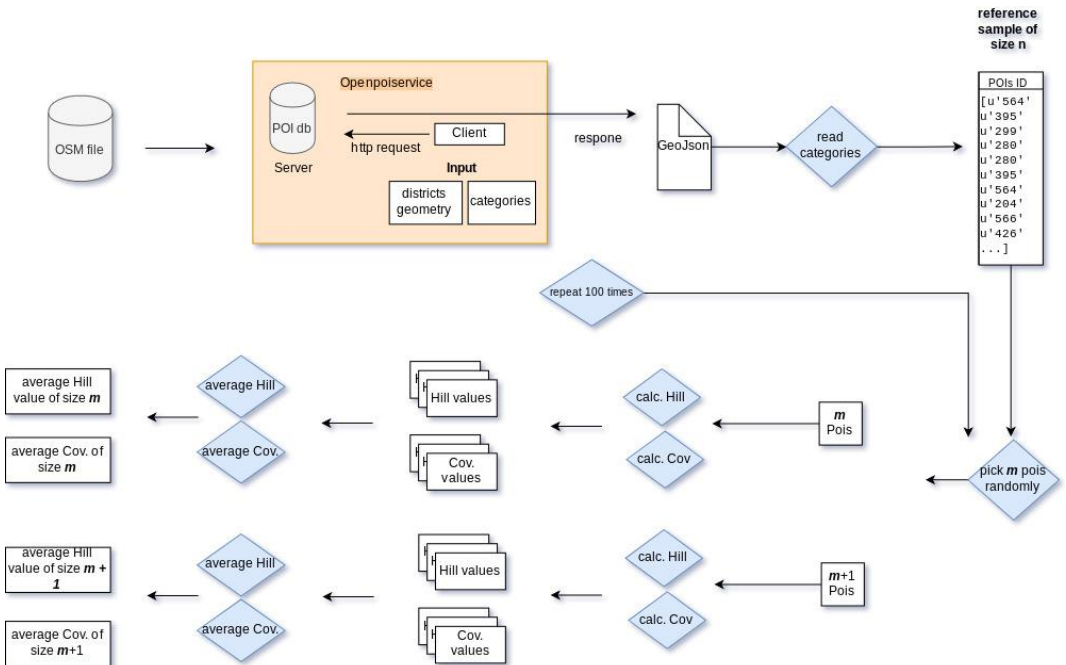


Figure 1: Workflow to calculate POI category diversity. For each city quarter Hill number and coverage were calculated. Uncertainty was estimated by a bootstrap approach.

While ecologists commonly refer to the terms species and individuals (Chao, 2014), in an urban context, we can consider categories as species and POIs as individuals. A city quarter is equal to an assemblage consisting of N total POIs, where each POI belongs to one of the C categories. Since we assume that the completeness of POIs in OSM vary from region to region, we consider a reference sample of n POIs from each city quarter from an underlying true assemblage that is unknown. The total number of categories observed in the reference sample is C_{obs} . X_i is the number of POIs of the i th category that is observed in the sample, $i = 1, 2, \dots, C$. Thus $p_i = X_i/n$ is the relative abundance of each observed category in the sample. Furthermore, f_k is the number of categories represented by exactly k POIs, $k = 0, 1, \dots, n$. From the definitions above it follows:

$$n = \sum_{i=1}^c X_i = \sum_{k \geq 1} k f_k \quad (1b)$$

$$C_{obs} = \sum_{k \geq 1} f_k \quad (1a)$$

Species richness represents (in our case POI category richness) the simplest and yet most popular measure of diversity, describing the number of categories in a given area. However, one main limitation is that the observed categories are highly sensitive to the sample size. Furthermore, species or POI category richness does not take into account any information about the relative abundance of categories (Chao et al., 2014). Addressing the abundance problem, the Shannon and Simpson indices combine species richness and the relative abundance of each category into a single metric. While the Shannon Index weighs each category exactly by their frequency, the Simpson Index is a dominance index that gives more weight to common or dominant categories (Ricotta, 2002; Jiang et al., 2017). However, the diversity indices are based on percentage composition, thus, they approach a constant value if sample size increases (Loya, 1972). Jost (2006) emphasises that the Shannon and Simpson are not necessarily themselves “diversity” indices; the Shannon index in particular represents an entropy reflecting the uncertainty in the outcome (Jost, 2006).

Hill numbers (Hill 1973) integrate species richness, Shannon, and Simpson index into a class of diversity measures. Thus, all measures include the following single expression for diversity:

$$D^q = \left(\sum_{i=1}^C p_i^q \right)^{1/(1-q)} \quad (2)$$

in which C is the number of categories in the assemblages, and the i th category has relative abundance p_i . The exponent q is also called the order of the diversity, thus, q determines the sensitivity to common or rare categories. The diversity of order 0 is completely insensitive to the relative frequencies of the categories, and is known as species richness (H^0) in ecology. If q is less than unity diversities favour rare categories, while all values of q greater than unity favour the most common categories (see Table 2). Order 1 is the exponential of Shannon entropy, while order 2 describes the inverse of the Simpson concentration (Chao et al, 2012).

Table 2: Conversion of common indices to Hill numbers

Index x:	Diversity in terms of x:	Hill numbers in terms of p_i :	Order:
Species richness	$x = \sum_{i=1}^c p_i^0$	x	$\sum_{i=1}^c p_i^0$ Hill ⁰
Shannon entropy	$x = - \sum_{i=1}^c p_i \cdot \ln(p_i)$	$\exp(x)$	$\exp\left(- \sum_{i=1}^c p_i \cdot \ln(p_i)\right)$ Hill ¹
Simpson concentration	$x = \sum_{i=1}^c p_i^2$	1/x	$1/\sum_{i=1}^c p_i^2$ Hill ²

Hill numbers offer the advantage that they fulfil a doubling property. Therefore, if a city quarter is twice as diverse as another city quarter, the ratios of Hill numbers are always 2.00. Furthermore, traditional diversity indices can be converted to Hill numbers by simple algebraic transformation (see Table 2). Hill numbers are all expressed in units of effective number of categories, which are the number of equally abundant categories required to give the same value of diversity measure. Since Hill numbers have the same units, it is possible to graph them as a function of order q (see Fig. 2). The steepness of the curve reflects the evenness of a city quarter. Regarding Figure 2, if a city quarter has equally abundant categories, the curve is a constant at the level of Hill⁰ (species richness). The ratios of Hill numbers can be used to obtain the evenness value as a single measure.

$$E_{a:b} = H^a / H^b \tag{3}$$

H_a and H_b are diversity numbers of order a and b based on q . Since Hill⁰ (species richness) is highly dependent on sample size (see Fig. 3), we will use the ratio Hill² and Hill¹, which stabilizes with increasing sample size. The resulting value ranges between 0 and 1, if the quarter comprises of completely even distributed categories the evenness value is 1. In contrast, 0 means one category is dominating the whole quarter.

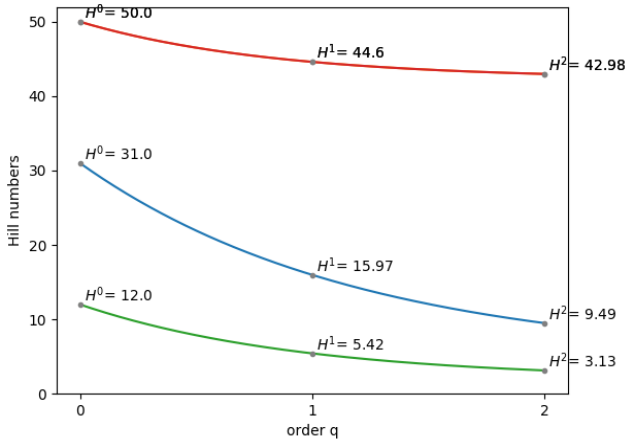


Figure 2: Hill numbers as a function of q . Steepness of the curve indicates, how even/uneven the distribution of the categories is. The red curve represents the most even city quarter, followed by the green curve. The blue curve indicates the most uneven distribution.

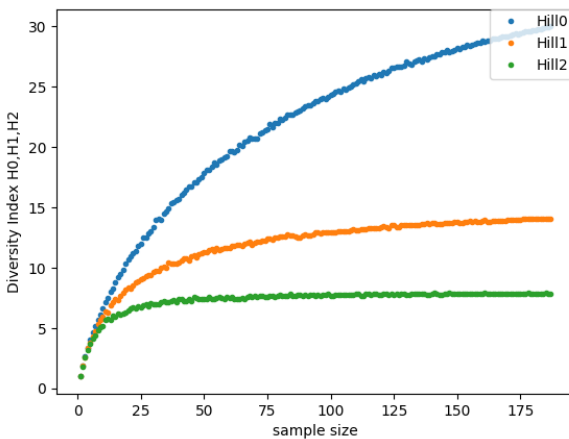


Figure 3: Hill numbers and sample size dependence. Hill0 (blue dots) is sensitive to sample size. Contrary, Hill1 (orange dots) and Hill2 (green dots) stabilize with increasing sample size.

As shown in Figure 3 Hill numbers, in particularly Hill0, is sample size dependent. Rarefaction describes an approach used in ecology to correct for this effect (Gotelli & Colwell, 2001). Rarefaction uses rarefaction curves to calculate category richness for a given number of individual samples. These curves plot the number of species as a function of the number of samples. They are based on a multiple resampling of the samples, and then plot the average number of species found in each sample (Gotelli & Colwell, 2001). However, if samples standardized by size are compared with each other, they will usually have a different degree of completeness. Chao & Jost (2012) suggest using a coverage-based standardization approach ensuring a comparison of samples of equal coverage. Based on these functional relationships the estimated Hill numbers are estimated.

4 Results

The estimated sample coverage values for the respective quarters were almost complete (see Table 1). To make the diversity of the five- quarter comparable, the respective quarters were rarefied down to the lowest base coverage of 94% (see dotted vertical line in Fig. 4). All three Hill numbers are evidently different for most city quarters. However, at 94% coverage the 95% confidence intervals of Hill⁰ and Hill² for Eschersheim and Kalbach-Riedberg overlap, indicating that the POI diversity of these two city quarters is not significantly different.

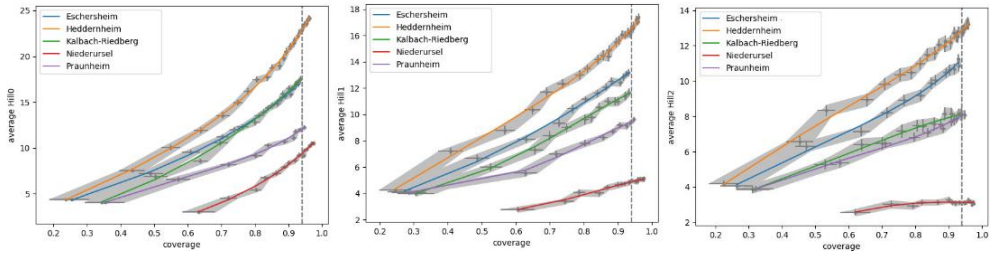


Figure 4: Sample completeness curves and Hill numbers ($q=0, 1, 2$) for the five city quarters. The grey areas indicate the 95% confidence bands derived from the bootstrap.

Table 3: diversity values ($q=0,1,2$) based on 0.94 basecoverage

City quarter	Hill ⁰	Hill ¹	Hill ²	evenness	Sample size
Eschersheim	16.9	13.5	11.0	81%	69
Heddernheim	22.5	16.5	12.9	78%	125
Kalbach-Riedberg	17.3	11.8	8.0	68%	70
Niederursel	8.8	4.8	3.1	66%	89
Praunheim	11.4	9.6	8.0	83%	51

Jost (2006) points out that Hill¹ is a fair choice as a single diversity index because it weighs categories exactly by their frequencies. Table 3 shows that Heddernheim has the highest diversity, followed by Eschersheim and Kalbach-Riedberg, while Niederursel has the lowest Hill¹ value. However, since Hill¹ focusses on both the richness and evenness, it is difficult to tell which factor contributed more simply by looking at the index. The richness (Hill⁰) and evenness indicator provide additional information. Although Praunheim consists of few categories (11.4), the high evenness (83%) indicates an even distribution. Niederursel showed the lowest richness (8.8) and the lowest evenness (66%). Heddernheim consisted of the highest number of categories, hence showed the highest Hill¹ value. Eschersheim and Kalbach-Riedberg showed almost the same number of categories, but due to its lower evenness, Kalbach-Riedberg had a lower Hill¹ value.

5 Discussion

Biodiversity measures such as Species richness, Shannon's, and Simpson's index are quantitative measures reflecting the number of categories and their relative frequencies. While these widely used indices are non-linear and not sufficient to compare multiple areas, Hill numbers are more intuitive and meet a doubling property (Jost, 2006).

To compare the diversities of multiple quarters by a single numerical value, we suggest Hill1. However, Hill1 and Hill2 incorporates both richness and evenness, hence it is difficult to tell which factor contributed more simply by looking at the index. We recommend calculating a separate evenness measure in combination with species richness (Hill0), to derive further characteristics of the respective quarter.

Ecologists consider a site as diverse when it consists of a high number of species, and if the species are well balanced in terms of abundance. When applying this terminology in an urban context, the following question arises: Are high richness and evenness sufficient for a diverse area in an urban context? Thus, the degree of diversity should always be considered with other factors, such as the population density and the resulting demand for specific services.

Moreover, diversity indices measure diversity quantitatively, they do not pay attention to qualitative aspects. For instance, a perfect mix of schools, grocery stores, and healthcare services scores identical to the same proportions of banks, estate agents, and companies.

In this study, we considered OSM POIs as a reference sample of an underlying true assemblage. However, if POI data is complete, standardization methods are unnecessary because the absolute number of POIs are also an indicator for the diversity of an area. Standardization methods are only useful when an area has not reached high completeness. Even though OSM-based POIs for urban areas in Germany seem almost complete, this work provided standardization methods so that the introduced methods are also applicable to areas with lower coverage. Overviews on methods for estimating completeness and other data quality indicators in OSM are given in Degrossi et al. (2018), Ludwig et al. (2019), Barron et al. (2003) and related analysis frameworks like ohsome.org (Raifer et al 2019). For how those methods have been adapted for biodiversity see Jacobs & Zipf (2017).

6 Conclusion

In conclusion, this paper has discussed the application of biodiversity indices in an urban context. Evidently, a high diversity of services and facilities can support economic groups, families, urban planners, as well as local authorities to identify attractive areas or areas that lack a high diversity. The proposed diversity indicator can be used in regression analyses as a proxy to explain socioeconomic variations. Regarding the effectiveness of the introduced indices, further studies might focus on revealing associations between diversity and other relevant social factors.

References

- Barron, C., Neis, P., & Zipf, A. (2014). A Comprehensive Framework for Intrinsic OpenStreetMap Quality Analysis. *Transactions in GIS*, 18(6), 877–895. <https://doi.org/10.1111/tgis.12073>
- Berger, A. N., Demirguc-Kunt, A., Levine, R., & Haubrich, J. G. (2004). Bank Concentration and Competition: An Evolution in the Making. *Journal of Money, Credit, and Banking*, 36(3b), 433–451. <https://doi.org/10.1353/mcb.2004.0040>
- Chao, A., Gotelli, N. J., Hsieh, T. C., Sander, E. L., Ma, K. H., Colwell, R. K., & Ellison, A. M. (2014). Rarefaction and extrapolation with Hill numbers: A framework for sampling and estimation in species diversity studies. *Ecological Monographs*, 84(1), 45–67. <https://doi.org/10.1890/13-0133.1>
- Chao, A., & Jost, L. (2012). Coverage-based rarefaction and extrapolation: Standardizing samples by completeness rather than size. *Ecology*, 93(12), 2533–2547. <https://doi.org/10.1890/11-1952.1>
- Degrossi, L. C., Albuquerque, J. P. de, Rocha, R. dos S., & Zipf, A. (2018). A taxonomy of quality assessment methods for volunteered and crowdsourced geographic information. *Transactions in GIS*, 22(2), 542–560. <https://doi.org/10.1111/tgis.12329>
- Frank, L. (1994). Impacts of Mixed Used and Density on Utilization of Three Modes of Travel: Single-Occupant Vehicle, Transit, Walking. *Transportation Research Record*, 1466, 44–52.
- Good, I. J. (1953). The Population Frequencies of Species and the Estimation of Population Parameters. *Biometrika*, 40(3/4), 237–264. <https://doi.org/10.2307/2333344>
- Goodchild, M. F. (2007). Citizens as sensors: The world of volunteered geography. *GeoJournal*, 69(4), 211–221. <https://doi.org/10.1007/s10708-007-9111-y>
- Gotelli, N. J., & Colwell, R. K. (2001). Quantifying biodiversity: Procedures and pitfalls in the measurement and comparison of species richness. *Ecology Letters*, 4(4), 379–391. <https://doi.org/10.1046/j.1461-0248.2001.00230.x>
- Grant, J. (2002). Mixed Use in Theory and Practice: Canadian Experience with Implementing a Planning Principle. *Journal of the American Planning Association*, 68, 71–84. <https://doi.org/10.1080/01944360208977192>
- Hill, M. (1973). Diversity and Evenness: A Unifying Notation and Its Consequences. *Ecology*, 54, 427–432. <https://doi.org/10.2307/1934352>
- Jacobs, C., & Zipf, A. (2017). Completeness of citizen science biodiversity data from a volunteered geographic information perspective. *Geo-Spatial Information Science*, 20(1), 3–13. <https://doi.org/10.1080/10095020.2017.1288424>
- Jiang, J., Shang, P., Zhang, Z., & Li, X. (2017). Permutation entropy analysis based on Gini–Simpson index for financial time series. *Physica A: Statistical Mechanics and Its Applications*, 486(C), 273–283.
- Jost, L. (2006). Entropy and diversity. *Oikos*, 113(2), 363–375. <https://doi.org/10.1111/j.2006.0030-1299.14714.x>
- Loya, Y. (1972). Community structure and species diversity of hermatypic corals at Elat, Red Sea. *Marine Biology*, 13, 100–123. <https://doi.org/10.1007/BF00366561>
- Ludwig, C., Hecht, R., Lautenbach, S., Schorcht, M., & Zipf, A. (2019). *Assessing the Completeness of Urban Green Spaces in OpenStreetMap*. <https://doi.org/10.5281/ZENODO.3387701>
- Manaugh, K., & Kreider, T. (2013). What is mixed use? Presenting an interaction method for measuring land use mix. *Journal of Transport and Land Use*, 6, 63–72. <https://doi.org/10.5198/jtlu.v6i1.291>
- Raifer, M., Troilo, R., Kowatsch, F., Auer, M., Loos, L., Marx, S., Przybill, K., Fendrich, S., Mocnik, F.-B., & Zipf, A. (2019). OSHDB: A framework for spatio-temporal analysis of OpenStreetMap history data. *Open Geospatial Data, Software and Standards*, 4(1), 3. <https://doi.org/10.1186/s40965-019-0061-3>
- Ricotta, C. (2002). Bridging the gap between ecological diversity indices and measures of biodiversity with Shannon's entropy: Comment to Izsák and Papp. *Ecological Modelling*, 152, 1–3. [https://doi.org/10.1016/S0304-3800\(01\)00468-9](https://doi.org/10.1016/S0304-3800(01)00468-9)

- Ritsema van Eck, J., & Koomen, E. (2008). Characterising urban concentration and land-use diversity in simulations of future land use. *The Annals of Regional Science*, 42(1), 123–140. <https://doi.org/10.1007/s00168-007-0141-7>
- Stadt Frankfurt am Main (2017). Statistisches Jahrbuch Frankfurt am Main. Retrieved from <https://frankfurt.de/service-und-rathaus/zahlen-daten-fakten/publikationen/statistisches-jahrbuch>
- Stadtplanungsamt Frankfurt am Main (2021). Am Riedberg. Projektbeschreibung. Retrieved from https://www.stadtplanungsamt-frankfurt.de/am_riedberg_5309.html
- Whittaker, R. H. (1965). Dominance and Diversity in Land Plant Communities: Numerical relations of species express the importance of competition in community function and evolution. *Science (New York, N.Y.)*, 147(3655), 250–260. <https://doi.org/10.1126/science.147.3655.250>

Mapping Nitrogen from Satellite Data to Improve Soil Quality - A Worked Example

Filippo Iodice¹, Federica D'Acunto¹ and Lorenzo Bigagli²

¹Uptoeearth GmbH, Germany

²CNR-IIA, Italy

Abstract

Soils are complex ecosystems. They play a key role in providing sustainable life on Earth, meeting the needs of humans and regulating several environmental processes. The United Nation's 2030 Agenda for Sustainable Development and the related 17 Goals include a commitment to the preservation of soil quality. However, the adopted indicators lack the measurement of a key nutrient: nitrogen. The aim of this paper is to call for the integration of two nitrogen indexes to measure soil quality and to present a worked example of geospatial technologies applied to nitrogen monitoring, aiding in farmland management and decision-making. Due to their inherent time/location precision, remote sensing data can provide insight in predicting the impact of agricultural practices and optimise their application.

Keywords: land degradation, soil quality, nitrogen

1 Introduction

Soil quality is *"The capacity of a soil to function within ecosystem and land-use boundaries to sustain biological productivity, maintain environmental quality, and promote plant and animal health"* (Doran & Parkin, 1996). This definition reflects the complexity of soil ecosystems and destinations of use. The latter aspect is especially complex, as changes in land use may be slow, making it difficult to detect changes in soil quality before non-reversible damage occurs (Nortcliff, 2002). Hence, it is crucial to identify a comprehensive and practical set of indicators to support quality assessment.

An attempt to measure soil quality is represented by SDG-15 Life on Land, namely by Indicator 15.3.1, which introduces three key indexes to quantify the loss of biological or economic productivity, and complexity of land: Land Cover Meta Language (LCML); Net Primary Production (NPP), to measure land productivity; and Soil Organic Carbon (SOC), to measure carbon stock (Global Mechanism of the UNCCD, 2016). However, this framework overlooks another key indicator: nitrogen. Nitrogen is a crucial nutrient for plants, contributes to keeping water bodies and air clean, and relates to severe soil threats, such as: contamination, erosion, soil organic matter decline, and biodiversity loss (Else K., Bünemann et al., 2016). Moreover, nitrogen is positively correlated to carbon stock.

If duly integrated into the analysis, an explicit reference to nitrogen will lead to a more complete understanding of the factors that contribute to healthy soil, and therefore to appropriate actions and interventions (see Table 1).

Table 1: EU Soil Framework Directive (European Commission, 2006) soil functions and threats, SDG targets and indicators where nitrogen should be integrated.

Soil function	Soil threats	SDGs target	SDGs indicator
Biomass production; Storing, filtering, transforming nutrients, carbon pool	Sealing; Compaction; Biodiversity loss; Erosion; SOM decline	2.4	2.4.1
Physical and cultural environment for humans; Source of raw materials; Archive of geological and archaeological heritage	Contamination; Biodiversity loss	3.9	
Physical and cultural environment for humans; Source of raw materials; Archive of geological and archaeological heritage	Contamination	12.4	
Biomass production; Storing, filtering, transforming nutrients substances and water; Biodiversity pool; Physical and cultural environment for humans; Carbon pool	Erosion; SOM decline; Biodiversity loss; Landslides/floods	13.2	13.2.2
Biomass production; Storing, filtering, transforming nutrients, substances and water; Biodiversity pool; Physical and cultural environment for humans; Carbon pool	Erosion; SOM decline; Contamination; Sealing; Compaction; Biodiversity loss; Salinization	15.3	15.3.1
Storing, filtering, transforming nutrients, substances and water; Biodiversity pool; Physical and cultural environment for humans; Archive of geological and archaeological heritage	Erosion; Contamination; biodiversity loss; Salinization	15.5	

The aim of this paper is twofold:

- to underline that, in order to evaluate soil quality, it is advisable to include Soil Total Nitrogen concentration (STN) and Nitrogen Nutrition Index (NNI);
- to present a worked example of remote sensing and geospatial technologies applied to nitrogen monitoring, to aid farmland management and decision-making.

STN is a pivotal indicator of fertility and is closely related to agricultural productivity. Therefore, reliable prediction of STN is critical for supporting sustainable agricultural development (Lausch et al., 2019). Up to date STN maps are of great interest to identify spatial variation and control factors, which can help maintain soil safety and provide a reference for climate change management. NNI is a plant-based diagnostic method used to determine the crop nitrogen distribution and status, to optimize its management in farming systems.

Remote sensing allows for open, precise, real-time, and localised data to be obtained, about how nitrogen is organized in soils or used by plants. Unlike traditional in-situ methodologies, it can show the impact of agricultural practices on large areas. Furthermore, when merged with other pieces of information, remote sensing supports the identification of the most suitable practices for each given soil. A seemingly passive monitoring tool subsequently turns into a

proactive planning methodology, supporting farmers to implement good practices strictly connected with the achievement of SDGs. For example, geospatial data concerning the loss of nitrogen in the atmosphere due to tillage interventions may suggest that crop rotation stores more nitrogen in the soil and increases its quality.

The outcome of our work is a dynamic, real-time nitrogen map conceived to help farmers to understand where and when to use fertilizers, usually containing nitrogen, and to promote sustainable soil management practices, such as crop rotation.

2 Materials and Methods

We considered the Sentinel-1 (S1) VH (vertical transmitted, horizontal received) and VV (vertical transmitted, vertical received) polarization modes, and computed the ratio VV/VH, which is less sensitive to vegetation cover (Vreugdenhil et al., 2021). SAR images are instrumental for mapping soil properties: Yang et al. (2019) demonstrated their correlation with in-situ data and possible errors in the sensitivity of backscatter intensity, changes in soil moisture, and soil surface conditions. They found a significant correlation between SAR backscatters and various soil properties (including SOC and STN) during the growing season and demonstrated that multi-temporal SAR data are useful for predicting soil chemical properties because they can capture soil properties. Also factoring in Maynard et al. (2017), we replicated their methodologies and tested them in our case study. Firstly, we examined the temporal variation of the canopy of Sentinel-2 (S2) vegetation and the soil-to-vegetation ratio using level-1 Single Look Complex (SLC) data from S1, we then built correlation models with in-situ data to predict soil properties. A total of 28 S1 and 22 S2 images were acquired during the soils' growing season.

Two sections of land were studied in an agricultural area of Po Valley (Northern Italy). Both study sites had crops in rotation (wheat/protein pea), undergoing minimal processing for five years: one section subject to Conservation Agriculture (CA), the other an Ecological Focus Area (EFA). Each area spanned three hectares. A comparison was therefore enabled for the two areas in the same environmental and cultural conditions but with different processing approaches.

Within the study area, we sampled thirty-six surveys of SOC and STN data over three years, including land use data and various soil texture data (0-10 cm - 10-30 cm). We then integrated the ground data with the SoilGrid-250 maps and LUCAS datasets, obtaining six additional samples useful for SOC (note that LUCAS does not contain information to validate NNI).

We pre-processed the SAR data utilising the ESA open-source Sentinel Application Platform (SNAP) toolbox, as depicted in the workflow in Figure-1 (Zhou et al., 2020). Finally, the S1 data were converted to dB scale with a backscatter coefficient with a resolution of 10 m. As for optical data, we downloaded L2 images, masking clouds and shadows and homologating the grid to the S1-data using a Digital Elevation Model at 10 m as a trace. We then calculated the backscatter coefficients of the VH and VV polarizations from the S1-images.

From the S2 MultiSpectral Instrument (MSI), we extracted the B2, B3, B4, B8A, B11, and B12 bands and computed the Normalized Difference Vegetation Index (NDVI), the Modified

Chlorophyll Absorption in Reflectance Index (MCARI), the Enhanced Vegetation Index (EVI), and the Soil Adjusted Total Vegetation Index (SATVI); to be used as SOC's predictors (Gholizadeh et al., 2018).

Following Zhou (2020), we processed the S1/S2 data using machine learning models to predict and model nitrogen maps. We built three models using S1, S2, S1/S2 images across Boosted Regression Trees (BRT) and Support Vector Machine (SVM) with three validation criteria: Root Mean Square Error (RMSE), coefficient of determination (R^2), and Mean Absolute Error (MAE).

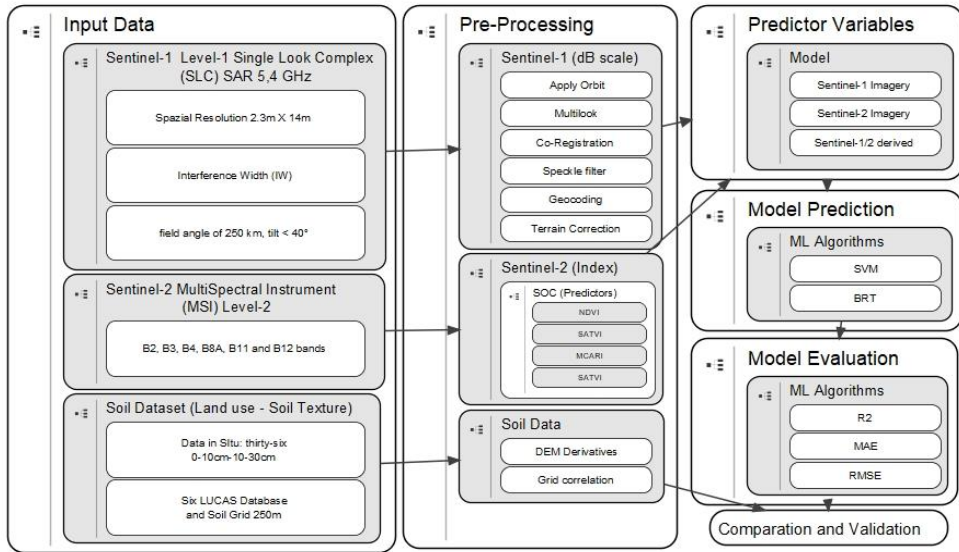


Figure 1: Summary of input data and related pre-processing workflow

The results in Table 2 confirmed the in-situ sampling data: crop rotation, applied on both areas, increases the SOC and STN levels, as foreseen by the literature. Both the EFA and the CA areas increased their nitrogen and carbon stocks over the three years. However, due to higher temporal sampling and a shorter review time, the satellite data highlight an additional dynamic, undetected by in-situ samples. Between one crop rotation and the next, the satellite can show the actual nitrogen loss, mainly due to processing, washout, and wind. For example, even if the EFA area did not undergo tillage in 2018, it suffered a substantial loss of nitrogen, unobserved by in-situ samplings, only highlighting the overall nitrogen and carbon balance, but not helping farmers to understand where to improve or identify any cause. Instead, the satellite shows what happens in a specific time frame and allows, using machine learning, to correct errors based on data and problems faced in the past. For example, in the EFA case, we could report to the farmer that the sowing process on sod was inaccurate in 2018; in addition, we could signal to postpone sowing for a week, due to very wet soil, resulting in abrupt losses due to ground runoff and wind. In the CA area, we could warn against the use

of compost in 2018, postponing it to 2019, when it was needed, resulting in a positive balance of nitrogen in 2020.

Maximum prediction accuracy was achieved for S1/S2 models, suggesting that multi-source approaches may be preferable for monitoring soil properties. Notably, SVM gave better results for CA, whereas BRT did for EFA.

Table 2: Model outputs for three years on the two case study areas, rotating wheat (grey) and protein pea (white) culture. The best correlations of satellite data with in-situ data are in green. The validation data in the two rightmost columns were obtained from the LUCAS database and in-situ data.

Modelling technique	Year	Farmland	STN						SOC						Analysis Standard Deviation	
			BRT			SVM			BRT			SVM			SOC	STN
			MAE	RMSE	R2											
Sensor																
Sentinel-1, Incident Angle +44, SL_C, IW, Descending VV/VH	2016 Balance	CA	0.26	0.33	0.09	0.22	0.28	0.08	0.21	0.28	0.08	0.22	0.34	0.05	0.34	0.22
		EFA	0.28	0.39	0.07	0.26	0.30	0.15	0.22	0.34	0.13	0.24	0.36	0.07		
		CA	0.23	0.22	0.16	0.24	0.21	0.05	0.30	0.33	0.13	0.29	0.40	0.04		
		EFA	0.29	0.28	0.12	0.25	0.22	0.06	0.32	0.35	0.14	0.26	0.41	0.06		
		CA	0.41	0.48	0.24	0.37	0.43	0.23	0.36	0.43	0.23	0.37	0.49	0.20		
		EFA	0.27	0.39	0.07	0.26	0.30	0.14	0.22	0.33	0.13	0.24	0.36	0.07		
	2018	CA	0.31	0.30	0.25	0.32	0.30	0.13	0.38	0.41	0.21	0.37	0.48	0.12	0.39	0.21
		EFA	0.31	0.30	0.14	0.27	0.24	0.08	0.34	0.37	0.16	0.28	0.43	0.10		
		CA	0.50	0.57	0.33	0.46	0.52	0.32	0.45	0.52	0.32	0.46	0.58	0.29		
		EFA	0.27	0.39	0.06	0.25	0.29	0.14	0.21	0.33	0.13	0.24	0.36	0.07		
		CA	0.31	0.30	0.25	0.32	0.30	0.14	0.38	0.41	0.21	0.37	0.48	0.13		
		EFA	0.35	0.34	0.18	0.31	0.28	0.12	0.38	0.41	0.20	0.32	0.47	0.14		
2020	CA	0.24	0.29	0.11	0.22	0.28	0.08	0.21	0.28	0.08	0.22	0.34	0.05	0.34	0.22	
	EFA	0.22	0.24	0.14	0.19	0.27	0.04	0.21	0.23	0.05	0.21	0.31	0.03			
	CA	0.21	0.21	0.17	0.24	0.19	0.04	0.31	0.32	0.12	0.31	0.35	0.06			
	EFA	0.27	0.26	0.14	0.23	0.21	0.05	0.32	0.35	0.13	0.27	0.27	0.07			
	CA	0.38	0.42	0.29	0.37	0.43	0.23	0.36	0.43	0.23	0.37	0.49	0.20			
	EFA	0.22	0.24	0.13	0.19	0.27	0.04	0.21	0.23	0.04	0.20	0.31	0.03			
Sentinel-2, L2A, No clouds, B2, B3, B4, B8A, B11 eB12	2016 Balance	CA	0.28	0.29	0.25	0.32	0.26	0.10	0.39	0.40	0.20	0.40	0.42	0.17	0.42	0.26
		EFA	0.28	0.27	0.16	0.24	0.22	0.06	0.34	0.37	0.14	0.29	0.28	0.12		
		CA	0.46	0.50	0.40	0.46	0.52	0.32	0.45	0.52	0.32	0.46	0.58	0.29		
		EFA	0.22	0.24	0.13	0.19	0.26	0.04	0.21	0.23	0.04	0.20	0.31	0.03		
		CA	0.29	0.29	0.26	0.32	0.26	0.10	0.40	0.40	0.20	0.40	0.42	0.17		
		EFA	0.32	0.31	0.20	0.28	0.26	0.10	0.38	0.41	0.18	0.33	0.31	0.16		
	2018	CA	0.19	0.21	0.19	0.21	0.21	0.10	0.19	0.24	0.19	0.22	0.28	0.21	0.34	0.22
		EFA	0.23	0.32	0.05	0.21	0.21	0.14	0.18	0.27	0.12	0.20	0.27	0.37		
		CA	0.28	0.17	0.36	0.29	0.28	0.08	0.37	0.43	0.14	0.36	0.48	0.24		
		EFA	0.34	0.23	0.32	0.30	0.29	0.09	0.39	0.45	0.15	0.33	0.49	0.26		
		CA	0.46	0.43	0.44	0.42	0.50	0.26	0.43	0.53	0.24	0.44	0.57	0.40		
		EFA	0.32	0.34	0.27	0.31	0.37	0.17	0.29	0.43	0.14	0.31	0.44	0.27		
2020	CA	0.36	0.25	0.45	0.37	0.37	0.16	0.45	0.51	0.22	0.44	0.56	0.32	0.42	0.26	
	EFA	0.36	0.25	0.34	0.32	0.31	0.11	0.41	0.47	0.17	0.25	0.51	0.30			
	CA	0.55	0.52	0.53	0.51	0.59	0.35	0.52	0.62	0.33	0.53	0.66	0.49			
	EFA	0.32	0.34	0.26	0.30	0.36	0.17	0.28	0.43	0.14	0.31	0.44	0.27			
	CA	0.36	0.25	0.45	0.37	0.37	0.17	0.45	0.51	0.22	0.44	0.56	0.33			
	EFA	0.40	0.29	0.38	0.36	0.33	0.15	0.43	0.51	0.21	0.39	0.55	0.34			

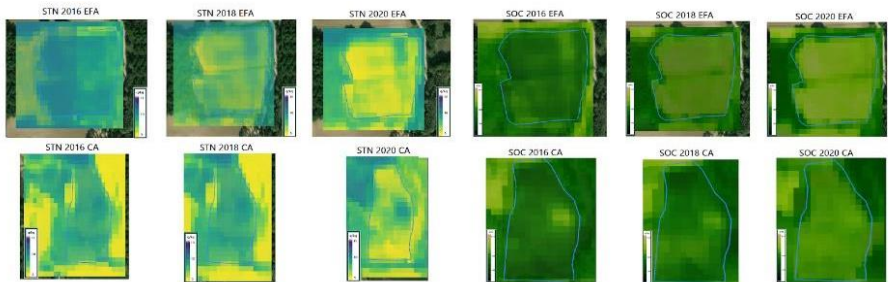


Figure 2: Annual graphical representation of STN-SOC data. The complete charts are available by [name deleted to maintain the integrity of the review process].

To produce NNI maps, we first pre-processed the satellite data to obtain biophysical variables such as: Leaf Area Index (LAI), Fraction of Vegetation Cover (FVC), and Chlorophyll Content of the Canopy (CCC). We used the biophysical processor inside SNAP to retrieve the variables: LAI_S2, CAB_S2, CCC_S2, which include all the green parts of the Green Area Index (GAI) plant. We assumed a linear relationship from the biophysical indices with the Actual quantity of Vegetable Nitrogen (PNUa) and the specific BioMass above ground (BM) to derive the Critical absorption of Vegetable Nitrogen (PNUc), according to a specific dilution curve of the crop. The methodology consists of calculating PNUa directly from CCC using linear relationships and then obtaining PNUc by estimating BM from the GAI data. NNI can then be calculated from the PNUa and PNUc estimations. We finally calculated the soil quality at the end of each phenological cycle as the sum of the total nitrogen in the crop (NNI) and in the soil (STN).

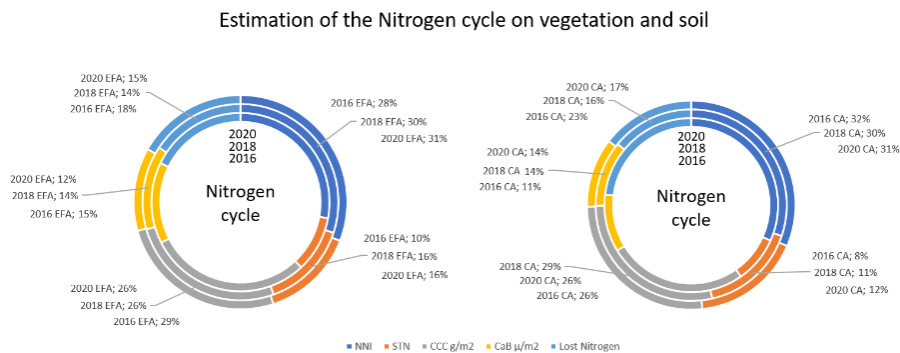


Figure 3: The graphs show an estimated “nitrogen cycle” for the CA (left) and EFA (right) areas over the three years of satellite monitoring. The cycle takes into account the nitrogen fixed by the crops, the nitrogen volatilization and the nitrogen in the soil.

In general, both fields were composed of very fertile clayey soil (67%), indicated in Table 1 by the high content of SOC (6-8%). Figure 3 highlights the importance of crop rotation, which helped to strengthen the biological, physical, and chemical components in both soils. Figures 2 and 3 suggest that no-tillage (EFA) may ensure better soil conservation than reduced tillage (CA), but the yield, vigour, and nitrogen supply of both practices are similar. The biological components are responsible for various processes such as: atmospheric nitrogen fixation, disintegration and degradation of the soil and its organic components, increase of organic substance, and simultaneously greater vigour to the crops. In conclusion, with soils richer in SOC and nitrogen, the quality of “fertile” soil improved by 6% and 4% respectively for the EFA and CA areas over the three-years period.

3 Conclusion

Although limited to the presented worked example, the nitrogen map promotes a more accurate definition of soil quality, demonstrating the relevance of nitrogen, proved to increase

the soil capacity to stock carbon. The study shows that high levels of SOC and nitrogen increase the fertility of soils, improve the production, and reduce the need for fertilizers. Moreover, by measuring the most relevant physical, chemical, and biological soil indicators, including nitrogen, the map offers an effective management tool for farmers, supporting them in implementing more sustainable practices.

Remote sensing proved to be a valuable ally in monitoring the entire phenological year for different farmlands. Satellite datasets allow access to historical data on a global scale every 6-days, and with a resolution precise enough (10 m) for monitoring the state of the soil. These datasets not only complement or enhance national and regional official data sources, especially when the latter are missing or incomplete, but also validate them due to satellites' time/location accuracy. The great advantage is having access to precise, historical, and locally calibrated data on a frequent schedule, which enables predicting the soil attitude to a specific treatment, supporting decision-making and management tools for farmers, such as the nitrogen map. In the future, we plan to present this tool to governments, to support countries in meeting their commitments in monitoring and reporting key soil quality indicators.

As shown in Table 1, several SDGs' targets and indicators are heavily interlinked with nitrogen functions, therefore should be integrated with its indicators to obtain a comprehensive overview of SOC stocks processes. By including one or more nitrogen indicators, the framework for the implementation of soil-related SDGs would better address the complexity of the soil ecosystem and its dynamics, facilitating the achievement and consolidation of Agenda 2030 both for farmers and policy makers. The former would be supported in applying sustainable practices; the latter would create more localised policies based on calibrated thresholds and indicators of soil quality.

References

- Doran, J.W., Parkin, T.B., 1996. Quantitative Indicators of Soil Quality: A Minimum Data Set. in: *Methods for Assessing Soil Quality*, (Eds.) J.W. Doran, A.J. Jones, Soil Science Society of America, pp. 25-37.
- Else K., Bünenmann et al., 2016. Concepts and indicators of soil quality – a review. *Interactive Soil Quality Assessment in Europe and China for Agricultural Productivity and Environmental Resilience - iSQAPER Project (GA n° 635750)*.
- European Commission. 2006. Proposal for a Directive of the European Parliament and of the Council establishing a framework for the protection of soil and amending Directive 2004/35/EC /* COM/2006/0232 final - COD 2006/0086 */
- Gholizadeh, H., Gamon, J., Townsend, P., Zyguelbaum, A., Helzer, C., Hmimina, G., Yu, R., Moore, R., Schweiger, A. and Cavender-Bares, J., 2019. Detecting prairie biodiversity with airborne remote sensing. *Remote Sensing of Environment*, 221, pp.38-49.
- Global Mechanism of the UNCCD, 2016. ‘Achieving Land Degradation Neutrality at the Country Level. Building Blocks for LDN Target Setting’.
- Lausch, A., et al., 2019. Linking Remote Sensing and Geodiversity and Their Traits Relevant to Biodiversity—Part I: Soil Characteristics. *Remote Sensing*, 11(20), p.2356.
- Maynard, J.J.; Levi, M.R., 2017. Hyper-temporal remote sensing for digital soil mapping: Characterizing soil-vegetation response to climatic variability. *Geoderma*, 285, 94–109.
- Nortcliff, S., 2002. Standardisation of soil quality attributes. *Agriculture Ecosystems & Environment*, 88(2), 161-168.
- Tóth, G., Hermann, T., da Silva, M. and Montanarella, L., 2018. Monitoring soil for sustainable development and land degradation neutrality. *Environmental Monitoring and Assessment*, 190(2).
- Vreugdenhil, M., Wagner, W., Bauer-Marschallinger, B., Pfeil, I., Teubner, I., Rüdiger, C. and Strauss, P., 2021. Sensitivity of Sentinel-1 Backscatter to Vegetation Dynamics: An Austrian Case Study.
- Yang, R.-M.; Guo, W.-W., 2019. Using time-series Sentinel-1 data for soil prediction on invaded coastal wetlands. *Environ. Monit. Assess*, 191, 462
- Zhou, T., Geng, Y., Chen, J., Pan, J., Haase, D. and Lausch, A., 2020. High-resolution digital mapping of soil organic carbon and soil total nitrogen using DEM derivatives, Sentinel-1 and Sentinel-2 data based on machine learning algorithms. *Science of The Total Environment*, 729, p.138244.

Dynamic Workflow Engine of Atmospheric Big Remote Sensing Data Processing Powered by Heterogeneous Platform for High Performance Computing

Sheng Zhang¹, Yong Xue¹ and Xiran Zhou¹

¹China University of Mining and Technology

Abstract

The development of big remote sensing data related technologies and applications poses a big challenge that massive computing capability is needed to support big data processing. In order to solve this challenge, this paper proposes an architecture of heterogeneous platform of high performance computing, which employs the computer hardware resources to improve the efficiency of big remote sensing data processing by optimizing scheduling strategies and designing high-performance algorithms. Furthermore, the proposed platform can dynamically incorporated with a workflow engine regarding big remote sensing data processing. These algorithms are modular to meet the flexible combination of different processes.

Keywords: high performance computing (HPC), heterogeneous computing platform, workflow engine, atmospheric big remote sensing data

1 Introduction

Currently, the ability to generate remote sensing data has achieved an unprecedented level. We have entered an era of big remote sensing data. Big remote sensing data are attracting more and more attentions from government officers, commercial investment planners, academic researchers, et al. (Liu et al., 2018).

Based on the requirements of big data technology and application, the methodological framework for multi-scale, long-term, and multi-source atmospheric remote sensing data processing is pressing needed. These framework generally include data preprocessing, spatial processing, denoising, fusion, inversion, classification, interpretation and so on (Ma et al., 2014). These complex, heterogeneous and massive computing tasks could generate a huge cost of time consuming and computing load. The traditional systems for remote sensing data processing can't meet the needs of efficient processing on atmospheric big remote sensing data (Xu et al., 2020).

With the development of parallel computing, distributed computing, grid computing, cluster computing and cloud computing technology, a number of high performance computing

(HPC) for remote sensing data big have emerged, which can significantly improve the efficiency of remote sensing data processing. However, there are still some challenges, including how to make rational using of heterogeneous computing resources, and how to access data and optimize task scheduling to reach the full utilization of computing power (Chi et al., 2016).

In this paper, the distributed computing resources and storage resources in atmospheric big remote sensing data computing are optimized by our proposed dynamic workflow engine, which can improve the logic dependent relation of data in different processing processes. In addition, for the specific needs of atmospheric big remote sensing data processing, we developed a parallel processing algorithm suitable for different GPU hardware. Thirdly, we build an extensible model library for atmospheric big remote sensing data processing.

2 Related Works

For big remote sensing data processing, many researchers proposed high-performance computing method based on GPU, and improved resource scheduling strategy based on workflow.

Jia Liu et al. (2015) proposed two high-performance computing architectures for aerosol optical depth (AOD) retrieval: one is multi-core processor architecture, and the other is GPU architecture, they are all based on OpenMP and CUDA Programming environment. According to the characteristics of orthorectification algorithm of remote sensing image, DAI. Chenguang et al. (2011) proposed a fast GPU-CPU collaborative processing algorithm based on CUDA, which realized the parallel processing of image resampling based on single GPU and multi-GPU. Ma Yan et al. (2015) proposed a parallel processing model for remote sensing image based on GPU, and established a set of parallel programming template which provides a simpler and more effective method for programmers to write parallel remote sensing image processing algorithm. Yang Xue et al. (2018) proposed a general, fast and effective denoising method, which combines Huber function and GPU adaptive partition technology, after analyzing the Markov random field prior model method. This method significantly improves the computational efficiency of processing massive remote sensing images. Wang Z et al. (2011) proposed a method to manage MODIS sensor data processing based on workflow engine, which can configure high-performance computing resources. It reduces the execution cost by using the existing program modules and distributed resources, and finally helps users manage and process a large number of remote sensing data through workflow. Based on Web services and Activiti 5.0 workflow engine, Fang Huang et al. (2020) built a high-performance computing service platform, which reduced the platform discrepancy between different high-performance exchange systems. This platform simplifies the operation of complex geospatial information processing applications in the field of high-performance geographic computing and realizes the efficient processing of massive data.

Overall, big remote sensing data computing and processing has accumulated some research results. However, in these achievements, the high-performance computing for atmospheric big remote sensing data processing is mainly to solve a specific problem, and there are still

deficiencies in modularization, integration ability, distributed scheduling, process optimization, etc., which cannot make full use of high-performance computing resources.

3 System Framework Design

The dynamic workflow customization technology proposed in this paper is based on a big data platform with 5-layer architecture (Fig. 1), which is composed of scheduling layer, hardware layer, data layer, algorithm layer, application layer.

Based on the workflow engine, the scheduling layer can realize the dynamic customization of remote sensing data processing process, the allocation of data resources, computing resources and storage resources, and solves the problem of dependence between different process data through the communication mechanism between different processing processes, so as to optimize the scheduling strategy. Therefore, the whole big remote sensing data processing is driven by the scheduling layer. The scheduling layer includes two key modules: task launcher and task scheduler. According to the workflow in terms of data processing designed by users, we design the task launcher to process each sub-task in parallel or serial order. In addition, we design the task scheduler for deciding the partition scheme of the whole task, to allocate every sub-task to a distributed computing node, and receive processing results.

The hardware layer provides storage and computing resources for the platform, and can dynamically add new computing nodes and new storage devices. Conversely, new storage and computing hardware resources need to be registered through the platform which dynamically monitors the computing resources and storage resources.

The data layer includes two kinds of data resources: remote sensing data and thematic data. Remote sensing data includes original data, process data and result data. Thematic data is used to assist remote sensing data processing, such as administrative boundaries, coordinate transformation parameters, digital high-range model data needed for orthorectification, etc. The data layer can be updated dynamically, and the first addition of data needs to be registered by providing metadata information of scope, type and time.

The algorithm layer is the program library related to atmospheric remote sensing data processing, including reading and writing, format conversion, projection, fusion, correction, splicing, cutting, inversion and other programs. The flexible customization of processing flow is realized through modular program, and other program tools are added dynamically through registration to expand the platform functions. According to the characteristics of data processing, algorithm layer tools support different GPU hardware.

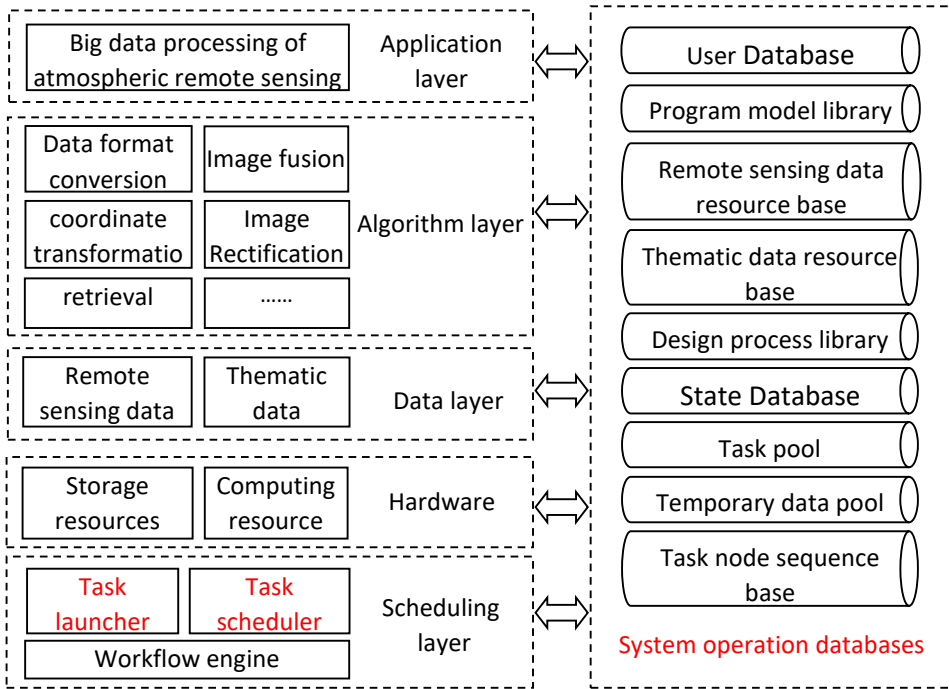


Figure 1: Architecture of the system framework

The application layer is oriented to professional users, customizes the remote sensing data processing flow through the visual window, configures the required data resources, computing resources and storage resources, makes full use of the distributed computing and storage resources, and optimizes the operation strategy by designing the processing flow and setting the interdependence between the processing flows.

The layers in the system mutually transfers information and exchanges data through nine databases. Users can customize and submit their data processing flow through the process designer. Then, the task scheduler automatically completes the task partition strategy according to the computing and storage resources, and distributes the partitined sub-task to each computing node. For each computing node, we design the task initiator to process its assigned task based on users' cunstermized processing flow, and transform the result to the master node. Finally, the task scheduler combines the results from each distributed computing nodes into the final one. Specifically, if the processing breaks unexpectedly due to an abnormal calculation node or unreasonable process design, we create the breakpoint continuation module to ensure the processing would still continue to reaching the completed point.

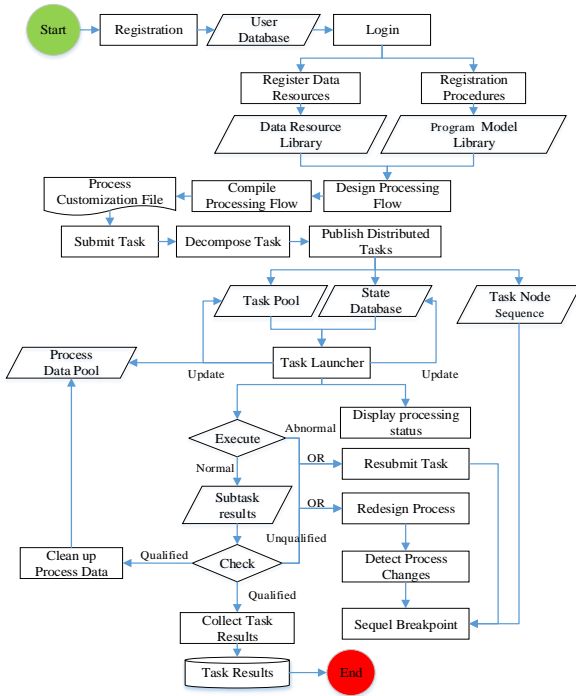


Figure 2: Task workflow procedure

4 Experiments

The experimental environment is shown in Figure 3, which is developed by six personal including one master node (management node) and five general computing nodes.

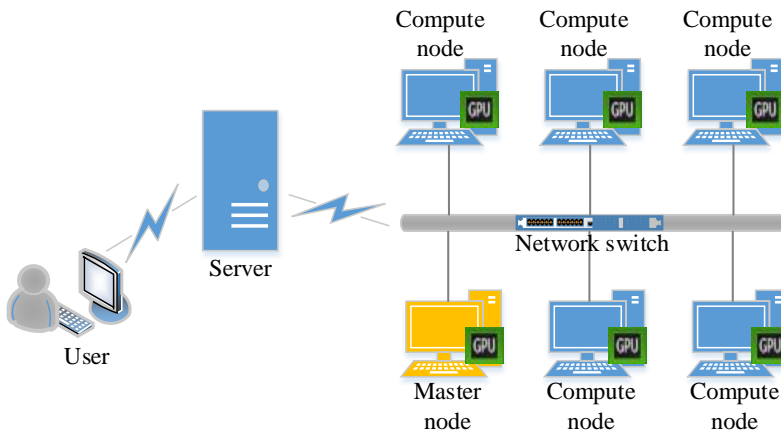


Figure 3: Supporting environment

Moreover, the hardware details of these six nodes are shown in Table 1.

Table 1: Configuration of the testing machines

Hardware category	Master node	Compute node
CPU Processor	Intel Core i7-10700F(2.90GHz ,16 CPUs)	Intel Core i7-10700F(2.90GHz ,16 CPUs)
RAM	16GB	8GB
GPU Processor	NVIDIA GeForce GTX 1660 SUPER(6GB)	NVIDIA GeForce GTX 1660 SUPER(6GB)
Hard disk	4TB(HDD)+1TB(SSD)	1TB(SSD)

The experiment regarding data processing is designed for the retrieval of satellite-based aerosol optical depth (AOD) data product. The data range is: 35°E -150°E (longitude) and 0°N -60°N (latitude). The satellite data is MODIS, and the data phase is April 9, 2017. We select the SRAP algorithm proposed by Yong Xue et al. (2014) as the AOD retrieval algorithm. The spatial resolution of the AOD retrieval result is 1KM.

Figure 4 shows the workflow designed for AOD retrieval with SRAP algorithm. The input data includes M*D02, M*D03 and M*D04_L2 (* stands for O or Y, which respectively refers to the Terra and Aqua satellite sensor).

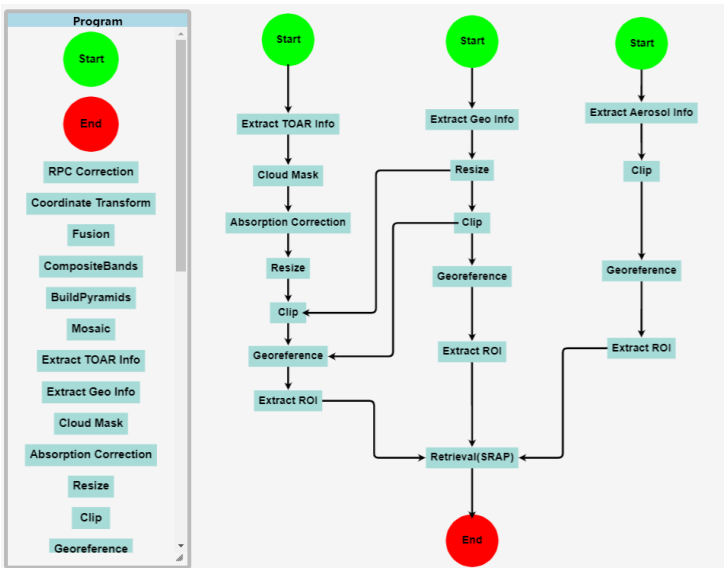


Figure 4: Workflow design of AOD retrieval

Table 2 shows the statistics of processing efficiency, which compares the method by a single machine processing and the proposed method.

Table 2: Statistics of processing efficiency

Satellite data	Ground resolution	Number	Data size	Processing time of Single machine			Processing time of this paper		
				Preprocessing	Retrieval	Total	Data interaction	Calculation	Total
M*D021KM	1km	61	8.7GB	153min					
M*D03	1km	61	2GB	5min	381	576	36 min	72	108
M*D04_L2	10km	61	156MB	37min	min	min		min	min

Compared with the traditional atmospheric remote sensing big data computing method, the previous test work proves that the platform proposed in this paper has advantages in the following aspects: Firstly, in the aspect of data processing systematicness, different processing tasks can be customized through this platform, which makes the integration of functions more convenient, systematic and processing content more flexible; Secondly, in terms of task computing efficiency, the overall efficiency is improved about 5 times.

5 Conclusions

In this paper, the computational efficiency of atmospheric big remote sensing data processing was improved by optimizing the scheduling strategy by the dynamic workflow and the parallel algorithm based on GPU. A variety of data processing modules were integrated into a platform to decrease the workload of big data platform, and facilitate the collaboration and communication among researchers in different disciplines. We focused on designing the workflow-driven modular processing and dynamic scaling to allow researchers for customizing their own developed program in the high performance computing.

In the future, the platform could be improved in terms of quality control, fault tolerance and so on. Due to the heterogeneous resources and poor quality of atmospheric remote sensing data, some data processing links might have an issue, resulting in reducing the operating effects of the overall data processing. Therefore, we believe that the improvement of fault tolerance and robustness, and the building of the front-end and process quality monitoring function are significance of developing the platform. We hope our work can facilitate the research regarding heterogeneous computing such as resource expansion, functional expansion, process expansion, etc.

References

- Liu, P., Di, L., Du, Q., & Wang, L. (2018). Remote sensing big data: Theory, methods and applications. *Remote Sensing*, 10(5). doi:10.3390/rs10050711.
- Ma, Y., Chen, L., Liu, P., & Lu, K. (2014). Parallel programming templates for remote sensing image processing on gpu architectures: Design and implementation. *Computing*, 98(1-2), 7-33. doi:10.1007/s00607-014-0392-y.
- Xu, C., Du, X., Yan, Z., & Fan, X. (2020). Scienceearth: A big data platform for remote sensing data processing. *Remote Sensing*, 12(4). doi:10.3390/rs12040607.
- Chi, M., Plaza, A., Benediktsson, J. A., Sun, Z., Shen, J., & Zhu, Y. (2016). Big data for remote sensing: Challenges and opportunities. *Proceedings of the IEEE*, 104(11), 2207-2219. doi:10.1109/jproc.2016.2598228.
- Liu, J., Feld, D., Xue, Y., Garcke, J., & Soddemann, T. (2015). Multicore processors and graphics processing unit accelerators for parallel retrieval of aerosol optical depth from satellite data: Implementation, performance, and energy efficiency. *IEEE Journal of Selected Topics in Applied Earth Observations and Remote Sensing*, 8(5), 2306-2317. doi:10.1109/jstars.2015.2438893.
- DAI C., & YANG J. (2011). Research on Orthorectification of Remote Sensing Images Using GPU-CPU Cooperative Processing.
- Ma, Y., Wu, H., Wang, L., Huang, B., Ranjan, R., Zomaya, A., & Jie, W. (2015). Remote sensing big data computing: Challenges and opportunities. *Future Generation Computer Systems*, 51, 47-60. doi:10.1016/j.future.2014.10.029.
- Yang, X., Li, F., Xin, L., Wang, C., Wang, XY., & Chang, X. (2018). Destriping methods for high resolution satellite multispectral remote sensing image based on GPU adaptive partitioning technology. *Conference on Remote Sensing for Agriculture, Ecosystems, and Hydrology XX*. doi:10.1117/12.2325311.
- Wang, Z., King, E., Smith, G., Bellgard, M., Broomhall, M., Chedzey, H., Fearn, P., Garcia, R., Hunter, A., Lynch, M., & Shibeci, D. (2011). RS-YABI: A workflow system for Remote Sensing Processing in AusCover. *MSSANZ 19th Biennial Congress on Modelling and Simulation (MODSIM)*, 1167-1173.
- Huang, F., Yang, H., Tao, J., & Zhu, Q. (2020). Universal workflow-based high performance geo-computation service chain platform. *Big Earth Data*, 4(4), 409-434. doi:10.1080/20964471.2020.1776201.
- Levin, N., Ali, S., Crandall, D., & Kark, S. (2019). World heritage in danger: Big data and remote sensing can help protect sites in conflict zones. *Global Environmental Change*, 55, 97-104. doi:10.1016/j.gloenvcha.2019.02.001.
- Xue, Y., He, X., Xu, H., Guang, J., Guo, J., & Mei, L. (2014). China collection 2.0: The aerosol optical depth dataset from the synergetic retrieval of aerosol properties algorithm. *Atmospheric Environment*, 95, 45-58. doi:10.1016/j.atmosenv.2014.06.019.

Energy from Biomass: Assessing Sustainability by Geoinformation Technology

Manuela Hirschmugl^{1,2}, Carina Sobe², Lorenzo Traverso³, David Cifuentes⁴, Alfonso Calera⁴, Cosette Khawaja⁵ and Marco Colangeli⁶

¹University of Graz, Austria

²Joanneum Research, Austria

³University of Tuscia, Italy

⁴University of Castilla-La Mancha, Spain

⁵WIP Renewable Energies, Germany

⁶IDEA2020

Abstract

Sustainable Development Goal (SDG) target 7.2 requests a substantial increase in the share of renewable energy in the global energy mix by 2030. Renewable energy production in all sectors has to be evaluated for its contribution to reach this target. Biomass for energy production has gained a bad reputation over the past years due to the “food versus fuel” debate or reported unsustainable practices. The BIOPLAT-EU project is employing geoinformation technologies combined with sustainability and economic expertise to more accurately evaluate the sustainability of bioenergy value chains. The project has three main parts: first, the generation of a pan-European map of marginal, underutilized, and contaminated (MUC) lands potentially usable for bioenergy production. This is realized by employing remote sensing time series, existing Copernicus, and other spatial data sets. Second, the generation of a web-based geographical information system (GIS) connecting the MUC lands with other important information sources necessary to assess sustainability. Third, the sustainability assessment includes not only typical social and environmental sustainability indicators like soil, water, or greenhouse gas emissions, but also economic sustainability indicators like employment. Current financial barriers are addressed by integrating innovative financing solutions considering SDG target 12.A.

Keywords: energy, sustainable production, biomass supply, time series, webGIS

1 Background and Introduction

Target 7.2 of the Sustainable Development Goals (SDGs) requests a substantial increase in the share of renewable energy in the global energy mix by 2030. Nevertheless, energy demand is growing in virtually all industrialized and even more so, in emerging economies worldwide (Capuano, 2020). Renewable energy production in all sectors has to be evaluated for its contribution to reach target 7.2. Sustainable feedstock supply is expected to play a central and crucial role not only for the production of biofuels (EC 2018/2001), but also for the

production of green hydrogen through innovative pre-treatment processes or pyrolysis oil production. However, the use of agricultural crops for energy production has gained a bad reputation over the past years due to the “food versus fuel” debate, and also due to reported unsustainable practices (Humpenöder et al, 2018; Robledo et al. 2017). This led to the adoption of the European Union (EU) Directive EC 2015/1513 to reduce indirect land use change for biofuels and bioliquids (EC 2015/1513).

In the last decade, many scientific studies have demonstrated how bioenergy crops have the potential to be grown profitably on surfaces of land which are currently marginal, underutilized, and/or contaminated (MUC). Additionally, studies also showed that MUC lands can be found in several EU and neighbouring countries (Alcantara et al. 2013, Estel et al. 2015, Lieskovský et al. 2015, Szatmári et al. 2018). Using these areas for bioenergy purposes could offer a source of income to local populations (Traverso et al, 2020) while contributing to achieving the targets of the new Renewable Energy Directive (RED II). Using MUC lands for bioenergy production contributes to SDG target 7.2 and, through the calculation of greenhouse gas (GHG) emissions within the sustainability assessment, also supports SDG 13.2. Intending to promote the market uptake of sustainable bioenergy in Europe using MUC lands, the BIOPLAT-EU project is employing geoinformation technologies combined with sustainability and economic expertise to more accurately evaluate the sustainability of bioenergy value chains. A database of MUC lands is compiled, which integrates different existing data sets, as well as results of a remote sensing mapping exercise based on satellite image time series. In parallel, a concept is developed, which permits the sustainability assessment of a selected bioenergy value chain from an economic, environmental, and social perspective. Both, the MUC land database and the sustainability assessment concept are integrated and implemented within a webGIS system.

2 Data and Workflow

A number of different data sets are used in this study in the various steps and for various purposes. Table 1 lists these data sets together with the source and usage in BIOPLAT-EU. The overall workflow is shown in Figure 1. It depicts how the individual data sets from Table 1 are being combined.

Table 1: Input data, source and usage in the study

Input data	Source	Usage
Sentinel-2 time series data	Copernicus/European Space Agency, GEE	Classification of underutilized lands
Landsat 8 time series data	NASA, GEE	
Copernicus High resolution layers (HRL)	Copernicus: land.copernicus.eu	Generation of training data for utilized land categories; Partly used for elimination of used land; Input for scenario projection
Corine land cover data (CLC)		
Ukrainian Landuse data (= national LCLU data)	Myroniuk (2020)	
Land Use/Cover Area frame statistical Survey (LUCAS) point data	LUCAS (2015)	Generation of training & validation data for underutilized land categories
Google Earth very high resolution (VHR) image data	Google Earth	
OpenStreetMap (OSM)	https://download.geofabrik.de/	Elimination settlements
Shuttle Radar Topography Mission digital elevation model (SRTM DTM) from NASA	www2.jpl.nasa.gov/srtm/	Elimination of steep slopes for identified MUC lands
Natura2000 layer of the European Environmental Agency	natura2000.eea.europa.eu/	Elimination of protected areas
Heavy metal concentrations in top soils	JRC, Toth et al. 2016	Input for the identification of contaminated lands
National contaminated land data sets	National sources	
Global Agricultural Ecological Zone (GAEZ) layers	Food and Agricultural Organization (FAO)	Sustainability assessment
Precipitation data	Copernicus: climate.copernicus.eu	Sustainability assessment
Local administrative units (LAU)	EUROSTAT, Ukrainian cadastre	Geometric extent of LAUs for scenario projections
Social and economic statistical data per administrative unit	EUROSTAT, Ukrainian statistical office	Input for scenario projections

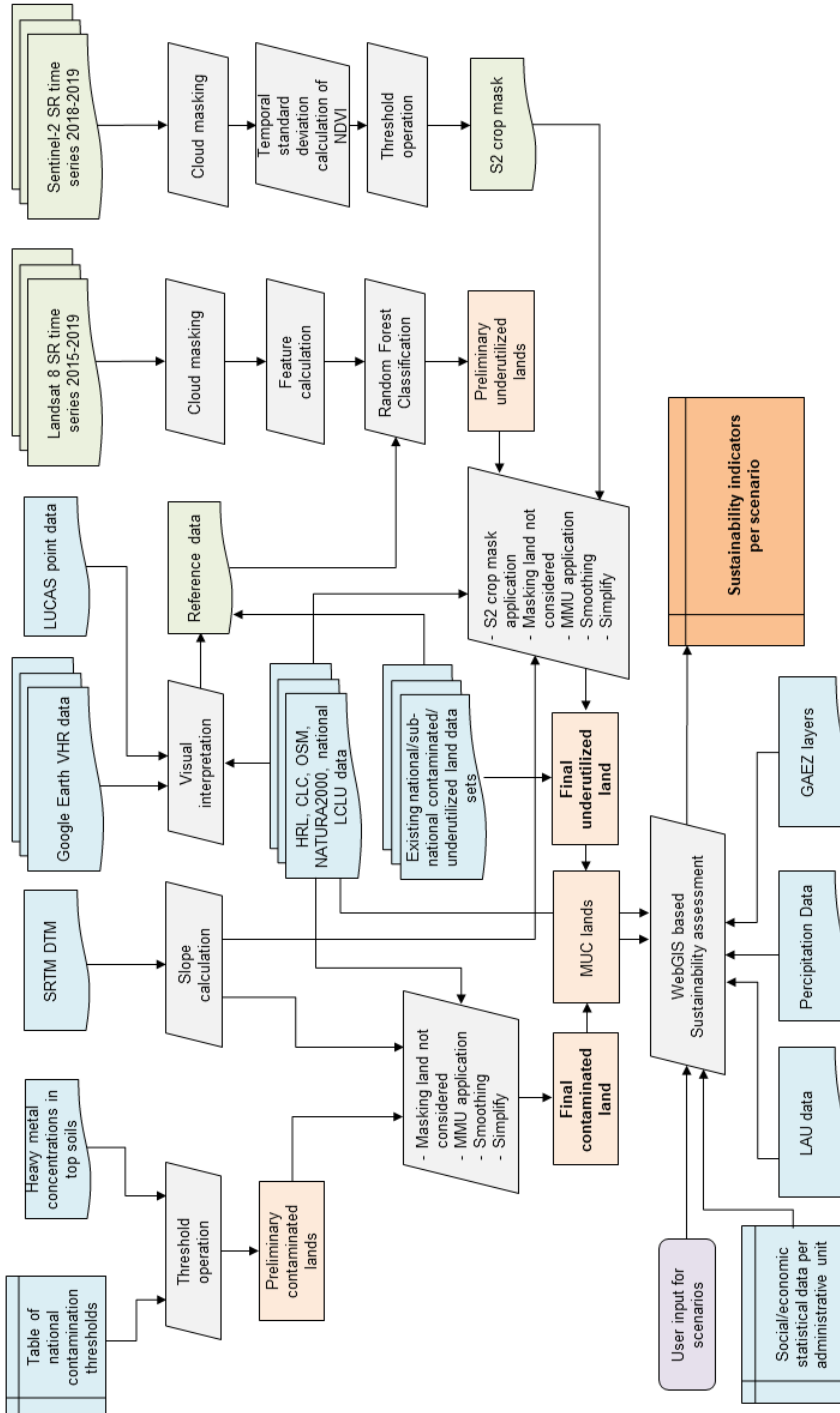


Figure 1: Overall workflow

3 The Spatial Solution

3.1 Generation of a pan-European data base of MUC lands

Marginal lands are difficult to define, as marginality can be understood in different ways: spatially, economically, or in terms of soil quality for example. Due to the “food versus fuel” debate, the project’s precondition was set to consider only land which is currently not used or not usable (due to contamination) for food production. Analyses of existing databases of marginal lands (e.g. results from other projects such as SEEMLA or MAGIC) revealed that marginal lands are often being used for food production despite their marginality. Examples include traditional agricultural practices, of which areas of olive cultivation in Southern Italy are a significant example in terms of expanse. To avoid controversial discussions, it was decided to include only marginal lands, which are not cultivated. This characteristic of “no utility” would then make those lands fall in the underutilized lands category which are considered as lands that had no signs of human activity (including grazing) in the last five years.

For the identification of **underutilized land**, the envisaged wall-to-wall, continental-wide detection can only be achieved at reasonable effort by remote sensing approaches. Landsat 8 data for 2014 – 2019 was used to fulfil the five-year requirement and was complemented by Sentinel-2 data from 2018 and 2019. The analysis was carried out in a stratified manner by biogeographical region and country using Google Earth Engine (GEE). GEE is an online cloud-based processing engine for geospatial analyses, available free of charge for research projects (Gorelick et al, 2017). Separate assessments for each biogeographical region are needed, as underutilized lands show significantly different properties depending on their climatic, elevation, and soil properties. The employed random forest classifier requires training data of underutilized and utilized lands in each region. The utilized training data was generated from sampling within the Copernicus High-resolution layers (HRL) and Corine Land Cover data (CLC). The underutilized training data was generated based on a multitemporal assessment of areas within Google Earth using the LUCAS points to pinpoint possible locations. All details on the processing can be found in Hirschmugl et al (2021). The classification suggests that a total of 5.3 million ha of underutilized land in Europe are potentially available for agricultural bioenergy production. The results show an overall accuracy of more than 85 %, with a confidence interval of 1.55 % at the 95% confidence level.

For the identification of **contaminated land**, the initial attempt was to collect national data and aggregate them into a pan-European map. Although most member states report statistics on contaminated lands (shares of total land), many countries either do not have or do not share the underlying spatial data sets due to legal restrictions. In many cases (e.g. Hungary), only point-wise data is available. In other countries, such as Romania, the official contaminated land layer is still under evaluation and thus, not yet released. These limitations led us to the second option: a top-down approach using an EU-wide map of contaminations, which we derived from the Joint Research Centre (JRC) in the “Heavy metals in soils” product based on LUCAS 2009 heavy metal (HM) data (Toth et al., 2016). This map (available at <https://esdac.jrc.ec.europa.eu/content/maps-heavy-metals-soils-eu-based-lucas-2009-hm-data-0>) has a spatial resolution of 1x1 km and covers 27 EU member states (not including Croatia). Maps of nine different heavy metals are provided: Arsenic, Cadmium, Chromium,

Cobalt, Copper, Mercury, Nickel, Lead, Manganese, and Antimony. For each of the heavy metals, thresholds had to be defined to separate contaminated from non-contaminated soils. If a threshold is exceeded, the use of this soil for food and fodder are not allowed/advisable. The relevant EU directive (Council of the European Union, 2002) gives only ranges of values rather than a specific threshold value. Previous studies (Toth et al., 2016) used Finnish thresholds for the whole of Europe, as these thresholds are well in line with the EU-directive. In our study, we collected national thresholds and applied them to the relevant country's territory completing with the above mentioned Finnish thresholds for countries without national thresholds. It is clear, that the resulting data set is not as accurate, nor as detailed as potential national maps, however, it was the only feasible option to produce a pan-European layer. In addition, for countries with available national maps, such as Italy, we included both layers. Figure 2 shows the resulting map of underutilized and contaminated lands for Europe. Please note, that no contaminated land information is available for Ukraine, as the above mentioned JRC data is not available for Ukraine. Further, contamination due to any other agents than the heavy metals mentioned above, like for example Cobalt-60 in Ukraine caused by the Chernobyl accident, was not included.

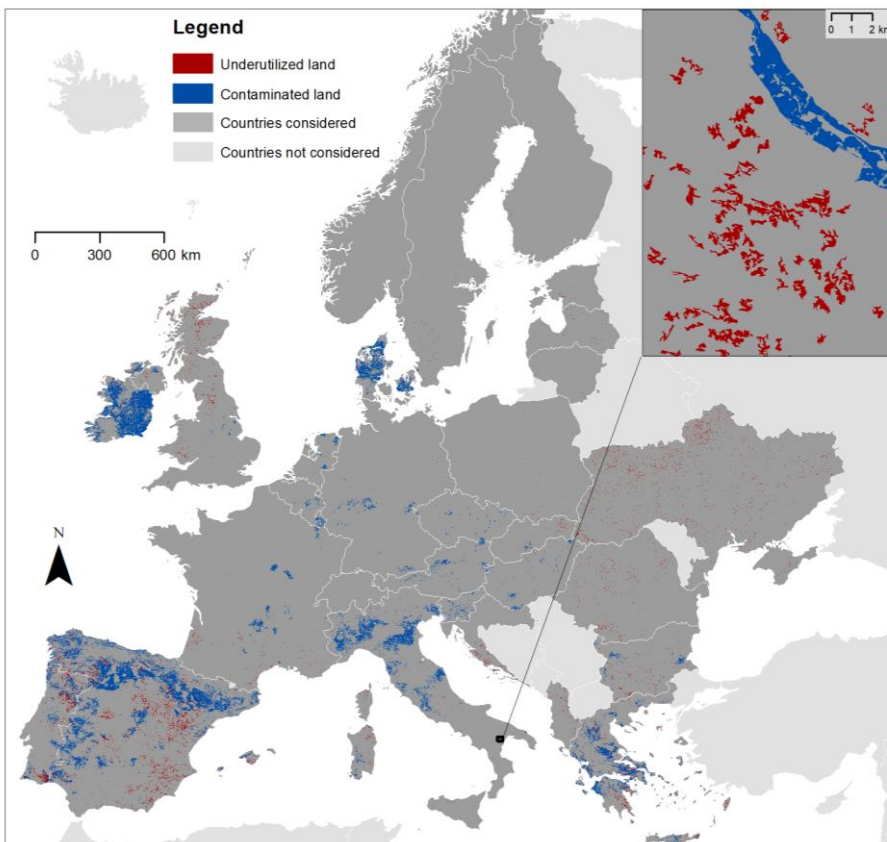


Figure 2: Pan-European map of underutilized and contaminated lands (country boundaries may be disputed)

3.2 Development of a webGIS platform for highly automated sustainability analysis

Sustainability assessment tools provide a better understanding of the three pillars of sustainability (economic, environmental and social) by conceptualizing and explaining the relationships and dependencies among them, aiming to help decision-makers to provide along more sustainable solutions. The methodology is described in detail in Traverso et al (2020). In these contexts, a suite of effective indicators and institutional frameworks were developed for assessing and measuring the sustainable production of bioenergy. They are intended to provide stakeholders with a set of analytical tools for policy decision making, management strategies' design, and alternative value chains comparative analyses. The most widely known and recognized tools for supporting the decision-making process include indicators proposed by the Global Bioenergy Partnership (GBEP, 2018), the Roundtable on Sustainable Biomaterials (2021), and others (Pulighe et al, 2019). The sustainability assessment is structured as the analysis of the difference in impacts caused by two (or more) projections: baseline vs target scenarios projections. A baseline scenario is projected into the future to present the foreseeable development of each selected sustainability indicator given the current circumstances and conditions, thus without the existence of the bioenergy value chain studied. This first projection, called "baseline", will consist of offsetting the current environmental, social and techno-economic features into the future for a reference period defined as relevant. For instance, the baseline scenario of the soil quality indicator is described as the trajectory that the specific soil quality parameter will have if no action is taken. The timeframe has to be explicitly set at the beginning of each analysis and it must be consistent for all scenario projections. The second projection, called "target", consists of the same indicators and their (different) behaviour and development if a new bioenergy value chain would be in place. More details can be found in Traverso et al (2020). These assessments are usually based on a lot of location-specific data, which is difficult to access. In order to move from such case-by-case assessment to an automated process, a webGIS system has been built including basic data available for the whole area of interest (i.e. Europe and Ukraine) either as fixed tables (such as the greenhouse gas emissions from the use of petrol versus other biomass sources), or as geospatial data sets. The latter included a layer of local administrative units including attributes on population, gross domestic product (GDP), different employment figures, etc. collected from various sources, mainly EUROSTAT and national statistics (see Table 1). Furthermore, several layers are needed to provide information on suitability for all feedstock types considered in the system. For this purpose, the Global Agricultural Ecological Zone (GAEZ) layers were employed (IIASA/FAO, 2012). This part is needed to assess the potential yield of different crops in a specific area.

Figure 3 shows the overall scheme of the sustainability assessment in the webGIS solution with the backend covering the MUC maps and all other geospatial and tabular data mentioned above, and the frontend with the user interaction. The user interaction includes inputs for location and scenarios selection and output of the final results, which are the assessments of the sustainability indicators for the selected scenarios. There are two levels of users: the standard user, and the advanced user. For advanced users (upon registration), the tool will even allow an in-depth analysis by adjusting pre-defined settings and integrating own values and results in the sustainability assessment. The webGIS tool is currently under finalization

and will be made available through the BIOPLAT-EU website (www.bioplat.eu) in July 2021 with fine-tuning until the end of the project in October 2021.

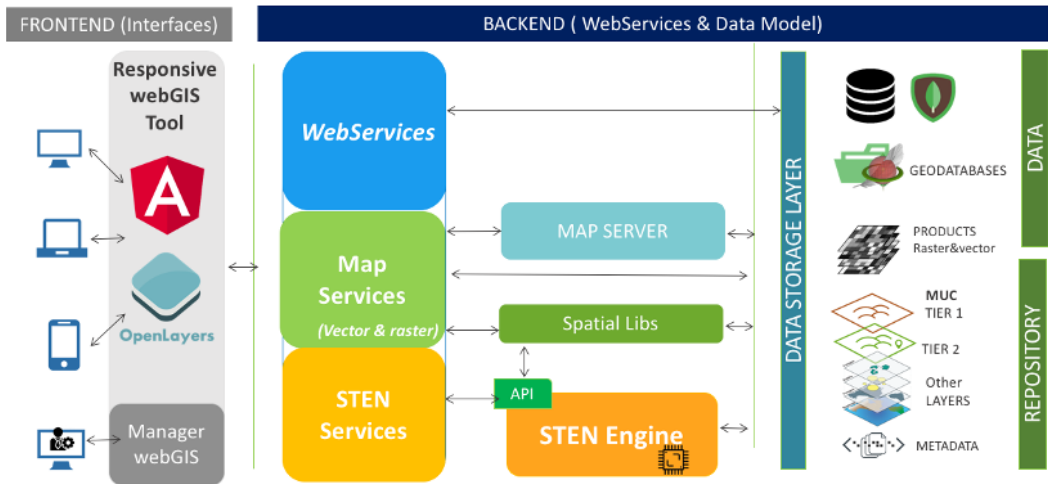


Figure 3: Set-up of the webGIS tool for automated sustainability assessment (STEN stands for the sustainability assessment tool used)

4 Conclusion & Outlook

This study employed geoinformation technologies combined with sustainability and economic expertise to more accurately evaluate the sustainability of bioenergy value chains. The proposed solution facilitates access to sustainability assessment tools by providing necessary input data and algorithms. The presented webGIS tool, which assesses the sustainability of different bioenergy value chains on selected MUC lands in an automated manner, represents a major step forward towards supporting data-based decisions. It also improves the overall understanding of existing dependencies among different indicators in an easily accessible way. Further, it will clearly help to improve indicator 7.2.1: “share of renewable energy in the total final energy consumption” by providing this tool for sustainability assessment together with measures to remove existing barriers in bioenergy production. By providing free access to this webGIS tool BIOPLAT-EU also fosters SDG target 12.2: “By 2030, achieve the sustainable management and efficient use of natural resources”. In order to potentially roll out the solution to areas outside Europe in future, existing barriers, such as lack of appropriate financing options, must be addressed. Based on the webGIS solution described above, innovative financing solutions can be developed supporting SDG indicator 12.a.2: “International financial flows to developing countries in support of clean energy research and development and renewable energy production, including in hybrid systems”. Sustainable energy, including research and development, challenges in many aspects of finance theory following capital asset pricing models (Sharpe, 1964) and the role development finance institutions play in including the private sector in the energy transition in developing countries. New business models will emerge with a more balanced approach between public and private sectors with often the

public sector as initial mover in making grants available in breakthrough innovations in the biofuels and biorefineries sector as witnessed in the launch of the Innovation Fund, and through recent calls for proposals for sustainable energy projects at early technology readiness levels between EU and Africa (26th Jan 2021), and between EU and India (Dec 2020).

References

- Alcantara, C.; Kuemmerle, T.; Baumann, M.; Bragina, E.V.; Griffiths, P.; Hostert, P.; Knorn, J.; Müller, D.; Prishchepov, A.V.; Schierhorn, F.; et al. Mapping the Extent of Abandoned Farmland in Central and Eastern Europe Using MODIS Time Series Satellite Data. *Environ. Res. Lett.* 2013, 8, 035035.
- Capuano, L. (2020). *S. International Energy Outlook 2020 (IEO2020)*. U.S. Energy Information Administration, available at <https://www.eia.gov/outlooks/ieo/pdf/ieo2020.pdf> (last accessed 12.03.2021)
- EC 2018/2001: Directive of the European Parliament and of the Council of 11 December 2018 on the promotion of the use of energy from renewable sources. PE/48/2018/REV/1. Available online: <http://data.europa.eu/eli/dir/2018/2001/oj> (accessed on 12 March 2021).
- EC 2015/1513: Directive of the European Parliament and of the Council of 9 September 2015 amending Directive 98/70/EC relating to the quality of petrol and diesel fuels and amending Directive 2009/28/EC on the promotion of the use of energy from renewable sources. OJ L 239, 15.9.2015, p. 1–29. Available at: <https://eur-lex.europa.eu/eli/dir/2015/1513/oj> (last accessed on 12 March 2021).
- Estel, S.; Kuemmerle, T.; Alcántara, C.; Levers, C.; Prishchepov, A.; Hostert, P. Mapping Farmland Abandonment and Recultivation across Europe Using MODIS NDVI Time Series. *Remote Sens. Environ.* 2015, 163, 312–325.
- GBEP: The Global Bioenergy Partnership; 2018. Accessible at <http://www.globalbioenergy.org> (accessed on 16 March 2021).
- Gorelick, N.; Hancher, M.; Dixon, M.; Ilyushchenko, S.; Thau, D.; Moore, R. Google Earth Engine: Planetary-Scale Geospatial Analysis for Everyone. *Remote Sens. Environ.* 2017, 202, 18–27, <https://doi:10.1016/j.rse.2017.06.031>.
- Hirschmugl, M.; Sobe, C.; Khawaja, C.; Janssen, R.; Traverso, L. Pan-European Mapping of Underutilized Land for Bioenergy Production. *Land* 2021, 10, 102. <https://doi:10.3390/land10020102>.
- Humpenöder, F.; Popp, A.; Bodirsky, B.L.; Weindl, I.; Biewald, A.; Lotze-Campen, H.; Dietrich, J.P.; Klein, D.; Kreidenweis, U.; Müller, C.; et al. Large-Scale Bioenergy Production: How to Resolve Sustainability Trade-Offs? *Environ. Res. Lett.* 2018, 13, 024011, <https://doi:10.1088/1748-9326/aa9e3b>.
- IIASA/FAO, 2012. *Global Agro-ecological Zones (GAEZ v3.0)*. IIASA, Laxenburg, Austria and FAO, Rome, Italy. Available at: http://www.fao.org/fileadmin/user_upload/gaez/docs/GAEZ_Model_Documentation.pdf (last accessed on 07 February 2021)
- Lieskovský, J.; Bezák, P.; Špulerová, J.; Lieskovský, T.; Koleda, P.; Dobrovodská, M.; Bürgi, M.; Gimmi, U. The Abandonment of Traditional Agricultural Landscape in Slovakia—Analysis of Extent and Driving Forces. *J. Rural Stud.* 2015, 37, 75–84.
- LUCAS 2015: Land use and land cover survey of the European Union. <https://ec.europa.eu/eurostat/statistics-explained/index.php/LUCAS>, (last accessed on 12 March 2021).

- Myroniuk, V.; Kutia, M.; Sarkissian, A.J.; Bilous, A.; Liu, S. Regional-Scale Forest Mapping over Fragmented Landscapes Using Global Forest Products and Landsat Time Series Classification. *Remote Sens.* 2020, 12, 187.
- Pulighe, G., Bonati, G., Colangeli, M., Morese, M., Traverso, L., Lupia, F., Khawaja, C., Janssen, R. and Fava, F. Ongoing and emerging issues for sustainable bioenergy production on marginal lands in the Mediterranean regions. *Renewable and Sustainable Energy Reviews*, Volume 103, 2019, 58-70, ISSN 1364-0321, <https://doi.org/10.1016/j.rser.2018.12.043>.
- Robledo-Abad, C.; Althaus, H.-J.; Berndes, G.; Bolwig, S.; Corbera, E.; Creutzig, F.; Garcia-Ulloa, J.; Geddes, A.; Gregg, J.S.; Haberl, H.; et al. Bioenergy Production and Sustainable Development: Science Base for Policymaking Remains Limited. *GCB Bioenergy* 2017, 9, 541–556, <https://doi:10.1111/gcbb.12338>.
- Roundtable on sustainable biofuels. Accessible from <http://rsb.org> (accessed on 16 March 2021).
- Sharpe, W.F. (1964) Capital Asset Prices: A Theory of Market Equilibrium under Conditions of Risk. *Journal of Finance*, 19, 425-442.
- Szatmári, D.; Kopecka, M.; Feranec, J.; Goga, T. Abandoned Agricultural Land Mapping Using Sentinel-2a Data. In *Proceedings of the 7th International Conference on Cartography and GIS*, Sozopol, Bulgaria, 18–23 June 2018; Bandrova, T., Konečný, M., Eds.; 2018. Available online: https://www.researchgate.net/publication/325644850_ABANDONED_AGRICULTURAL_LAND_MAPPING_USING_SENTINEL-2A_DATA (accessed on 21 January 2021).
- Tóth, G., Hermann, T., Silva, M. D., and Montanarella, L. (2016). Heavy metals in agricultural soils of the European Union with implications for food safety. *Environment International*, 88:299–309.
- Traverso, L., Colangeli, M., Morese, M., Pulighe, G., and Branca, G. 2020. Opportunities and constraints for implementation of cellulosic ethanol value chains in Europe. *Biomass and Bioenergy*, Volume 141, ISSN 0961-9534, <https://doi.org/10.1016/j.biombioe.2020.105692>.

A Methodology for Implementing a Digital Twin of the Earth's Forests to Match the Requirements of Different User Groups

Matti Möttus¹, Matthias Dees², Heikki Astola¹, Stanisław Dątek³, Eelis Halme¹, Tuomas Häme¹, Monika Krzyżanowska³, Annikki Mäkelä⁴, Gheorghe Marin⁵, Francesco Minunno⁴, Gero Pawlowski², Juho Penttilä⁶ and Jussi Rasinmäki⁶

¹VTT Technical Research Centre of Finland

²Unique GmbH, Freiburg, Germany

³Cloudferro Sp z o.o., Warszawa, Poland

⁴University of Helsinki, Finland

⁵Institutul Național de Cercetare-Dezvoltare în Silvicultură Marin Drăcea (INCDS), Bucharest, Romania

⁶Simosol OY, Riihimäki Finland

Abstract

Europe has acknowledged the need to develop a very high precision digital model of the Earth, a Digital Twin Earth, running on cloud infrastructure to bring data and end-users closer together. We present results of an investigation of a proposed submodel of the digital twin, simulating the world's forests. We focus on the architecture of the system and the key user needs on data content and access. The results are based on a user survey showing that the forest-related communities in Europe require information on contrasting forest variables and processes, with common interest in the status and forecast of forest carbon stock. We discuss the required spatial resolution, accuracies, and modelling tools required to match the needs of the different communities in data availability and simulation of the forest ecosystem. This, together with the knowledge on existing and projected future capabilities, allows us to specify a data architecture to implement the proposed system regionally, with the outlook to expand to continental and global scales. Ultimately, a system simulating the behaviour of forests, a digital twin, would connect the bottom-up and top-down approaches of computing the forest carbon balance: from tree-based accounting of forest growth to atmospheric measurements, respectively.

Keywords: Digital Twin Earth, forest, carbon, modelling

1 Introduction

Forests make up approx. 1/3 of the Earth's land surface (FAO, 2020). They influence climate through physical, chemical, and biological processes that affect planetary energetics, the hydrologic cycle, and atmospheric composition (Bonan, 2008). Forest biomass is a central component in the terrestrial carbon balance: together with agriculture, it contributes close to

10% of the total greenhouse gases (Tubiello *et al.*, 2015). European countries have agreed to take carbon emissions under meticulous political attention with the Paris agreement. Furthermore, forests are an important economic resource and provide ecosystem services to communities. The global forest sector had a direct contribution of more than US\$539 billion and a total contribution of more than US\$1298 billion to the world GDP (Li *et al.*, 2019).

The value of Earth Observation (EO) for forestry is widely accepted: if certain baseline requirements on data availability and technology are fulfilled, the technology can provide forest area and deforestation rate, and also on more in-depth information, e.g., biodiversity (Anderson *et al.*, 2017). Currently, information on forests is available, for example, as a part of Copernicus Core Services; the EU has also launched a new Forest Information System for Europe, based heavily on remote sensing. Recently, high-level EU documents, the Green Deal and EU Data Strategy called for bringing together European scientific and industrial excellence to develop a very high precision digital model of the Earth. The Digital Twin Earth (DTE) will provide a leading-edge capability to “visualize, monitor and forecast natural and human activity on the planet in support of sustainable development thus supporting Europe’s efforts for a better environment”. The Destination Earth (DestinE) policy document (European Commission, 2021) specifically foresees the creation of a Digital Twin on Climate Change Adaptation, which will also include specialised DTE’s of Earth system components.

Here, we present a methodology for a spatially explicit EO data analysis and modelling tool supporting the top-level policy goals to create a specialized DTE of Earth’s forests. We start with describing user needs based on a Europe-wide user survey. We consider the spatial and temporal resolutions needed by the users, and the resulting requirements of the DTE. Finally, we present a layout of the DTE, fitting the structure of DT on Climate Change Adaptation.

2 Methods

We performed 30 one-hour interviews with leading data users in forestry and forest science. As the DestinE policy targets European entities, the addressed entities were chosen from Europe, many with an international scope. They were, somewhat subjectively, divided into categories such as forest enterprises, scientific and institutional users, etc. (Table 1). We also assigned home countries to the entities, which represented their main location or home market. Many of the users are international and work with global data (e.g., most science users) or treat Europe, or even the entire globe, as their home market, but only European and international intergovernmental institutions are classified as international in Table 1.

We asked all users eleven questions, including both open-ended and multiple-choice ones (Table 2). The answers to the questions were used to determine the key estimation and prediction needs, as well as spatial and temporal resolutions and ranges for the DTE. Finally, we analysed the requirements on the available forest models and computing infrastructure to address the needs determined in the survey. The analyses were constrained by the requirements of openness and interoperability set out in the policy documents, and the key European infrastructures foreseen to be used for the tasks.

Table 1: User categories involved in the user needs study. Country codes: DE – Germany, ES – Spain, FI – Finland, GB – United Kingdom, PL – Poland, RO – Romania, SE – Sweden, INT – international (acting at European or global scales only).

User category	number	countries
Forest enterprises	5	DE,FI,RO
Governmental bodies & international organizations	9	DE,FI,PL,RO,INT
Forest and Wood Industry	3	FI,SE
Service Companies	1	DE
Scientific users	7	DE,FI,GB, RO
Public research institutes	5	DE,ES,FI,RO
total	30	

Table 2: The questions guiding the interview. The column "Open" indicates whether the question was open-ended.

no.	Question text	Open
1	What is the key question to be answered by a forest modeling system?	yes
2	What are further priorities to be simulated?	no
3	How should the results be presented?	no
4	What is the spatial unit of the analysis you would like to carry out?	yes
5	What is the temporal scope of the analysis you would like to carry out?	yes
6	In what region on Earth do you typically carry out analyses?	yes
7	What is the size of the study area you are focusing?	yes
8	What kind of data could you contribute?	yes
9	When using the platform, would you contribute your data to the digital twin?	no
10	What systems do you have in place for analyzing the status of forests and the future development of the forests?	yes
11	At which spatial dimension could you provide data?	yes

3 Results and Discussion

The question most commonly asked to be addressed by the digital twin was forest carbon stocks and their changes (**Figure 1**). Due to the role of forests in the carbon cycle, its relevance to institutional and scientific users is not a surprise. However, this topic was also relevant for commercial entities, as indicated by the high importance of “organizational carbon balance”, which quantifies the carbon footprint of the activities of an entity, including its forest-related products. Next in line were topics related to hazards and risks, including shifts in the geographic area of the climatic conditions suitable for specific overstory species. “Sustainable

timber productivity” was not very high on the list, but considering the small share of commercial users in the survey, it cannot be ignored by the digital twin.

Open-ended questions included those related to carbon and climate (*What does climate change mean for the entire forest carbon cycle? How can we mitigate the effects of the wood industry to global warming?*); species and risk mitigation (*Which tree species will still occur in 100 years and where will they occur? What will be the natural borders of tree species in 2050 or 2100? What does climate change mean for individual tree species? What species to plant now in order to guarantee a continuous forest cover?*), and forestry (*Which forest type will retain its forest function in the long run? Where can forests be secured in the future, and where can timber still be produced? Where will trees still grow old enough in order to harvest timber?*).

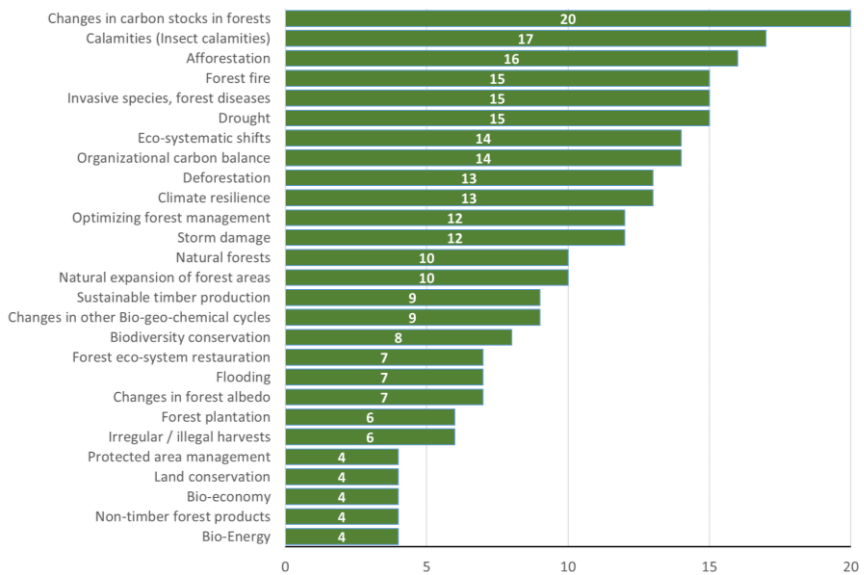


Figure 1: The number of times a need was mentioned by users. Each user was asked for three priorities.

On average, the time to be simulated was 54 years. National research centres interviewed by us are legally obliged to provide long-term simulations between 10 and 40 years. 45% of the interviewed stakeholders mentioned the need for seasonal or yearly forecasts, with one request for near real-time operations. The required time step varied from weekly and bi-weekly to monthly. Shorter steps were mentioned regarding hazards such as bark beetle disturbances or drought and fire threats. The required modelling scale varied largely between the interviewed users, ranging from a single tree to $16 \times 16 \text{ km}^2$, with possible aggregation to regional/country level. A specific requirement stated by commercial users is the need to enforce access rights to data: to achieve their requirements for accuracy and reliability, commercial users need to use their privately-owned forestry data for simulations, which should not be accessible to other users of the digital twin. The visualisation and data output requirements for almost all users included geographically tagged rasters (e.g., geotiffs; NetCDF was explicitly mentioned once). More enhanced visualisations, including a fully realistic 3D and interactive representation of

the forest, was not a high priority but mentioned as a tool for outreach (non-commercial users) or attracting customers (commercial users).

To answer the different tasks raised by the potential users and to match the definition of the DTE as expressed in the DestinE policy (“digital replicas of various aspects of the Earth system”; European Commission, 2021), the following modelling components need to be used: (1) forest structure retrieval, (2) forest growth model, (3) forest disturbance risk prediction, (4) forest management and scenario model, (5) wood product life cycle model, and (6) estimation of direct climate forcing of forest. As dictated by the policy documents, the digital twin will need to interact with the foreseen Digital Twin on Climate Change Adaptation, which will provide the forest twin with the scenarios to simulate, weather and climate data, parts of a user interface, etc. (Figure 2). Visualization will form a natural part of the DTE, implemented on the landscape scale, displaying the spatial variation in predicted key forest properties.

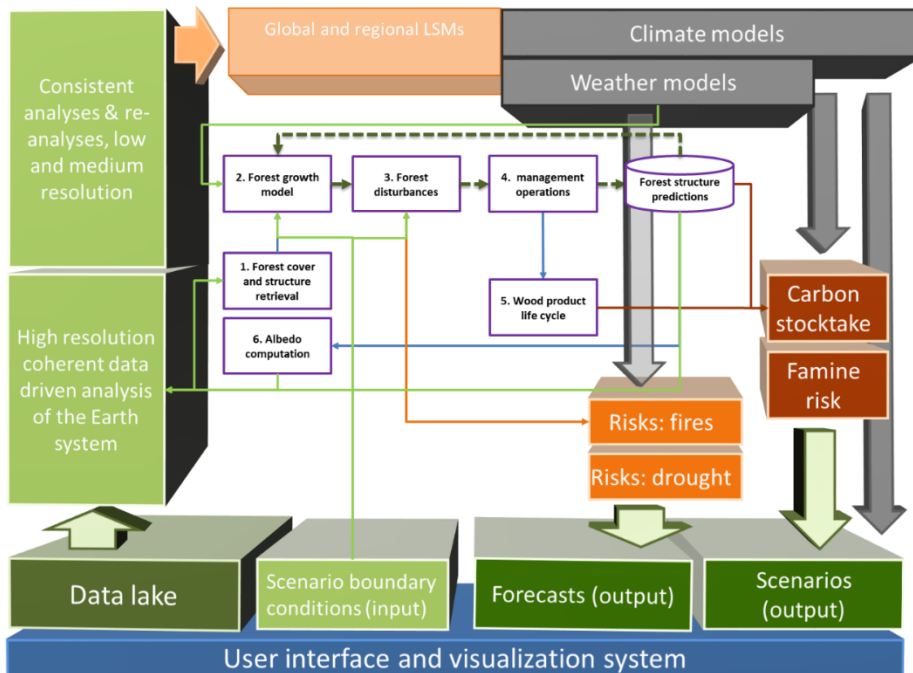


Figure 2: Positioning of the digital twin of forests (represented as a set of numbered blocks) inside the Digital Twin on Climate Change Adaptation to be implemented according to the DestinE policy.

To start the simulations, existing forests need to be mapped in the simulation area. Next, the forest productivity model needs to predict the productivity (e.g., net ecosystem exchange and the distribution of assimilated carbon in the different pools in the forest) and translate this into forest growth. In interaction with forest management and disturbance models, the forest structure should be altered in time steps required by users, quantify the side flows of carbon (e.g., into wood products), and determine the status of the forest for the next iteration. A single forest productivity and growth model can be adopted, calibrated for different biomes (e.g.,

Tian *et al.*, 2020) or several biome-specific models could be combined. Great attention must be paid to model validation: model prediction errors consist of inherent model errors and model calibration (parameterization) errors, with the former contributing up to 50% of model performance (Dietze *et al.*, 2014). Forest management models need to be up-to-date regarding national forest policies and regulations, while forest damage assessment still requires expert knowledge (e.g., Jactel *et al.*, 2012).

Due to the nature of the models, optical multispectral data is recommended (Sirro *et al.*, 2018) for estimating the forest variables and initializing the modelling process. For global coverage and unlimited accessibility, Sentinel-2 and Landsat are the preferred sources. Auxiliary data (field plot measurements, airborne laser scanning, very high resolution imagery, future hyperspectral and chlorophyll fluorescence imagery, etc.) should be included where and when available. In addition to providing the required EO data, the computing environment should support the implementation of the forest models mentioned above and provision of environmental and weather data required by the forest growth model. Such infrastructure in Europe is provided by the Copernicus Data and Information Access Services (DIAS), initially funded by the European Commission.

The key components and competences for a successful implementation of a digital twin of the Earth's forests exist in Europe. The biggest challenge is to implement the system at the very high resolution required by the forestry sector, while still achieving compatibility with the global estimates of carbon fluxes from the variations in the CO₂ concentration in the atmosphere (i.e., merging bottom-up and top-down approaches of carbon flux estimations). Based on the work presented here, the policy-driven enthusiasm in Europe is supported by real user-side interest and technological readiness.

References

- Anderson, K., Ryan, B., Sonntag, W., Kavvada A., Friedl, L. (2017). Earth observation in service of the 2030 Agenda for Sustainable Development. *Geo-spatial Information Science*, 20(2), 77-96, doi: 10.1080/10095020.2017.1333230
- Bonan, G. B. (2008), Forests and climate change: Forcings, feedbacks, and the climate benefits of forests, *Science* 320, 1444–1449.
- Dietze, M.C., Serbin, S.P., Davidson, C., Desai, A.R., Feng, X., Kelly, R., Wang, D. (2014). A quantitative assessment of a terrestrial biosphere model's data needs across North American biomes. *Journal of Geophysical Research. Biogeosciences*. 119 (3), 286–300. doi:10.1002/2013JG002392
- European Commission (2021). Destination Earth (DestinE) | Shaping Europe's digital future. <https://ec.europa.eu/digital-single-market/en/destination-earth-destine>
- FAO 2020. Global Forest Resources Assessment 2020 – Key findings. Rome. doi:10.4060/ca8753en.
- Jactel, H., Branco, M., Duncker, P., Gardiner, B., Grodzki, W., Langstrom, B., . . . Tojic, K. (2012). A Multicriteria Risk Analysis to Evaluate Impacts of Forest Management Alternatives on Forest Health in Europe. *Ecology and Society*, 17(4), 52., doi:10.5751/ES-04897-170452
- Kondo, M., Patra, P. K., Sitch, S., Friedlingstein, P., Poulter, B., Chevallier, F., . . . Ziehn, T. (2020). State of the science in reconciling top-down and bottom-up approaches for terrestrial CO₂ budget. *Global change biology*, 26(3), 1068–1084. doi:10.1111/gcb.14917
- Li, Y., Mei, B., Linhares-Juvenal, T. (2019). The economic contribution of the world's forest sector. *Forest Policy and Economics* 100, 236-253. doi: 10.1016/j.forpol.2019.01.004
- Nunes, L. J. R., Meireles, C. I. R., Pinto Gomes, C. J., & Almeida Ribeiro, N. M. C. (2020). Forest Contribution to Climate Change Mitigation: Management Oriented to Carbon Capture and Storage. *Climate*, 8(2), 21. doi:10.3390/cli8020021
- Sirro, L., Häme, T., Rauste, Y., Kilpi, J., Hämäläinen, J., Gunia, K., De Jong, B., Paz Pellat, F. (2018). Potential of different optical and SAR data in forest and land cover classification to support REDD+ MRV. *Remote Sensing* 10(6), 942. doi:10.3390/rs10060942
- Tian, X, Minunno, F, Cao, T, Peltoniemi, M, Kalliokoski, T, Mäkelä, A. (2020). Extending the range of applicability of the semi-empirical ecosystem flux model PRELES for varying forest types and climate. *Global Change Biology* 26(5), 2923–2943. doi:10.1111/gcb.14992
- Tubiello, F. N., Salvatore, M., Ferrara, A. F.; . . . Smith, P. (2015). The Contribution of Agriculture, Forestry and other Land Use activities to Global Warming, 1990–2012. *Global Change Biology* 21(7), 2655–2660. doi:10.1111/gcb.12865

Helping forest owners to manage forest carbon – the Forest Flux project

GI_Forum 2021, Issue 1
Page: 137 - 142

Best Practice Paper

Corresponding Author:

tuomas.hame@vtt.fi

DOI: 10.1553/gjscience2021_01_s137

Tuomas Häme¹, Laura Sirro¹, Matthias Dees², Annikki Mäkelä³, Juho Penttilä⁴, Gheorghe Marin⁵ and Margarida Tomé⁶

¹VTT, Finland

²UNIQUE forestry and land use GmbH, Freiburg, Germany

³University of Helsinki, Finland

⁴Simosol Oy, Finland

⁵National Institute for Research and Development in Forestry Marin Dracea (I.N.C.D.S.), Romania

⁶University of Lisbon, Portugal

Abstract

Forest Flux <https://www.forestflux.eu/> will renew forestry value-added services in Earth Observation (EO) by creating and piloting cloud-based services for committed users on forest carbon assimilation and structural variable prediction. Forest Flux exploits the explosive increase of high-resolution EO data from the Copernicus program and developments of cloud computing technology. It implements a world-first service platform for high-resolution maps of traditional forestry variables together with forest carbon fluxes. Forest Flux will allow the users to improve the profitability of forest management while taking care of ecological sustainability. The Forest Flux services are implemented on the Forestry Thematic Exploitation cloud platform <https://f-tep.com/>. In 2020, nearly 700 thematic maps on forest stand and carbon flux variables were delivered to nine specific users in a form that was applicable to their operational forest management systems. The last project year 2021 focuses on map product refinement and improving user services, which eventually lead to operational service concepts. Forest Flux is an Innovation Action project of the European Union, Grant Agreement No. 821860.

Keywords: forestry, carbon, satellite, earth observation, biomass, cloud platforms

1 Introduction

Until recently, detailed information on the forest carbon cycle has not been available due to a lack of scientific understanding, spatial data availability, limited processing capacity, and the complexity of implementing this information in business processes.

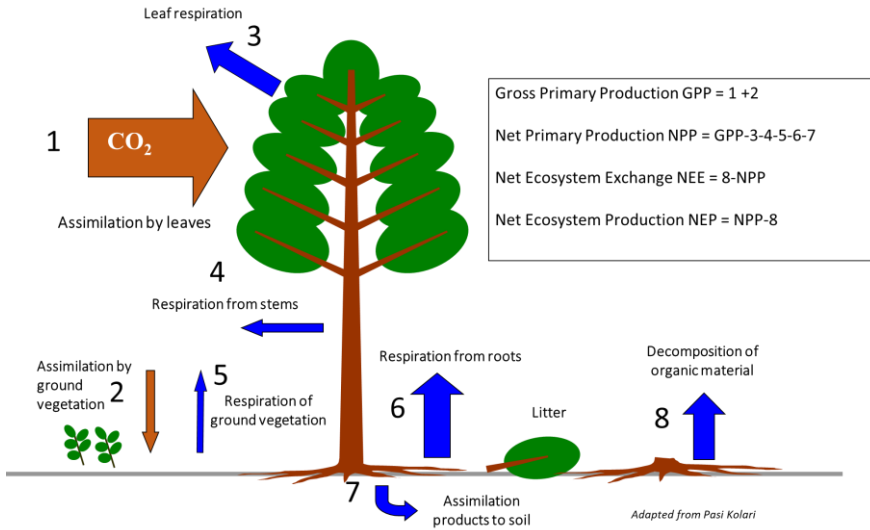


Figure 1: Carbon flux variables computed in Forest Flux project.

Forest Flux will renew forestry value-added services in Earth Observation (EO) by creating and piloting cloud-based services for committed users on forest carbon assimilation and structural variable prediction (Figure 1). The services utilize Copernicus satellite data. The services are driven by sustainable forest management, EU forest strategy, the Bioeconomy Action Plan, and the demands of environmentally aware end-users of wood industry products.

Forest Flux exploits the explosive increase of high-resolution Earth observation data with 10-to-20 metre resolution, particularly from the Sentinel 2 satellite of the Copernicus program. The recent developments of cloud computing technology are utilized in data value-adding. It implements a world-first service platform for high-resolution maps of traditional forestry and carbon flux variables. Forest Flux will allow the users to improve the profitability of forest management while taking care of ecological sustainability. Forest Flux is an Innovation Action project of the European Union's Horizon 2020 program, Grant Agreement 821860. The project started in 2019 and will be completed at the end of 2021.

Forest Flux uses a holistic approach in a single processing chain. Already during the project, forestry and carbon data are integrated into the decision-making processes of selected core users. The Forest Flux services are implemented on the Forestry Thematic Exploitation cloud platform <https://f-tep.com/>. It uses the CreoDIAS infrastructure as the satellite data supply and processing infrastructure.

Forest Flux will establish the leadership of European industry in the sustainable utilization of forest resources. The computing infrastructure is specifically targeted for EO data and forestry users, and it will be fully functional by the end of the project. The web-based human and machine interfaces will enable market access unrestricted by country boundaries, and facilitate easy commercial interactions of players of different sizes and backgrounds.

2 Concept

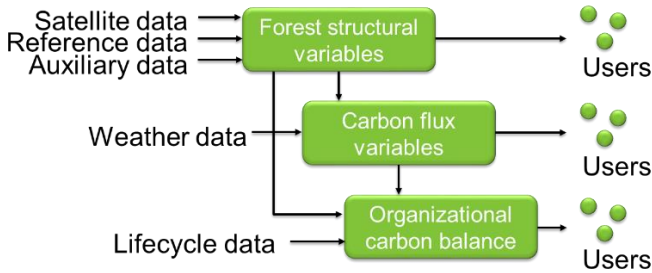


Figure 2: The three service groups of Forest Flux.

The services of Forest Flux are composed of three main blocks: 1) Forest structural variable services, 2) Carbon flux services, and 3) Organizational carbon balance services (Figure 2).

Forest structural variable services comprise of forest cover mapping and estimation of forest variables that have been traditionally measured in the field. The provided information includes tree height, basal area, stem diameter, stem volume, density, and tree species. The forest inventory service can be implemented for several years, or at defined intervals.

Forest change services are also part of the service block of structural variables. These services offer mapping of changes in forest cover between given target years. Possible change types include changes between land cover classes due to forest harvests, or forest damage.

Forest ecology inventory services include two types of products: fragmentation and structural diversity products. The products of this service are computed from outputs of forest inventory service. The Forest ecology inventory indicators indicate the proportion of wooded area within a selected grid cell area (e.g. 1 km²), number of wooded patches with a unit area, wooded area perforation density, number of tree species, and tree height variability within the selected grid cells.

Forest ecology change computes changes between two ecology products that represent different points of time.

The forest structural variable services provide information on forest area, forest status, and their changes. The inventory considers one target year, whereas the change services provide information about forest changes between the years.

Carbon flux services provide information on the **biomass and carbon balance of the forests**. Forest structural variables derived from EO are used to initialize the forest model PREBAS (Minunno et al., 2019; Tian et al., 2020). Carbon (C) stocks and fluxes are computed for the year of the structural variable mapping and for the future, providing forest growth and C balance forecasts.

The outputs of the biomass and carbon balance service are: maps of above and below-ground tree biomass, soil C stocks, vegetation carbon, yearly averaged Evapotranspiration, Gross Primary Production (GPP), Net Primary Production (NPP), Net Ecosystem Exchange (NEE)

(Figure 1). Mapping using the PREBAS model allows spatial identification of carbon sinks and sources and monitoring particular vegetation stresses, such as water stress.

Biomass and carbon fluxes can be monitored for years for which ground reference, satellite, and weather data are available. Several structural forest variable estimations over years help to improve the carbon flux and growth models. Forecasts for future fluxes and forest growth can be computed by applying different climatic and forest management scenarios.

The **organizational carbon balance** builds on the previous service layers: forest structural variable estimation and carbon storage and fluxes while adding one additional layer: the wood harvested from the forest and manufactured into wood-based products.

The carbon storages and fluxes from the previous step, carbon in trees and soil, the fluxes between these storages and atmosphere, are in other words augmented with third carbon storage, wood-based products, and the associated carbon fluxes. Part of these fluxes are carbon emissions from the execution of wood harvesting, transport, and manufacturing processes, including recycling. Another aspect considered for the wood-based carbon product storage is the substitution of non-renewable materials with renewable ones.

Dedicated user involvement, strong commercial interests, rapidly developing online markets, and demonstrated excellence of the consortium make the Forest Flux service platform sustainable beyond the end of the project.

3 Pilot services

Pilot services were conducted for nine users in five countries in Europe and South America. In total, approximately 700 thematic maps were delivered for the forest management systems of the users. For each user, a Service Agreement was prepared. This agreement defined the site and desired contents of the services. The users assessed the delivered maps and associated information of uncertainties. The assessment results were used to improve the services for the second pilot that has been conducted in 2021.

The main high-resolution (HR) satellite data were Copernicus Sentinel-2 Multispectral Instrument (MSI) images with a ten-metre spatial resolution that was also the resolution of the output maps except for the ecology products where the resolution was one square kilometre. Supplementary satellite data for before the year 2015 were obtained from Landsat 8 Operational Land Imager (OLI). The wall-to-wall satellite data were augmented by a sample of Very High Resolution (VHR) satellite imagery with sub-metre resolution. Images from several VHR satellites including Worldview-2, GeosEye-1, Pleiades, Deimos, and Kompsat 3, available on the Data Warehouse of Copernicus, were analysed. These data were used to augment incomplete ground reference data on some pilot sites.

The ground reference data were mostly provided by the users. Openly available ground sample plot data of high quality were available for the whole country in Finland. These data were used for the training of the models for satellite image interpretation and for uncertainty analyses. The principal method for the estimation of forest structural variables was the Probability method of VIT (Häme et al., 2013, 2001).

For changes, VTT's Autochange method was applied (Häme et al., 2020). Probability and Autochange software were run on the Forestry cloud TEP platform. A significant amount of new software for the improvement of the image analysis process was developed in Forest Flux. Figure 3 and Figure 4 give examples of the Forest Flux maps.

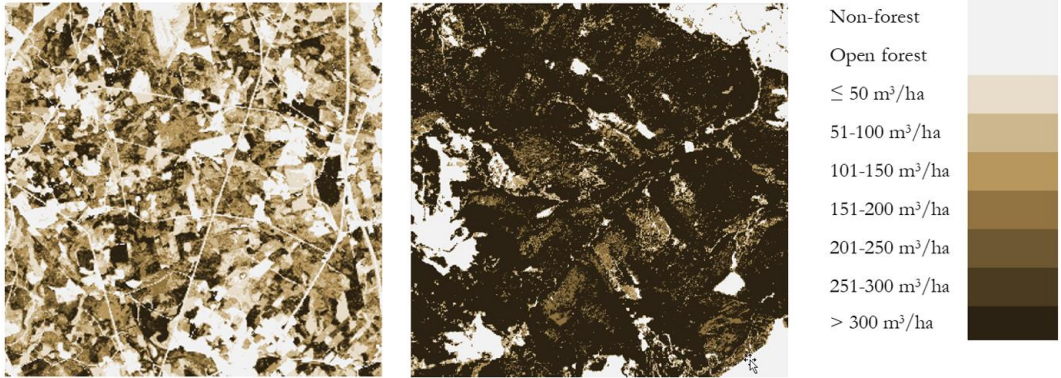


Figure 3: Stem volume maps computed in the first pilot services Forest Flux on 7 km x 7 km areas in Finland and Romania. The relative RMSE was in Finland 52% and bias 0.1 m³/ha and in Romania 59% and 2.3 m³/ha, respectively. The uncertainties were computed at the level of ground sample plots using an independent plot sample. The uncertainties are smaller for larger areas.

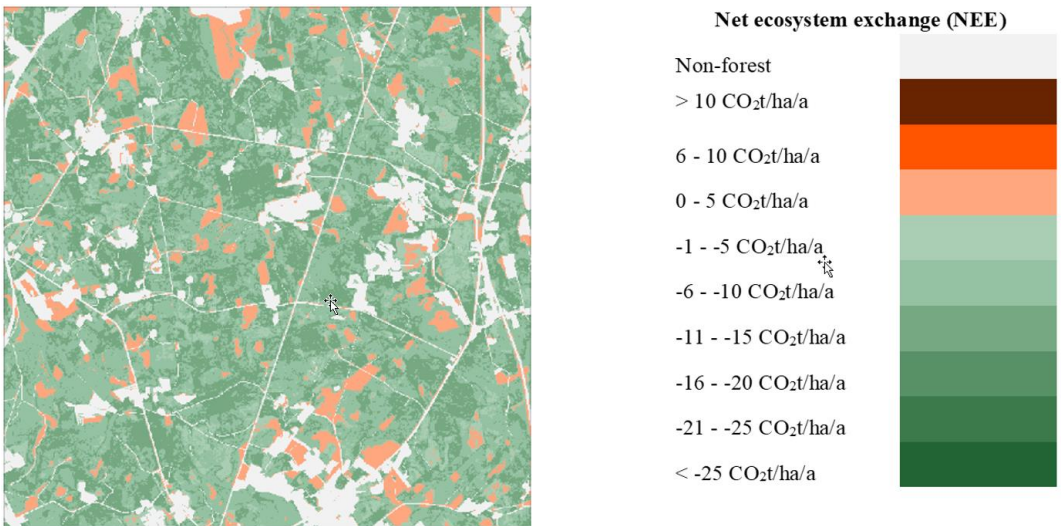


Figure 4: Net ecosystem exchange for in the Finnish study site. Negative values mean carbon assimilation and positive carbon emission. The emission sites represent recent regeneration areas.

Conclusions

Relatively complex production chains were developed during the two first years of the Forest Flux project. The second pilot services for the same users means approaching an operational status of the service provision. All the users were willing to continue receiving Forest Flux services in pilot stage two. The feedback showed requirements for increasing the accuracy of estimations. A positive assessment was received from sites where the ground reference data were poor because also the earlier information on forest resources was inaccurate. In Finland, where the quality of the reference data was good, the existing information of forest resources is also accurate. The satellite data will be augmented with Airborne Laser Scanner (ALS) observations when demand for accuracy is high and these data are available.

During the last project year, a business plan for the operational services will be developed together with the provision of the second pilot services.

References

- Häme, T., Kilpi, J., Ahola, H. A., Rauste, Y., Antropov, O., Rautiainen, M., ... Bounpone, S. (2013). Improved mapping of tropical forests with optical and sar imagery, part i: Forest cover and accuracy assessment using multi-resolution data. *IEEE Journal of Selected Topics in Applied Earth Observations and Remote Sensing*, 6(1), 74–91. <https://doi.org/10.1109/JSTARS.2013.2241019>
- Häme, T., Sirro, L., Kilpi, J., Seitsonen, L., Andersson, K., & Melkas, T. (2020). A Hierarchical Clustering Method for Land Cover Change Detection and Identification. *Remote Sensing*, 12(11), 1751. <https://doi.org/10.3390/rs12111751>
- Häme, T., Stenberg, P., Andersson, K., Rauste, Y., Kennedy, P., Folving, S., & Sarkeala, J. (2001). AVHRR-based forest proportion map of the Pan-European area. *Remote Sensing of Environment*, 77(1), 76–91. [https://doi.org/10.1016/S0034-4257\(01\)00195-X](https://doi.org/10.1016/S0034-4257(01)00195-X)
- Minunno, F., Peltoniemi, M., Härkönen, S., Kalliokoski, T., Mäkinen, H., & Mäkelä, A. (2019). Bayesian calibration of a carbon balance model PREBAS using data from permanent growth experiments and national forest inventory. *Forest Ecology and Management*, 440, 208–257. <https://doi.org/10.1016/j.foreco.2019.02.041>
- Tian, X., Minunno, F., Cao, T., Peltoniemi, M., Kalliokoski, T., & Mäkelä, A. (2020). Extending the range of applicability of the semi-empirical ecosystem flux model PRELES for varying forest types and climate. *Global Change Biology*, 26(5), 2923–2943. <https://doi.org/10.1111/gcb.14992>

Monitoring Land Degradation from Space

GI_Forum 2021, Issue 1

Page: 143 - 149

Best Practice Paper

Corresponding Author:

filippo.iodice@uptoearth.eu

DOI: 10.1553/giscience2021_01_s143

Filippo Iodice¹, Federica D'Acunto¹ and Lorenzo Bigagli²

¹Uptoearth GmbH, Germany

²CNR-IIA, Italy

Abstract

Unsustainable practices and increasing pressure on soil jeopardise the achievement of land degradation neutrality, targeted by 2030. Land degradation is costing billions in terms of land restoration and is heavily impacting human health and climate change. Sustainable Development Goals' (SDGs) target 15.3 focuses on the issue, and several methodologies are proposed to address land degradation. However, all present some limitations in terms of accuracy. This paper aims to present a more comprehensive approach based on the application of remote sensing technology. We show that the Copernicus Sentinel-1 and Sentinel-2 satellite imagery archives can be used on the one hand to detect the current soil conditions, on the other hand to predict the future balance of Soil Organic Carbon (SOC). A case study illustrates that SOC, tillage and bare soil are key quality indexes that can facilitate quantifying and achieving a land degradation-neutral world.

Keywords: land degradation, soil quality, soil organic carbon

1 Introduction

Soil is a complex ecosystem that hosts several organisms and influences several services and mechanisms, such as water quality, food production, and climate regulation. Moreover, soil is a crucial non-renewable resource for humankind and its economic system (European Commission, 2020).

The Sustainable Development Goals (SDGs) try to establish a transnational commitment to promoting more sustainable management of Earth resources (Mancebo, 2015). Sustainability, intended as the “*dynamic and unstable equilibrium between the natural and social systems capability to soak in shocks, keeping their functions, without collapsing (resilience), and losing that capability (vulnerability)*” (IAEG-SDGs, 2016), represents the common theme of the whole framework. Whereas the previous Millennium Development Goals presented an independent list of objectives, the 2030 Agenda establishes a systematic foundation for sustainability, where the single SDGs are not 17 separate purposes but interlinked goals requiring systemic planning and intervention.

This close interconnection is clear with regards to soil: food security (SDGs 2 and 6) and safety (SDG 3), mitigation and adaptation to climate change (SDG 13) and sustainability of terrestrial

ecosystem services (SDG 15), for instance, all directly depend on soil conditions, while indirect correlations with other SDGs (e.g., 7, 12) can be easily identified. Moreover, a specific target (15.3) has been established to combat land degradation (Tóth et al., 2018).

Land degradation represents one of the main threats for the Earth and its inhabitants: it affects at least 3.2 billion people and costs about €5.5-10.5 trillion per year and 10% of the annual global gross product in terms of biodiversity and ecosystem services. In addition, land degradation and climate change feed mutually (Keesstra et al., 2018; IPBES, 2018). According to Keesstra (2018), it is possible to identify three types of land degradation: physical, chemical, and biological. Physical degradation refers to phenomena like erosion and compaction, which imply the dislocation and relocation of soil particles without modifying their chemical composition. In contrast, chemical degradation also involves such alteration, for example, in case of overuse of fertilisers, insecticides, and herbicides, or inadequate water management, leading to salinisation of (semi)arid regions. Biological degradation refers to loss of Soil Organic Matter (SOM) connected to change in land destination (e.g., the conversion of forests in arable lands). This overview underlines, even more, the interconnection between land degradation and the entire sustainable development framework and poses an urgent challenge: on the one hand, water management (SDG 6), responsible production (SDG 11), and sustainable economic growth (SDG 8) are negatively impacted by land degradation; yet, on the other hand, the targets of other SDGs related to food, health, water, and climate, pose a high pressure on land and soil.

Looking at SDGs, target 15.3 calls for “land degradation neutrality - LDN” as “a state whereby the amount and quality of land resources necessary to support ecosystem functions and services and enhance food security remain stable or increase within specified temporal and spatial scales and ecosystem”. LDN is measured (in hectares or km²) by indicator 15.3.1 as the “proportion of land that is degraded over total land area” (IAEG-SDGs, 2016) and by three sub-indicators referring to land cover (measured as Land Cover Meta Language - LCML), land productivity (indicated as Net Primary Production - NPP) and carbon stock (expressed as Soil Organic Carbon - SOC) (UNSD, 2018).

In practical terms, the United Nations Convention to Combat Desertification (UNCCD) called for the application of remote sensing to monitor land degradation, and several satellite-based methods already provide an algorithm for calculating 15.3.1. This paper aims to promote a more comprehensive analysis for the design of supporting tools to help especially farmers turn SDGs’ commitments into agricultural practices.

2 Materials and Methods

In order to improve the understanding of the primary soil degradation dynamics, it is necessary to ensure the interconnection of a broad network of data and monitor them at a global scale. The methodology we propose differs from traditional and other satellite-based studies. It defines soil texture, weather conditions, agronomic intervention (tillage, fertilisation, etc.) and anthropic elements directly from satellites instead of using land cover maps to precisely predict carbon balance. Both historical and real-time data about carbon balances allow to forecast the impact of agricultural practices and to support the farmer in optimising their application.

In particular, data from Sentinel-1 (S1) and Sentinel-2 (S2) on agricultural areas are used, with the aim of creating binary maps of the variations in surface roughness related to tillage practices and the related loss or storage of carbon in the soil. The adopted strategy includes a pre-processing phase for both sensors and final modelling of data consolidation and correlation. The multispectral data underwent a classification and a pre-processing of some indices such as the selection of values <0.36 NDVI (normalised difference between band 8 and 4) and Normalized Burn Ratio 2 (NBR2) index thresholds from 0,05 to 0,1, which helped to identify the bare or sparsely vegetated soils where tillage practices are usually performed.

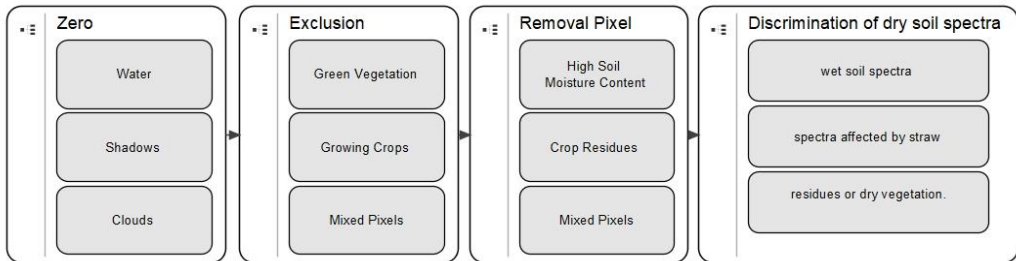


Figure 1: The image masking process

The SAR data, on the other hand, were used for detecting the processing change. The pre-processing of the S1-SLC images was accomplished using SNAP Toolbox S1. In the second phase, the adjacent meteorological stations within a radius of three km were added to the study and sorted for the hourly frequency close to the satellite pass. This allowed us to mask pixels that received more than 1 mm of rain within the five hours before image capture.

The pre-processing chain for SLC images consists of applying precise S1A orbits, calibrating, removing thermal noise, de-bursting and ground correction with SRTM 1 sec. The values of the digital numbers have been converted to dB scale with a backscatter coefficient with a resolution of 25 m. Analysing the temporal changes of S1 on the VH polarisation allowed us to identify the variations due solely to tillage practices since the roughness of the surface on agricultural land varies unevenly in space. In contrast the soil humidity usually varies uniformly (Mercier et al., 2020). The analysis of S2 data concentrated on two spectral wavelength ranges: 700-865 nm and 1375-2190 nm. These spectral ranges were selected since the Near Infra-Red (NIR), and the Short Wave Infra-Red (SWIR) regions have spectral characteristics associated with SOC (Sorenson et al., 2017). The algorithm was validated by observing various types of tillage practices collected at different sites. Among the study areas, we selected three homogeneous cereal crops farms: two practice conservation agriculture and the third traditional agriculture. In addition, 16 samples (8 before and 8 after tillage) were collected at 0-30 cm depth and used for validating the satellite data.

The temporal changes of S1 on the VH polarisation are shown in Figure 2 and allow us to identify the processing mechanisms that took place on the different soils. It is clear that traditional processing affects more the VH polarisation. On the other hand, in Figure 2, it can be seen that the unploughed soil does not go under any variation of VH polarization between one crop and another.

The presented methodology allows to create soil tillage change maps from S1 data. The methodology based on multiscale time change detection on S-1 VH-backscatter on bare soil areas or poorly vegetated areas has an overall accuracy of tillage/no-tillage land identification of 90%. Based on the observations collected for the three agricultural lands, errors were found on the perimeter areas of the land due to delimitation trees or anthropogenic objects.

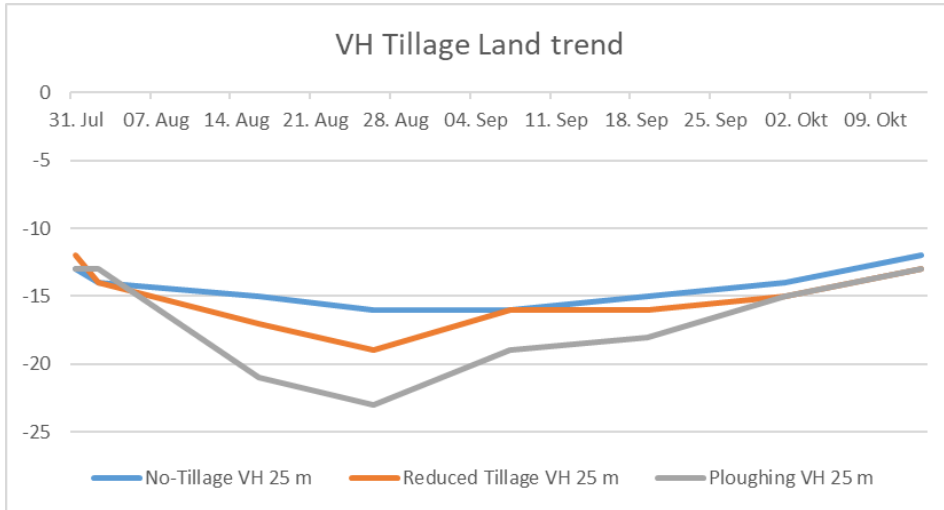


Figure 2: Monitoring of agricultural operations with the S1 VH polarisation in the pre-sowing period.

Once tillage was identified from the satellite, two models were developed based on Random Forest (RF) and Support Vector Machine (SVM) neural networks that use S2 images on the VNIR and NIR-SWIR bands. Each spectrum was pre-processed using Continuous Wavelet Transform (CWT) within the WMTSA package in R (Percival et al., 2016). Spectral data were calibrated against a pre-and post-processing SOC calibration dataset (Table-1).

Table 1: Summary of S2 elaboration and related validation of in-situ data.

Sensor	Parameter	SOC content %											
		No-Tillage				Reduced Tillage				Ploughing			
		SVM		RF		SVM		RF		SVM		RF	
		Before	After	Before	After	Before	After	Before	After	Before	After	Before	After
	Bare Soil	NO	NO	NO	NO	YES	YES	YES	YES	YES	YES	YES	YES
Data in Situ	SOC Validation Standard Deviation	0.26	0.26	/	/	0.28	0.23	/	/	0.29	0.18	/	/
S2	VNIR	0.27	0.29	0.32	0.3	0.31	0.24	0.29	0.24	0.28	0.19	0.32	0.21
	NIR-SWIR	0.22	0.21	0.25	0.24	0.25	0.19	0.23	0.14	0.22	0.13	0.26	0.17

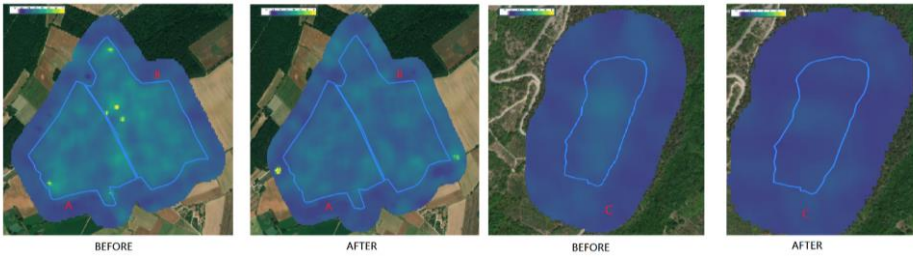


Figure 3: Annual graphical representation of S2 SOC data. The complete charts are available by [name deleted to maintain the integrity of the review process]. Study area A: No-Tillage; Study area B: Reduced Tillage; Study area C: Ploughing

Although the study analyses the variants that represent a different soil tillage system, it can be concluded that the no-tillage system is characterised by less impact on the soil and therefore favours a higher presence of organic carbon. Taking tillage into account, the use of reduced tillage compared to a no-tillage soil resulted in a 22% decrease in SOC. On the other hand, the land that has undergone conventional ploughing resulted in a 36% reduction in SOC, which means nearly twice the emissions of no-tillage. While in the case of a comparison between reduced tillage and conventional tillage, the latter is responsible for increasing 14% of soil organic carbon.

We believe that time series are fundamental to determine causes of carbon loss that are not visible with annual coring: SOC/soil ratio and soil tillage must be monitored over a medium/long period of time, and the satellite guarantees constant monitoring over the soil. In conclusion, as shown in Figure 4, the entire research is based on a 3D map adding an additional time dimension that enables to correlate the processing of agricultural land and SOC. The first dimension consists of a binary map (full 1-byte raster images) containing an information class on the cultivated/uncultivated land, the second dimension refers to the tillage monitored by S1 “tillage/no-tillage”. The third and last dimension contains the variation of the organic substance detected by S2 through a linear correlation between reflectance indices and in-situ data.

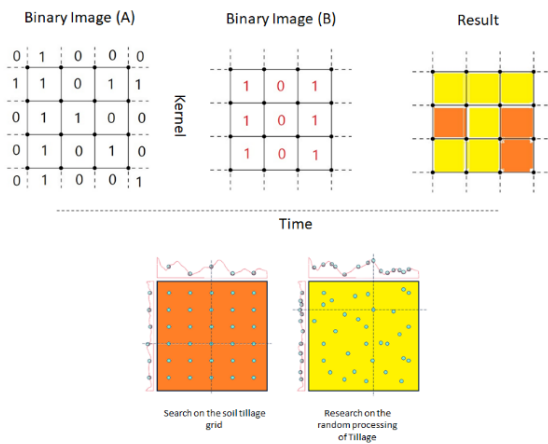


Figure 4:

Graphic representation of 3D map + Time. From the top left: cultivated/uncultivated land map; tillage/no-tillage grid; S2 SOC grid. The bottom part shows the resampling methods for homologating the different data resolutions.

Satellite data has helped demonstrate that farmers who implement these practices can significantly reduce soil erosion rates and indirectly increase the amount of organic matter in the soil. The same data can help farmers create a monitoring system of their land and their practices to further reduce the impact of agriculture on climate change. Further analyses will be carried out on the phenological cycles of 2020 and 2021 to train the neural networks better and reduce the error with in-situ data.

3 Conclusion

Many scholars and the United Nations themselves noted that the Millennium Development Goals (MDGs) missed a chance both in terms of purposes and methodology (Death & Gabay, 2015; United Nations, 2015). The post-2015 debate promoted vivacity for the definition of the “post”, which resulted in the creation of 17 new goals, the Sustainable Development Goals (SDGs), with 169 targets to be achieved by 2030.

Although several initiatives at transnational and European level have been launched, such as the Common Agriculture Policy (CAP) and the Zero Pollution Action Plan for Air, Water and Soil, to achieve the commitment on land degradation neutrality, there is no consensus about how to effectively pursue it. Our research (still ongoing in three areas in Italy and Germany) wants to contribute to the implementation of the SDGs framework with a bottom-up approach: while SDGs targets directly address governments, most land degradation processes take place in the private sphere, where farmers play a key role (Keesstra et al., 2018). The solution proposed in this paper suggests that this realignment can be facilitated by introducing an innovative monitoring system that promotes sustainable use and management of soil among farmers. The facilitation of soil monitoring and management at the farmers’ level will, on the one hand, improve SDGs accessibility and applicability. On the other hand, promote a uniform methodology, compliant to the international commitments (the 2030 Agenda) and the internationally recognised strategies to contrast global change, like the Intergovernmental Panel on Climate Change Guidelines.

References

- Death, C., & Gabay, C., 2015. Doing Biopolitics Differently? Radical Potential in the Post-2015 MDG and SDG Debates. *Globalizations*, 12(4), 597-612.
<http://dx.doi.org/10.1080/14747731.2015.1033172>
- European Commission, 2020. EU Biodiversity Strategy for 2030. Bringing nature back into our lives. COM (2020) 380 final.
- IAEG-SDGs, 2016. 'IAEG-SDGs — SDG Indicators'. Sustainable Development Goals.
<http://unstats.un.org/sdgs/iaeg-sdgs/metadata-compilation/>
- IPBES, 2018. Summary for policymakers of the assessment report on land degradation and restoration of the Intergovernmental Science-Policy Platform on Biodiversity and Ecosystem Services. (eds.). IPBES secretariat, Bonn, Germany.
- Keesstra, S., Mol, G., de Leeuw, J., Okx, J., Molenaar, C., de Cleen, M. and Visser, S., 2018. Soil-Related Sustainable Development Goals: Four Concepts to Make Land Degradation Neutrality and Restoration Work. *Land*, 7(4), p.133.
- Mancebo, F., 2015. Introduction. In F. Mancebo & I. Sachs, *Transitions to sustainability* (1st ed.). London: Springer.
- Mercier, A., Betbeder, J., Baudry, J., Le Roux, V., Spicher, F., Lacoux, J., Roger, D. and Hubert-Moy, L., 2020. Evaluation of Sentinel-1 & 2 time series for predicting wheat and rapeseed phenological stages. *ISPRS Journal of Photogrammetry and Remote Sensing*, 163, pp.231-256.
- Percival, D.B., Walden, A.T., William, A., Percival, D., and Constantine, M.W., 2016. Wavelet methods for time series analysis. [Online]. Available: <https://cran.r-project.org/package=wmtsa>
- Sorenson, P., Small, C., Tappert, M., Quideau, S., Drozdowski, B., Underwood, A. and Janz, A., 2017. Monitoring organic carbon, total nitrogen, and pH for reclaimed soils using field reflectance spectroscopy. *Canadian Journal of Soil Science*, 97(2), pp.241-248.
- Tóth, G., Hermann, T., da Silva, M. and Montanarella, L., 2018. Monitoring soil for sustainable development and land degradation neutrality. *Environmental Monitoring and Assessment*, 190(2).
- United Nations, 2015. *The Millennium Development Goals Report 2015* (pp. 1-9).
- UNSD, 2018. SDG Indicators. Metadata Repository for target 15.3.1. [Online]. Available: <https://unstats.un.org/sdgs/metadata/?Text=&Goal=15&Target=>

Using Open-Source Data and Software to Analyse Land-Use Changes and Deforestation in Marqués de Comillas, Chiapas, Mexico (Work in Progress)

Iskar Jasmani Waluyo Moreno¹, José García Hernández², Agustín Bolóm Gómez¹ and Julio Cesar García Sampayo¹

¹Centro de investigación en Ciencias de Información Geoespacial, México

²Universidad de Chalcatongo, México

Abstract

This project aimed to exploit existing open data and open-source software to allow visualising and finding spatial coincidences between three groups of indicators: 1) agricultural activity, 2) land use and forest cover changes, and 3) spatial distribution patterns of vegetation loss. This paper presents preliminary results of developing an interactive map using R, Leaflet, and QGIS to perform a simple overlay analysis of layers containing better policy and decision-making indicators. The map uses open data available through the Mexican government platforms, and all processing, storage and publication are done using free open-source software tools. The data used in this project was limited to the Marqués de Comillas municipality because of its importance in Mexico's forest ecosystem. The maps are a work in progress and a continuation of research done for a geomatics graduate program in Centro de Investigación en Ciencias de Información Geoespacial.

Keywords: overlay analysis, Chiapas deforestation, open source geospatial data, open source geospatial software

1 Introduction

Agricultural expansion continues to be one of the main drivers of deforestation and forest fragmentation, and the associated loss of forest biodiversity. The deforestation rate in the 1990s was 16 million hectares per year and 10 million hectares per year from 2015 to 2020. (FAO & UN, 2020). Decisions on land use have prioritized the benefits of agriculture over forest conservation, which in large part explains continued deforestation in the tropics. In the short term, deforestation allows greater productivity, but long-term effects may be inverse due to soil degradation (Benhin, 2006). Although simplistic, analysing links between agricultural activity and deforestation can provide preliminary information regarding the drivers of land-use changes and deforestation (Benhin, 2006).

Deforestation drivers in Mexico is strongly influenced by contradictory public policies that, on the one hand, promote conservation and, on the other, promote productive activities in forest

ecosystems. Most recently, the federal program “Sembrando Vida” provides economic support to farmers who have access to at least 2.5 ha of workable land for agroforestry projects and are located in municipalities with social lag. The broad goals of the program are: promoting food auto sufficiency, increasing employment levels and improving forest cover. A review of newspaper notes and research papers regarding the program revealed mixed results. While the program has had positive results, it has also contributed to the deforestation of natural and endemic forest cover (Olvera, 2019; Forbes Staff, 2016; Acosta and Vera-Herrera, 2019; Arturo, 2020; Enciso, 2020; Quadri, 2020; CONEVAL, 2020). However, state-level data regarding the program is clear, at municipal levels the information about the “Sembrando Vida” program is not (Colter et al., 2020). Furthermore, no current evaluations or recommendations were found that analyse the effects of the program on forest coverage. In this regard, this article presents preliminary results of a interactive map prototype intended to use open data and open source software to facilitate monitoring land use changes and agricultural activities at a sub-municipal level that could provide useful information for better evaluation and monitoring of programs such as these.

2 Proposal

There is a large amount of data regarding forest cover, land use and agricultural activities in Mexico. Additionally, satellite imagery from several different sources is also freely and widely available. Although easily accessed, the data used is often stored in different repositories and in different formats and dimensions, making combining data of related phenomena, such as agriculture and deforestation, complex. The following table compares three platforms that allow visualisation of this type of data in Mexico.

Table 1: Comparison of existing portals with georeferenced data in Mexico

	GAIA INEGI	Geoportal CONABIO	Geoweb Chiapas
Datasets	20	>13000	>200
Allows data download	Not all layers	Yes	Yes
Code is available	No	No	No
Allows overlays	No	No	No
Regional or National	National	Both	Regional
Can filter data by region	Not all layers	No	NA

Albeit not exhaustive, none of the platforms reviewed allowed overlaying layers of data at state or municipal levels, and none of them provided code or development information. Exploiting the full potential of all of this data requires it to be easily visualised and compared, which we consider as important as developing new models and generating new data. In this sense, this paper presents preliminary results of a prototype of a simple GIS that allows basic data visualisation by homologating data from different open data sources and open-source software. The map is intended to allow simple overlay analysis of the data that contributes to

finding likely or best locations for a specific phenomenon (ArcGIS, 2020). The system is designed to help to answer three general but essential questions at a local scale:

1. Where are the changes in land use and forest cover clustering?
2. What are the main agricultural activities where these clusters are occurring?
3. What may the different combinations of these clusters/activities indicate?

This work is not focused on designing or implementing a complex model but rather on attempting to configure, process and compare readily available data from different sources in a simple interactive map that allows overlay analysis of the following groups of data (see table 2):

Group 1: Agricultural activities

Group 2: Land cover change

Group 3: Spatial autocorrelation of vegetation loss

End users will be able to select different combinations of layers data and overlay analysis of these combinations as well as access raw and processed data used.

3 Case Study: Marques de Comillas Chiapas, Mexico

This pilot project was limited to the Marqués de Comillas municipality because of its relevance Mexico's forest; it is located in the last redoubts of high evergreen forest in the country, an ecosystem that went from 10 million hectares to just over 1 million that contains remnants of the forest that allow the mobility of different species and also bordered the Montes Azules Biosphere Reserve which preserves the greatest diversity of species in Mexico (Carabias, de la Maza & Cadena, 2015; Flores, 2019). Productive activities in this region are in constant conflict with forest conservation; finding ways to guarantee the population's well-being should balance productive capacity with conserving the ecosystem. It is widely accepted that agriculture is a driver of tropical deforestation and its large scale environmental consequences. Thus through proxies such as plot size, it may be possible to analyse details that provide accurate data regarding forest cover changes (Dang, 2019).

4 Data Processing and Map Development

Data sources: Data from Censo Agropecuario 2007¹ (INEGI, 2007), AMCA 2016² (INEGI, 2016), USV series III and VI³, was pre-processed in R in order to generate data frames that could be easily concatenated with maps and compared with land cover change information. The results were then stored as .Rdata and .geojson files in a Github account.

¹ Censo Agrícola, Ganadero y Forestal 2007 – Agriculture, Livestock and Forestry Census 2007

² Actualización del Marco Censal Agropecuario 2016 – Update of the Agriculture, Livestock and Forestry Census 2016

³ Uso de suelo y vegetación serie III and serie VI – Land use series III and series IV are nationwide maps of landuse published in 2005 and 2016 respectively.

Data Processing: Data processing was divided into three groups, as shown in the following table.

Table 2: Groups and indicators

* The census was taken in 2007 and 2016 do not allow comparing data directly. Only data from 2016 data was used for creating thematic maps for the time being.

Group 1: Agricultural activities (2016)*	Group 2: Land cover change (2007-2016)	Group 2: Spatial autocorrelation of vegetation loss (2007-2016)
Parcels with some kind agricultural activity.	Continued anthropic activity (% of ha)	Spatial autocorrelation of changes in primary vegetation (no scale)
Agricultural activities (% of parcels)	Conserved forest cover (% of ha)	Spatial autocorrelation of changes in secondary vegetation (no scale)
Productive forestry activities (% of parcels)	Increase of agricultural activity (% of ha)	Spatial autocorrelation of changes in vegetation (includes primary and secondary vegetation) (no scale)
Livestock activities (% of parcels)	Increase of primary vegetation (% ha)	
	Increase of secondary vegetation (% ha)	
	Reduction of primary vegetation (% ha)	
	Reduction of secondary vegetation (% ha)	
	Increase in urbanized area (% ha)	

Interactive Map Development: Processed data was uploaded to Github and then processed again using R and its Leaflet library to create thematic map layers of the aforementioned data groups. Afterwards, the Shiny library was used to deploy the maps in an interactive map in shinyapps.io (Shiny, 2020). Initially, data was read directly from Github through shinyapp.io; this made the process slow and surpassed the shinyapp.io server free account limits. However, this was solved using the .Rdata file because it allowed loading “pre-processed” data. Data and code are stored in Github⁴, and an experimental version of the map is available on a free Shiny Apps⁵ account.

⁴ https://github.com/iskarwaluyo/mapa_agricultura_masaforestal/

⁵ https://iskarwaluyo.shinyapps.io/mapa_agricultura_masaforestal_comillas/

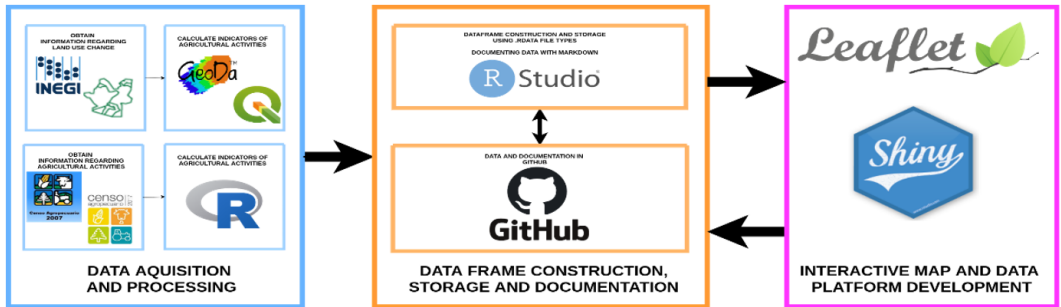


Figure 1: Project development scheme

5 Preliminary Results

The following figures show overlays of layers of autocorrelation of vegetation loss and percentage of plots with agricultural, livestock and forest activities. Although rudimentary, these types of visualisations allow quick identification of combinations of clusters of vegetation loss and main agricultural activities, theoretically providing quick contextual information for decision takers and policymakers.

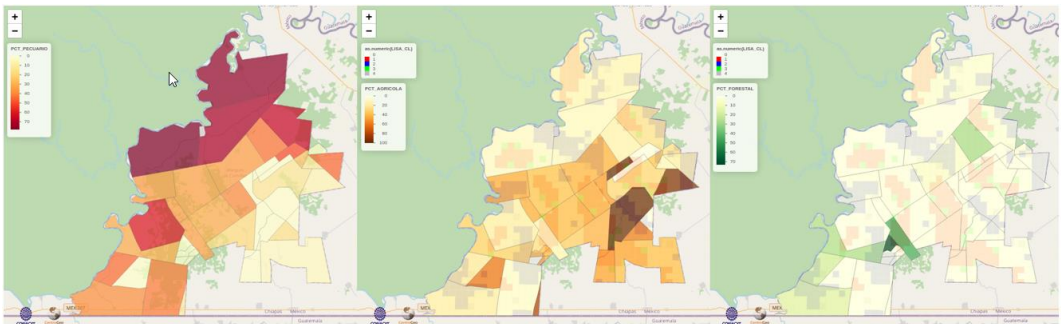


Figure 2: Overlays with autocorrelation of vegetation loss from left to right a) livestock activity, b) agricultural activity and c) productive forestry activity

A visual analysis of the layers may illustrate overlaps between data may better explain land-use changes in the region. For example, it was found that AC 07116010-1007 occupies 46% of plots with forestry activities. However, it also had a positive autocorrelation of total vegetation loss which seems contradictory; a closer look allows noticing that the net vegetation loss is negative due to secondary vegetation loss, but primary vegetation is increasing. A hypothesis that arises from this pattern is that overlaps of clusters with secondary vegetation loss and primary vegetation gain may indicate reforestation or forest stand maturity.

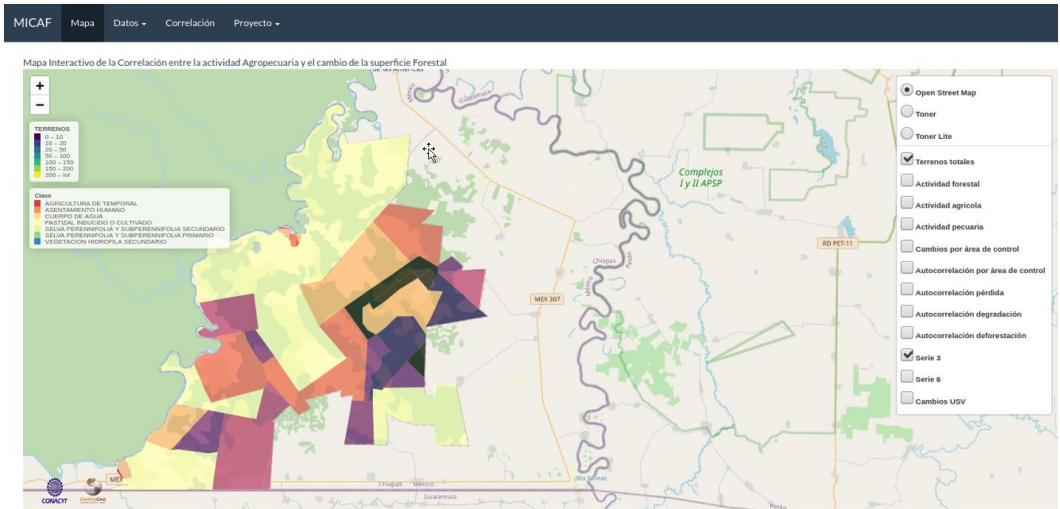


Figure 3: Screenshot of interactive map deployed in shinyapps.io

Another quick pattern that stands out is that most livestock production activity occurs near the northern natural border of the municipality, a river that borders the conservation area. Thus agroforestry programs such as the ones being promoted currently in Mexico could be beneficial in these specific areas of the municipality.

6 Conclusions

After reviewing a number of platforms, we sustain that although there is a large amount of data available, there is a need to develop lighter, less robust platforms designed for end-users. Current platforms are excellent data repositories but require a lot of data manipulation by specialists to exploit the data. Given the urgency many institutions, organisations, leaders and decision-makers have to decide sometimes; we believe that current platforms do not allow easy access to the data they contain. The prototype we present is practical and allows relatively quick overlays and data queries. Although our results are not detailed, they allow an overview that we consider helpful for end-users who often need to make general data consultations and comparisons. Additionally, the cost and time of development are relatively low, which is advantageous for areas where the cost of data analysis and software development are limiting factors for progressing towards the UNSDGs. Nonetheless, our project is only a prototype and its scalability, and real-world use is unknown at this point. We recognize that further research regarding the needs of end-users and computational costs of expanding our work is needed in order to determine the potential of using open-source data and software to develop quicker, lighter and cheaper speciality platforms such as the one we present in this paper. Additionally, it is important that our results be validated; although we are confident that the data used is reliable, further developments could include validating our results with other processes such as NDVI.

References

- Anselin, L. (2004). GeoDa 0.95i Release Notes. Spatial Analysis Laboratory (SAL). Department of Agricultural and Consumer Economics, University of Illinois, Urbana-Champaign, IL. http://geoda-center.github.io/workbook/6a_local_auto/lab6a.html
- ArcGIS. (2020). Comprender El Análisis De Superposición—Ayuda | Arcgis for Desktop. Retrieved June 30, 2020, from <https://desktop.arcgis.com/es/arcmap/10.3/tools/spatial-analyst-toolbox/understanding-overlay-analysis.htm>.
- Arturo, P. (2020, June 13). Sembrando Vida, la reforestación más grande del mundo. Retrieved January 30, 2021, from <https://www.excelsior.com.mx/nacional/sembrando-vida-la-reforestacion-mas-grande-del-mundo/1387883>
- Benhin, J., (2006). "Agriculture and Deforestation in the Tropics: A Critical Theoretical and Empirical Review," *AMBIO: A Journal of the Human Environment* 35(1), 9-16. <https://doi.org/10.1579/0044-7447-35.1.9>
- Quadri de la Torre, G. (2020). Sembrando Vida, la otra catástrofe. Retrieved January 30, 2021, from <https://www.eleconomista.com.mx/opinion/Sembrando-Vida-la-otra-catastrofe--20200820-0130.html>
- Enciso, A. L. (2020, October 12). Sembrando Vida no rescata bosques: ONG. Retrieved January 30, 2021, from <https://www.jornada.com.mx/ultimas/sociedad/2020/10/12/sembrando-vida-no-rescata-bosques-ong-3923.html>
- Carabias, J., de la Maza, J., Cadena, R. (2015). Conservación y desarrollo sustentable en la Selva Lacandona 25 años de Actividades y experiencias. *Natura y Ecosistemas Mexicanos*, A.C.
- Cheng, G. (2020). Leaflet. (Version 2.0.4.1) [Software library for R]. <https://rstudio.github.io/leaflet/>
- Chang, W. (2020). Shiny. (Version 1.6.0) [Software library for R]. <https://cran.r-project.org/web/packages/shiny/index.html>
- CONEVAL (Consejo Nacional de Evaluación de la Política de Desarrollo Social). (2020). Evaluación de Diseño con Trabajo de Campo del Programa Sembrando Vida 2019-2020. Mexico City.
- Cotler, H., Manson, R., Nava, J.D. (2020). Evaluación de la focalización del Programa Sembrando Vida. Retrieved January 30, 2021, from https://www.centrogeo.org.mx/cgeo_archivo/200518_evaluacion-de-la-focalizacion-del-programa-sembrando-vida.pdf
- Dang DKD, Patterson AC, Carrasco LR (2019). An analysis of the spatial association between deforestation and agricultural field sizes in the tropics and subtropics. *PLoS ONE* 14(1): e0209918. <https://doi.org/10.1371/journal.pone.0209918>
- FAO and UNEP. 2020. The State of the World's Forests 2020. Forests, biodiversity and people. Rome. <https://doi.org/10.4060/ca8642en>
- Flores, M.L. (2019). Los alcances en la producción agrícola chiapaneca. Una reflexión sobre la soberanía alimentaria en la región. *región y sociedad*, 31, e1177. doi: 10.22198/rys2019/31/1177
- Forbes Staff. (2019, July 11). Talan árboles en Veracruz para entrar al programa 'Sembrando Vida' • Actualidad • Forbes México. Retrieved January 30, 2021, from <https://www.forbes.com.mx/pobladores-talan-arboles-para-entrar-al-programa-sembrando-vida/>
- Gentleman, R., Ihaka, R. (2019). R. (Version 3.6.1) [Computer software]. <https://www.r-project.org/>
- INEGI. (2005). Uso del suelo y vegetación, escala 1:250000, serie III (continuo nacional). Retrieved June 30, 2020, from http://www.conabio.gob.mx/informacion/gis/?vns=gis_root/usv/inegi/usv250ks3gw
- INEGI. (2007). Censo Agrícola, Ganadero y Forestal 2007. Retrieved June 30, 2020, from <https://www.inegi.org.mx/programas/cagf/2007/#Documentacion>
- INEGI. (2016). Actualización del Marco Censal Agropecuario 2016. Retrieved June 30, 2020, from <https://www.inegi.org.mx/programas/amca/2016/>

- INEGI. (2016). Uso del suelo y vegetación, escala 1:250000, serie VI (continuo nacional). Retrieved June 30, 2020, from http://www.conabio.gob.mx/informacion/gis/?vns=gis_root/usv/inegi/usv250ks3gw
- Olvera, D. (2020, March 06). No se debió sembrar en primer año del programa Sembrando Vida, se saltaron la planeación: Expertos. Retrieved January 30, 2021, from <https://www.economiahoy.mx/nacional-eAm-mx/noticias/10400116/03/20/No-se-debio-sembrar-en-primer-ano-del-programa-Sembrando-Vida-se-saltaron-la-planeacion-expertos.html>
- Pontius, R. G. Jr., E. Shusas and M. McEachern (2004), “Detecting important categorical land changes while accounting for persistence”, *Agriculture, Ecosystems and Environment*, no. 101, pp. 251–268.
- Sherman, G. (2020). Quantum GIS. (Version 3.16) [Computer software]. <https://www.qgis.org/>

Nationalization of Indicators for Sustainable Development Goals in the Republic of Kazakhstan through Geoinformation Technologies

GI_Forum 2021, Issue 1
Page: 158 - 168
Best Practice Paper
Corresponding Author:
gulnara.nyusupova@kaznu.kz
DOI: 10.1553/giscience2021_01_s158

Gulnara Nyussupova¹, Gaukhar Aidarkhanova¹, Madiyar Kadylbekov¹, Laura Kenespayeva¹, Roza Kelinbayeva¹ and Bazaraly Kozhakhmetov¹

¹Al-Farabi KazNU, Kazakhstan

Abstract

From the first days of independence, Kazakhstan has paid attention to sustainable development and successfully achieved the Millennium Development Goals and in 2015 launched the implementation of the 2030 Agenda for Sustainable Development. The article discusses the issues of monitoring and reporting on the SDGs in Kazakhstan, the priority of nationalization of indicators, the creation of a statistical database on the SDGs, the definition of data sources, and methodology for calculation. Geospatial data are inevitable for the integration of information about society, economy and environment. A web-portal developed by the authors is presented that allows to assess the quality of life of the population in different regions based on the SDG indicators.

Keywords: sustainable development goals, geospatial information, geoinformation technologies, atlas information system, Republic of Kazakhstan

1 Introduction

In 2015 in New York, the UN adopted the "The 2030 Agenda for Sustainable Development" - aimed at achieving progressive, sustainable development of all countries of the world (United Nations, & Nations, U. (2015). Kazakhstan, among other states, also took an active part in the development of this Agenda.

The Sustainable Development Goals (SDGs) are a set of goals for future international cooperation that replaced the Millennium Development Goals (https://www.un.org/ru/documents/decl_conv/declarations/) at the end of 2015. The SDG goals are planning to achieve from 2015 to 2030. To track progress on each goal developed a set of quantifiable indicators, targets, and observables specific to each goal. The final document, "Transforming Our World: the 2030 Agenda for Sustainable Development," contains 17 global goals and 169 related targets. The SDGs adopted by 193 UN member states.

The targets of the SDGs largely coincide with the priorities of the Republic of Kazakhstan outlined in the development documents: the Development Strategy "Kazakhstan-2050", the Strategic Development Plan until 2025, the "National Plan – 100 Concrete Steps" for the implementation of five institutional reforms, Five social initiatives of the Head of State and the State Program "Ruhani Zhangyru" (https://www.akorda.kz/ru/official_documents/-/strategies_and_programs). These national programs and initiatives aimed at improving the quality of life of all segments of the population, creating a sustainable economy and strengthening human capital in the republic. To date, about 80% of the SDG objectives are reflected in the documents of the state planning system of Kazakhstan.

The 2030 Agenda and its 17 goals call for a balance of social, economic and environmental dimensions to ensure inclusive and sustainable economic growth, social inclusion and environmental sustainability. Thus, Kazakhstan sets the main guidelines of its state policy to ensure social justice and environmental sustainability, the transition from short-term planning to long-term vision. The assumption of social and environmental costs as investments in sustainable development, and the limited recognition of planetary boundaries and the need for systemic change "by enhancing well-being and quality of life of the population of Kazakhstan and the country's entry into the top 30 most developed countries of the world while minimizing the burden on the environment and degradation of natural resources." (Decree of the President of the Republic of Kazakhstan 2013).

Thus, the SDGs are in many respects consistent with Kazakhstan's development efforts and can serve as a useful and convincing strategic framework for addressing national challenges.

Monitoring and reporting on the SDGs are receiving close attention. Nationalization of indicators, creation of a statistical database on SDGs, identification of data sources, and methodology for calculation are in priority.

2 Material and Methods

Research uses theoretical and methodological analysis of scientific literature, methods of comparative and structural analysis, grouping and systematization of databases, and geoinformation technologies. Statistical and analytical data are collected from the national SDG reporting platforms of the Republic of Kazakhstan, monographs, scientific articles, publications and reports of the UN, etc.

3 Results and Discussion

The role of big data in the analysis of SDG indicators has been considered by many scientists (MacFeely 2019; Breuer et al., 2019; Allen et al., 2019).

Information about the physical, chemical, and biological systems of the planet that are needed to achieve, monitor, and monitor the SDGs can be detected using remote sensing technologies (Masó et al., 2019). Remote sensing and GIS methods use satellite data that provide a synoptic overview with global and local coverage at different spatial resolutions. These approaches can

also be used to monitor the impact of climate change on various components of aquatic and terrestrial ecosystems, in addition to field survey data (Avtar et al., 2013).

Location plays a huge role in integrating information about society, the economy, and the environment, and is key to tracking progress towards each of the SDGs. The UN recognizes the role of location in integrating information about society, economy, and environment, while also simply tracking each of the SDGs. Over the years, the organization has worked to combine geospatial and statistical information to visualize patterns, address data gaps, and effectively channel resources into areas most in demand to improve overall development outcomes (Paul Cheung 2015).



Figure 1: Correlation of SDGs with the goals and objectives of documents of the State Planning System of the Republic of Kazakhstan

The United Nations Statistics Division (UNSD) is now teaming up with ESRI to conduct research for testing a data center that will help target Member States measure, track and report on their progress towards achieving the SDGs in a geographical context.

This data research makes it possible to store all the information in one place. As part of the project, several participating countries are leveraging their existing data systems and deploying the ArcGIS Hub together with ArcGIS Enterprise to help their national statistical

organizations integrate SDG-related data into their work. The event also aims to ensure that national statistical organizations align their data and systems with other SDG stakeholders in the country, including mapping agencies, ministries, natural resources and environment agencies.

Kazakhstan, as a country that has committed itself to achieving the Sustainable Development Goals, is actively working in all areas and contributing to the successful achievement of global goals. The state planning system is consistent with the SDG targets (Figure 1).

Monitoring and reporting on the SDGs are receiving close attention in the Republic of Kazakhstan. Nationalization of indicators, creation of a statistical database on SDGs, identification of data sources, and methodology for calculation are in priority. The main government body responsible for collecting, processing and disseminating data on the SDGs is Bureau of National Statistics of the Agency for Strategic Planning and Reforms of the Republic of Kazakhstan. As a result of the work carried out to nationalize the Sustainable Development Goals, a nationalized list of 17 goals, 169 targets and 297 indicators was approved (with the addition of 76 national indicators, 35 of which are proposed additionally) (Figure 2).

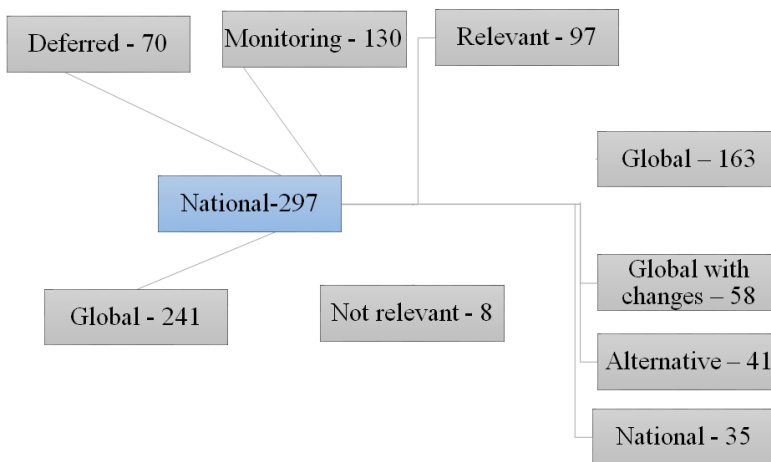


Figure 2: Nationalized list of SDG indicators in the Republic of Kazakhstan

At the same time, according to the results of the analysis, the indicators were grouped into four categories, including:

- Relevant indicators, which are the highest priority for policy implementation - 97;
- Some of the indicators that need to be monitored taking into account the current policy were proposed for monitoring - 130;
- Deferred indicators for which there are currently no calculation methodology or baseline values - 70;
- Not relevant for the country - 8.

At this stage, it is planned to carry out monitoring in the first two categories, where the initial data have already been determined. Work on deferred indicators will be phased in as the methodology is agreed globally and national data sources are identified.

The national SDG monitoring and reporting system consists of two main elements: the integration of SDG indicators into documents of the state planning system and official statistics. The data are published on the official web resources of state bodies in the form of official statistics and conclusions based on the results of monitoring and evaluation of strategic and program documents. Official statistics will play a key role in providing data for monitoring the SDGs and related targets. The Bureau of National Statistics of the Agency for Strategic Planning and Reforms of the Republic of Kazakhstan has also developed a national SDG reporting platform, which is under development and is available at: <https://kazstat.github.io/sdg-site-kazstat/> (Figure 3).

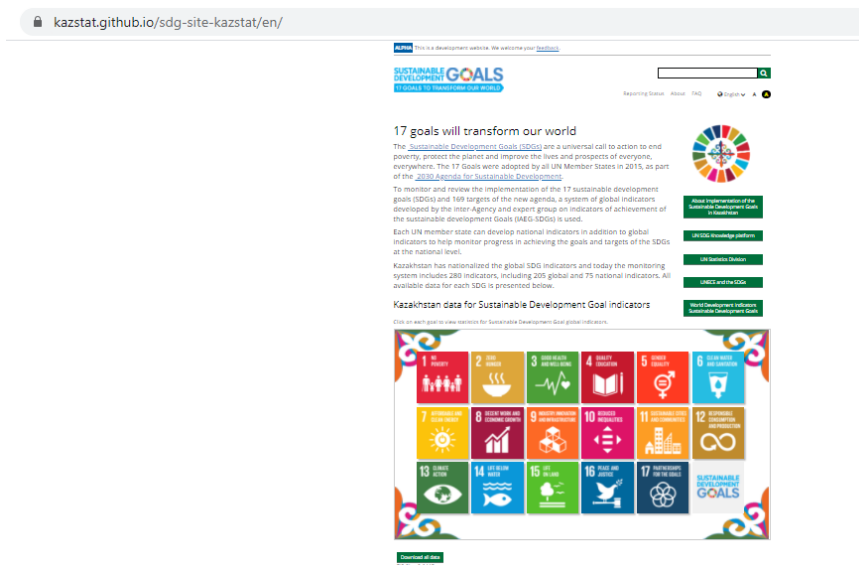


Figure 3: National SDG reporting platform Bureau of National Statistics of the Agency for Strategic Planning and Reforms of the Republic of Kazakhstan <https://kazstat.github.io/sdg-site-kazstat/>

The purpose of this platform is to provide Kazakhstan with data on both global indicators of the achievement of the Sustainable Development Goals (SDGs) and national indicators. In addition, it provides the interested public with constantly updated information on the status of the SDG indicators in Kazakhstan and detailed information on their calculation methodology. Data from monitoring SDG indicators in Kazakhstan are presented on the website in the form of tables and graphs (Figure 4).

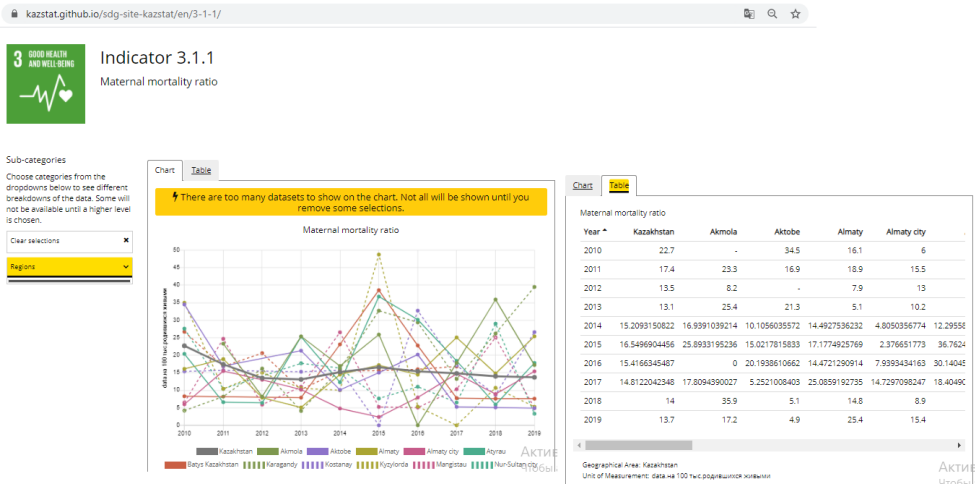


Figure 4: Indicator "Maternal mortality ratio" on the national SDG platform of the Republic of Kazakhstan <https://kazstat.github.io/sdg-site-kazstat/en/>

Unfortunately, geospatial data is not yet presented in the national SDG platform of the Republic of Kazakhstan. The continuous flow of information to adapt management methods to the changing situation during the implementation of the SDGs emphasizes the importance and feasibility of introducing a geographic information system for researching territorial aspects and addressing SDG issues. In this regard, work is underway in Kazakhstan to create a geospatial database for SDG indicators. On the basis of Al-Farabi KazNU a scientific study "Development of an atlas information system for a comprehensive spatial analysis of the quality of life of the population of the regions of the Republic of Kazakhstan as part of the implementation of the program" Digital Kazakhstan" was carried out, where the quality of life of the population of the regions was assessed using SDG indicators. During the work, a geodatabase was created for SDG indicators, thematic maps on the website of the developed atlas information system.

The Atlas Information System of the Quality of Life of the Population is a geo-informational web system for poly-scale organization of data, mapping, modeling and forecasting the situation in the field of research of indicators (economic, social, demographic and natural-ecological, SDGs) of the quality of life of the population. The main feature of the atlas information system in comparison with the geographic information system is the expanded capabilities of the cartographic representation of spatial data in the AIS.

Of course, the management of QoL indicators for the SDGs requires an exhaustive set of input data, including natural and socio-economic topics. Depending on the presence or absence of a particular set of data, various types of analysis will be available and, accordingly, management decisions of different complexity and flexibility will be available. On the basis of the considered QoL indicators, as well as the experience of using GIS in the management of QoL indicators, a conceptual scheme for the use of geoinformation technologies is proposed (Figure 5).

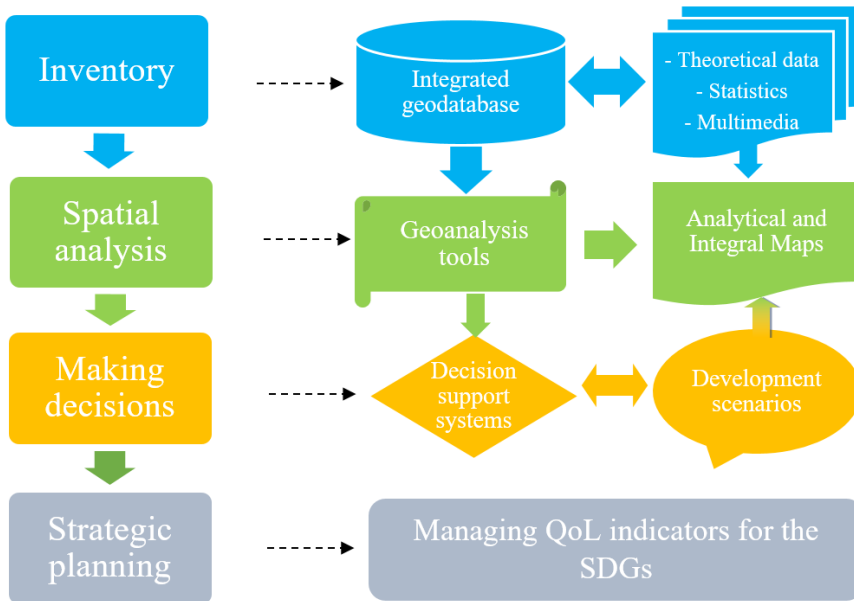
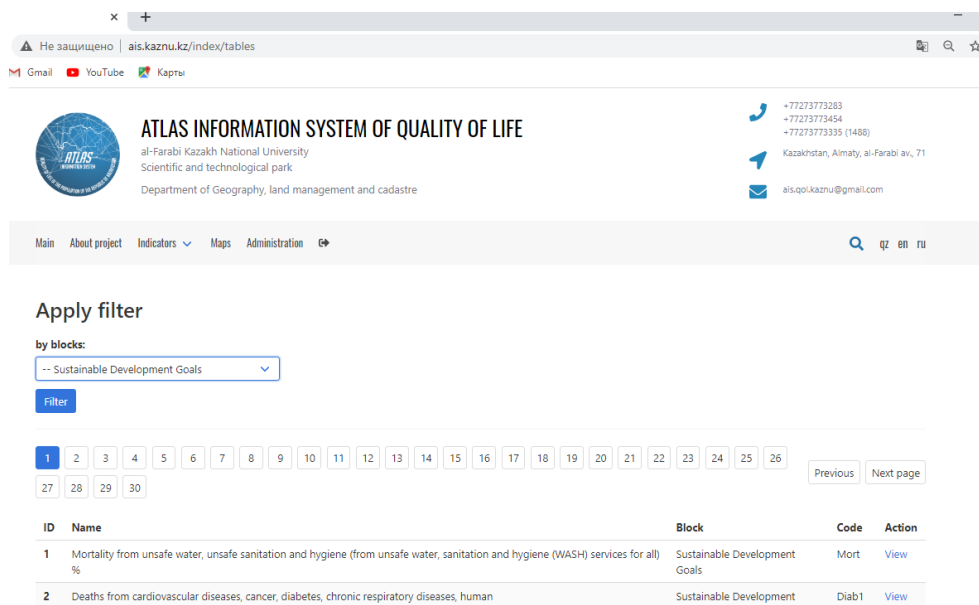


Figure 5: Algorithm for the use of geoinformation technologies in the management of QoL indicators for the SDGs

AIS QoL is characterized by a multi-level structure, consisting of blocks of information - the main groups of indicators characterizing the quality of life of the population: economic, social, demographic and natural-ecological, SDGs. Each of the blocks has two structural components. The first is the structure of files by type (maps and schematic maps, text descriptions, graphic material, tables). The second is the corresponding internal structure (blocks-sub-blocks-indicators), developed based on the content of the block. AIS QoL made it possible to integrate data from various sources, to form and collect information in the form of a single geoinformation base, varied in detail, time coverage, methods of obtaining, a set of indicators, types of presentation. So, to ensure the functioning of the AIS, a structure was developed and a geodatabase (GDB) was formed according to objective indicators of the quality of life of the population, consisting of two types of information: statistical and spatial. The spatial database is represented by vector layers previously created and processed in GIS and corresponding to the basic requirements of vector information (detail, reliability, accuracy, unity of the coordinate system and projection, etc.). Methods of geoinformation analysis, ERS processing, and digital mapping methods were used through ArcGIS Desktop in creating a digital basis. Each layer of the base is accompanied by attributive information in three languages about the qualitative and quantitative characteristics of the object.

The statistical data of the AIS QoL database are partial and integral indicators of the quality of life of the population for the following groups of indicators: economic, social, demographic, natural and ecological, SDGs. A total of 340 indicators were collected, including 71 SDG indicators (Figure 6).



The screenshot shows the website interface for the Atlas Information System of Quality of Life. At the top, there is a navigation menu with links for Main, About project, Indicators, Maps, and Administration. A search bar and language options (qz en ru) are also present. The main content area features a filter section where 'Sustainable Development Goals' is selected. Below the filter is a pagination control showing a grid of numbers from 1 to 30, with '1' highlighted. A table of indicators is displayed below the pagination, with the first two rows visible:

ID	Name	Block	Code	Action
1	Mortality from unsafe water, unsafe sanitation and hygiene (from unsafe water, sanitation and hygiene (WASH) services for all) %	Sustainable Development Goals	Mort	View
2	Deaths from cardiovascular diseases, cancer, diabetes, chronic respiratory diseases, human	Sustainable Development	Diab1	View

Figure 6: SDG indicators on the AIS QoL website <http://ais.kaznu.kz/index>

The development of AIS QoL in the form of a website began with the formation of the database structure and dependencies between the database tables. PostgreSQL 9 was chosen as the database management system, which supports tools for creating and storing procedures.

Geographic data, previously created and processed in GIS, are uploaded to the site as a cartographic base for all future thematic maps of AIS QoL. The formation of thematic maps of QoL was carried out by linking the statistical indicators of QoL uploaded to the site to the vector cartographic layer of administrative regions.

An important feature of the website is the ability for the user to further replenish and update the database and automatically compile new thematic maps based on requests, using the site's statistical data on indicators. This creates conditions for further monitoring and research of QoL indicators of regions, both in the context of regions and in the context of districts of cities of republican significance.

The visualization function of AIS QoL data is a presentation of QoL indicators in the form of maps, tables, texts and graphs and is the result of geoanalysis in the most understandable and convenient form for solving specific problems of monitoring and managing the level of QoL development in the regions of the Republic of Kazakhstan. AIS QoL allows to make inquiries and visualize processes.

The function of geoanalysis and modeling of AIS QoL allows a means of overlaying thematic layers - indicators of economic, social, demographic and natural-ecological blocks of QoL indicators of the regions of Kazakhstan for 1999-2018 to carry out interactive implementation of integrated maps. These cartographic models make it possible to analyze the situation, identify patterns of development, relationships in spatial distribution, identify trends in the development of processes for solving specific problems, in this case for monitoring and

managing QoL indicators and making decisions to increase the QoL level in the regions of Kazakhstan.

When creating the site, the determining factors were: the ability to implement information retrieval functions; the possibility of integrated processing of cartographic and text data; convenient forms of dialogue with the user; the ability to adapt the atlas to changes in the forms of input and output documents; the presence of a variety of data models specialized in information processing tasks, closely integrated with a supporting atlas information system; flexibility in choosing the architecture of the system supporting the atlas; openness to external programs.

Thematic maps of AIS QoL reflect the indicators of the SDGs in the field of education, health care, social sphere, employment, as well as environmental changes in the regions of the Republic of Kazakhstan. Visualization of thematic maps by the method of cartograms gives a clear picture of the intensity of certain processes and phenomena, allows to reveal the spatial differentiation of the development of regions by the level of QoL and SDG indicators (Figure 7).

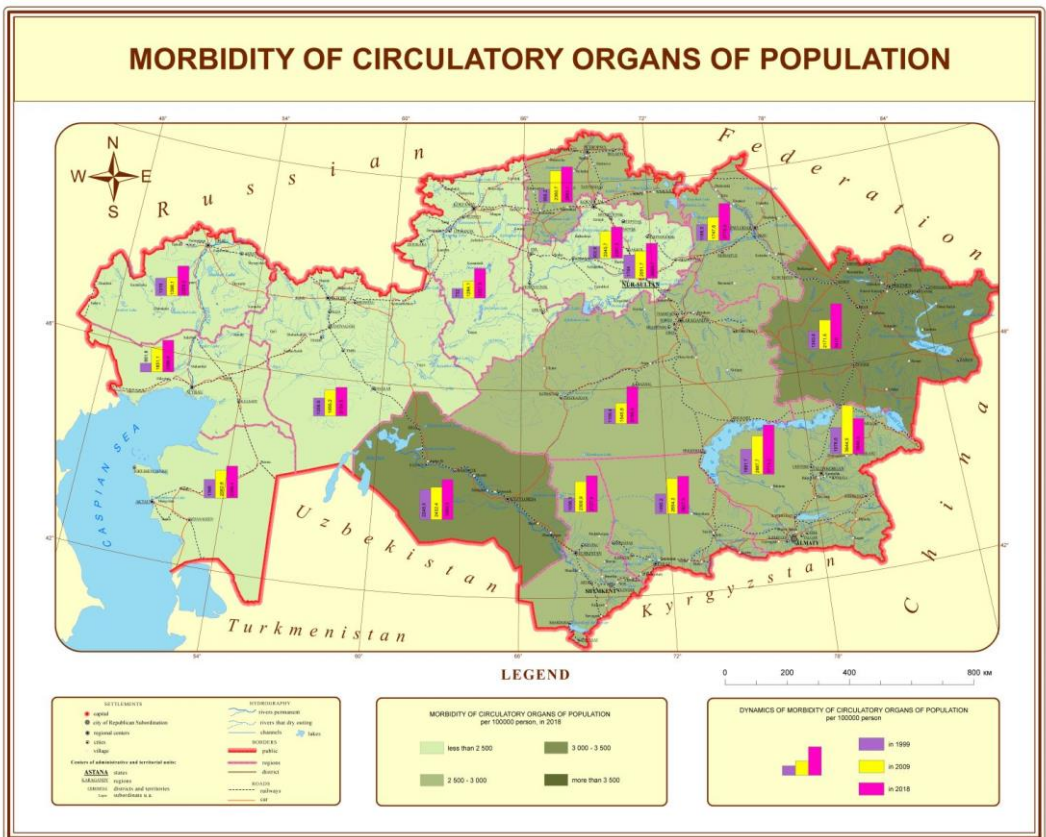


Figure 7: Morbidity of circulatory organs of population in Republic of Kazakhstan

SDG 1 is poverty eradication. The use of alternative methods based on GIS and digital AIS QLM maps (the share of the population with incomes below the subsistence level, poverty indicators, average per capita nominal monetary incomes of the population, subsistence minimum, regional distribution of poverty) based on geospatial data, provide information on the spatial differences of the regions of the republic, related to various SDG 1 indicators. These maps are an important tool for developing effective policies aimed at reducing regional inequality through the implementation, regulation and improvement of social protection programs for the allocation of subsidies, pension payments, efficient resource use, unemployment insurance, etc. (Avtar et al., 2019).

Health system indicator maps, along with indicators of infant and maternal mortality in the regions of Kazakhstan, allow to identify regional differences for effective and intensive allocation of budgetary funds and human resources in areas with low indicators to improve the situation to achieve SDG 3.

SDG 4 - getting quality education is the most important condition for improving the quality of life of people and sustainable development. Maps of the education system, reflecting indicators in the field of preschool, school and higher education in the regions of Kazakhstan, as well as teaching staff and educational coverage of the population, clearly reflects the relationship, deficit and surplus of places, professional staff in these institutions. Also relevant during the COVID-19 pandemic and distance learning is a map of access to the Internet in the regions, which demonstrates the access of students and teachers to educational platforms and learning resources. Geospatial representation allows you to identify problem regions for effective and intensive coverage of the population with education, personnel and Internet accessibility.

AIS QoL maps reflect certain aspects of SDG 5. These are maps of the ratio of the male and female population in the regions, gender and age structure, indicators of male and female population life expectancy, incomes and wages of men and women, etc., which allow identifying patterns and conducting a retrospective analysis of gender aspects of the quality of life.

The AIS QoL considers the cities of republican significance Nur-Sultan and Almaty, where 15% of the population of the republic lives. These megacities are centers of economic growth, providing more than 30.5% of GDP. Rapid urbanization leads to an increase in inadequate and congested infrastructure and services (such as waste collection and water and sewerage systems, roads and transport), worsening air pollution and unplanned urban sprawl. Cartographic visualization allows to display the disproportions in the development of individual indicators of the quality of life of the population in the administrative districts of cities. Research data reflect challenges for SDG 11.

The introduction of AIS QoL in the process of teaching bachelors, undergraduates and doctoral students of the university, work with SDG indicators within the AIS QoL is a key moment in the implementation of the implementation of the SDGs in universities. In particular, it provides a basic understanding and visual representation of the subject areas of each of the SDGs, allows to provide in-depth knowledge in the field of both geographic information systems and for the implementation of the SDGs, and expand opportunities for building the potential of future specialists to solve sustainable development problems.

4 Conclusion

Achieving the SDGs undoubtedly requires a huge global concerted effort to effectively leverage the sharing, processing and aggregation of data in a multidisciplinary framework. National Geospatial Information Agencies will need to work closely with national professional communities in the area of statistics and Earth observation

At present, it is becoming easier to obtain spatial geographic data, but the key point is the collection, organization, and management of databases to correctly use this data for analysis, monitoring, and management when making strategically important decisions of states. Spatial analysis plays an important role in determining the causes and effects of a given phenomenon, e.g. for agriculture, global health or nature protection, based on classic GIS procedures like map overlays and assessing the relationships between them.

References

- Allen, C., Metternicht, G., & Wiedmann, T. (2019). Prioritising SDG targets: assessing baselines, gaps and interlinkages. *Sustainability Science*, 14(2), 421-438. <https://doi.org/10.1007/s11625-018-0596-8>.
- Avtar, R., Takeuchi, W., & Sawada, H. (2013). Full polarimetric PALSAR-based land cover monitoring in Cambodia for implementation of REDD policies. *International Journal of Digital Earth*, 6(3), 255-275. <https://doi.org/10.1080/17538947.2011.620639>
- Avtar R, Aggarwal R, Kharrazi A, Kumar P, Kurniawan TA. Utilizing geospatial information to implement SDGs and monitor their Progress. *Environ Monit Assess*. 2019 Dec 11;192(1):35. doi: 10.1007/s10661-019-7996-9. PMID: 31828438.
- Breuer, A., Janetschek, H., & Malerba, D. (2019). Translating sustainable development goal (SDG) interdependencies into policy advice. *Sustainability (Switzerland)*, 11(7). <https://doi.org/10.3390/su1102092>.
- Decree of the President of the Republic of Kazakhstan No. 577, Concept for the transition of the Republic of Kazakhstan to a "green economy", May 30, 2013, https://greenkaz.org/images/for_news/pdf/npa/koncepciya-po-perehodu.pdf
- MacFeely, S. (2019). The big (data) bang: opportunities and challenges for compiling SDG indicators. *Global Policy*, 10 (January), 121-133. <https://doi.org/10.1111/1758-5899.12595>
- Masó, J., Serral, I., Domingo-Marimon, C., & Zabala, A. (2019). Earth observations for sustainable development goals monitoring based on essential variables and driver-pressure-state-impact-response indicators. *International Journal of Digital Earth*, 1-19. <https://doi.org/10.1080/17538947.2019.1576787>.
- Paul Cheung (2015) "National Statisticians Embracing Location-Based Information" *ArcNews*
- United Nations, & Nations, U. (2015). Transforming our world: the 2030 agenda for sustainable development. General assembly 70 session (Vol. 16301). <https://doi.org/10.1007/s13398-014-0173-7.2>

Mapping Flooded Paddy-Rice Fields in the Landscape between Turin and Milan: A GIS-Based Method for Detecting Scenic Routes for Experiential Tourism

Alessandro Scandiffio¹

¹Politecnico di Milano, Italy

Abstract

The current research aims to explore the potential of ESA Sentinel-2 time-series satellite imagery, for detecting the seasonal landscape changes of paddy-rice fields, in the north-west of Italy, by using GIS mapping tools. On a regional scale context, paddy-rice mapping has several implications for agricultural monitoring, precision farming, food production, water management and climate change. However, it also concerns their high scenic value in the landscape perception, which can be a great resource for sustainable tourism. The defining characteristic of paddy-rice is that rice plants grow on flooded soils. In the field of slow tourism, such a temporary site-specific condition of the landscape can become an unconventional tourist destination. The research has been applied to territories in between cities: Turin and Milan, where the phenomenon of paddy-rice flooding, in the spring season, generates an outstanding scenic perception of the rural landscape. The research shows the effectiveness of the GIS workflow to compute the vegetation indices, which are sensitive for mapping flooded paddy-rice fields. The final outcome is a thematic map highlighting the scenic routes in the existing road network that allows experiencing such seasonal landscape conditions.

Keywords: seasonal landscape, vegetation index, paddy-rice, mapping scenic routes, Sentinel-2

1 Introduction

Seasonal landscape changes are strongly interlaced with the annual cycle of plants and human actions impacting the earth. In the last decades, many research efforts have been developed in the field of the earth observation, with the aim of finding new ways to monitor environmental phenomena that occur on the earth's surface. Since 2014, the European Commission, in cooperation with other partners such as ESA and EUMETSAT, has started the ambitious programme for earth observation named: Copernicus. This program consists of seven Sentinel satellites in orbit, which supply geospatial data and geo-information referring to six thematic streams: land monitoring, marine environment monitoring, atmosphere monitoring, security, emergency management and climate change (European Commission, 2015).

2 Seasonal landscape changes and sustainable tourism

The current research aims to investigate the relationships between the seasonal landscape changes related to paddy-rice fields and sustainable tourism. Seasonal landscape changes can affect specific environments such as forests, paddy-rice, vineyards and grasslands that, over the seasons, can assume a high scenic value in landscape perception. Such site-specific phenomena that occur seasonally, such as autumn foliage colouring, spring-blooming of lavender fields and grasslands, and flooding of paddy-rice fields are major attractions for the tourism sector and contribute to increasing the attractiveness of the places (Spotts & Mahoney, 1993), (Hall et al. 2011), (Chen et al., 2016), (Rozenstein & Adamowski, 2017). Paddy-rice fields mapping can play an important role in the field of experiential tourism and perception of agricultural landscapes. In fact, the unique feature of paddy-rice fields is that rice plants grow on flooded soils. On regional-scale contexts, such a temporary condition of the landscape can become an unexpected and unconventional tourist destination. Furthermore, the growth of a new form of tourism, such as experiential tourism, requires new digital tools for supporting personal user's travel-planning. The flooding stage is a time-defined period that is also related to different parameters (temperature, water availability, weather forecasts etc.) that individual farmers consider for their cultivation schedule. On regional-scale contexts, the scenic value of large portions of the rural landscape can be detected through remote sensing and mapped by using GIS techniques. Paddy-rice mapping is a very challenging topic that affects many research fields such as food production, water management, agricultural monitoring, precision farming, water management, and climate changes (Dong & Xiao, 2016b), which are also strongly interlaced with UN SDGs (United Nations, 2015). Examples of these SDGs include: SDG n.2 for sustainable agriculture, SDG n.9 for building resilient and sustainable infrastructure, SDG n.11 for safe, resilient and sustainable human settlements, SDG n.13 actions for climate change, SDG n.15 for sustainable use of the land and environment. Referring to SDGs, the current research will show the application of digital earth observation and GIS mapping techniques, as a tool to support new strategies for sustainable tourism. In this research field, a global-scale continuously updated map showing where and when the flooding of the paddy-rice fields occurs is required. In this framework, the open-access availability of the huge quantities of Sentinel satellite imagery is a vital data source for supporting research activities and decision-making for sustainable tourism management.

3 Study area

The current research has been centred on the *in-between* territories the cities of Turin and Milan, in the north-west of Italy, south of the Alps (province of Vercelli 45°19'26"40 N, 08°24'59"04 E); a complex landscape made up of open spaces, mobility infrastructure, towns, rural settlements, and natural protected areas, which is the result of a long process of interaction between natural elements and human activities. The historically rural landscape, used in intensive agriculture (rice cultivation, vineyards, orchards etc.) is supported by a network of artificial waterways, such as the Cavour canal, built between 1863 and 1866, which is a vital resource for this territory (Segre, 1983), (Monti, 2002), (Occelli et al. 2012), (Rolando & Scandiffio, 2016), for both food production and tourism. Furthermore, the historical network

of local roads is widespread, well maintained and ensures the accessibility to the scenic landscape of paddy-rice fields over the year. The pilgrimage path, Via Francigena (from Canterbury to Rome), that is ridden by many pilgrims over the year, crosses these territories from the Alps to Po valley, and it is a great resource for slow tourism. The study area has been selected within the towns Vercelli and Santhià, where there is a high concentration of paddy-rice fields between the Cavour canal, the river Sesia, and the high-speed railways connecting Turin and Milan (Fig.1).

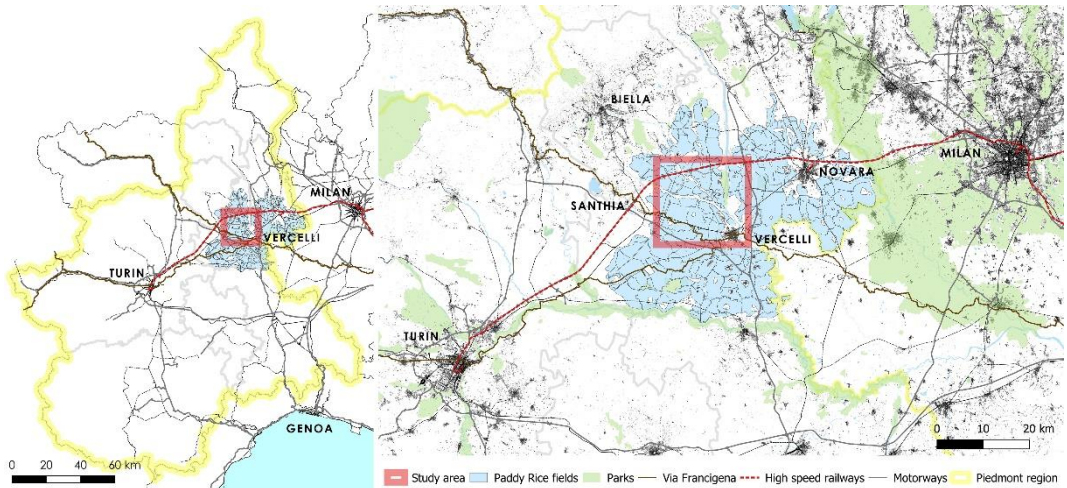


Figure 1: On the left, scheme of the Piedmont region in the northwest of Italy, with evidence of the study area in-between the cities of Turin and Milan, where a high concentration of paddy-rice fields is localized. On the right, the study area has been highlighted in the rural landscape of the paddy-rice fields. The study area has been localized in-between the towns of Vercelli, Santhià and the high-speed railways connecting Turin and Milan.

Furthermore, Italy is the largest rice producer in Europe (FAO, 2004). To better understand the importance of rice production in the Piedmont region, regional and national data were compared. In 2019, the paddy-rice land cover in Italy was 220.027,24 ha; while the paddy-rice land cover in the Piedmont region was 111.632,07 ha, split up the province of Vercelli 67.577,86 ha, the province of Novara 32.104,14 ha, and the province of Biella 3.651,82 ha (Ente Risi, 2021). The three mentioned provinces have covered more than 92% of the regional paddy-rice land cover and 47% of the Italian paddy-rice land cover. All these factors contribute to the uniqueness of these territories and support new investigations for local economies and tourism management.

4 Methodology: the GIS workflow

In this perspective, the current research explores how satellite imagery from ESA Sentinel-2 mission (European Space Agency, 2015) can be applied for computing vegetation indices and

consequently mapping the spatial distribution of the flooded paddy-rice fields during the spring season. The workflow exploits the specific physical feature of rice plants, that they grow on flooded soils (Xiao et al., 2006). In this study, the GIS workflow was created by using the graphical modeller, in order to improve the effectiveness of the processing. The following scheme shows the GIS workflow, from the input to the outputs (fig.2). In the following sections, the workflow will be analyzed step by step.

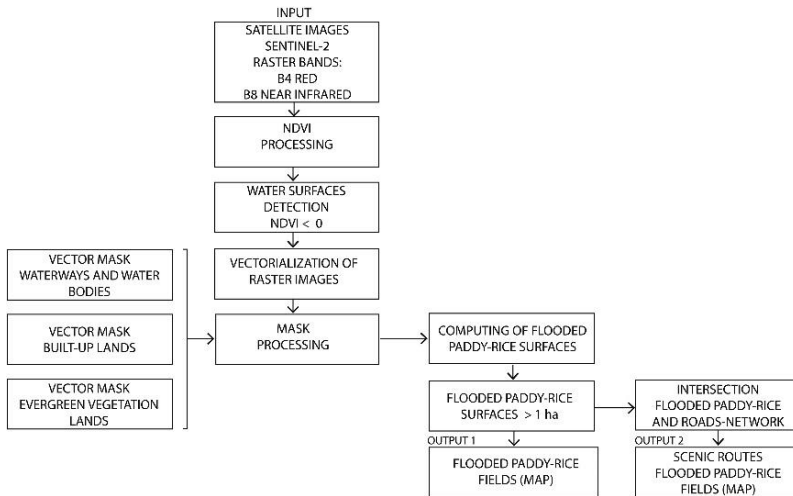


Figure 2: Scheme of the GIS workflow. Satellite images from Sentinel-2 have been considered as input data (Bands: Band 3 Green 543-578 nm – Resolution 10 m, Band 4 Red 650-680 nm – Resolution 10 m; Band 8 Near Infrared 785-899 nm – Resolution 10 m).

4.1 Data source and vegetation indices

Sentinel-2 is a European wide-swath, high-resolution, multi-spectral imagery mission that contributes to the ongoing multi-spectral observations and benefits Copernicus services and applications such as land management, agriculture, forestry and disaster relief (European Space Agency, 2015). Sentinel-2 contributes to land monitoring, by providing input data such as multi-spectral imagery with high resolution (10 m, 20 m and 60 m), which supports the computing of Vegetation Indices (VI), such as Normalized Difference Vegetation Index (NDVI) and Normalized Difference Water Index (NDWI). In the scientific literature, several approaches have been identified to observe landscape seasonal changes at ground level, particularly forests (Motohka et al., 2010) (Motohka et al., 2011), but also paddy-rice mapping, by exploiting satellite imagery (Dong & Xiao, 2016b), (Kaplan & Avdan, 2017), computing vegetation indices (e.g. NDVI, NDWI, EVI, LSWI etc.), and using multi-spectral bands (Xiao et al. 2006) (Dong et al. 2016a). During the flooding period, the land surface of paddy-rice fields is a mixture of water and green rice plants, with water depths usually between 2 and 15 cm (Xiao et al. 2006). This specific condition of paddy-rice fields can be captured, by computing vegetation indices. NDVI exploits the surface reflectance of near-infrared 785-899 nm and red 650-680 nm; NDWI exploits the surface reflectance of near-infrared 785-899 nm

and green 543-578 nm. (McFeeters, 1996). NDVI and NDWI have been calculated according to the following equations:

$$(1) \text{NDVI} = \frac{\text{B8 NIR} - \text{B4 Red}}{\text{B8 NIR} + \text{B4 Red}} \quad (2) \text{NDWI} = \frac{\text{B3 Green} - \text{B8 NIR}}{\text{B3 Green} + \text{B8 NIR}}$$

The NDVI and NDWI values can range between -1 and +1. The pixel-based recognition of the flooded paddy-rice fields have been conducted with high-resolution bands (10 m), using thresholds: $\text{NDVI} < 0$, and $\text{NDWI} > 0$, to compare the results of both indices. In order to verify the threshold method, a comparison was made between the pixel-based recognition (1st of June 2018) and ground observations (2nd of June 2018). The comparison between the pixel-based recognition and the ground observation shows good match for both indices in the selected locations (fig. 3). Both thresholds perform very well in respect to the scope of current research; the NDVI threshold allows to capture a wider area than NDWI. Therefore, the NDVI threshold has been assumed for the processing of the current research.

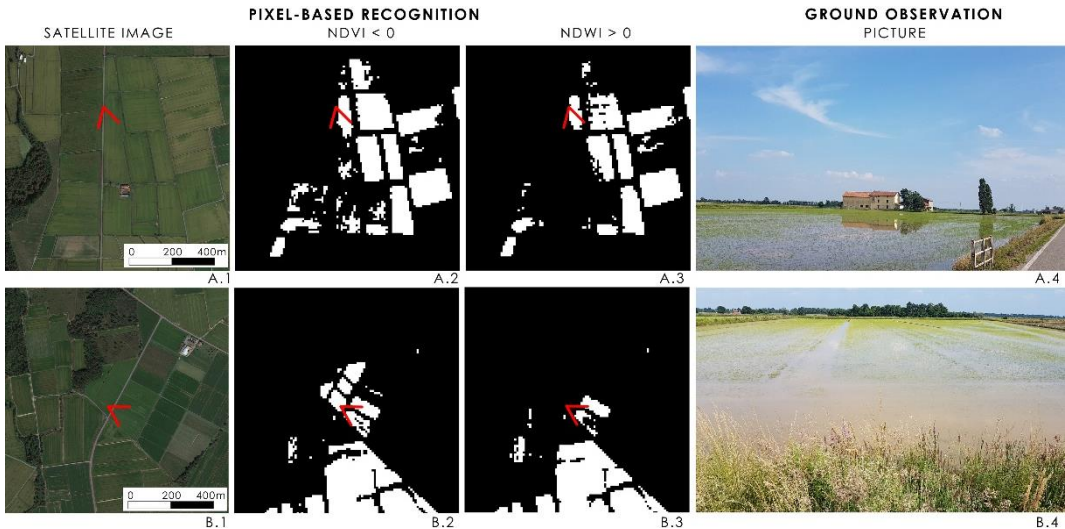


Figure 3: location a) lat: 45.514488, long: 8.270235. Location b) lat: 5.542138, long: 8.275017. The figure shows the comparison between satellite pixel-based recognition of flooded paddy-rice (1st of June 2018) and ground observation (2nd of June 2018). In the figure, it is also possible to compare NDVI and NDWI thresholds.

In the current research, the flooding monitoring was carried out in spring 2020, over three months (March, April and May are the traditional flooding months in this area), selecting the satellite imagery within a cloud cover of 5% in order to avoid misleading information. The following images refer to Sentinel-2 image of a typical day (11th April 2020), selected at the beginning of the flooding season (Product: Sentinel-2A, cloud cover 1,30 %, zone: 32TMR, min lat: 45.0852, max lat: 46.0535, min lon: 7.70695, max lon: 9.12617) (fig. 4a). The NDVI has been performed according to equation (1). The NDVI values (between -1 and +1) have been visualized by using a colour ramp from red to green (fig. 4b).

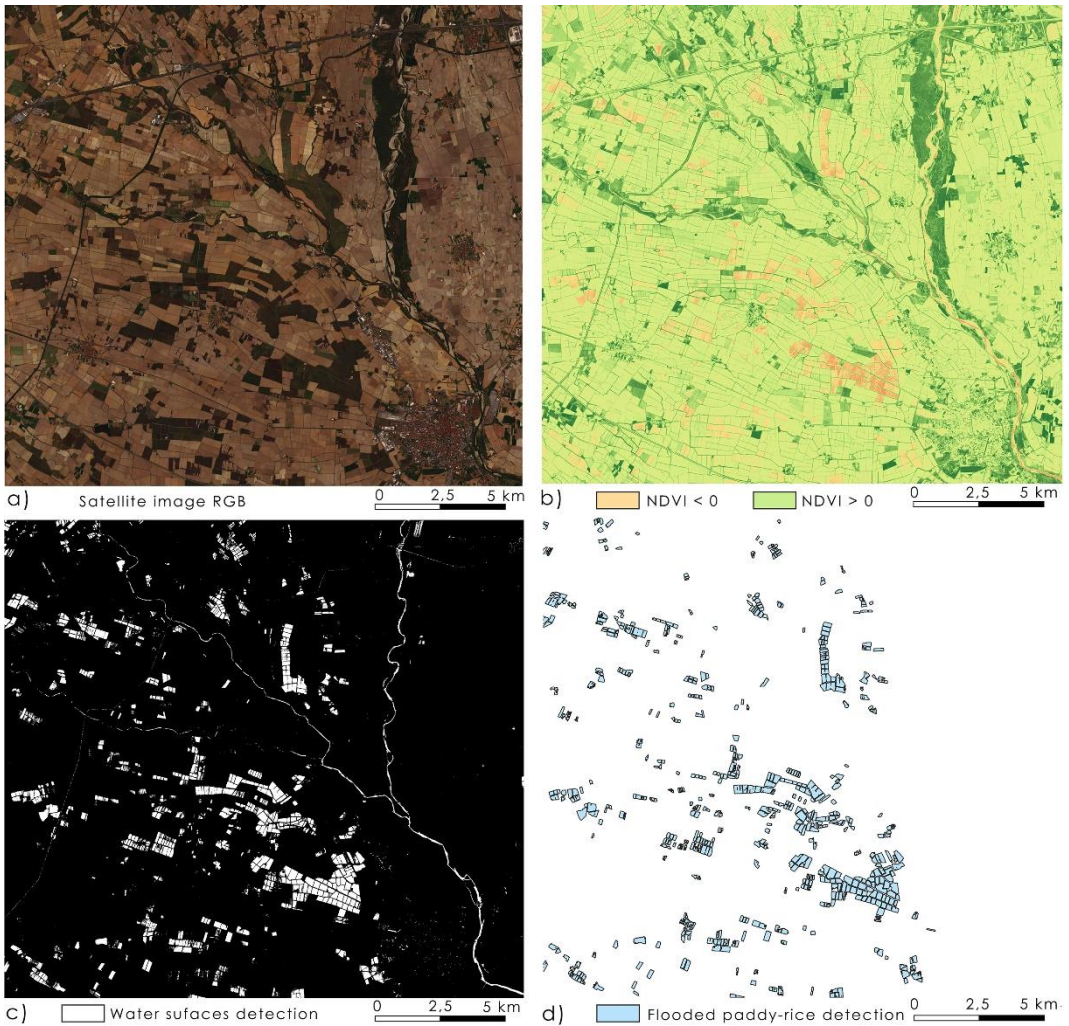


Figure 4: a) Satellite images from Sentinel-2 RGB. b) NDVI processing. High values have been mapped by dark green; low values, which correspond to the water surfaces, have been mapped by red. c) Pixel-based detection by using the threshold $NDVI < 0$. This threshold allows the detection of water surfaces, but also other heterogeneous objects. d) The mask and vectorization process enables the isolation of the flooded paddy rice-fields into the map.

4.2 The mask processing

In a regional-scale context, the performed vegetation indices thresholds enable the detection of different typologies of water surfaces and other heterogeneous objects such as flooded paddy-rice fields, rivers, waterways, wetlands, permanent water bodies, and particular roofs in built-up areas (Dong & Xiao, 2016b) (fig. 4c). Delete misleading information from the whole pixel-based recognition was performed by applying the vectorization process to the thresholded raster images. The mask process has been successfully performed by using the open-access available vectorial datasets (e.g. regional open data and open street map datasets).

Mask processing was carried out using several datasets: built-up areas, permanent waterbodies, waterways, and wooded land cover datasets. The application of the masks to the pixel-based recognition is a fundamental step of the workflow as it enables isolating the flooded paddy-rice fields from the other detected heterogeneous surfaces. In terms of tourism attractiveness of flooded paddy-rice fields, it has been computed for the surface of each areal entity and applied the following threshold: flooded paddy-rice surface > 1 ha. This threshold allows the detection of the most significant sections of flooded paddy-rice fields in the study area. The first outcome of the GIS workflow is the flooded paddy-rice map, which shows, on a certain date of the year, the spatial distribution of the flooded paddy-rice fields (fig. 4d).

5 Experiencing the flooded paddy-rice fields through scenic routes

The final goal of the research is the processing of a thematic map that shows the scenic routes in the existing road network. This tool informs a range of end-users decisions in the field of tourism and environmental contexts. The scenic routes map should be perceived as a “trip-advisor” tool, able to support tourists, interested in the perception of this scenic phenomenon, in the route-choice. The scenic routes detection is the result of the overlapping between the roads-graph, available through the open-access vector datasets (e.g. Open Street Map dataset), and the flooded paddy-rice fields map. The roads-graph has been overlapped with the flooded paddy-rice fields map, with the aim to identify single stretches of the road network that intersect with flooded areas. An offset distance of 50 m from the road axis for the both sides was established to determine the geometrical intersection between the flooded areas and the offset lines of the roads. The thematic map visualises the single stretches of the road network where the flooded paddy-rice fields are within sight (fig. 5). The workflow can be reiterated over the flooding period of paddy-rice fields to redetermine the map of scenic routes every week.

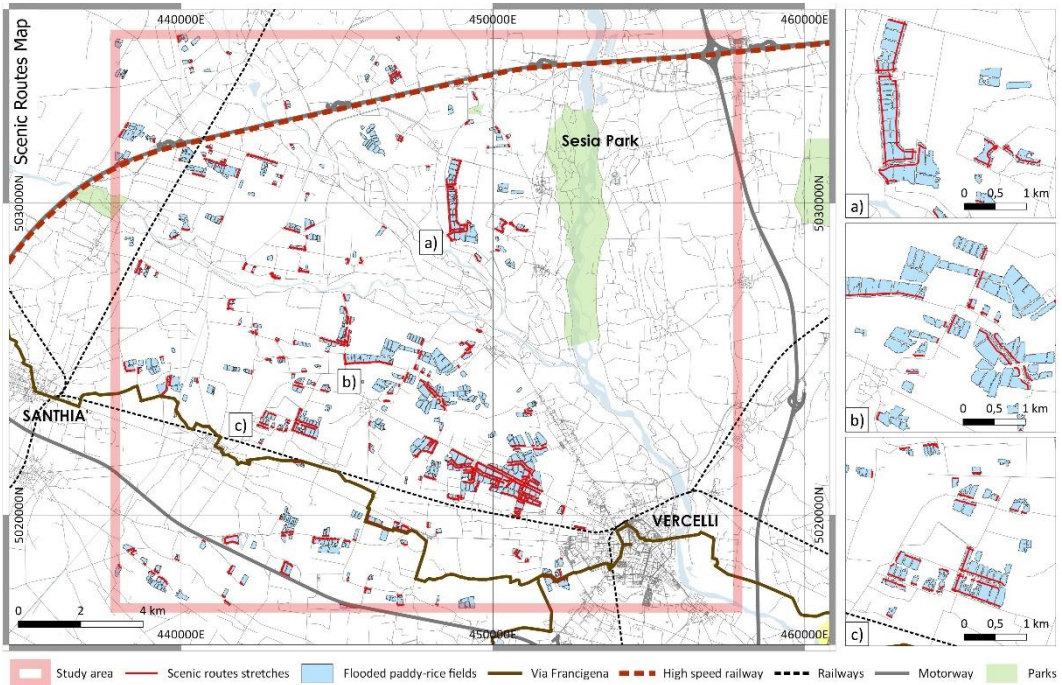


Figure 5: On the left, The Scenic Routes Map. SR WGS84/UTM 32 N. The map highlights the scenic routes stretches in the existing roads-network. On the right, the detailed sections (a, b and c) highlight the single stretches of the roads-network from where flooded paddy-rice fields are perceivable.

6 Discussion

The research shows the effectiveness of the workflow, combining earth observation tools and GIS mapping techniques for detecting flooded paddy-rice fields and determining the scenic routes map for sustainable tourism. Firstly, the application of the GIS modeller to the workflow allows reiterating the process every 3 days (time for Sentinel-2 data acquisition at mid-latitude) over the spring season, showing the variability of landscape conditions in a dynamic map. The high frequency of Sentinel-2 data acquisition would enable mapping the seasonal changes of paddy-rice fields to support the creation of a widespread tourist-destination offer, year-round. In the current research, the workflow has been applied to a limited extension area (about 20 km by 20 km), but the method is replicable and scalable in other territories around the world, where such scenic landscape conditions occur seasonally. Secondly, the applied NDVI threshold can be further improved, to perform mapping of the different rice-growing stages, with higher detection accuracy, even considering formulas which combine multiple vegetation indices. Finally, this method uses the vectorization processing of raster images in the mask processing, coherently with the targets of the research. This aspect could be considered as a limit for large areas, where no uniform vectorial datasets are available yet, and can require long processing. In a regional-scale context, such as the performed one in the research, the available vectorial datasets can be used successfully in the mask processing.

7 Conclusions

Over the year, many seasonal phenomena occur regularly in different environments (e.g. the spring blooming of grasslands and lavender, the autumn colouring foliage). New mapping tools, which combine earth observation and GIS mapping tools, can inspire the development of new strategies for sustainable tourism, which may also contribute to SDGs, particularly addressing the revitalization of inner-areas economies, promoting more efficient use of the places, reducing emissions, and overpressures on the environment. New digital services may contribute in capturing the seasonal conditions of the landscape and enhancing the tourist experience of the places especially if they are localized in marginalized and remote landscapes. Better integration of earth observation tools and GIS mapping tools can contribute to the “digital earth” by supplying tools that support sustainable actions for the future of our planet.

References

- Chen, B., Qiu, Z., Nakamura, K. (2016). Tourist preferences for agricultural landscapes: a case study of terraced paddy fields in Noto Peninsula, Japan. *Journal of Mountain Science*, 13, 1880–1892. <https://doi.org/10.1007/s11629-015-3564-0>
- Dong, J., Xiao, X., Menarguez, M. A., Zhang, G., Qin, Y., Thau, D., Biradar, C., & Moore, B. (2016a). Mapping paddy rice planting area in northeastern Asia with Landsat 8 images, phenology-based algorithm and Google Earth Engine. *Remote sensing of environment*, 185, 142–154. <https://doi.org/10.1016/j.rse.2016.02.016>
- Dong, J., Xiao, X. (2016b). Evolution of regional to global paddy rice mapping methods: A review. *ISPRS Journal of Photogrammetry and Remote Sensing*, 119, 214–227. <https://doi.org/10.1016/j.isprsjprs.2016.05.010>
- Ente Risi, (2021). Retrieved from: http://www.enterisi.it/servizi/seriestoriche/superfici_fase01.aspx
- European Commission (2015). *Copernicus Europe’s eyes on the Earth*. Copernicus Brochure, European Commission, Directorate-General for Communication, Retrieved from: https://www.copernicus.eu/sites/default/files/documents/Brochure/Copernicus_Brochure_EN_WEB.pdf
- European Space Agency (2015). Sentinel-2 User Handbook. Retrieved from: https://earth.esa.int/documents/247904/685211/Sentinel-2_User_Handbook
- FAO (2004), International year of rice 2004, Retrieved from: <http://www.fao.org/rice2004/en/p7.htm>
- Hall, C.M., Scott, D., Gössling, S. (2011). Forests, Climate Change and Tourism. *Journal of Heritage Tourism*, 6, 353–363. <https://doi.org/10.1080/1743873X.2011.620252>
- Kaplan, G., Avdan, U. (2017). Object-based water body extraction model using Sentinel-2 satellite imagery. *European Journal of Remote Sensing*, 50:1, 137-143. <https://doi.org/10.1080/22797254.2017.1297540>
- McFeeters, S., K. (1996). The use of the Normalized Difference Water Index (NDWI) in the delineation of open water features, *International Journal of Remote Sensing*, 17:7, 1425-1432 [doi:10.1080/01431169608948714](https://doi.org/10.1080/01431169608948714)
- Monti, P. (2002). *Storie d’acqua. Le canalizzazioni del Vercellese e gli ecomusei del Piemonte*. Pavone Canavese: Priuli & Verlucca.
- Motohka, T., Nasahara, K.N., Murakami, K., Nagai, S. (2011). Evaluation of Sub-Pixel Cloud Noises on MODIS Daily Spectral Indices Based on *in situ* Measurements. *Remote Sensing*, 3, 1644-1662. <https://doi.org/10.3390/rs3081644>

- Motohka, T., Nasahara, K., N., Oguma, H., Tsuchida, S. (2010). Applicability of Green-Red Vegetation Index for Remote Sensing of Vegetation Phenology. *Remote Sensing*, 2(10), 2369-2387. <https://doi.org/10.3390/rs2102369>
- Occelli, C., Palma R., Sassone M. (2012). *La ciclostrada del canale Cavour. Una via a bassa velocità tra Torino e Milano*. Boves: Araba Fenice.
- Rolando, A., Scandiffio, A. (2016), *The Central Park in between Torino and Milano*. In AA.VV. Proceedings of 53rd IFLA World Congress, Tasting the Landscape. Turin.
- Rozenstein, O., Adamowski J. (2017). Linking Spaceborne and Ground Observations of Autumn Foliage Senescence in Southern Québec, Canada. *Remote Sensing*, 9(6), 630. <https://doi.org/10.3390/rs9060630>.
- Segre, L. (1983). *Agricoltura e costruzione di un sistema idraulico nella pianura piemontese (1800-1880)*. Milano: BCI.
- Spotts, D.M., Mahoney, E.M. (1993). Understanding the Fall Tourism Market. *Journal of Travel Research*, 32, 3–15. <https://doi.org/10.1177/004728759303200202>
- United Nations (2015). Transforming our world: the 2030 Agenda for Sustainable Development. Retrieved from: https://www.un.org/ga/search/view_doc.asp?symbol=A/RES/70/1&Lang=E
- Xiao, X.M., Boles, S., Frolking, S., Li, C.S., Babum J.Y., Salas, W, Moore, B., (2006). Mapping paddy rice agriculture in South and Southeast Asia using multi-temporal MODIS images. *Remote Sensing of Environment*, 100, 95–113. <https://doi.org/10.1016/j.rse.2005.10.004>

Citizen Science Tools for Lake Monitoring in the Framework of the United Nations Sustainable Development Goals: The Project SIMILE

Alberto Vavassori¹, Carlo Andrea Biraghi¹, Gorica Bratic¹, Daniela Carrion¹, Giorgio Zamboni¹ and Maria Antonia Brovelli¹

¹Politecnico di Milano, Italy

Abstract

SIMILE (Informative System for the Integrated Monitoring of Insubric Lakes and their Ecosystems) is a cross-border Italian-Swiss project aiming to improve the management of the Insubric lakes and their ecosystems with different technologies as well as the participation of citizens and stakeholders in water resources monitoring. In this project, water monitoring and management was carried out through different technologies: in situ sensors, satellite imagery, and data coming from citizen science. This paper focuses in particular on this last source of information, describing how data sourced from citizen science can contribute to the Sustainable Development Goals (SDGs) of the United Nations (UN). The report illustrates the tools that have been developed for the collection and management of information provided through citizen science; a mobile cross-platform application for smartphones that can be used by any citizen and a Web application for administrators, useful for data management and editing.

Keywords: lake monitoring, water quality, citizen science, Sustainable Development Goals

1 Introduction

Lakes are a fundamental resource for the environment, not only in terms of water consumption for agricultural and domestic usage, but also for the touristic and leisure activities that benefit from them (Carrion et al., 2020). Recently, scientific and technological development has provided useful tools for improving the management and monitoring of water resources.

SIMILE (Informative System for the Integrated Monitoring of Insubric Lakes and their Ecosystems) is a cross-border Italian-Swiss project. It aims to improve the collaboration and coordination between public administrations and stakeholders; for the management of the Insubric lakes (Lugano, Como and Maggiore) and their ecosystems, as well as monitoring water resources quality. The project involves both technical/scientific partners (Politecnico di Milano, Fondazione Politecnico, Water Research Institute – National Research Council and University of Applied Sciences and Arts of Southern Switzerland) and institutional partners

(Lombardy Region and Ticino Canton), yet also benefits from the involvement of schools, general public, and associations (Carrion et al., 2020).

The project's aim is the development of a business intelligence platform supporting decision and policy making for the public administrations regarding the Insubric lakes' management (Brovelli et al., 2019). This platform will integrate all the data retrieved in the context of the project. In particular, the technologies used for data collection including low-cost in-situ sensors (installed on dedicated buoys) that make high-frequency measurements, free and open satellite images (for example, those provided by the European Space Agency Sentinels), and information derived through a citizen science approach.

This paper primarily focuses on a citizen science approach, particularly tools developed for the collection and management of data coming from citizen science. Albeit, it is worth underlining that the business intelligence platform will integrate all the data collected and elaborated in the framework of the project. Therefore, data retrieved from satellite images and in-situ sensors represent relevant components as well.

The project strongly links to the purpose of the 6th Sustainable Development Goal (SDG) of the United Nations ("Ensure availability and sustainable management of water and sanitation for all"). There is a particular focus on targets 6.3 (stressing the importance of improving water quality and encouraging the recycling and safe reuse of water on a global level) and 6.5 (highlighting the importance of a coordinated management of water resources, including a transboundary cooperation). As SIMILE aims to strengthen the coordinated management of the water resources and the participation of citizens in water quality monitoring, we can view it as a form of "geospatial enabler" monitoring the SDG 6 (Brovelli et al., 2019).

2 Existing tools for the collection and management of citizen science data

The development of the above-mentioned applications started from an in-depth research of existing tools.

As for the mobile application, a detailed analysis of similar tools is described in a paper from Jovanovic et al. (2019). The authors presented six different applications used for water quality monitoring with a citizen science approach. These tools allow the user to provide information about different water quality related parameters (such as water colour, reflectance, transparency, and turbidity). Even though most applications are free, none of them is open source. For this reason, a new mobile application has been designed according to the following criteria: it should provide user support, it has to be user-friendly, able to work offline, free, and open source (Jovanovic et al., 2019).

In terms of the integrated system mobile/Web application, there are existing tools developed for the collection and visualization of crowdsourced data. For example, EpiCollect+ allows users to collect spatially referred data with a smartphone by completing a single questionnaire. Users have the possibility of attaching photos, short videos, sound clips, and measurements. The mobile app is integrated with a Web page dedicated to data visualization, downloading, and management (Aanensen et al., 2014). Another example is the Ultra Mobile Field GIS

system, which consists of a mobile component dedicated to real-time data collection and a Web-GIS application for data visualization, downloading, and analysis (Lwin et al., 2011). Two other examples based on free and open source technologies are the projects: PoliCrowd 2.0 and The Paths of Via Regina. In both cases, data is collected with a smartphone, and a Web platform enables their visualization. With crowdsourced data displayed on a Virtual Globe, users can edit the data visualization, create customized maps, and use a time bar to investigate temporal distribution (Brovelli et al., 2016).

Although the above-mentioned systems have not been developed specifically for lake monitoring, there were some similarities with the tool created for SIMILE. The latter consists of a client-side with both the mobile and Web applications; and a server side with servers used to host, install, and execute the applications, the database, and a workstation processing collected images (Jovanovic et al., 2019). In the following section the system's functionalities will be introduced.

3 Description of the mobile application and administration interface

The first tool is a cross-platform, open-source mobile application called "SIMILE – Lakes Monitoring" (Biraghi et al., 2020). The application interface opens with a map centred on the user's current position and showing the contents uploaded by all users. In the application, a user can: share observations relative to the lake status (presence of algae, foams, oil stains, litters, odours, drains, and fauna), measure the water quality (transparency, temperature, pH, oxygen, and bacteria concentration), participate in education and sensibilisation events (such as clean-ups and workshops), and learn more about the lake ecosystem (through a glossary available in the app).

The user can report strange phenomena or measure one of the water-quality parameters by adding a new observation to the map. A single observation consists of a georeferenced image and a series of attributes, selected through a guided interface (a list of entries is available for every indicator). A dedicated interface offers more precise information for every item, and a help button provides explanations about concepts that the user might not be familiar with. These contributions can be provided by any user, as they do not require particular competencies nor additional tools with respect to the smartphone. Additional instruments are necessary for actual measurements; for example, the Secchi disk to evaluate the water transparency and a thermometer to measure the water temperature. This functionality, which is available for everyone, allows sharing the results of lake monitoring through a simple tool. Once the fields are completed, the observation can be submitted, and it will become visible to all the users.

Figure 1 shows some functionalities of the mobile app.

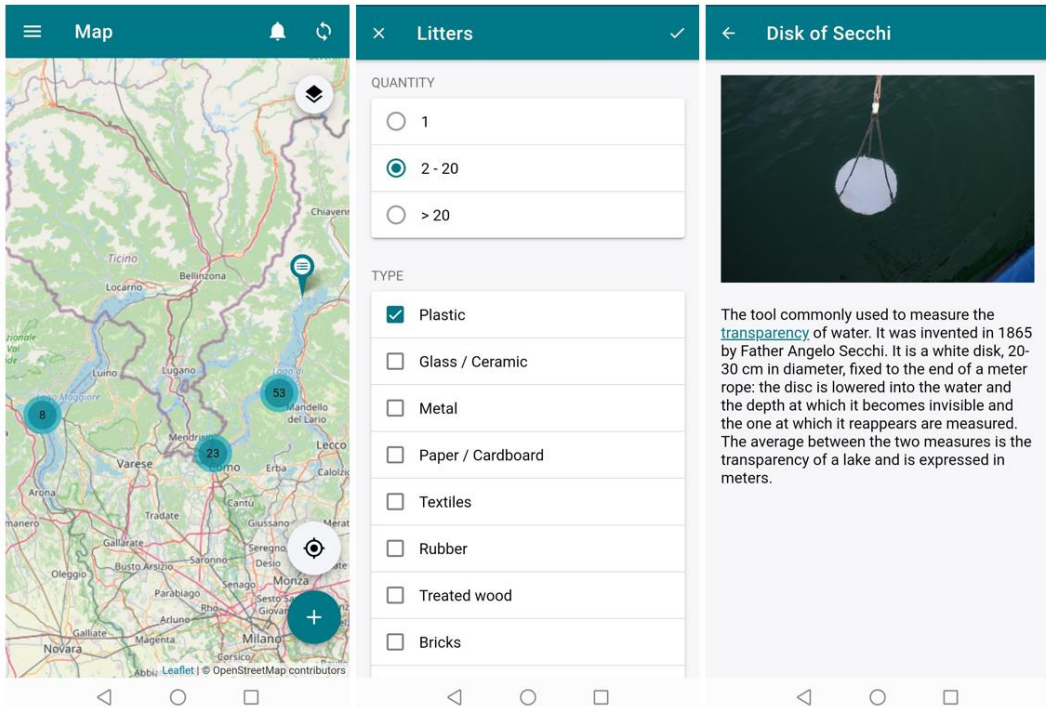


Figure 1: screenshots representing the functionalities of the mobile app. From left to right: cartographic representation displaying the position of events and observations; guided interface for adding a new observation; glossary.

In case of particularly dangerous or severe conditions, it is possible to contact the competent authorities through their official channels. The observations and the photographs uploaded through the app can be advantageous for a preliminary evaluation of the phenomenon.

Thanks to the mobile application, public and private authorities can promote public events with subjects relating to the project, directly addressing all application users. Uploaded events are visible in the dedicated section, accessible from the main menu, through an icon symbolizing a bell and the map itself. In the same section, the user can also find important communications published by the project partners or the competent authorities about environmental issues. This functionality can be quite helpful in case of weather warnings (or other types of alerts).

The information provided by citizens through the app is collected and managed with a dedicated Web application. The administration interface allows the user to visualize, delete, and edit the data provided with the app. The two applications are synchronized, thus, the edits performed on the database through the Web app are visible on the mobile app and vice versa. The information provided through the app is visible and editable with the Web app.

On the home page of the Web interface, it is possible to easily access all the functionalities through a series of buttons, each one dedicated to a specific theme (Figure 2). Data is provided

either in a table format and through cartographic representation; therefore, it is possible to visualize their spatial distribution (either singularly or grouped in spatial clusters).

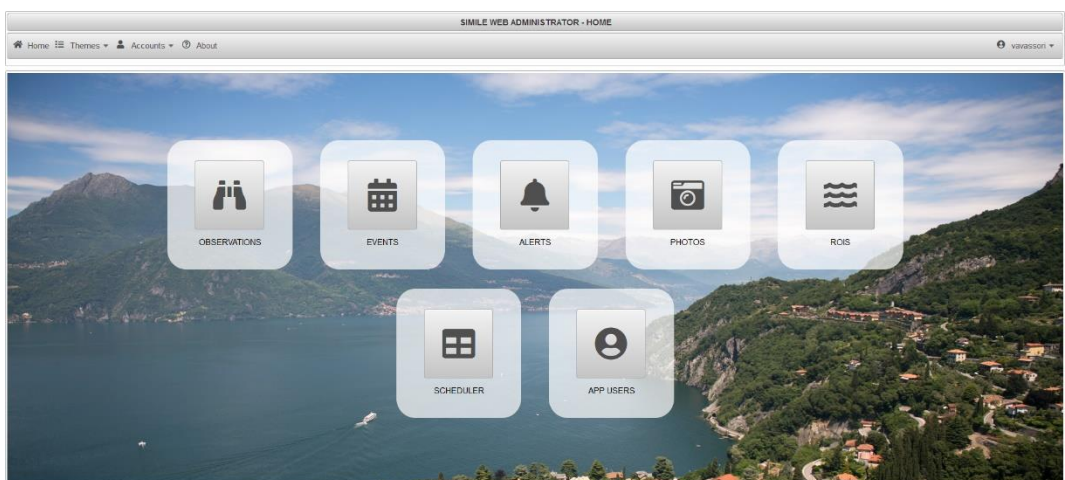
The themes accessible through the app are also available in the Web app. With proper credentials, it is possible to edit the database. For instance, a user can delete or edit existing observations, or improve their geographic position. Deleted data can be consulted applying an adequate filter to the table, and they can be recovered at any time.

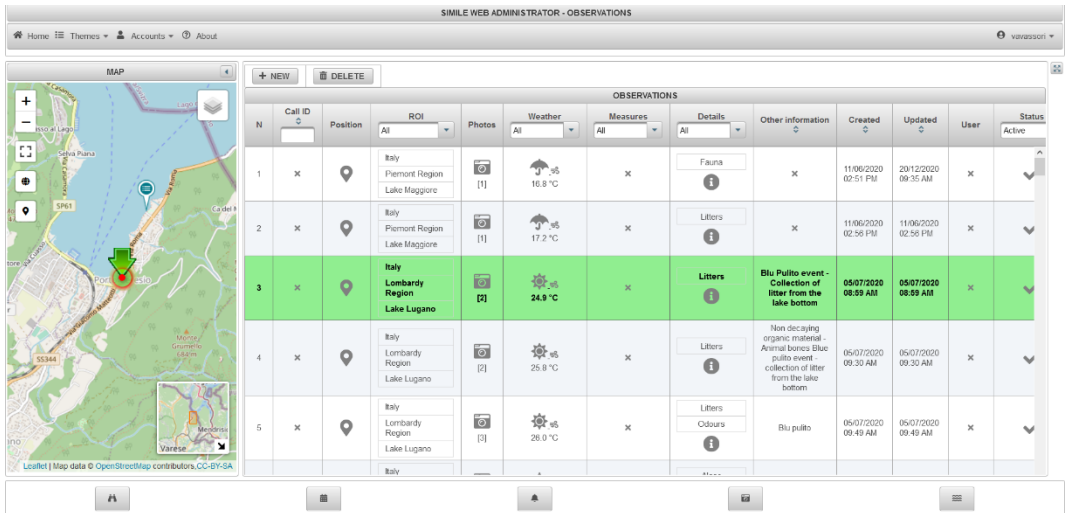
Provided here is a short description of the available functionalities. Firstly, it is possible to consult, delete, and edit observations submitted by the users and create new observations (theme “observations”). The system can visualise graphs of some numerical variables (temperature, oxygen, and pH) as functions of depth. The Web interface is intuitive and well guided. The user can choose pre-set attributes for each field and manually add the value of the numerical variables.

Similarly, the user can consult or edit events and add new events (theme “events”). The possibility to modify or create a new event is available only on the Web application (through the mobile app, the user can only consult existing events). Similar functionalities are available for alerts (theme “alerts”); however, alarms have an “expiry date” after which they are no longer visible.

The Web app displays photographs uploaded by the users (theme “photos”), with all corresponding observation information in chronological order. Moreover, it is possible to visualize the boundaries of the different sub-areas within the region of interest (theme “ROIs”, Region Of Interests). All the uploaded news, events and observations in either application are visualized on a dedicated calendar (theme “scheduler”) or time bar (theme “timeline”).

Finally, the Web application allows performing some analyses on the data (theme “analysis”): in particular, a user can filter the observations based on their attributes and visualize some useful statistics and trends.





SIMILE WEB ADMINISTRATOR - OBSERVATIONS												
OBSERVATIONS												
N	Call ID	Position	ROI	Photos	Weather	Measures	Details	Other information	Created	Updated	User	Status
1	X	Italy Piemont Region Lake Maggiore		[1]	☁️ 16.8 °C	X	Fauna	X	11/06/2020 02:51 PM	20/12/2020 09:35 AM	X	Active
2	X	Italy Piemont Region Lake Maggiore		[1]	☁️ 17.2 °C	X	Litters	X	11/06/2020 02:56 PM	11/06/2020 02:56 PM	X	Active
3	X	Italy Lombardy Region Lake Lugano		[2]	☁️ 24.9 °C	X	Litters	Blu Pulpito event - Collection of litter from the lake bottom	05/07/2020 08:59 AM	05/07/2020 08:59 AM	X	Active
4	X	Italy Lombardy Region Lake Lugano		[2]	☁️ 25.9 °C	X	Litters	Non-decaying organic material - Animal bones Blue pulpito event - collection of litter from the lake bottom	05/07/2020 09:30 AM	05/07/2020 09:30 AM	X	Active
5	X	Italy Lombardy Region Lake Lugano		[3]	☁️ 26.0 °C	X	Litters Odours	Blu pulpito	05/07/2020 09:49 AM	05/07/2020 09:49 AM	X	Active

Figure 2: above, home page of the administration interface; below, interface for the management of observations.

4 Conclusions

This paper describes the tools that have been developed in the framework of SIMILE Interreg Italy-Switzerland project: allowing citizens to get involved in monitoring the Insubric lakes and the public administrations to manage the data provided with a citizen-science approach.

The project provides an example of how citizen science activities can contribute to the monitoring and management of water resources. The project involves citizens and public administrations along with schools, local leisure associations, and regular lake visitors. The goal is for more conscious management of the water resources and increasing awareness of citizens about the problems regarding water quality and preservation. For this reason, the project is consistent with the sixth SDG (in particular, targets 6.3 and 6.5) of the UN, encouraging the reduction of pollution for the water quality improvement and the coordinated management of this resource.

The proposed tools are a cross-platform mobile application and a Web-based application that can be used by any citizen or specific users with administrator credentials. The mobile app is currently promoted through online or public events among public administrations, schools, leisure associations (such as rowers and fishermen), and environmental associations (e.g. Legambiente) demonstrating app functionalities. Public events include clean-ups, mapathons and workshops, where participants can collect observations and measurements on lake conditions, or suggest improvements for app functionalities, aiming at attracting their interest for water preservation. A push notification service is enabled on significant “international days” (i.e. Earth Day, Environment Day, Water Day). The Web application is presumed to be used by a limited number of people (i.e. project partners and regional institutions) that can edit and manage the data provided by citizens. Therefore, dedicated courses are organized to teach the application functions.

This data alone is not sufficient for monitoring purposes. It will be integrated with satellite images and data from in-situ sensors, through the business intelligence platform, for a broader, more comprehensive view of the lake conditions. Citizen science contributions are currently being used by the project partners for monitoring purposes, as they contribute to validate the other data and improve their spatial and temporal coverage. They will be used by politicians and public administrations as a decision support system. In any case, data can be accessed and used by anyone.

Approximately 100 contributions have been uploaded so far; hopefully they will keep increasing, thanks to newly scheduled events and the involvement of more people. These contributions have already revealed to be effective in detecting potentially dangerous phenomena occurring in the lakes. For instance, a user observed an active outlet draining into the lake for five consecutive days, leading the competent regional authority to intervene for further inspections.

These tools are currently being tested and will be released as open-source software. The mobile application is already available for Android devices and will soon be available for iOS. In the next months, the measurement campaigns will be activated, and new algorithms will be introduced in the software dedicated to data management. The project will be concluded by January 2022.

Acknowledgements

The research described in this paper is part of SIMILE project (ID: 523544), which has been funded with the support from the European Commission within the Interreg Italy-Switzerland 2014-2021 programme.

References

- Aanensen D. M., Huntley D. M., Menegazzo M., Powell C. I., Spratt B. G. (2014). EpiCollect+: linking smartphones to web applications for complex data collection projects [v1; ref status: indexed, <http://f1000r.es/3vk>], *F1000Research*, 3:199. doi: <https://doi.org/10.12688/f1000research.4702.1>
- Biraghi, C. A., Pessina, E., Carrion, D., Brovelli, M.A. (2020). VGI Visualisation to Support Participatory Lake Monitoring: the Case Study of SIMILE Project. *International Archives of the Photogrammetry, Remote Sensing and Spatial Information Sciences, XLIII-B4-2020*, 245-251. <https://doi.org/10.5194/isprs-archives-XLIII-B4-2020-237-2020>
- Brovelli, M. A., Cannata, M., Rogora, M. (2019). SIMILE: a Geospatial Enabler of the Monitoring of Sustainable Development Goal 6 (Ensure Availability and Sustainability of Water for All). *International Archives of the Photogrammetry, Remote Sensing and Spatial Information Sciences, XLII-4/W20*, 3-10. <https://doi.org/10.5194/isprs-archives-XLII-4-W20-3-2019>
- Brovelli M. A., Kilsedar C. E., Zamboni, G. (2016). Visualization of VGI data through the new NASA Web World Wind Virtual Globe. *International Archives of the Photogrammetry, Remote Sensing and Spatial Information Sciences, XLI-B4*, 205-209. Doi: <https://doi.org/10.5194/isprsarchives-XLI-B4-205-2016>
- Carrion, D., Pessina, E., Biraghi, C. A., Bratic, G. (2020). Crowdsourcing Water Quality with the SIMILE App. *International Archives of the Photogrammetry, Remote Sensing and Spatial Information Sciences, XLIII-B4-2020*, 245-251. <https://doi.org/10.5194/isprs-archives-XLIII-B4-2020-245-2020>
- Jovanovic, S., Carrion, D., Brovelli, M. A. (2019). Citizen science for water quality monitoring applying FOSS. *International Archives of the Photogrammetry, Remote Sensing and Spatial Information Sciences, XLII-4/W14*, 119-126. doi: <https://doi.org/10.5194/isprs-archives-XLII-4-W14-119-2019>
- Lwin K. K., Murayama Y. (2011). Web-Based GIS System for Real-Time Field Data Collection Using a Personal Mobile Phone. *Journal of Geographic Information System*, 3(04):382-389. doi: <https://doi.org/10.4236/jgis.2011.34037>
- SIMILE Website: <https://progetti.interreg-italiasvizzera.eu/it/b/78/sistemainformativoperilmonitoraggiointegratodeilaghiinsubriciedeiloroe>

Using Information and Communication Technologies to Facilitate Mobility Behaviour Change and Enable Mobility as a Service

Henry Martin^{1,2}, Daniel Reck¹ and Martin Raubal¹

¹ETH Zurich, Switzerland

²Institute for Advanced Research in Artificial Intelligence (IARAI), Austria

Abstract

Our mobility is responsible for substantial global greenhouse gas emissions and urban problems such as air pollution, usage of public spaces for infrastructure and parking, and congestion. Therefore, the transformation of our mobility towards sustainability is essential to achieve the sustainable development goals #11 (sustainable cities and communities) and #13 (climate action).

Mobility as a Service (MaaS) is a core concept for this transformation; however, there are still many open questions and challenges due to its novelty and complexity. The Empirical use and Impact Analysis of MaaS (EIM) project conducts a large-scale user study during the roll-out of a MaaS offer in Switzerland to gather empirical data that help to address and answer challenges and open questions.

Keywords: sustainability, mobility, MaaS, mobility behaviour change, ICT

1 Introduction

A large portion of our GHG emissions can be traced back to the movement of people and goods. In 2018, the transport sector was responsible for 24 % of the global GHG emissions (IEA, 2020), for 26 % of the GHG emissions in the European Union (Pilzecker et al., 2020) and for 32.4 % of the GHG emissions in Switzerland (Schilt, 2020). Tackling climate change, therefore, requires significant action in the transport sector.

Apart from the severe impact on climate change, the transport sector is linked to additional problems that are especially relevant for cities, such as air pollution, injuries, an increase of impervious cover for infrastructure (Gössling, 2020) and more traffic and congestion, which already results in high economic costs (Reed, 2019).

The primary source of these problems, including GHG emissions in the transport sector, is the private ownership of fossil fuel-based internal combustion engine cars (ICEV), therefore transitioning of the transport sector towards sustainability will have to focus on a sustainable alternative to ICEV based trips.

The most promising path for fast decarbonisation of the transport sector is the aggressive roll-out of battery electric vehicles (BEV) due to their significantly smaller environmental impact than ICEVs (Haasz et al. 2018; Cox et al., 2020). However, simply replacing ICEVs with BEVs leaves many challenges unresolved. Individual motorised transportation will still block large areas of public space for parking and infrastructure instead of using it for housing or recreational space. The problem of increasing traffic would persist.

In this paper, we will discuss the main strategies for the transition of individual human mobility towards sustainability in the sense of the Sustainable Development Goals (SDG) #11 “Sustainable Cities and Communities” and #13 “Climate Action”. We thereby relate to the case study YUMUV, a novel Mobility as a Service (MaaS) platform in Switzerland and its associated research project Empirical use and Impact Analysis of Maas (EIM), which studies its impact as an enabler of sustainable mobility.

2 MaaS key challenges:

MaaS is a mobility concept that integrates shared modes with public transport to facilitate intermodal travel (Reck, 2020). One goal of MaaS is to decrease private car ownership. This is a significant challenge as it requires individuals to undergo a significant behaviour change (Weiser et al., 2016; Raubal et al., 2020).

The integration of shared modes and public transport creates a high degree of complexity as many stakeholders such as mobility service providers (MSP), public transport operators and regulators need to synchronise to create a MaaS offer. The creators of these offers have a large degree of freedom along ten design dimensions such as the geography of the offer, the included modes, or the subscription cycle (Reck et al. 2020). Using this design space, several key factors are required for the resulting MaaS offer to be attractive to a broad audience:

- **Attractive and easy pricing:**
Apart from an attractive price, the offer needs a comprehensible pricing structure, i.e., avoiding different pricing schemes for each mode of transport.
- **Easy access:**
The user should be able to access all modes via a single gateway, such as a single app, instead of using a different gateway per mode of transport.
- **Optimal availability and mobility options:**
The core of the MaaS package is the offered mobility. The desired modes of the user should be sufficiently available in space, time, quantity and sufficiently diverse to cover mobility demands in different situations.

The correct design of a MaaS offer concerning these factors is of utmost importance as they can potentially impact how a MaaS offer is used and its potential to decrease private car ownership. First evidence supports the claim that MaaS could decrease private car usage (Hensher et al., 2021); however, due to a lack of substantial behavioural data, it remains unclear how these design decisions influence the perception and the impact of MaaS and to what degree and how MaaS can change travel behaviour (e.g., mode choice, car ownership).

With these rather design-oriented questions, there are novel challenges regarding the technical realisation of a MaaS offer. The (large-scale) analysis of individual mobility behaviour poses the problem of combining heterogeneous data from various sources such as tracking data, context data or booking data all from different providers, different vehicles, and users. This is especially true for spatial tracking data, as there are many different possibilities to record a person's position with varying spatio-temporal granularity (e.g. GPS tracking data or public transport smart card data) (Miller and Goodchild, 2015). To answer questions about MaaS usage that help support the design of MaaS offers, the data must be collected, stored, filtered, integrated, and enriched with relevant context data.

One goal of MaaS is to cover the current mobility demand with less but optimised resources. This requires predictive knowledge about individual mobility behaviour and the available resources to solve tasks such as the optimal redistribution of mobility tools, optimised charging and maintenance cycles and the improvement of intermodal route recommendations. In the past years, machine learning has become the predominant tool for the prediction of human mobility (LUCA et al., 2020). However, most approaches assume mobility recordings to be independent and identically distributed or use simplistic 1st order Markov assumptions (Kulkarni et al., 2019), thereby omitting the information that lies in the highly regular structure of individual human mobility (Schneider et al., 2013). We, therefore, see great potential in expanding current work on the prediction to incorporate the spatio-temporal structure of human mobility and relevant context data to support a more efficient operation of MaaS.

3 study – The EIM project and YUMUV:

The EIM project is a collaboration between the Swiss Federal Railways (SBB) and ETH Zürich to fill the gap of lacking empirical data. For this, we designed a user study based on YUMUV¹ - a new MaaS offer that was introduced as a collaboration of SBB and the public transport providers in Zürich, Bern, and Basel.

YUMUV aggregates various mobility service providers (MSP) such as car-sharing, bike-sharing and shared e-scooters as a mobility platform and allows users to access all transport modes via mobility bundles – a subscription acting as an easy-to-understand pricing scheme for all MSPs. These bundles are city-specific, and in the case of Zürich, users can choose between a 30- or 60-minutes monthly subscription (shown in Figure 1 on the right), which allows using all modes of transport for a total of the respective minutes. The user can book different mobility options via the YUMUV app (shown in Figure 1 on the left), created in collaboration with trafi².

¹ <https://yumuv.ch/en>

² <https://www.trafi.com/>

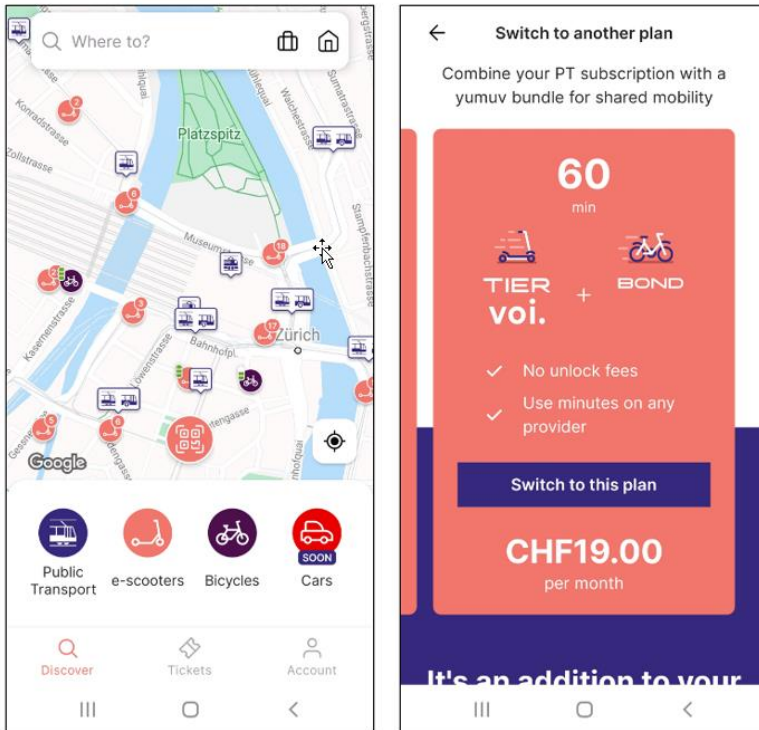


Figure 1: Two screenshots of the YUMUV android app. The left side shows the overview of available modes at Zurich main station, the right side shows one of the available bundles

The case study took place between August and October 2020 in the agglomeration of the city of Zürich and consisted of 71 persons in the treatment group and 417 persons in the control group. All participants were tracked for 3 month, and participants in the treatment group got access to a mobility bundle after 4 weeks.

During the study period, all participants recorded their movement using an app on their smartphone and provided labels for activities and modes of transport. The treatment group recorded booking data from the YUMUV app, and all users participated in a survey at the beginning and the end of the tracking period.

4 Takeaways from the data preprocessing phase

A crucial part of this project is integrating tracking data with context data for the subsequent analysis of the impact of MaaS on mobility behaviour and mode choice behaviour. In the following, we describe takeaways to keep in mind when designing a similar case study.

Label correction using different data sources:

In this study, all users were required to regularly label their recorded movement data with the mode of transport and activity categories in the tracking app. These labels are of great importance for the analysis of transport behaviour. However, they are often noisy as users might forget the labelling task or save effort and validate an incorrect label. During the preprocessing, it was very valuable that we could use the recorded booking data to validate and correct the user-provided labels. Even though it increases complexity, we recommend planning redundant tracking from different sources to reduce the noise in labels.

An early collection of context data:

The availability of shared modes in proximity plays a vital role in the mode choice for a trip. To analyse this influence, we started logging the locations of all relevant micro-mobility modes every 5 minutes in the study area during the study period. The resulting dataset has more than 600'000 entries per day and is used to calculate availability measures at the beginning of each trip.

We recommend planning the context data acquisition (e.g., by scraping) and the necessary infrastructure as early as possible in the project so that all context data is recorded in the same period as the tracking data and easily accessible.

Increase impact and reproducibility by contributing to open source projects:

Today, there are plenty of excellent open-source frameworks for processing and analysing spatial data. In this project, we used the open-source routing machine³ for map matching, PostgreSQL⁴ with PostGIS⁵ extension for data management and relied on the many spatial Python libraries such as GeoPandas⁶. However, many niches, such as the processing of tracking data libraries, are missing or incomplete. We, therefore, decided to implement all suitable methods within the trackintel⁷ framework and contribute to this open-source project. This increases code quality, reproducibility and the impact of this work as it allows others to benefit from it.

5 Outlook and expected contributions:

MaaS is expected to play a major role in the transport sector's contribution to achieving the sustainable development goals of climate action (#13) and creating sustainable cities and communities (#11). An essential next step to test the potential of MaaS to improve the sustainability of transport systems is the analysis of the impact of bundles on travel behaviour. Hopes are that multimodal transport bundles can reduce car usage in the short term and reduce car ownership in the long term (Mulley, 2017; Hensher et al., 2020; Ho et al., 2021). Substitution effects such as using shared cars instead of owned cars have to be carefully accounted for to measure the net effect of bundles on transport emissions (Reck et al., 2021).

³ <http://project-osrm.org/>

⁴ <https://www.postgresql.org/>

⁵ <https://postgis.net/>

⁶ <https://geopandas.org/>

⁷ <https://github.com/mie-lab/trackintel>

Thus, comprehensive mobility profiles of trial participants are needed. The YUMUV trial allows analyses of these effects at unprecedented accuracy due to the broad scope of the collected data, including each participant's comprehensive mobility profile (tracking data, booking data, context data). Our trial set-up further includes a control group which is a first in studies aiming to analyse the impact of multimodal transport bundles.

The following step proceeding data preprocessing is to estimate YUMUV bundles impact on participants' mode choice using discrete choice models. In doing so, we expect to make a substantial contribution towards understanding the potential of MaaS to improve the sustainability of transport systems to inform policy-making towards more sustainable and integrated future mobility.

References

- Banister, D. (2008). The sustainable mobility paradigm. *Transport policy*, 15(2), 73-80.
- Bundesamt für Energie (2020). *Energiaperspektiven 2050+. Zusammenfassung der wichtigsten Ergebnisse*. <https://www.bfe.admin.ch/bfe/de/home/politik/energieterspektiven-2050-plus.html>
- Bundesamt für Statistik (2017). *Verkehrsverhalten der Bevölkerung 2015*, <https://www.bfs.admin.ch/bfsstatic/dam/assets/1840604/master>
- Cox, B., Bauer, C., Mendoza Beltran, A., van Vuuren, D. P., & Mutel, C. L. (2020). Life cycle environmental and cost comparison of current and future passenger cars under different energy scenarios. *Applied Energy*, 269, 115021.
- Gössling, S. (2020). Why cities need to take road space from cars—And how this could be done. *Journal of Urban Design*, 25(4), 443–448.
- Haasz, T., Gómez Vilchez, J. J., Kunze, R., Deane, P., Fraboulet, D., Fahl, U., & Mulholland, E. (2018). Perspectives on decarbonizing the transport sector in the EU-28. *Energy Strategy Reviews*, 20, 124–132.
- Hensher, D. A., Mulley, C., Ho, C. Q., Wong, Y., Smith, G. & Nelson, J. D. (2020). *Understanding Mobility as a Service (MaaS): Past, present and future*. Elsevier.
- Hensher, D. A., Ho, C. Q., & Reck, D. J. (2021). Mobility as a Service and private car use: evidence from the Sydney MaaS trial. *Transportation Research Part A: Policy and Practice*, 145, 17-33.
- Ho, C. Q., Hensher, D. A. & Reck, D. J. (2021). Drivers of participant's choices of monthly mobility bundles: Key behavioural findings from the Sydney Mobility as a Service (MaaS) trial. *Transportation Research Part C: Emerging Technologies*, 124, 102932.
- IEA. (2020). *CO2 Emissions from Fuel Combustion*. IEA. <https://www.iea.org/reports/co2-emissions-from-fuel-combustion-overview>
- Kulkarni, V., Mahalunkar, A., Garbinato, B., & Kelleher, J. D. (2019). On the Inability of Markov Models to Capture Criticality in Human Mobility. In I. V. Tetko, V. Kůrková, P. Karpov, & F. Theis (Eds.), *Artificial Neural Networks and Machine Learning – ICANN 2019: Image Processing* (pp. 484–497). Springer International Publishing.
- Luca, M., Barlacchi, G., Lepri, B., & Pappalardo, L. (2020). Deep Learning for Human Mobility: A Survey on Data and Models. *ArXiv:2012.02825 [Cs]*. <http://arxiv.org/abs/2012.02825>
- Miller, H. and M. Goodchild (2015) Data-driven geography, *GeoJournal*, 80, 449-461.
- Mulley, C. (2017). Mobility as a Service (MaaS) – does it have a critical mass? *Transport Reviews*, 37(3), 247-251.
- Pilzecker, A., Fernandez, R., Mandl, N., & Rigler, E. (2020). *Annual European Union greenhouse gas inventory 1990–2018 and inventory report 2020*. European Environment Agency.

- Raubal, M., Bucher, D., & Martin, H. (2021). *Geosmartness for personalized and sustainable future urban mobility*. In W. Shi, M. Goodchild, M. Batty, M.-P. Kwan, & A. Zhang (Eds.), *Urban Informatics*: Springer.
- Reck, D. J., Hensher, D. A., & Ho, C. Q. (2020). MaaS bundle design. *Transportation Research Part A: Policy and Practice*, 141, 485-501.
- Reck, D. J., Axhausen, K. W., Hensher, D. A. & Ho, C. Q. (2021). Multimodal Transportation Plans: Empirical Evidence on Uptake, Usage and Behavioural Implications from the Augsburg MaaS Trial. Paper presented at the *100th Annual Meeting of the Transportation Research Board*, Washington, D. C., January.
- Reed, T. (2019). *INRIX Global Traffic Scorecard*.
- Schäfer, A.W., Yeh, S. (2020). A holistic analysis of passenger travel energy and greenhouse gas intensities. *Nature Sustainability* 3, 459–462.
- Schneider Christian M., Belik Vitaly, Couronné Thomas, Smoreda Zbigniew, & González Marta C. (2013). Unravelling daily human mobility motifs. *Journal of The Royal Society Interface*, 10(84), 20130246.
- Schilt, A. (2020). *Emissionen von Treibhausgasen nach revidiertem CO2-Gesetz und Kyoto-Protokoll, 2. Verpflichtungsperiode (2013–2020)*. Bundesamt für Umwelt BAFU.
- Shoup, D. C. (1997). The high cost of free parking. *Journal of planning education and research*, 17(1), 3-20.
- United Nations Environment Programme (2019). *Emissions Gap Report 2019*
- United Nations Environment Programme (2020). *Emissions Gap Report 2020*
- Weiser, P., Scheider, S., Bucher, D., Kiefer, P., & Raubal, M. (2016). Towards sustainable mobility behavior: research challenges for location-aware information and communication technology. *GeoInformatica*, 20, 213-239.

Observing Cyclists' Mobility Patterns for better Decisions

Martin Loidl¹ and Ursula Witzmann-Müller¹

¹University of Salzburg, Austria

Abstract

Although the amount of data, generated in the mobility domain, has been increasing dramatically over the past years, specific cycling-related data are still hardly ever employed as the evidence base for cycling promotion. This is due to lacking data availability and accessibility on the one hand and to the absence of frameworks for integrating data from a different source on the other hand. We, therefore, propose a Bicycle Observatory, which facilitates a continuous observation of cycling mobility and serves as decision support in the broader context of cycling promotion. In this study, we investigate the contribution of a Bicycle Observatory achieving of strategic goals in cycling promotion and summarize major requirements and recommendations for establishing a Bicycle Observatory.

Keywords: cycling, bicycle observatory, evidence base, cycling promotion, monitoring

1 Introduction: cycling data

Cycling data are commonly regarded as essential for planning and decision-making processes. Due to the rise of cycling in many cities and regions, the demand for valid data as an evidence base has constantly been rising. In parallel to this development, advancements in the ICT and wearable sector have led to growing amounts of generated data. Over the past ten years, numerous studies contributed to an optimistic perspective on transport data availability in the broader context of “Smart Cities” and the “Internet of Things” (IoT). Miller and Shaw (2015) see huge potential in data from mobile sensors when it comes to the investigation of mobility patterns and behaviour. In the context of big data and smart urbanism, Kitchin (2014) appraises new opportunities for gaining insights into cities and their governance. Anda et al. (2017) regard big data, opportunistically collected by wearables, as game-changer in transport modelling.

In a recent review of available pedestrian and bicycle data, Lee and Sener (2020) distinguished between traditional data sources, such as counts and travel surveys, and emerging data. The latter are all generated by wearables with location sensors, ranging from GNSS to Wi-Fi and Bluetooth, and user-generated data, such as system data from bike-sharing systems or feedback in citizens' apps. The authors point to the fact that there are still a lot of open questions connected to emerging data sources. These range from mode detection, data validity, sampling

bias, privacy, to a lack of contextual information and costs for obtaining and utilizing the data. Thus, it is not surprising that a substantial gap between theoretical opportunities and common daily practice becomes evident. Steenberghen et al. (2017) investigated the availability of mobility data from cyclists and pedestrians in the European Union, plus Norway and Switzerland. In interviews with national representatives, the authors found that only 40% were able to determine the average distance cycled per person at the national level. For cities and regions, where a sound evidence base for planning decisions and implementing measures is most needed, the situation is expected to be even worse.

Independent from data availability, different data sources need to be integrated for a holistic perspective (Romanillos et al., 2016, Conrow et al., 2018). However, a standardized framework for how to relate different data to a common picture of cycling mobility does not exist yet. Consequently, we are facing two interlinked issues: a lack of data availability and accessibility, especially at a local scale level, and the absence of concepts, frameworks or tools for data integration. Against this backdrop, we introduce a concept for a geospatial Bicycle Observatory (Loidl et al., 2020), which serves as an integrator of different data and allows for monitoring bicycle mobility in an integrated way. In this study, we are aiming for determining a Bicycle Observatory's contribution to achieving strategic goals with regard to cycling and identify the cornerstones of such a platform.

2 Bicycle Observatory

Instead of single measurements at specific locations and time periods, a Bicycle Observatory facilitates continuous and integrated measurements of cycling-related parameters. The concept is well established in different observational disciplines, such as astronomy, biology or economy. The application of an observatory for geographic information was proposed by Janowicz et al. (2014) and further elaborated by Miller (2017). Geographic Information Observatories (GIOs) facilitate holistic insights into geographic data and underlying phenomena. Since mobility is spatial and all data that are relevant for capturing aspects of cycling mobility, we applied the concept of a GIO and developed the concepts for a Bicycle Observatory (Loidl et al., 2020).

For this, the following data sources are tapped and technically integrated: spatial data (infrastructure, physical environment, and weather), movement data (trajectories from mobile applications), statistical data (census, crash reports), mobility surveys and qualitative data (surveys, data from feedback apps). These data have different temporal characteristics (sporadically or periodically updated, real-time) and spatial resolutions. However, the geographical reference facilitates the linking of these data sources. Decentral storage of the data ensures maximum efficiency in terms of data ownership and updating. In order to integrate data, spatial and temporal re-sampling methods need to be employed. Semantic interoperability is supported by Semantic Web technologies, such as ontologies (see Reda et al. 2018) for an example in a related domain). We refer to existing approaches for dealing with heterogeneous and erroneous data (Loidl and Keller, 2015, Vaccari et al., 2009), which need to be user-tailored for the specific data set and purpose.

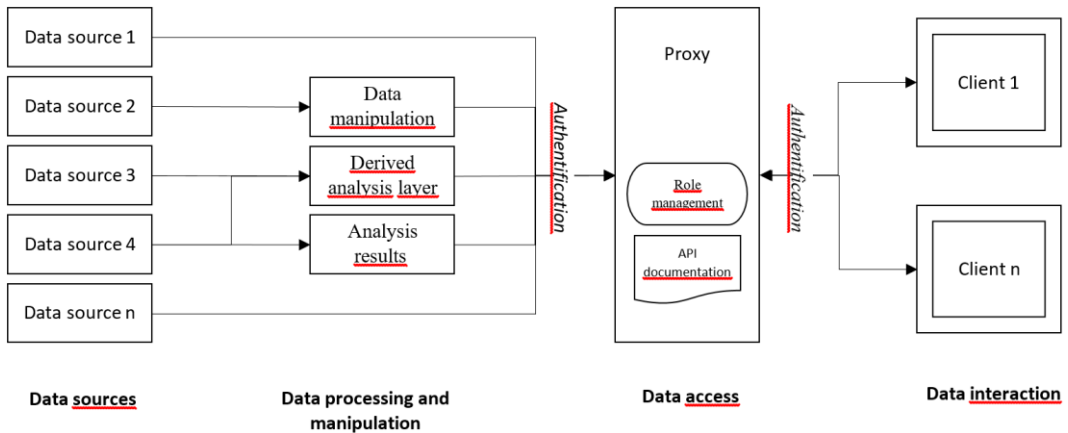


Figure 1: Concept of a Bicycle Observatory with decentral data storage (modified from (Loidl et al., 2020))

The Bicycle Observatory platform refers to the data sources and provides standardized interfaces for different clients (Figure 1). In a proof of concept (POC), we established a Bicycle Observatory for Salzburg and adjacent municipalities (Loidl et al., 2020, Leitinger et al., 2020, Heym et al., 2020, Brocza and Kollarits, 2020). The following investigations are based on this POC.

3 Supporting cycling promotion strategies

When it comes to supporting a modal shift towards cycling, cycling promotion strategies are fundamental for political decisions and implementation processes. In order to conduct an effective and credible cycling policy, sound data for status-quo analyses and monitoring are essential. We evaluated the contribution of a Bicycle Observatory to this demand. For this, we selected cycling promotion strategies at different administrative levels: the European Cycling Strategy by the European Cyclists' Federation (ECF)¹, the Masterplan for Cycling by the Austrian ministry for climate action (BMK)², the cycling strategy of the Austrian province of Vorarlberg³ and the cycling strategy of the city of Salzburg⁴.

We extracted all action fields and measures mentioned in the four strategies and evaluated how the integrated data provision in a Bicycle Observatory supports efficient implementation of the respective measure. The matching matrix revealed a strong relation, especially at a local level (Table 1).

¹https://ecf.com/eu_cycling_strategy (last access: 2020-09-28)

²https://www.klimaaktiv.at/mobilitaet/radfahren/masterplan_RF_2025.html (last access: 2020-09-28)

³<https://vorarlberg.at/documents/21336/80850/Kettenreaktion+Radverkehrsstrategie+Vorarlberg/> (last access: 2020-09-28)

⁴<https://www.stadt-salzburg.at/smartcity/smarte-mobilitaet/radverkehrsstrategie-2025/> (last access: 2020-09-28)

Table 1: Matching of action fields and measures in cycling promotion strategies with a Bicycle Observatory.

Cycling promotion strategy	Number of action fields and measures	Number of matches
European Cycling Strategy	4	2
Austrian Masterplan for Cycling	25	7
“Kettenreaktion” - cycling strategy Vorarlberg	21	8
“Radverkehrsstrategie 2025+” - cycling strategy Salzburg	25	16

In a subsequent step, the most supported strategy by a Bicycle Observatory, namely the cycling strategy Salzburg, was investigated in-depth. For this, we developed an assessment matrix. We described the ideal status after implementing all suggested measures, the current status, and the gap (necessary actions) between the two. Moreover, we assessed the availability and accessibility of the data that could support the achievement of the respective goals. The necessary data for seven out of sixteen measures, which data from a Bicycle Observatory could support, are currently available. The data are partly available for seven measures and currently not available for two measures. None of these data sets is currently entirely accessibly as open data; seven are partly provided as open data.

Table 2: Example for the assessment of action fields and measures defined in a local cycling strategy.

Action field	Ideal status	Current status	Required actions	Data available	Data accessible
Planning consistent main bicycle network	The main bicycle network is designed based on data on the existing infrastructure, bicycle traffic flows, as well as sources and destinations. The current situation before the measures are implemented is recorded and periodically compared with counting and tracking data in order to monitor the effect of the measures. In addition, user feedback is used for the qualitative evaluation of the measures	The main bicycle network of the city of Salzburg was designed by traffic planners in 2018. The planning was based on expert knowledge, an assessment of potential routes and an experimental simulation of effects.	Monitoring of bicycle traffic flows (dense network of cycle counting stations, processed trajectories) and analysis of user feedback.	Yes	Partly

Table 2 provides an example for how action fields in the cycling strategy Salzburg could be supported by data and insights from a Bicycle Observatory and to which degree necessary data are available and accessible.

4 Requirements for the establishment of a Bicycle Observatory

Since the contribution of a Bicycle Observatory to achieving strategic goals is evident, we identified the requirements for the establishment in a consecutive step. For this purpose, we launched an international web survey among experts (which is going to be published elsewhere) and conducted expert interviews with representatives of four institutions (two academic, two companies). From these inputs, we derived requirements in three different categories.

4.1 Requirements and recommendations with regard to data

We identified the accessibility of data as the major bottleneck for establishing a Bicycle Observatory. Thus, we recommend publishing all cycling-related data as open data for two reasons. Firstly, open data contribute to value creation in various application fields. This holds especially true for authoritative data, which are generated with public money anyway. Examples of this are road status data, counting data, or socio-demographic data. Secondly, open data usage leads to permanent quality control of the data and a subsequent improvement. In this context, we see huge potential for secondary data usage. Data that is initially generated for another purpose could be re-used in a Bicycle Observatory if it was made accessible. For instance, data from navigation apps, where the location is sensed in order to optimize the service for individual users, could be perfectly re-used in aggregated form for analysis purposes at a population level. Independent from the data source, the spatial and temporal resolution of available data is identified as being crucial for in-depth analysis. However, we found that most data are not available at the necessary resolution and quantity. In addition to data availability and accessibility, research gaps with regard to data integration became evident. For example, it remains unclear how crowdsourced trajectories (GNSS tracks) can be linked conceptually to stationary counting data. To the best of our knowledge, no method set exists beyond map matching trajectories and calculates correlation coefficients at selected locations. We, therefore, call for further research in the GIS domain in order to facilitate true integration, in addition to overlay analyses or visual inspections.

4.2 Requirements and recommendations with regard to data management

The effective handling of large amounts of data is only feasible with rigorous data management and the usage of data standards. Since data are integrated and linked based on geographical reference, we used data and service standards by the Open Geospatial Consortium (OGC). For managing the data, we recommend using a comprehensive data management plan (DMP), as for example, developed and provided as an Open Source template by Leitinger et al. (2020). This template describes data layers individually and contains core metadata, compatible with national and international metadata standards. For the operation of a Bicycle Observatory, the following information in a DMP is regarded as essential: geographical extent and coverage, update cycle, licence and privacy issues. On the basis of these four categories, the suitability of data for a Bicycle Observatory can be determined.

4.3 Organizational and legal requirements and recommendations

The organizational effort for establishing a Bicycle Observatory increases with the number of integrated data layers. This holds especially true if third-party data is used. In this case, data usage contracts need to be concluded, which is commonly associated with considerable effort. In addition to the data management, the success of a Bicycle Observatory very much depends on continuous conceptual, technical and content-related support. Regardless of whether a Bicycle Observatory is established within administrative bodies or outsourced to external service providers, a project owner is highly recommended.

With regard to privacy, we recommend not using individual data with direct reference to individual persons. Instead, anonymized and aggregated data are sufficient for the most common purposes of a Bicycle Observatory, where the observation of the entire system is key (and not the surveillance of individuals!).

5 Conclusion and outlook

Cycling data are essential for an evidence-based promotion of cycling mobility, as we revealed by a structured analysis of cycling promotion strategies. Although the number of sensors has increased at an unprecedented pace over the past years and huge amounts of data are being generated in the transport sector, we found that relevant cycling data are still sparsely available and accessible, respectively. A Bicycle Observatory would provide a suitable framework for integrating relevant data and provide them to decision-makers, planners and cycling communities. The framework of a Bicycle Observatory is adaptable and transferable. The POC, evaluated in this study, serves best activities at a local and regional level. However, the organizational and technological architecture can be employed for other scale levels and regions in the world as well. Against this backdrop, we call for further investments in data acquisition and provision and publish existing data to generate additional value through secondary data usage.

Acknowledgments

Research presented in this paper was conducted in the project Bicycle Observatory (FFG Nr. 865176), which received funding by the Austrian Ministry for Climate Action, Environment, Energy, Mobility, Innovation and Technology (BMK) under the program “Mobility of the Future”.

References

- Anda, C., Erath, A. & Fourie, P. J. 2017. Transport modelling in the age of big data. *International Journal of Urban Sciences*, 21, 19-42.
- Brocza, U. & Kollarits, S. 2020. Dashboard Radverkehr: alles im Blick. *AGIT – Journal für Angewandte Geoinformatik*, 2020, 238-243.
- Conrow, L., Wentz, E., Nelson, T. & Pettit, C. 2018. Comparing spatial patterns of crowdsourced and conventional bicycling datasets. *Applied Geography*, 92, 21-30.
- Heym, L., Werner, C., Innerebner, G. & Kofler, P. 2020. Mission Impossible: Typologisierung von Radfahrenden – ein Designsoziologischer Ansatz. *AGIT – Journal für Angewandte Geoinformatik*, 2020, 244-254.
- Janowicz, K., Adams, B., McKenzie, G. & Kauppinen, T. 2014. Towards Geographic Information Observatories. *GIO 2014: Proceedings of the Workshop on Geographic Information Observatories 2014, collocated with the 8th International Conference on Geographic Information Science (GIScience 2014)*. Vienna.
- Kitchin, R. 2014. The real-time city? Big data and smart urbanism. *GeoJournal*, 79, 1-14.
- Lee, K. & Sener, I. N. 2020. Emerging data for pedestrian and bicycle monitoring: Sources and applications. *Transportation Research Interdisciplinary Perspectives*, 4, 100095.
- Leitinger, S., Wagner, A. & Kremser, W. 2020. Erfahrungen bei der Umsetzung eines Datenmanagementplans für räumliche Daten des Radverkehrs. *AGIT – Journal für Angewandte Geoinformatik*, 2020, 255-262.
- Loidl, M. & Keller, S. 2015. An intrinsic approach for the detection and correction of attributive inconsistencies and semantic heterogeneity in OSM data. In: HAKLAY, M. & MCCONCHIE, A. (eds.) *AAG Annual Meeting, Workshop OpenStreetMap Studies*. Chicago.
- Loidl, M., Wagner, A., Kaziyeva, D. & Zagel, B. 2020. Bicycle Observatory – eine räumlich differenzierte, kontinuierliche Beobachtung der Fahrradmobilität. *AGIT – Journal für Angewandte Geoinformatik*, 2020, 263-271.
- Miller, H. J. 2017. Geographic information science I: Geographic information observatories and opportunistic GIScience. *Progress in Human Geography*, 41, 489-500.
- Miller, H. J. & Shaw, S.-L. 2015. Geographic Information Systems for Transportation in the 21st Century. *Geography Compass*, 9, 180-189.
- Reda, R., Piccinini, F. & Carbonaro, A. 2018. Towards Consistent Data Representation in the IoT Healthcare Landscape. *Proceedings of the 2018 International Conference on Digital Health*. Lyon, France: Association for Computing Machinery.
- Romanillos, G., Zaltz Austwick, M., Ettema, D. & de Kruijf, J. 2016. Big Data and Cycling. *Transport Reviews*, 36, 114-133.
- Steenberghen, T., Tavares, T., Richardson, J., Himpe, W. & Crabbé, A. 2017. Support study on data collection and analysis of active modes use and infrastructure in Europe. Brussels: European Commission, DG Mobility and Transport.
- Vaccari, L., Shvaiko, P. & Marchese, M. 2009. A geo-service semantic integration in Spatial Data Infrastructures. *International Journal of Spatial Data Infrastructures Research*, 4, 24-51.

Extraction of Dwellings of Displaced Persons from VHR Radar Imagery – A Review on Current Challenges and Future Perspectives

Andreas Braun^{1,2}

¹ Paris Lodron University of Salzburg, Austria

² University of Tübingen, Germany

Abstract

While many studies exist to identify buildings from optical satellite images, radar-based approaches are still lacking in humanitarian contexts. This article outlines the main challenges related to scattering mechanisms returning from huts, tents, informal dwellings, and their natural surroundings, but also from geometric distortions caused by the side-looking radar aperture. An outlook summarizes how these limitations can be overcome by image enhancement or multi-image composites, but also by advanced methods on building extraction, such as convolutional neural networks (CNNs). This article aims to stimulate scientific debate and to lay a foundation for the development of new methods.

Keywords: synthetic aperture radar (SAR), earth observation, humanitarian aid, building extraction

1 Introduction

Satellite images are increasingly used in humanitarian work. They effectively deliver consistent and accurate information over large areas, especially when they are remote or dangerous. Images help to allocate and count displaced persons, monitor natural resources and environmental changes, and therefore support the planning of missions, the distribution of goods and services, and the protection of people in need (Lang et al., 2020). Radar images are especially helpful in this context because they map physical surface characteristics independently from cloud cover, therefore, allowing quick response to emergencies (Boccardo et al., 2015). Their use for humanitarian action has been demonstrated in various cases, for example, for mapping settlements or identifying natural resources and hazards (Braun, 2020). However, while numerous approaches exist using very high resolution (VHR) optical imagery, radar-based studies are rare, particularly in the detection of dwellings as a crucial information for humanitarian work. This article discusses the reasons for this research gap and outlines how this issue can be addressed in the future. Furthermore, it provides examples on the interaction of microwaves with informal settlements to provide a basic understanding necessary for the design and conduction of studies in this domain.

2 Current limitations

2.1 Spatial resolution

One reason for the scarcity of radar studies on building extraction is the low availability of VHR radar images. Compared to optical satellites with sub-meter resolutions which have operated since the beginning of the 21st century, the development of VHR SAR satellites shows a delay of 10-20 years which, of course, also affects the methodological development. Among the small number of existing studies on building extraction from single VHR SAR images, sufficient results were only achieved for medium-size and large buildings with regular shapes (Ferro et al., 2012). Studies on small and irregular buildings are still missing. As a foundation for future studies, Table 1 lists the currently available radar data operating at very high spatial resolution.

Table 1: Selection of suitable SAR missions for dwelling detection

Sensor / Image Mode	Azimuth resolution	Range resolution	Availability
TerraSAR-X / HighRes Spotlight	0.6 m	1.1 m	2007 - today
Radarsat-2 / Spotlight	0.8 m	1.6 m	2008 - today
TerraSAR-X / Staring Spotlight	0.24 m	0.6 m	2013 - today
COSMO SkyMed / Spotlight	0.9 m	1.0 m	2014 - today
RISAT-1 / HighResolution	1.0 m	0.67 m	2012 - 2017
Kompsat-5 / Ultra HighResolution	< 0.85 m	< 0.85 m	2015 - today
COSMO SkyMed SG / Spotlight 2A	0.35 m	0.55 m	2020 - today
ICEYE / Spotlight	0.5 m	0.5 m	2020 - today
ICEYE / Spotlight High	0.25 m	0.5 m	2020 - today
Capella / Site	0.5 m	1.0 m	2021 - today
Hisea-1 / Spotlight	< 1.0 m	1.0 m	2021 - today
Capella / Spot	0.4 m	0.6 m	planned for 2022
Umbra / Staring Spotlight	0.25 m	0.25 cm	planned for 2022
XpressSAR / Spotlight	< 1.0 m	< 1.0 m	planned for 2024

2.2 Information content

Radar images are formed by microwaves of several centimetres length. This makes them sensitive to physical characteristics (roughness, moisture, material, shape and orientation) of surfaces and objects (Ulaby et al., 2019). A systematic comparison of how buildings of different materials react to radar waves is provided in Figure 1. As shown by the TerraSAR-X (Spotlight) image in Figure 1b, the buildings of Goz Beïda (Chad) produce high radar backscatter, mainly because of the corner reflection of signals from buildings. However, high returns are also received by trees in the eastern part (volume scattering) and wetlands in the north (specular scattering). The identification of buildings by high radar backscatter from single images is therefore a challenge. Besides the ambiguity of the radar signal, a significant limitation in humanitarian settings is the material of the buildings.



Figure 1: Goz Beïda (a, b), Lilleström (c, d) and Minawao (e, f) in VHR optical and radar images. Green outlines indicate building footprints retrieved from the optical image. TerraSAR-X © DLR 2021

Buildings covered by natural materials (straw on tukuls), or fabric or canvas (tents) produce distinctively less backscatter than solid clay or metal roof tiles. While solid buildings in the city of Lillestrøm (Norway) are characterized by locally high backscatter in Figure 1d, the regularly arranged tents in the refugee camp of Minawao (Cameroon) are mostly penetrated by the radar signal (Figure 1f) and therefore produce no backscatter. These low signals are often even superimposed by volume scattering of hedges or shrubs, which are used in arid regions to separate households in refugee camps, as demonstrated in Figure 2a showing the refugee camp of Dagahaley (Kenya). Accordingly, the potential of radar data often depends on the type of dwellings and their materials which can range from textile or natural materials (low visibility) to all kinds of solid coverage (higher visibility) in refugee camps or informal settlements.

Lastly, due to interference of different signal returns, radar images are characterized by speckle: a granular pattern (Figure 2b and Figure 5) which complicates both visual interpretation and the automated extraction of information (Lee et al., 1994). It can be partially mitigated by adaptive filters, as demonstrated in section 3.2.

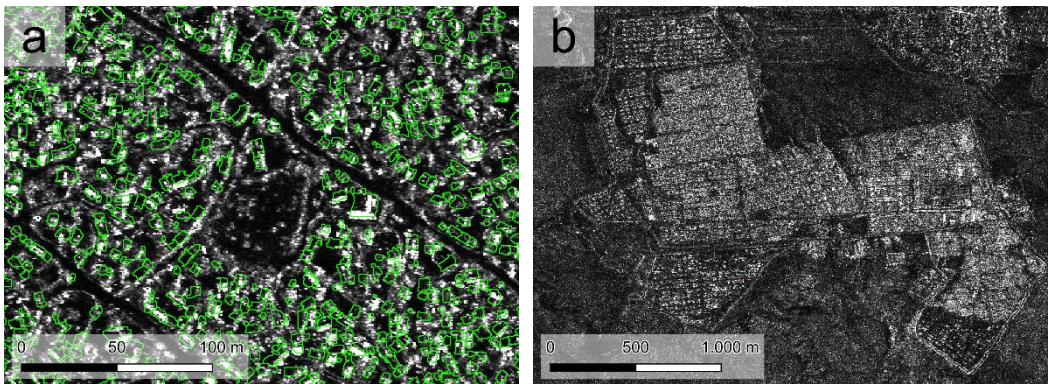


Figure 2: Volume scattering in a TerraSAR-X image of Dagahaley (a), and speckle in an unfiltered ICEYE image of Al Hol (b). TerraSAR-X © DLR 2021

2.3 Acquisition geometry

The active nature of a radar sensor requires a side-looking geometry of the satellite, resulting in incidence angles between 25 and 45 degrees. This introduces several geometric and radiometric distortions in the image, which require careful pre-processing (Oliver et al., 2004). Most of them can be compensated by the integration digital elevation model. However, with increasing spatial resolutions, freely available DEMs are no longer sufficient, especially for reducing signal saturation at slopes facing towards the sensor (Figure 3a). Besides these topographic effects, the orientation of buildings combined the flight and look direction of the radar sensor has a considerable impact on their backscatter intensity. As shown in Figure 3b, even solid administrative buildings in camp Minawao (Cameroon) are only visible as a thin line because the incoming microwave is reflected by just one wall. This brings new challenges regarding the delineation of building footprints.

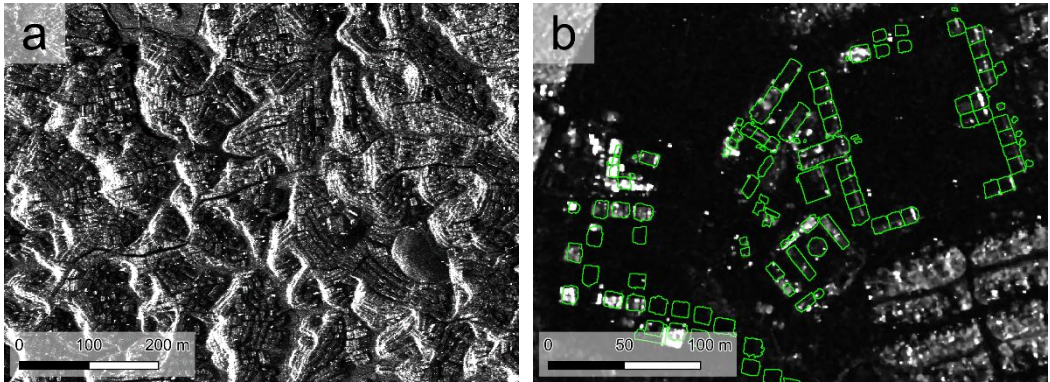


Figure 3: Geometric effects in radar images of Kutupalong (a) and Minawao (b). TerraSAR-X © DLR 2021

3 Solutions and future developments

3.1 Using proxy measures

The previous examples have shown that some types of dwellings do not produce a distinct backscatter signal which can be used to allocate them, for instance because of their material, their orientation, or their size. When the spatial resolution is not sufficient to delineate single buildings, one alternative is dwelling density. The relationship between dwelling density and backscatter intensity has been investigated and utilized in studies for Dagahaley (Figure 4; Braun, 2020) and Maiduguri (Lang et al., 2020). Combined with knowledge of household sizes, these approximations can then be used to estimate the number of residents. However, this requires collecting reference statistics on household sizes in the field and is not a precise method for subtle changes within informal settlements.

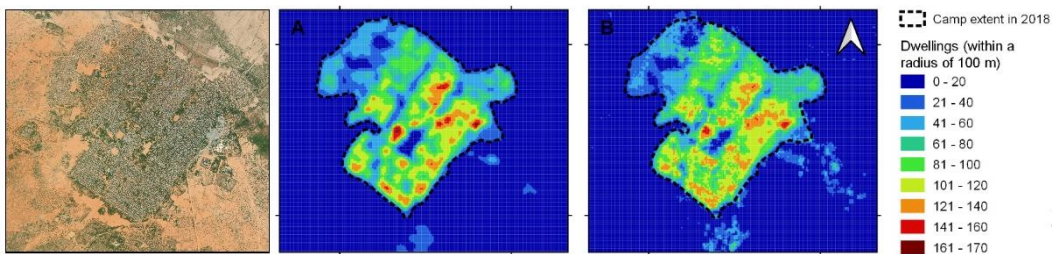


Figure 4: Observed (A) and predicted (B) dwelling density of camp Dagahaley (Braun, 2020)

3.2 Image enhancement

While most speckle filters were designed for SAR satellites such as ERS, ENVISAT or ALOS, they approach speckle at pixel resolutions between 10 and 30 meters. Accordingly, they are not entirely suitable to address patterns within VHR data, because the concept of a moving

window with the size of a few pixels is not applicable at this scale. For these VHR products, filters based on region-growing algorithms, such as the intensity-driven adaptive-neighborhood (IDAN) filter (Vasile et al., 2006), have proven to be more effective because they suppress speckle while keeping the outlines of very bright pixels sharp. This is illustrated in Figure 5 (top): While traditional filters, such as Lee Sigma, Frost or Boxcar struggle with locally high values, the region-growing IDAN filter preserves the outlines of the building while smoothing its surroundings. Still, more filter techniques adapted to very high resolutions have to be developed.

Another way of increasing the quality of a radar image is to combine images from multiple dates using temporal averaging of the backscatter intensity. As shown in Figure 5 (bottom), a single scene can contain a large proportion of random signal contributions. A clearer image is produced by increasing number of images, these are systematically suppressed. However, this requires a large number of images, preferably within a short time frame. Therefore, this approach is not ultimately applicable in cases of emergencies where no archived images exist.

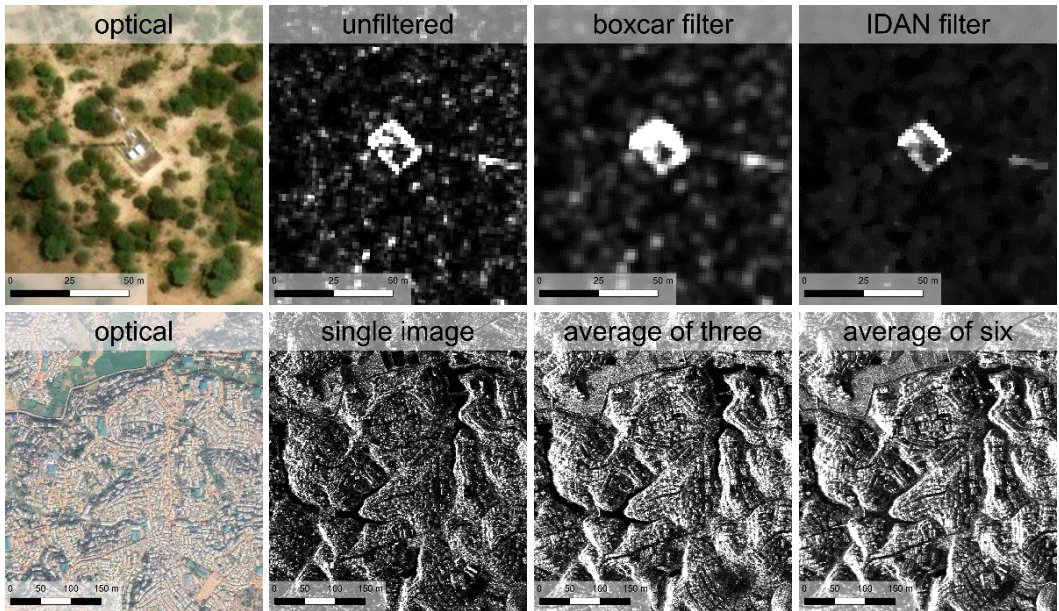


Figure 5: Top: Effect of different filters on a single dwelling in Namibia. Bottom: Effect of image averaging on TerraSAR-X © DLR 2021

Lastly, little backscatter of buildings made of light construction materials can be mitigated by a fusion of VHR optical and radar images, for example, as demonstrated by Spröhnle et al. (2017), who systematically compared the information content of WorldView-2 and TerraSAR-X Spotlight products for the extraction of dwellings in the Al Zaatari refugee camp (Jordan). They confirm that only metal buildings can be reliably identified in radar images, nevertheless, reporting that the fusion of both sensors brings the highest accuracy. A benchmark dataset for the systematic evaluation of approaches based on optical and radar imagery in urban areas

(SARptical) is provided by Wang and Zhu (2019). On the downside, fusion methods increase the dependency of users from several product sources, which unfortunately is counterproductive in emergencies.

3.4 Advanced approaches

As shown in the previous chapters, traditional pixel-based methods fail to reliably identify buildings of displaced persons because of insufficient spatial resolution, little backscatter intensity compared to their surroundings, and geometric effects on building and landscape levels. For this reason, advanced methods which aggregate pixels to segments or semantic objects can be used. Object-based image analysis (OBIA) has already been applied in urban areas using VHR radar imagery, but primarily for change detection based on multi-temporal approaches and not identifying dwellings from single images (Pirrone et al., 2020). One key to successfully identifying dwellings is the understanding and exploitation of typical patterns of double-bounce and signal shadow caused by solid buildings and how these relate to the actual footprint (Soergel, 2010). Once more, this is complicated by partial lacking of backscatter from buildings containing natural construction materials. Advancements in machine learning or pattern recognition, particularly in the training and application of convolutional neural networks (CNN), can help overcome these gaps. Nonetheless, they do currently struggle with the asymmetric dynamic range of the radar signals in urban areas, which require suitable histogram normalization (Zhu et al., 2020). Lastly, the integration of phase information can greatly enhance the quality of urban footprint delineation, for example, by methods of SAR tomography (Wang & Zhu, 2019). Nevertheless, these require large numbers of systematic image acquisitions and are currently not tested for rural areas.

4 Discussion and outlook

Concludingly, the development of radar-based approaches for the identification of buildings for humanitarian purposes still faces many challenges. Predominantly, the variety of different settings brings difficulties for the creation of both accurate and transferable methods, which can then be used in operational settings with low dependencies on specific sensors, acquisition geometries, or extensive data preparation. Future SAR missions will bring new opportunities for spatial resolution and data quality (Table 1), especially in combination with advancements in Deep Learning. Methods adapted to buildings of light construction materials and rural settlements still have to be developed. However, these will still require a sufficient number of input images (SAR only or combined with optical data) and training samples, for example, from previous dwelling extractions. Finally, the availability of in-situ information is crucial for developing methods contributing to both the calibration of models and the validation of generated results. As areas of interest can be hard or even dangerous to access, this is only possible in close collaboration with humanitarian organizations deployed in such regions. To grant results with an accuracy sufficient for humanitarian decision making, the development of approaches should, therefore initially, focus on specific sites or settings instead of aiming at universally transferable methods.

Acknowledgements

This study was funded by the Christian Doppler Forschungsgesellschaft within the Christial Doppler Laboratory for Earth Observation for Humanitarian Action (CDL GEOHUM).

References

- Boccardo, P., Tonolo, F. G. (2015). Remote sensing role in emergency mapping for disaster response. In G. Lollino, A. Manconi et al. (Eds.), *Engineering Geology for Society and Territory* (pp. 17–24). Cham: Springer. doi:10.1007/978-3-319-09048-1_3
- Braun, A. (2020). Spaceborne radar imagery: An under-utilized source of information for humanitarian relief. *Journal of Humanitarian Engineering*, 8(1).
- Ferro, A., Brunner, D., Bruzzone, L. (2012). Automatic detection and reconstruction of building radar footprints from single VHR SAR images. *IEEE Transactions on Geoscience and Remote Sensing*, 51(2), 935–952.
- Lang, S., Füreder, P., Riedler, B., Wendt, L., Braun, A. et al. (2020). Earth observation tools and services to increase the effectiveness of humanitarian assistance. *European Journal of Remote Sensing*, 53(sup2), 67–85.
- Lee, J. S., Jurkevich, L., Dewaele, P., Wambacq, P., Oosterlinck, A. (1994). Speckle filtering of synthetic aperture radar images: A review. *Remote Sensing Reviews*, 8(4), 313–340. doi:10.1080/02757259409532206
- Oliver, C., Quegan, S. (2004). *Understanding Synthetic Aperture Radar Images*: SciTech Publishing.
- Pirrone, D., Bovolo, F., Bruzzone, L. (2020). An Approach to Unsupervised Detection of Fully and Partially Destroyed Buildings in Multitemporal VHR SAR Images. *IEEE Journal of Selected Topics in Applied Earth Observations and Remote Sensing*, 13, 5938–5953. doi:10.1109/JSTARS.2020.3026838
- Soergel, U. (2010). Review of radar remote sensing on urban areas. In U. Soergel (Ed.), *Radar remote sensing of urban areas* (pp. 1–47). Berlin: Springer.
- Spröhnle, K., Fuchs, E.-M., Aravena Pelizari, P. (2017). Object-Based Analysis and Fusion of Optical and SAR Satellite Data for Dwelling Detection in Refugee Camps. *IEEE Journal of Selected Topics in Applied Earth Observations and Remote Sensing*, 10(5), 1780–1791. doi:10.1109/JSTARS.2017.2664982
- Ulaby, F. T., Dobson, M. C., Álvarez-Pérez, J. L. (2019). *Handbook of radar scattering statistics for terrain* ([Revised and updated]). *Artech House Remote Sensing Library*. Norwood, MA: Artech House.
- Vasile, G., Trounev, E., Lee, J.-S., Buzuloiu, V. (2006). Intensity-driven adaptive-neighborhood technique for polarimetric and interferometric SAR parameters estimation. *IEEE Transactions on Geoscience and Remote Sensing*, 44(6), 1609–1621. doi:10.1109/TGRS.2005.864142
- Wang, Y., Zhu, X. X. (2019). The Challenge of Creating The Sarptical Dataset. In *IGARSS 2019* (pp. 5714–5717). IEEE. doi:10.1109/IGARSS.2019.8899803
- Zhu, X. X., Montazeri, S., Ali, M., Hua, Y., Wang, Y., Mou, L., . . . Bamler, R. (2020, June 17). *Deep Learning Meets SAR*. URL: <https://arxiv.org/pdf/2006.10027>

Multi-Feature Sample Database for Enhancing Deep Learning Tasks in Operational Humanitarian Applications

GI_Forum 2021, Issue 1

Page: 209 - 219

Research Paper

Corresponding Author:

stefan.lang@sbg.ac.at

DOI: 10.1553/giscience2021_01_s209

Stefan Lang¹, Lorenz Wendt¹, Dirk Tiede¹, Yunya Gao¹, Vanessa Streifender¹, Hira Zafar¹, Adebawale Adebayo¹, Gina Schwendemann² and Peter Jeremias¹

¹University of Salzburg, Salzburg, Austria

²Spatial Services GmbH, Salzburg, Austria

Abstract

Amongst the many benefits of remote sensing techniques in disaster- or conflict-related applications, timeliness and objectivity may be the most critical assets. Recently, increasing sensor quality and data availability have shifted the attention more towards the information extraction process itself. With promising results obtained by deep learning (DL), the notion arises that DL is not agnostic to input errors or biases introduced, in particular in sample-scarce situations. The present work seeks to understand the influence of different sample quality aspects propagating through network layers in automated image analysis. In this paper, we broadly discuss the conceptualisation of such a sample database in an early stage of realisation: (1) inherited properties (quality parameters of the underlying image such as cloud cover, seasonality, etc.); (2) individual (i.e., per-sample) properties, including *a.* lineage and provenance, *b.* geometric properties (size, orientation, shape), *c.* spectral features (standardized colour code); (3) context-related properties (arrangement). Several hundred samples collected from different camp settings were hand-selected and annotated with computed features in an initial stage. The supervised annotation routine is automated so that thousands of existing samples can be labelled with this extended feature set. This should better condition the subsequent DL tasks in a hybrid AI approach.

Keywords: humanitarian action, earth observation, deep learning, data assimilation, hybrid AI, sample quality, automation

1 Shifting demands in operational humanitarian EO

1.1 Time criticality vs reliability

Remote sensing and Earth observation (EO) derived products play a growing role in providing relevant and up-to-date information for humanitarian operations (Lang et al., 2019). Amongst the many benefits of remote sensing techniques in disaster- and conflict-related applications, timeliness and objectivity may be regarded as the most critical assets (Denis et al., 2016; Voigt et al., 2016). This applies, for example, to refugee camp mapping or dwelling extraction routines in deprived urban areas for population estimation, where otherwise such figures are

missing or largely outdated (Quinn et al., 2018). About a decade ago, when the humanitarian community started to adopt EO technologies in operations, both aspects of actuality (i.e., up-to-date and trustworthy information) were mainly referred to image (source) quality. Reluctance with respect to image provision, image manipulation, limited spatial resolution, cloud contamination, etc., was the main concern with respect to operational use. Recently, increasing sensor quality, data fusion techniques, and data availability have shifted the attention more towards the information extraction process itself (Lang, Füreder, et al., 2019). The increasing acceptance has experienced a synchronous shift in attention of the larger EO community from data management to data exploitation (Giuliani et al., 2017; Sudmanns et al., 2019; Voigt et al., 2016).

In highly demanding operational settings, timeliness and reliability may be considered mutually exclusive, if not contradictory, even. In demanding tasks, innovation in the automation process is limited, making the information extraction process ‘stagnant’ and dominated by and manual delineation. Recently, the community saw many approaches labelled as “semi-automated”, attempting to best implement computer vision with (GE-)OBIA techniques (Lang, Hay, Baraldi, Tiede, & Blaschke, 2019) and to overcome the tedious delineation process of small features which occurs in large frequencies and diversities (Füreder et al., 2015). In particular, in well-structured camp arrangements with distinct structures, the performance of region-based segmentation routines are satisfying and – once the delineation of dwellings has been achieved – object features such as size, colour, shape, etc., can be used to categorise them. The process is challenging when a clear distinction of individual dwellings is hampered by the complexity of the arrangement, and even visual inspection reaches its limits, and inter-subject objectivity is no longer guaranteed among experts.

With promising results obtained by deep learning (DL) in various applications (Ghorbanzadeh, Tiede, Wendt, Sudmanns, & Lang, 2020; Quinn, et al., 2018; Tiede, Wendt, Schwendemann, Alobaidi, & Lang, 2021) humanitarian community adopts to data science techniques as well. This also applies to computer vision, which gradually evolves from static rule-based strategies to a more dynamic, self-adaptable machine learning-based approach. The limitation for the latter, however, is the existence and quality of samples. Despite the inherent improvement capabilities of machine learning, DL is not agnostic to input errors (Ghorbanzadeh, Tiede, Dabiri, Sudmanns, & Lang, 2018) or biases introduced, in particular in sample-scarce situations. Sample scarcity in humanitarian applications may be attributed to the complexity and required level of detail (e.g., complex urban settings or organically grown refugee camps), for which samples on a generalised level do not exist in sufficient number or quality. Even though tents and other dwelling types can be generalised and described according to standard building codes, the confusion with other and similar features, mixed in and intermingled, is high and the appearance on EO imagery greatly depends on seasonal conditions (dry vs. humid periods, overgrown by vegetation, etc.). The detection and correct interpretation of different dwelling types, in a degree relevant to humanitarian organisations, is a dedicated expert task. While support is increasingly available through community-mapping approaches such as Humanitarian Open Street Map (HOT OSM or Missing Maps), utilising crowd-sourced information needs, therefore, to be curated and the existing dwelling delineations need to be evaluated and characterised (Albuquerque, Herfort, & Eckle, 2016; Elia, Balbo, & Boccardo, 2018).

The challenge remains: compromising reliable results for the sake of increased automation is a tricky decision in operational humanitarian settings, where actions and decisions may have severe implications for human lives and wellbeing. Taking the ‘best of two worlds’, we try to apply hybrid approaches, which are aware of the physical properties of the target dwellings, which rests upon the experience of operational mapping task of the last ten years. Based on this legacy, an annotated dwelling sample database is foreseen, which documents sample provenance and characteristics in a way that observations and dwelling models are well attuned in a hybrid AI and data assimilation approach.

1.2 Hybrid AI and data assimilation

Artificial intelligence (AI) simulates processes characteristic to human intelligence and thereby mimics human actions. Among the cognitive relevant AI tasks includes knowledge representation, automated reasoning, machine learning (ML) and teaching. Types of AI are distinguished by adaptability, performance, proficiency as compared to the human brain ranging from narrow AI and general AI to Super AI. Physics-aware or hybrid AI is a strategy to better condition ML/DL tasks by employing physical models, principles, or even laws. These principles into consideration using general conditions and constraints utilising machine teaching as an enabler (Lang, Hay, et al., 2019). One strategy is data assimilation.

Data assimilation aims to foster data integration and data harmonisation in a bi-directional way between the measured and the modelled reality (Lahoz and Schneider, 2014). In Earth observation, data assimilation compensates for the fact that a specific site may be observed in a variety of measurements by satellites with different sensor types, at different dates, different angular geometries and viewing directions, illumination conditions (solar time), observation frequencies, etc. (Verhoef and Bach, 2003). In particular, for monitoring purposes, measurements over time need to assure to actually measure the status of the system or object and not the divergence in observation. For vegetation and crop type monitoring, radiative transfer modelling (RTF) is being used as an example (Graf, Papp, & Lang, 2020; Verhoef and Bach, 2003). In general, when interpreting images and overcoming the semantic gap, rigorous classifiers based on solid spectral models, acting across sensors, are available. Semantic enrichment of satellite data (Augustin, Sudmanns, Tiede, Lang, & Baraldi, 2019). For satellite image time-series (SITS), the seasonal dynamics and the variability the appearance of the target classes are relevant. Data assimilation can also bridge non-availabilities of EO data and other observations to provide estimates or prediction for geographical variables. A related aspect is data imputation, i.e. filling gaps in observations, e.g. by other, complementary data sets (e.g. Radar imagery in the absence of VHR data under cloudy weather conditions).

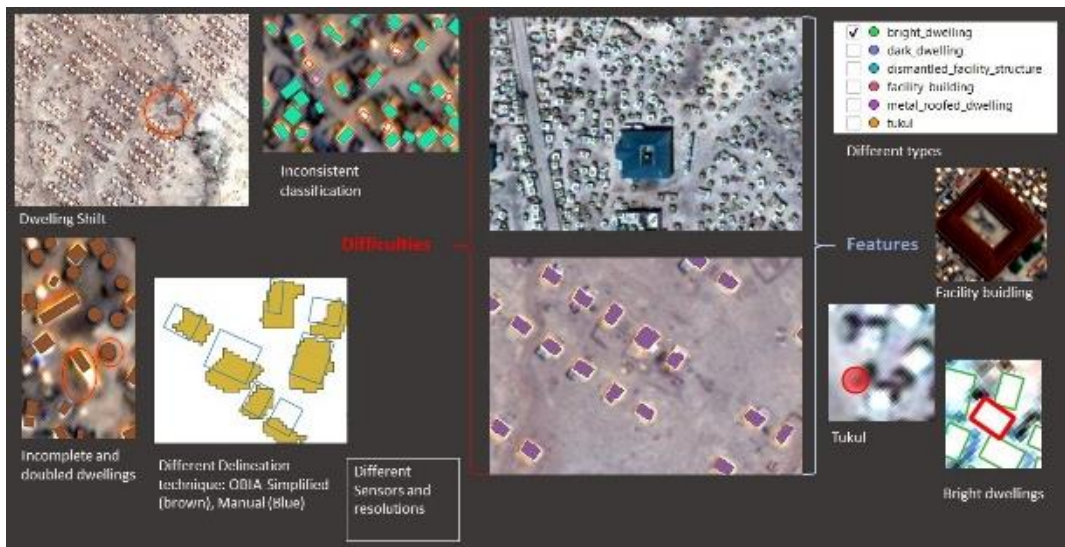
2 Quality-controlled samples

2.1 Rationale in the context of dwelling extraction

A better understanding of sample quality is a critical requirement to improve automated DL tasks in image analysis. Our aim is to investigate systematically how various imperfections in the delineation and provision of samples affect the result of machine learning. We, therefore,

in a first step, defined and tested a set of quality indicators, computed and recorded in a database next to each sample's label (dwelling category). These indicators comprise: (1) inherited properties (quality parameters of the underlying image such as cloud cover, seasonality, etc.); (2) individual (i.e., per-sample) properties, including a. lineage and provenance, b. geometric properties (size, orientation, shape), c. spectral features (standardized colour code); (3) context-related properties (spatial arrangement). Currently, the approach is 'static' and does not consider the temporal dynamics of dwelling evolution, meaning we record quality indicators per image timeslot (epoch). Several hundred samples collected from different camp settings were selected and annotated using the expert-based selection of quality indicators in an initial stage. It is foreseen that thousands of existing samples and future delineations are labelled automatically with this set of quality-relevant features.

The following figures illustrate the challenges encountered in documenting the quality indicators of the samples using mixed methods for dwelling delineation in an operational production environment. We deal with different sensors and image resolutions, limitations due to cloud cover and atmospheric conditions, problems of geometric correction (shifts), incomplete interpretation or extraction (false positives and negatives), different delineation techniques (segmentation-based vs. manual delineation), and inconsistencies in the classification and labelling (see figure 1). Some of these aspects influence the quality of the samples globally, i.e. per image. Atmospheric conditions and cloud contamination or any other aspects of image correction introduce a global bias to the extraction process. While difficult to estimate, this bias is an important aspect of data provenance in the process of turning primary (continuous image) data into secondary (discrete object) data.



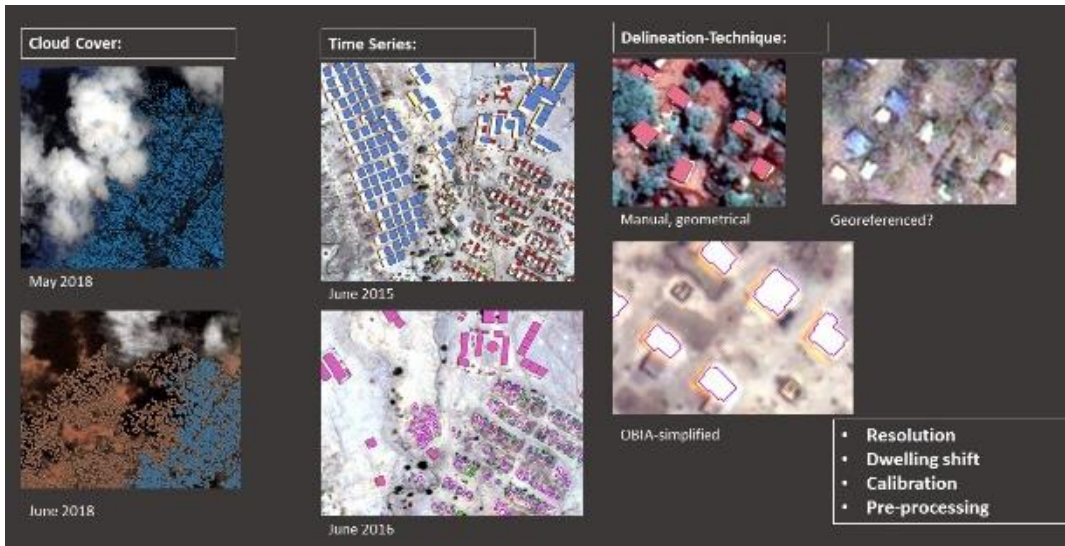


Figure 1: Various aspects to consider in estimating quality parameters of extracted dwellings (see text for further explanation).

Global (per-image) quality indicators. We aim to use quality-proven polygon data as input for training tasks of ML algorithms rather than labelled imagery. We, therefore, have to ensure that the extracted dwelling polygons have a unique image source assigned. What sounds trivial is sometimes impaired by the complexity of operational tasks, using multiple input data (e.g. VHR satellite images, drones), or observing dwellings over a certain longer time period with updated image data (monitoring). Once a unique match of source and dwelling object is assured, the produced dwelling data will inherit the global image quality indicators, like cloud cover, incidence angle, atmospheric conditions, geometric shift, etc. This is another crucial aspect of data provenance and reproducibility because only polygon data with a unique source should be considered a matching pair to be used as training samples.

In the absence of an alternative option, we are currently experimenting with a global quality score for judging the data provenance as a combination of image resolution, cloud cover and feature delineation (including shifts). Table 1 shows a draft version of such a grading scheme, which would attest all samples taken from one input image at a certain epoch a global quality score. Those with a quality score 1 could be used as testing samples to start the model training without any bias. Further, samples with a lesser quality can be used for training to increase the robustness of the model. Samples of quality scores 3 or 4 might suffer inconsistencies in spatial registration or delineation type but may still be used for sample augmentation purposes. Quality score 6 would indicate a status of non-correspondence between image and extracted dwellings.

Table 1: Grading scheme for assessing the overall quality of data provenance (draft)

Delineation	Image resolution	Cloud cover	Quality score
Nearly perfect delineation, minor differences in delineation	High	none	1
Minor differences in delineation	high-medium	none	2
Larger difference in delineation; repairable dwelling shift	High-medium	partly	3
Dwellings partly missing; repairable dwelling shift	High-medium	partly	4
Many dwellings missing; shift not repairable	Medium-Low	large	5
no correspondence in delineation	-	-	6

2.2 Quality features per dwelling

The present work is a precursor to a larger investigation that aims at documenting systematically how different aspects of quality of samples propagate through artificial neural network layers, thereby judging how this reflects in the result of the DL task. An extensive number of annotated samples, semi-automatically derived and manually revised, are collected, representing features suitable for enumerating and estimating the actual local population; they are stored and made accessible in a dedicated sample database. The samples consist of vector representations (polygons) of dwellings of different types like tents, huts, tukuls, facility buildings, etc.; hence have a different characteristic to be taken into account for the structure of the database. Next to the labels, the dwelling samples are characterised by a set of quality indicators assessing their spectral and spatial properties (table 2).

Table 2: Dwelling sample quality indicators

Dwelling delineation process	
Dwelling shift	Polygons do not match the source image and show offsets
Inconsistency in classification	Different labels depending on the source of the footprints and image
Incomplete and double count of dwellings	Dwellings double-counted or do not totally cover the apparent dwelling on the source image
Delineation strategy	Manual, semi-automated (OBIA), etc.
Image characteristics (inherited by dwellings)	
Cloud cover	Not all dwelling in the imaged scene captured
SITS	Evolution of a camp and seasonal effects
Delineation strategy	(see above)
Dwelling individual properties	
Representation	As polygon, as point (centroid)
Spectral properties	Colour categories (SIAM-based)
Neighbourhood, context	Embeddedness in dwellings of the same type
Geometrical attributes	Size, position (centroid)
Shape	Compactness, regular fit, orientation, etc.
SITS	Dwelling dynamics (emergence, disappearance, etc.)

Spectral features. Spectral characteristics are recorded based on standardised colour categories using a knowledge-based feature space partitioning system called SIAM®. The idea is to generate standardised categories (semi-concepts) fully automated from VHR imagery (figure 2). This requires calibration (as far as possible), even in operational, demanding application contexts. The advantage is to have stable categories rather than subjective colour impressions (“light-blue tents”, “brownish tukul”, “bright dwellings”, etc.). This helps enrich the sample database because we have a (certain level of) semantic understanding of the global image content (e.g. dominance of dwelling type X) and a per-object uniform colour label to support the classification. The standardised colour categories are based on a fully automated pre-classification of the multi-spectral properties from VHR images; this process involves radiometric calibration of the images into top-of-atmosphere (TOA) reflectance followed by a knowledge-based feature classifier. The image calibration process includes the absolute radiometric calibration factors provided by the VHR image vendors; this ensures the baseline for multiple sensors data integration and fusion in every operational and demanding application contexts. The predefined colour codes consist of a discrete and fixed number of cross-sensor spectral categories (e.g. 33 or 61) whose degree of semantic information – while lower than common land cover classes – is superior to non-semantic image data. This provides a stable and uniform representation of object primitives labelled to support recognition and classification by the model.

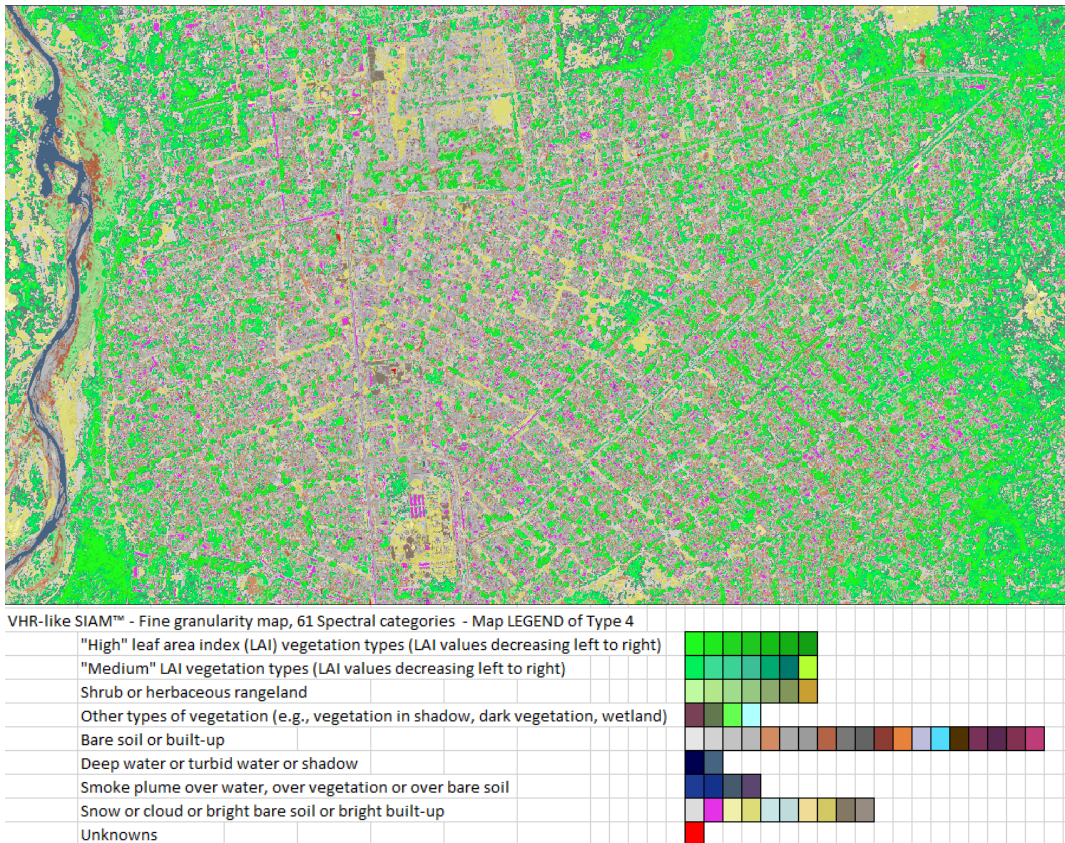


Figure 2: Fully automatic pre-classification of calibrated VHR Pléiades imagery into a fixed set of 61 spectral categories using SIAM®. Different vegetation, water, built-up, and other low-level semantic classes are discerned in a standardised and transferable manner,

Spatial features. Spatial properties comprise geometric properties and spatial arrangement. The azimuth angle is the angle between two points in the Cartesian plane; it is calculated between the centroid of the dwelling itself and the neighbouring dwelling. The orientation angle was calculated to show the orientation of individual dwellings against geographic North. The shape index measures the deviation of a given polygon from the circularity of a perfect circle of the same size. For any set of geometric forms of a given area, the circle has the shortest perimeter in relation to the area; thus its compactness is highest. Any other form exhibiting the same area shows less compactness and a higher shape index. The proximity index is well suited for indicating the embeddedness of an extracted dwelling in its surrounding, i.e. to which degree a dwelling differentiate from neighbours in terms of size and distance. It was calculated for each dwelling by identifying the dwellings that were within the buffer distance of the indexed dwelling and then calculating the size to distance ratio for each of the n dwellings identified within the buffer.

2.3 Annotated sample database – a prototypical implementation

A spatial database in PostgreSQL stores the quality indicators of the image source and the respective dwellings (vector data). This database aims to store spatial and spectral characteristics of the dwellings analysed in the area of investigation. The simplified database schema (figure 3) consists of two main tables: the Image table and the Dwelling table connected via image ID as primary and foreign key. The dwellings delineated from each image were originally stored in separate individual tables per country and now collated in one single schema. The Image table serves as the main table containing information about individual dwellings in all images in one place. The Image table contains information about image characteristics of the image (radiometric, etc.) properties. The Dwelling table contains information about spatial characteristics of individual dwellings, as described above.

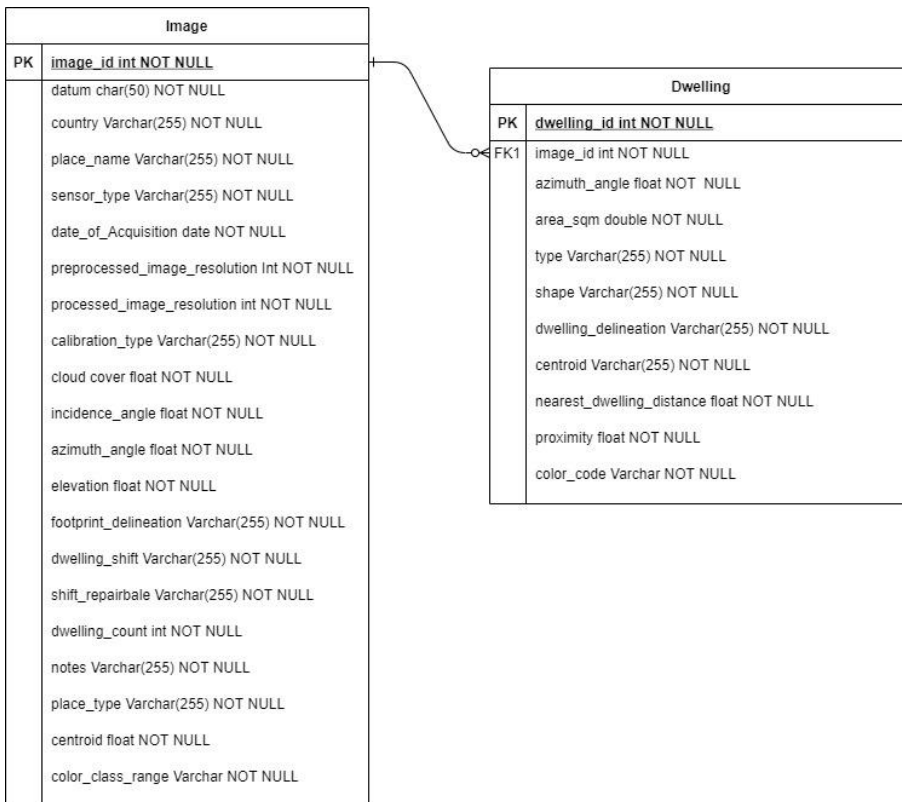


Figure 3: Simplified ER diagram of sample DB

3 Outlook

The described conceptual framework for quality indicators of dwelling extraction is currently investigated and expert-evaluated in terms of impact on the performance of various DL tasks. Being in an early stage of development, we plan to consider temporal aspects of dwelling evolution by deriving quality indicators not from single epochs but from multi-temporal (and potentially semantically enriched) data cubes.

Prospectively, hundreds of thousands of existing samples are going to be labelled automatically with this extended set of quality indicators. This should better condition the subsequent mapping tasks using a hybrid AI approach and improve existing operational mapping routines. It may also serve as a stimulating reference dataset for benchmark contests.

References

- Albuquerque, J. P., Herfort, B., & Eckle, M. (2016). The tasks of the crowd: a typology of tasks in geographic information crowdsourcing and a case study in humanitarian mapping. *Remote Sensing*, 8(10), p 859.
- Augustin, H., Sudmanns, M., Tiede, D., Lang, S., & Baraldi, A. (2019). Semantic Earth observation data cubes. *Data*, 4(3), pp. 102-115. doi:10.3390/data4030102
- Baraldi, A. (2011). Satellite Image Automatic Mapper™ (SIAM™). A turnkey software button for automatic near-real-time multi-sensor multi-resolution spectral rule-based preliminary classification of spaceborne multi-spectral images. *Recent Patents on Space Technology*(1), pp. 81-106.
- Denis, G., de Boissezon, H., Hosford, S., Pasco, X., Montfort, B., & Ranera, F. (2016). The evolution of Earth Observation satellites in Europe and its impact on the performance of emergency response services. *Acta Astronautica*, 127, pp. 619-633.
- Elia, A., Balbo, S., & Boccardo, P. (2018). A quality comparison between professional and crowdsourced data in emergency mapping for potential cooperation of the services. *European Journal of Remote Sensing*, 51(1), pp. 572-586.
- Füreder, P., Lang, S., Hagenlocher, M., Tiede, D., Wendt, L., & Rogenhofer, E. (2015). Earth observation and GIS to support humanitarian operations in refugee/IDP camps. In Palen, Büscher, Comes & Hughes (Eds.), *Geospatial Data and Geographical Information Science*. Kristiansand.
- Ghorbanzadeh, O., Tiede, D., Dabiri, Z., Sudmanns, M., & Lang, S. (2018). Dwelling extraction in refugee camps using CNN - first experiences and lessons learnt. *The International Archives of the Photogrammetry, Remote Sensing and Spatial Information Sciences*, XLII(1), pp. 161-168.
- Ghorbanzadeh, O., Tiede, D., Wendt, L., Sudmanns, M., & Lang, S. (2020). Transferable instance segmentation of dwellings in a refugee camp - integrating CNN and OBIA. *European Journal of Remote Sensing*, pp. 1-14. doi:10.1080/22797254.2020.1759456
- Giuliani, G., Chatenoux, B., Bono, A. D., Rodila, D., Richard, J.-P., Allenbach, K., . . . Peduzzi, P. (2017). Building an Earth observations data cube: lessons learned from the Swiss Data Cube (SDC) on generating Analysis Ready Data (ARD). *Big Earth Data*, 1(1-2), pp. 1-18. doi:doi.org/10.1080/20964471.2017.1398903
- Graf, L., Papp, L., & Lang, S. (2020). OBIA4RTM – towards an operational open-source solution for coupling object-based image analysis with radiative transfer modelling. *European Journal of Remote Sensing*, pp. 1-12. doi:10.1080/22797254.2020.1810132
- Lahoz, W. A., & Schneider, P. (2014). Data assimilation: making sense of Earth Observation. *Frontiers in Environmental Science*, 2, p 16. doi:doi.org/10.3389/fenvs.2014.00016

- Lang, S., Füreder, P., Riedler, B., Wendt, L., Braun, A., Tiede, D., . . . Hochschild, V. (2019). Earth observation tools and services to increase the effectiveness of humanitarian assistance. *European Journal of Remote Sensing*, pp. 1-19. doi:10.1080/22797254.2019.1684208
- Lang, S., Hay, G., Baraldi, A., Tiede, D., & Blaschke, T. (2019). GEOBIA achievements and spatial opportunities in the era of big Earth observation data. *ISPRS International Journal of Geo-Information*, 8, pp. 474-483. doi:doi.org/10.3390/ijgi8110474
- Quinn, J. A., Nyhan, M. M., Navarro, C., Coluccia, D., Bromley, L., & Luengo-Oroz, M. (2018). Humanitarian applications of machine learning with remote-sensing data: review and case study in refugee settlement mapping. *Philosophical Transactions of the Royal Society A*, 376(2128)
- Sudmanns, M., Tiede, D., Lang, S., Bergstedt, H., Trost, G., Augustin, H., . . . Blaschke, T. (2019). Big Earth data: disruptive changes in Earth observation data management and analysis? *International Journal of Digital Earth*, pp. 1-19. doi:10.1080/17538947.2019.1585976
- Tiede, D., Wendt, L., Schwendemann, G., Alobaidi, A., & Lang, S. (2021). Mask R-CNN-based building extraction from VHR satellite data in operational humanitarian action. *Transactions in GIS*, (in press)
- Verhoef, W., & Bach, H. (2003). Remote sensing data assimilation using coupled radiative transfer models. *Physics and Chemistry of the Earth*, 28(1-3), pp. 3-13.
- Voigt, S., Giulio-Tonolo, F., Lyons, J., Kučera, J., Jones, B., Schneiderhan, T., . . . Guha-Sapir, D. (2016). Global trends in satellite-based emergency mapping. *Science*, 253(6296), pp. 247-252. doi:doi:10.1126/science.aad8728

Testing Transferability of Deep-Learning-Based Dwelling Extraction in Refugee Camps

Getachew Workineh Gella¹, Lorenz Wendt¹, Stefan Lang¹, Andreas Braun^{1,2}, Dirk Tiede¹, Barbara Hofer¹, Yunya Gao¹, Barbara Riedler¹, Ahmad Alobaidi³ and Gina Marciela Schwendemann³

¹University of Salzburg, Austria

²University of Tübingen, Germany

³Spatial Services, Salzburg, Austria

Abstract

For effective humanitarian response in refugee camps, reliable information concerning dwelling type, extent, surrounding infrastructure, and respective population size is essential. As refugee camps are inherently dynamic in nature, continuous updating and frequent monitoring is time and resource-demanding, so that automatic information extraction strategies are very useful. In this ongoing research, we used labelled data and high-resolution Worldview imagery and first trained a Convolutional Neural Network-based U-net model architecture. We first trained and tested the model from scratch for Al Hol camp in Syria. We then tested the transferability of the model by testing its performance in an image of a refugee camp situated in Cameroon. We were using patch size 32, at the Syrian test site, a Mean Area Intersection Over Union (MIoU) of 0.78 and F-1 score of 0.96, while in the transfer site, MIoU of 0.69 and an F-1 score of 0.98 were achieved. Furthermore, the effect of patch size and the combination of samples from test and transfer sites are investigated.

Keywords: deep learning, dwelling extraction, refugee camp, transferability, U-net

1 Introduction

Humanitarian aid organizations, human rights groups, and concerned parties working in emergency response need accurate and reliable information related to the camp extent, dwelling type, number, and structure of dwellings of camps of refugees and internally displaced persons (IDP). Especially in the absence of exact population numbers, estimating the number of people in need of relief from these proxies is a viable option. Earth observation is routinely used to this end when information collection on the ground would be too time-consuming or dangerous (e.g., Lang and Füreder, 2015; Bjorgo, 2000; Lang et al., 2020).

Despite recent advances in computer vision and particularly deep learning for information extraction from satellite images (Ma et al., 2019; Li et al., 2020), manual digitization or at least extensive clean-up of automatically extracted dwelling features is still required. Quinn et al. (2018), who demonstrated the potential of deep learning for automatic dwelling counting,

noted problems of transferability of models emanated from differences in sensors and inherent characteristics of dwelling structures. To overcome these challenges, Ghorbanzadeh et al. (2018) investigated combining object-oriented and deep learning approaches for dwelling extraction to improve the transferability of classifiers from one satellite scene to another.

The large number of dwellings we extracted from satellite images of refugee and IDP camps in an operational setting for a major international humanitarian organization over the past years now enables us to experiment on the optimal combination of sample-based machine learning / deep learning techniques, prior-knowledge based machine teaching methods and an optimized selection of samples. As part of ongoing work, this study focuses on the spatial transferability of deep learning-based dwelling extraction. More specifically, it has the following contributions: firstly, it tests the U-net architecture (Ronneberger, Fischer, & Brox, 2015) for dwelling extraction in two refugee camps; secondly, it investigates the impact of patch size on model capability for dwelling extraction; thirdly, it explores the transferability of the model trained at one site to another refugee camp situated in a different geographic region; finally, it compares the performance of U-net segmentation network trained on local samples, samples from a different camp setting, and network using a combined set of samples.

2 Methodology

2.1 The test sites

The study is based on the two refugee camps in Al Hol, Syria, and Minawao, Cameroon. The two camps are characterized by a large fraction of standard-issue shelters as used by UNHCR and other organizations but are located in a different part of the world. Therefore, these sites allow testing the generalization capability of the trained model from one geographic setting to the other. Al Hol consisted of approximately 19,396 dwellings at the time of the investigation. It has a total area of 289 hectares with dwelling density ranging from below 15 dwellings per hectare at the outskirts of the camp towards 108 dwellings per hectare in the inner parts. Almost 97% of the dwellings are standard-issue tents (UNHCR, 2016). It has experienced a high population influx (Neil, 2020; REACH, 2020). Minawao has a camp area of 623 hectares with a total of 16,601 dwellings with a dwelling density of 1-2 dwellings per hectare towards 180 dwellings per hectare. The camps have different dwellings, which include small structures ($\sim 2\text{-}5\text{ m}^2$) towards large facility structures ($\sim 102\text{ m}^2$).

2.2 Data and sample generation

We used a WorldView-2 image with a spatial resolution of 0.5 meters for Al Hol acquired on 27 April 2020, and a WorldView-3 image with a resolution of 0.3 meters for Minawao acquired on 3 June 2016. The Worldview-3 image is resampled to Worldview-2 resolution. The labelled vector data used in this study were generated as part of ongoing operational humanitarian service by combining object-based image analysis (OBIA) and subsequent manual digitization with proper post-processing operations. For labelled data, a qualitative check is made for completely missing polygons and the presence of systematic positional shifts. Then these

vector files were converted to binary raster tiles (dwelling and non-dwelling), irrespective of dwelling type (Figure 1).

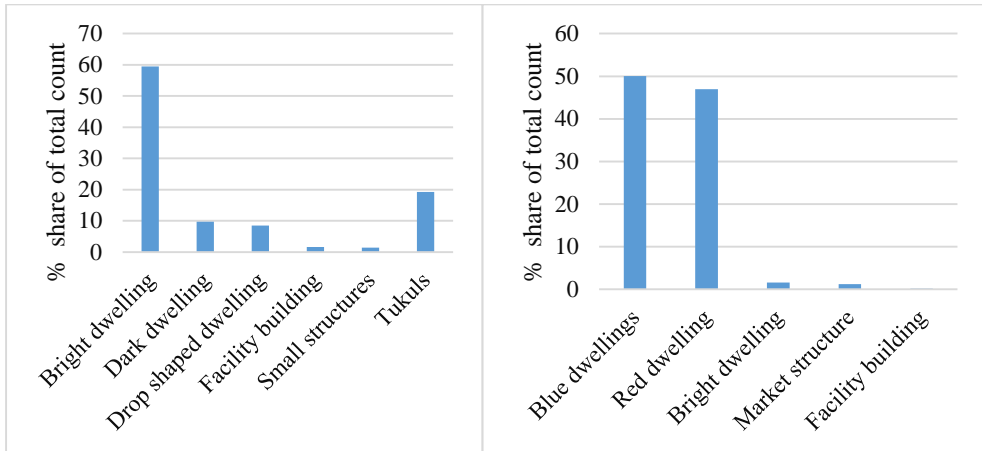


Figure 1: Dwelling types in Minawao (right) and Al Hol (left)

To train, validate and test the model, the test site in Syria is partitioned into training and test area. During this partitioning, some part of the area surrounding the camp is also included in training and validation samples to reduce model confusion on unseen features from the surrounding environment during the prediction phase both onsite and at the transferability test site. As patch size influences the variation of Fully Convolutional Network (FCN) model performance (Hamwood, Alonso-Caneiro, Read, Vincent, & Collins, 2018), from a training area, three sample sets with a mutually exclusive patch size of 32 by 32, 64 by 64, and 128 by 128 pixels were generated. To train the model, these sample sets are randomly partitioned into training and validation samples with a ratio of 0.8 and 0.2. Testing of the trained model is done with unseen samples taken from camp parts partitioned to test areas that are not included in the training and validation samples and also in the transferability test site. To see the impacts of training on mixed samples from test and transfer sites, we have also generated some samples from Cameroon and mixed them with samples from Al Hol Syria.

2.3 The model and training process

We used the U-net model architecture (Ronneberger et al., 2015). The model is a family of Convolutional Neural Network (CNN), which are FCN architectures (Long, Shelhamer, & Darrell, 2015) and was reported robust in many problems that need semantic segmentation, like medical (Ibtehaz & Rahman, 2020) and aerial (Ivanovsky, Khryashchev, Pavlov, & Ostrovskaya, 2019) image segmentation. The model mainly works with an encoder-decoder architecture where the contracting encoder extracts abstract features from an image while the expanding decoder block reconstructs segmented features (Ibtehaz & Rahman, 2020). Both encoder and decoder blocks are constructed from a stack of convolution, pooling, and activation layers with skip connections between the decoder and encoder blocks at some stage.

For the current study, decoder and encoder blocks used Rectified Linear Unit (ReLU) activation (Nair & Hinton, 2010; Zeiler et al., 2013). Weight updating and feature learning are done using a categorical cross-entropy loss and stochastic gradient descent (SGD) optimizer (Zaheer & Shaziya, 2019) with a learning rate of 0.01. To prevent model overfitting (Ying, 2019) and reduce unnecessary computational time, an early stopping strategy with a patience of 10 epochs taking validation cross-entropy loss as a target monitoring metric has been implemented. Final dwelling structure presence probabilities are predicted by using a softmax activation, which is further converted to hard binary classes of dwelling features. To see the pixel-wise overall model performance, the F-1 score is used. Given that pixel-based metrics yield relatively inflated values in segmentation tasks, especially in unbalanced samples, an object-based metric, Mean Intersection over Union (MIoU) (Atiqur & Yang, 2001), was used. This metric evaluates the spatial (geometric) congruency of predicted and reference objects where a perfect match gives MIoU of 1 while complete disjoint MIoU of 0.

3 Results

Table 1 shows dwelling extraction accuracy metrics for a model in Syria trained on Syria, Cameroon trained on Syria, and Syria and Cameroon trained on samples from both sites combined for different patch sizes. The accuracy is calculated over all dwellings, irrespective of their type (Figure 1). As model prediction is made on an image that includes areas outside of the camp, false positives outside the camp area are masked out before the calculation of evaluation metrics.

Obtained results show variation as per utilized patch size for model training. In terms of MIoU metrics, 78.2% areal fit is achieved when trained with patch sizes of 128 pixels by 128 in Syria and 79.5% in Cameroon. The combination of samples from the transferability test site to train the model has yielded MIoU values almost similar to outputs from the model trained on samples from a single site. The model transferability metric is also varying as per input patch size, where a model trained with a patch size of 128 performed better. This also holds the same for a model trained with samples mixed from model training and transferability site (Cameroon).

Table 1: Accuracy metrics for experiments

Test site	Syria			Cameroon		
	32	64	128	32	64	128
Patch size						
F-1 score	0.964	0.961	0.963	0.985	0.983	0.989
Mean IoU	0.781	0.776	0.782	0.691	0.758	0.795
	Combined samples			Combined samples		
F-1 score	0.963	0.961	0.963	0.986	0.983	0.988
Mean IoU	0.778	0.777	0.779	0.726	0.763	0.770

Figures 1 and 2 show a visual comparison of classification and reference data. In the first test site, except for lack of crispness at the edge of dwellings, it has extracted dwellings with good completeness. In the transferability test site (Cameroon), relatively, there are some dwellings flagged by a model as false negatives. Combining samples from both sites during model training has not added any accuracy improvements except for patch size 32 where combining samples resulted in a 3.5% improvement of MIOU.

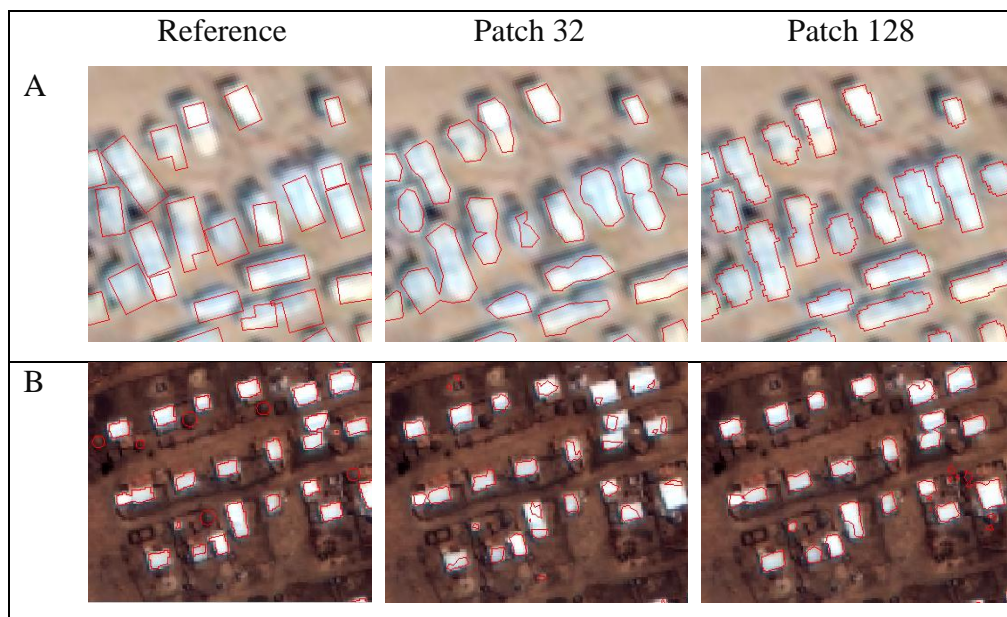


Figure 2: Dwelling extraction results in A) from Syrian test site and B) from Cameroon transferability test site

4 Discussion

Though the model fails to detect small and circular buildings made from natural materials, called tukuls (UNHCR, 2016) in the transferability test (Figure 1B), overall, the obtained results were in good agreement with segmentation results reported for building extraction (Rastogi, Bodani, & Sharma, 2020) and tent detection in refugee camps (Kahraman, Ates, & Kucur Ergunay, 2013). Current results were slightly better than segmentation results reported using the CNN with OBIA approach (Ghorbanzadeh et al., 2018), which achieved F-1 scores of 85.2%, 96.3%, and 93.3% for tunnel-shaped, rectangular, and large buildings, respectively. Variations in findings could also be attributed to differences in model architecture, patch size and details included in dwelling types. Increasing patch size has resulted in a reduction of false negatives within the dwelling blocks with respective trade-offs, including some reflective features like roads and bare land as false positives, especially in areas outside of the dwelling camp. Contrary to this, when the patch size is reduced, the model fails to properly segment larger and linearly attached dwelling structures (area >280 km²). This is especially prevalent in

the transferability test site. Using a different segmentation model, Ergunay et al. (2013) have also reported the same impact of window size on the proper segmentation of tents. It should be noted that though the dwellings structures are extracted with good performance, the segmentation is not exact at the edges. The samples for this study had been produced in a time-constraint operational setting, where outlining the dwellings precisely was not essential. At some blocks, even segmentation outputs have more precise outlines than reference polygons (Figure 1A). We assume that somewhat unsharp outlines in the samples resulted in a less-than-perfect segmentation, which also affects evaluation metrics.

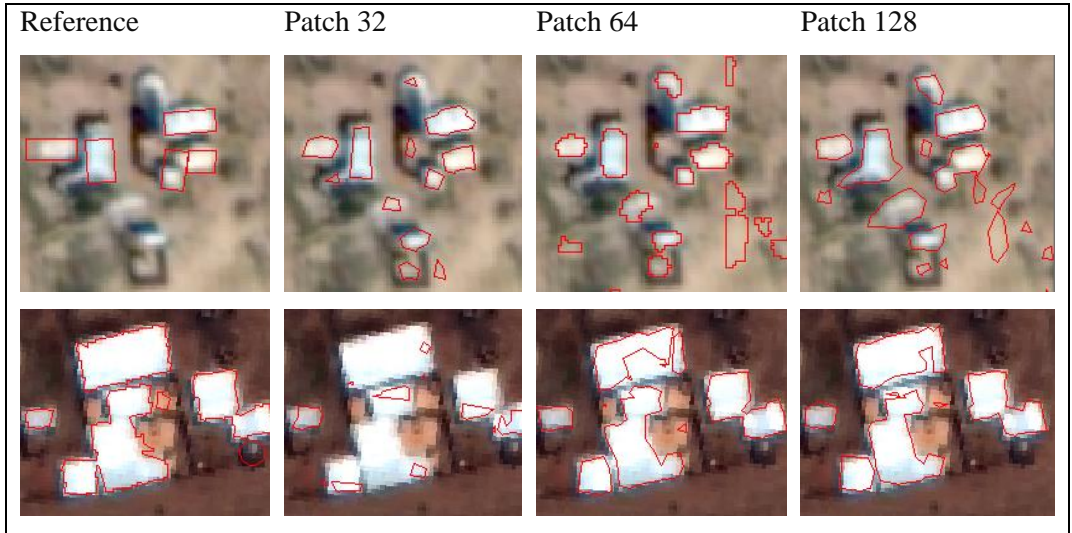


Figure 3: Confusion of background features with dwelling structures in Syria (first row) and patch wise variation of larger structure extraction (lower row)

5 Conclusion

Though the deep learning-based U-net model showed good overall performance, not all types of all dwelling structures were similarly well extracted. Structures that have good contrast with the background (bright and drop-shaped dwellings) are well extracted, while those with poor contrast (tukuls and small dark structures) were not well extracted. The model's capability to extract features varies with the patch sizes used for model training, especially to segregate background features with resembling reflectance characteristics. The model trained with a larger patch size can extract features in the transferability test site. In this study, except with patch size 32, the combination of samples from both sites has not changed the model performance. To get a more robust model that can universally extract dwelling structures, we plan further research with different pre-processing strategies that can enhance low contrast dwelling from its background, test segmentation models, and further detailed mapping of types of dwelling structures in the camp.

Acknowledgments

This work is undertaken under Christian Doppler Laboratory for Geospatial and EO-based Humanitarian Technologies (GeoHum) with support from the Christian Doppler Research Association and Médecins Sans Frontières (MSF) Austria. We are thankful for their support.

References

- Atiqur, R., & Yang, W. (2001). Optimizing Intersection-Over-Union in Deep Neural Networks for Image Segmentation. *International Symposium on Visual Computing ISVC 2016: Advances in Visual Computing*, 234–244.
- Bjorgo, E. (2000). Using very high spatial resolution multispectral satellite sensor imagery to monitor refugee camps. *International Journal of Remote Sensing*, 21(3), 611–616. <https://doi.org/10.1080/014311600210786>
- Ghorbanzadeh, O., Tiede, D., Dabiri, Z., Sudmanns, M., & Lang, S. (2018). Dwelling extraction in refugee camps using CNN - First experiences and lessons learned. *International Archives of the Photogrammetry, Remote Sensing and Spatial Information Sciences - ISPRS Archives*, 42(1), 161–166. <https://doi.org/10.5194/isprs-archives-XLII-1-161-2018>
- Hamwood, J., Alonso-Caneiro, D., Read, S. A., Vincent, S. J., & Collins, M. J. (2018). Effect of patch size and network architecture on a convolutional neural network approach for automatic segmentation of OCT retinal layers. *Biomedical Optics Express*, 9(7), 3049. <https://doi.org/10.1364/boe.9.003049>
- Ibtehaz, N., & Rahman, M. S. (2020). MultiResUNet: Rethinking the U-Net architecture for multimodal biomedical image segmentation. *Neural Networks*, 121, 74–87. <https://doi.org/10.1016/j.neunet.2019.08.025>
- Ivanovsky, L., Khryashchev, V., Pavlov, V., & Ostrovskaya, A. (2019). Building detection on aerial images using U-NET neural networks. *Conference of Open Innovation Association, FRUCT, 2019-April*, 116–122. <https://doi.org/10.23919/FRUCT.2019.8711930>
- Kahraman, F., Ates, H. F., & Kucur Ergunay, S. S. (2013). Automated Detection Of Refugee / IDP TENTS FROM Satellite Imagery Using Two-Level Graph Cut Segmentation. *CaGIS/ASPRS Fall Conference*, (September 2015). San Antonio, Texas.
- Lang, S., Füreder, P., Riedler, B., Wendt, L., Braun, A., Tiede, D., ... Hochschild, V. (2020). Earth observation tools and services to increase the effectiveness of humanitarian assistance. *European Journal of Remote Sensing*, 53(sup2), 67–85. <https://doi.org/10.1080/22797254.2019.1684208>
- Li, X., Liu, B., Zheng, G., Ren, Y., Zhang, S., Liu, Y., ... Wang, F. (2020). Deep-learning-based information mining from ocean remote-sensing imagery. *National Science Review*, 7(10), 1584–1605. <https://doi.org/10.1093/nsr/nwaa047>
- Long, J., Shelhamer, E., & Darrell, T. (2015). Fully convolutional networks for semantic segmentation. *Proceedings of the IEEE Computer Society Conference on Computer Vision and Pattern Recognition, 07-12-June*, 431–440. <https://doi.org/10.1109/CVPR.2015.7298965>
- Ma, L., Liu, Y., Zhang, X., Ye, Y., Yin, G., & Johnson, B. A. (2019). Deep learning in remote sensing applications: A meta-analysis and review. *ISPRS Journal of Photogrammetry and Remote Sensing*, Vol. 152, pp. 166–177. <https://doi.org/10.1016/j.isprsjprs.2019.04.015>
- Nair, V., & Hinton, G. E. (2010). Rectified linear units improve restricted Boltzmann machines. *ICML 2010 - Proceedings, 27th International Conference on Machine Learning*, 807–814.
- Neil, S. (2020). The Al Hol camp in Northeast Syria: health and humanitarian challenges. *BMJ Global Health*, 5(e002491). <https://doi.org/doi:10.1136/bmjgh-2020-002491>

- Quinn, J. A., Nyhan, M. M., Navarro, C., Coluccia, D., Bromley, L., & Luengo-Oroz, M. (2018). Humanitarian applications of machine learning with remote-sensing data: Review and case study in refugee settlement mapping. *Philosophical Transactions of the Royal Society A: Mathematical, Physical and Engineering Sciences*, 376(2128). <https://doi.org/10.1098/rsta.2017.0363>
- Rastogi, K., Bodani, P., & Sharma, S. A. (2020). Automatic building footprint extraction from very high-resolution imagery using deep learning techniques. *Geocarto International*. <https://doi.org/10.1080/10106049.2020.1778100>
- REACH. (2020). *Camp Profile: Al Hol/Al-Hasakeh governorate, Syria October 2020*. Retrieved from https://reliefweb.int/sites/reliefweb.int/files/resources/Al-Hol_camp-profile_October-2020_FINAL.pdf
- Ronneberger, O., Fischer, P., & Brox, T. (2015). U-net: Convolutional networks for biomedical image segmentation. In N. Navab, J. Hornegger, W. M. Wells, & A. F. Frangi (Eds.), *Lecture Notes in Computer Science (including subseries Lecture Notes in Artificial Intelligence and Lecture Notes in Bioinformatics)* (Vol. 9351, pp. 234–241). https://doi.org/10.1007/978-3-319-24574-4_28
- UNHCR. (2016). *SHELTER DESIGN CATALOGUE* (p. 68). p. 68. Retrieved from <https://cms.emergency.unhcr.org/documents/11982/57181/Shelter+Design+Catalogue+January+2016/a891fdb2-4ef9-42d9-bf0f-c12002b3652e>
- Ying, X. (2019). An Overview of Overfitting and its Solutions. *Journal of Physics: Conference Series*, 1168(2). <https://doi.org/10.1088/1742-6596/1168/2/022022>
- Zaheer, R., & Shaziya, H. (2019). A Study of the Optimization Algorithms in Deep Learning. *Proceedings of the 3rd International Conference on Inventive Systems and Control, ICISC 2019*, (Icisc), 536–539. <https://doi.org/10.1109/ICISC44355.2019.9036442>
- Zeiler, M. D., Ranzato, M., Monga, R., Mao, M., Yang, K., Le, Q. V., ... Hinton, G. E. (2013). On rectified linear units for speech processing. *ICASSP, IEEE International Conference on Acoustics, Speech and Signal Processing - Proceedings*, 3517–3521. <https://doi.org/10.1109/ICASSP.2013.6638312>

Suggestions on the Selection of Satellite Imagery for Future Remote Sensing-Based Humanitarian Applications

Yunya Gao¹, Stefan Lang¹, Dirk Tiede¹, Lorenz Wendt¹ and Getachew Workineh Gella¹

¹University of Salzburg, Austria

Abstract

Satellite imagery is an important information source for research on remote sensing (RS)-based humanitarian applications. The selection of satellite imagery is one of the most important steps for such research. This paper firstly shows the selection of satellite imagery in past research from 2015 to 2021. It can be found that most research on land cover and land use (LCLU) change caused by conflicts or refugees/internally displaced persons (IDPs) chose medium spatial resolution (MSR) imagery. Most research on dwelling detection of refugee/IDP camps applied high or very high spatial resolution (HSR/VHSR) imagery. There is much research that applied multiple types of satellite imagery for humanitarian applications. Then, the paper presents general characteristics of commonly available optical satellite imagery. Next, with the development of sensors, this paper suggests that data fusion of SPOT-5 and Sentinel-2 may be helpful in LCLU change detection caused by refugees/IDPs or conflicts. Smallsat imagery may be promising for research on humanitarian applications that require a high temporal frequency of imagery.

Keywords: remote sensing, satellite imagery, humanitarian applications

1 Introduction

Remote sensing (RS) technology has assisted humanitarian aid applications for the past few decades (Lang & Füreder, 2015). During a crisis, critical information for planning humanitarian operations, such as population in need and their spatial distribution, is usually hard to access by fieldwork (Witmer, 2015). Therefore, the major role of RS is to provide such information for users to support their humanitarian operations in hard-to-reach areas (Voigt, Schoepfer, Fourie, & Mager, 2014). Satellite imagery is a central information source for RS-based humanitarian applications. With the fast development of satellite sensors, more and more satellite imagery has become available. This paper firstly reviews the selection of satellite imagery in past research for humanitarian applications. Then it presents the latest collection of optical satellite imagery and discusses under-explored satellite imagery that may be beneficial for future research.

2 The selection of satellite imagery in past research

Different crises can result in different impacts on the ground with different spatial and temporal scales (Witmer, 2015). The selection of satellite imagery for different crises requires considering characteristics of both crises and imagery (Marx & Goward, 2013). Table 1 lists common research topics and the selection of satellite imagery from the most literature published from 2015 to 2021. The satellite imagery in Table 1 includes four categories that are optical imagery, synthetic-aperture-radar (SAR) imagery, nighttime light imagery, and the combination of multiple types of imagery. General characteristics of imagery, such as spatial resolution and revisit days, could be found in Table 2. Explanations of abbreviations in Table 1 and Table 2 could be found in Table 3.

Table 1: The selection of satellite imagery in past research

Type	Research topic	Sensors	Reference
Optical satellite imagery	LCLU change caused by refugee/IDP camps	Quickbird, WorldView-2, Pléiades-1A	(Rossi et al., 2019)
		SPOT-4, IKONOS, QuickBird	(Spröhnle, Kranz, Schoepfer, Moeller, & Voigt, 2016)
		Sentinel-2	(Bernard, Aron, Loy, Muhamud, & Benard, 2020)
		Landsat-5, Landsat-7, Landsat-8	(Alayyash, 2017; Hossain, Labib, & Patwary, 2018; Lu, Koperski, Kwan, & Li, 2020; Quinn et al., 2018; Ren, Calef, Durieux, Ziemann, & Theiler, 2020; Rossi et al., 2019)
		MODIS	(Maystadt, Mueller, Van Den Hoek, & Van Weezel, 2020)
	Vegetation cover and urban LST change caused by the influx of refugees/IDPs	Landsat-5, Landsat-8	(Rashid, Hoque, Esha, Rahman, & Paul, 2021; Shatnawi & Abu Qdais, 2019)
	Detecting dwellings of refugee camps	QuickBird, WorldView-2	(Tiede, Krafft, Füreder, & Lang, 2017)
		WorldView-3	(Ghorbanzadeh, Tiede, Dabiri, Sudmanns, & Lang, 2018)
		GeoEye-1, Pléiades-1A	(Jenerowicz, Wawrzaszek, Krupinski, Drzewiecki, & Aleksandrowicz, 2019)
		WorldView-2	(Lu et al., 2020)
GeoEye-1, WorldView-2		(Ghorbanzadeh, Tiede, Wendt, Sudmanns, & Lang, 2021)	
Dwelling infrastructure change detection for refugee/IDP camps	GeoEye-1, QuickBird, Worldview-1, Worldview-2, Worldview-3	(Tomaszewski, Tibbets, Hamad, & Al-Najdawi, 2016)	

	Dwelling change monitoring for refugee camps	Sentinel-2, (WorldView-2 and WorldView-3 used for comparison)	(Wendt, Lang, & Rogenhofer, 2017)
	LCLU change caused by conflicts/wars	Sentinel-2	(Hassan, Smith, Walker, Rahman, & Southworth, 2018)
		Landsat-5, Landsat-8	(Al-husban & Ayen, 2020)
		Pléiades-1A, Landsat-8, Landsat-5	(Aung, 2021)
	Village burnings caused by conflicts/wars	CubeSat 3U (Planet Dove)	(Marx, Windisch, & Kim, 2019)
	Satellite-derived drought indicators for humanitarian applications	MODIS	(Enekel et al., 2016)
SAR	Refugee camp sizes and their environmental impacts	ALOS-2, TerraSAR-X, RADARSAT-2	(Trinder, 2020)
	Environmental change around refugee/IDP camps	ALOS PALSAR, ALOS-2, (Landsat-7 and Landsat-8 used for comparison)	(Braun & Hochschild, 2017)
		ERS-2, Sentinel-1	(Braun, Lang, & Hochschild, 2016)
	Impacts of refugee camps on land surface elevation	Sentinel-1	(Braun, Höser, & Delgado Blasco, 2020)
	Change detection of refugee camps	TerraSAR-X	(Braun, 2020)
Nighttime light products	Detecting areas under conflicts	DMSP-OLS	(Coscieme, Sutton, Anderson, Liu, & Elvidge, 2017)
		DMSP-OLS, VIIRS	(Jiang, He, Long, & Liu, 2017)
	City light dynamics of human settlements during conflicts	DMSP-OLS, VIIRS	(Li, Li, Xu, & Wu, 2017)
Combination of multiple types of satellite imagery	Land cover classification around refugee/IDP camps	Sentinel-1, Sentinel-2	(Braun et al., 2016)
	Detecting dwellings of refugee camps	WorldView-2, TerraSAR-X	(Sprohnle, Fuchs, & Aravena Pelizari, 2017)
		Pléiades, TerraSAR-X	(Sprohnle et al., 2017)
	Environmental changes caused by refugee/IDP camps	ALOS-2, Sentinel-1, SRTM	(Braun, Fakhri, & Hochschild, 2019)
		Sentinel-1, Sentinel-2	(Fakhri & Gkanatsios, 2021)
		Pléiades-1A, VIIRS	(Aung, Overland, Vakulchuk, & Xie, 2021)

Dwelling destruction caused by conflicts/wars	GeoEye-1, WorldView-2, QuickBird	(Knoth & Pebesma, 2017)
Detecting anomalous fire and destroyed settlements	MODIS, VIIRS, Sentinel-1	(Ren et al., 2020)
Analyzing hazards and risks around refugee/IDP camps	Landsat-8, SRTM	(Ahmed, Firoze, & Rahman, 2020)

Based on summarization in Table 1, there are some common rules for selecting satellite imagery for humanitarian applications. Firstly, most research on LCLU change detection caused by the influx of refugees/IDPs or conflicts typically selected MSR satellite imagery. The selection is mainly because LCLU change detection usually requires large spatial scales and long-term series imagery. Landsat-5, together with Landsat-7 and Landsat-8, can provide long-term series imagery from 1984 until now. Thus, Landsat imagery is widely used for such research. Though in many cases, the performance of Sentinel-2 is better than Landsat imagery in LCLU classification (Sekertekin, Marangoz, Akcin, & Faculty, 2017). Sentinel-2 imagery is not broadly used for such research, possibly due to its short archived history. Most research on dwelling detection of refugee/IDP camps selected HSR/VHSR satellite imagery. Due to the small sizes of refugee/IDP camps, MSR imagery usually cannot capture details of dwellings. The applications of optical imagery usually are hacked by cloud covers. SAR imagery can reduce the influences of cloud covers and, thus, also plays a vital role in humanitarian applications (Braun et al., 2016). In recent years, the combination of optical imagery, SAR imagery, together with other data, has been paid more and more attention. These studies aim to make use of the advantages of different imagery to improve the performance of RS-based humanitarian applications.

3 Under-explored satellite imagery for humanitarian applications

In the past few decades, the development of satellite sensors is quite fast. Table 2 presents the general characteristics of currently common optical satellite imagery that may help researchers select the imagery for related research quickly.

In 2014, CNES announced that SPOT archive imagery older than five years is open for non-commercial purposes (Witmer, 2015). It may be valuable to combine satellite imagery from SPOT-5 (starting from 2002 to 2015) and Sentinel-2 (starting from 2015 until now) for LCLU change detection caused by refugees/IDPs or conflicts. The fusion may outperform Landsat imagery due to higher spatial resolution. Up to now, no similar studies have combined these two datasets specifically for LCLU change detection for humanitarian applications.

As shown in Table 2, the revisit days of several satellites can be within one day. Among them, SkySat and Jilin-1-Smart video can revisit the same location more than 5 times per day. This very high temporal resolution may be helpful for humanitarian applications, especially for emergent situations such as earthquakes and flooding. Compared to other traditional satellites, the size of these satellites is usually much smaller. Thus, they are called small satellites

(smallsats). Usually, the cost of smallsat imagery is lower than other traditional commercial satellite imagery such as WorldView (Datta, 2018). Currently, only one research on RS-based humanitarian applications used smallsat imagery (Planet Dove). It is proved that the smallsat imagery has high potentials for long-term monitoring of village burning in Myanmar (Marx et al., 2019). Hence, smallsat imagery may be valuable for research on humanitarian applications that require a high temporal resolution.

Table 2: General characteristics of common optical satellite imagery (European Space Agency, 2021)

Provider	Sensor	Spatial resolution / m and Spectral information		Revisit days	Availability
		PAN	RGB+NIR		
Digital Globe	IKONOS	0.8	3.2	3	1999-2015
	QuickBird	0.6	2.6	3	2001-2015
	GeoEye-1	0.5	1.8	3	2008-now
	WorldView-1	0.5		2	2007-now
	WorldView-2	0.5	0.5	2	2009-now
	WorldView-3	0.3	1.2	1	2014-now
	WorldView-4 (GeoEye-2)	0.3	1.2	<1	2016-2019
CNES	Pleiades-1A, 1B	0.5	2	<1	2011-now
	SPOT4	10	20	2 - 3	1998-2013
	SPOT5	2.5-5	10	2 - 3	2002-2015
	SPOT6	1.5	6	1	2012-now
	SPOT7	1.5	6	1	2014-now
Planet Lab	SkySat (1,2,3,4,5,6,7)	0.8	1	7 times/ day	2013-now
	PlanetScope		3	1	2009-now
	RapidEye (1,2,3,4,5)		5	5.5	2008-2020
DSC	TripleSat	0.8	3.2	1	2015-now
CAST	Gaofen-2	0.8	3.2	5	2014-now
CGST	Jilin-1-Optical	0.7	2.9	3.3	2015-now
	Jilin-1-Hyperspectral		5	2 - 3	2019-now
	Jilin-1-Smart video		1.1 (only RGB)	5-7 times/day	2017-now
ESA	Sentinel-2		10	5	2015-now
NASA	Landsat-5 TM		30	16	1984-2013
	Landsat-7 ETM+	15	30	16	1999-now
	Landsat-8 OLI-TIRS	15	30	16	2013-now
	MODIS		250/500/1000	1-2	1999-now

Table 3: Explanations of abbreviations

Abbreviation	Explanation
CAST	China Association for Science and Technology (China)
CGST	Chang Guang Satellite Technology Company (China)
CNES	National Centre for Space Studies (France)
DSC	Dhawan Space Centre (India)
DMSF-OLS	The Defence Meteorological Program Operational Line-Scan System
MODIS	Moderate Resolution Imaging Spectroradiometer
PAN	Panchromatic
SRTM	Shuttle Radar Topography Mission
RGB+NIR	Red, Green, Blue, Near-Infrared
VIIRS	Visible Infrared Imaging Radiometer Suite

4 Conclusion and Outlook

This paper first presents satellite imagery selection in numerous research on RS-based humanitarian applications from 2015 to 2021. It can be observed that MSR satellite imagery is usually selected for LCLU change detection caused by conflicts or refugees/IDPs. For detecting dwellings of refugee/IDP camps, most research chose HSR/VHSR satellite imagery due to the small size of camps. In addition to optical imagery, SAR imagery also plays an important role in humanitarian applications. Recently, quite a lot of research combined multiple types of imagery to explore more possibilities of improving RS-based humanitarian applications. Then, this paper displays some general characteristics of current optical satellite imagery, as shown in Table 2. This summarization may help researchers have a quick understanding of existing optical satellite imagery, and thus, be helpful for related research. At last, with some latest development in satellite imagery, the paper provides two suggestions for future research. The first suggestion is to combine SPOT-5 and Sentinel-2 data to create a long-term-series dataset that may help LCLU change detection for humanitarian applications. The second suggestion is considering smallsat imagery that usually has a lower cost and a higher temporal resolution. The smallsat imagery may be helpful for research or applications that require very high temporal frequency, such as natural disasters.

Acknowledgment

This work is funded within the Christian Doppler Laboratory for geospatial and EO-based humanitarian technologies (GEOHUM) by the Christian Doppler Research Association. We thank Médecins Sans Frontières Austria for their support.

Reference

- Ahmed, N., Firoze, A., & Rahman, R. M. (2020). Machine learning for predicting landslide risk of Rohingya refugee camp infrastructure. *Journal of Information and Telecommunication*, 4(2), 175–198. <https://doi.org/10.1080/24751839.2019.1704114>
- Al-husban, Y., & Ayen, A. (2020). The impact of the Syrian civil war on land use/land cover in Al-Yarmouk basin during 2010 – 2018, (September 2015), 147–153.
- Alayyash, S. M. (2017). Rainfall Floods as a Result of Land Use Alteration in a Syrian Refugee Camp in Jordan R =, 9(2), 65–71.
- Aung, T. S. (2021). Satellite analysis of the environmental impacts of armed-conflict in Rakhine, Myanmar. *Science of The Total Environment*, 781, 146758. <https://doi.org/10.1016/j.scitotenv.2021.146758>
- Aung, T. S., Overland, I., Vakulchuk, R., & Xie, Y. (2021). Using satellite data and machine learning to study conflict-induced environmental and socioeconomic destruction in data-poor conflict areas: The case of the Rakhine conflict. *Environmental Research Communications*, 3(2), 025005. <https://doi.org/10.1088/2515-7620/abedd9>
- Bernard, B., Aron, M., Loy, T., Muhamud, N. W., & Benard, S. (2020). The impact of refugee settlements on land use changes and vegetation degradation in West Nile Sub-region, Uganda. *Geocarto International*, 0(0), 1–19. <https://doi.org/10.1080/10106049.2019.1704073>
- Braun, A. (2020). Space borne radar imagery – An under-utilised source of information for humanitarian relief. *Journal of Humanitarian Engineering*, 8(1). <https://doi.org/https://doi.org/10.36479/jhe.v8i1.164>
- Braun, A., Fakhri, F., & Hochschild, V. (2019). Refugee camp monitoring and environmental change assessment of Kutupalong, Bangladesh, based on radar imagery of Sentinel-1 and ALOS-2. *Remote Sensing*, 11(17), 1–34. <https://doi.org/10.3390/rs11172047>
- Braun, A., & Hochschild, V. (2017). A SAR-based index for landscape changes in African savannas. *Remote Sensing*, 9(4). <https://doi.org/10.3390/rs9040359>
- Braun, A., Höser, T., & Delgado Blasco, J. M. (2020). Elevation change of Bhasan Char measured by persistent scatterer interferometry using Sentinel-1 data in a humanitarian context. *European Journal of Remote Sensing*, 54(1), 1–18. <https://doi.org/10.1080/22797254.2020.1789507>
- Braun, A., Lang, S., & Hochschild, V. (2016). Impact of Refugee Camps on Their Environment A Case Study Using Multi-Temporal SAR Data. *Journal of Geography, Environment and Earth Science International*, 4(2), 1–17. <https://doi.org/10.9734/jgeesi/2016/22392>
- Coscieme, L., Sutton, P. C., Anderson, S., Liu, Q., & Elvidge, C. D. (2017). Dark Times: nighttime satellite imagery as a detector of regional disparity and the geography of conflict. *GIScience and Remote Sensing*, 54(1), 118–139. <https://doi.org/10.1080/15481603.2016.1260676>
- Datta, A. (2018). Top five small satellite start-ups that are transforming the EO industry. Retrieved May 2, 2021, from <https://www.geospatialworld.net/blogs/top-small-satellite-start-ups-that-are-transforming-the-eo-industry/>
- Enenkel, M., Steiner, C., Mistelbauer, T., Dorigo, W., Wagner, W., See, L., ... Rogenhofer, E. (2016). A combined satellite-derived drought indicator to support humanitarian aid organizations. *Remote Sensing*, 8(4). <https://doi.org/10.3390/rs8040340>
- European Space Agency. (2021). EARTH ONLINE - Earth Observation information discovery platform. Retrieved May 2, 2021, from <https://earth.esa.int/eogateway/>
- Fakhri, F., & Gkanatsios, I. (2021). Remote Sensing Applications : Society and Environment Integration of Sentinel-1 and Sentinel-2 data for change detection : A case study in a war conflict area of Mosul city. *Remote Sensing Applications: Society and Environment*, 22(November 2020), 100505. <https://doi.org/10.1016/j.rsase.2021.100505>
- Ghorbanzadeh, O., Tiede, D., Dabiri, Z., Sudmanns, M., & Lang, S. (2018). Dwelling extraction in

- refugee camps using CNN - First experiences and lessons learnt. *International Archives of the Photogrammetry, Remote Sensing and Spatial Information Sciences - ISPRS Archives*, 42(1), 161–166. <https://doi.org/10.5194/isprs-archives-XLII-1-161-2018>
- Ghorbanzadeh, O., Tiede, D., Wendt, L., Sudmanns, M., & Lang, S. (2021). Transferable instance segmentation of dwellings in a refugee camp - integrating CNN and OBIA. *European Journal of Remote Sensing*, 54(sup1), 127–140. <https://doi.org/10.1080/22797254.2020.1759456>
- Hassan, M. M., Smith, A. C., Walker, K., Rahman, M. K., & Southworth, J. (2018). Rohingya refugee crisis and forest cover change in Teknaf, Bangladesh. *Remote Sensing*, 10(5), 1–20. <https://doi.org/10.3390/rs10050689>
- Hossain, N., Labib, S. M., & Patwary, S. H. (2018). Environmental Cost of Refugee Crisis: Case Study of Kutupalong Balukhali Rohingya Camp Site A Remote Sensing Approach Environmental Cost of Refugee Crisis: Case Study of Kutupalong-Balukhali Rohingya Camp Site A Remote Sensing Approach. *Proceedings of the 26th ...*, (September). <https://doi.org/10.13140/RG.2.2.14086.22085>
- Jenerowicz, M., Wawrzaszek, A., Krupinski, M., Drzewiecki, W., & Aleksandrowicz, S. (2019). Applicability of Multifractal Features as Descriptors of the Complex Terrain Situation in IDP/Refugee Camps. *International Geoscience and Remote Sensing Symposium (IGARSS)*, 2662–2665. <https://doi.org/10.1109/IGARSS.2019.8898588>
- Jiang, W., He, G., Long, T., & Liu, H. (2017). Ongoing conflict makes Yemen dark: From the perspective of nighttime light. *Remote Sensing*, 9(8), 1–18. <https://doi.org/10.3390/rs9080798>
- Knoth, C., & Pebesma, E. (2017). Detecting dwelling destruction in Darfur through object-based change analysis of very high-resolution imagery. *International Journal of Remote Sensing*, 38(1), 273–295. <https://doi.org/10.1080/01431161.2016.1266105>
- Lang, S., & Füreder, P. (2015). Earth Observation for Humanitarian Operations. *GI_Forum*, 1(July 2018), 384–390. <https://doi.org/10.1553/giscience2015s384>
- Li, X., Li, D., Xu, H., & Wu, C. (2017). Intercalibration between DMSP/OLS and VIIRS night-time light images to evaluate city light dynamics of Syria's major human settlement during Syrian Civil War. *International Journal of Remote Sensing*, 38(21), 5934–5951. <https://doi.org/10.1080/01431161.2017.1331476>
- Lu, Y., Koperski, K., Kwan, C., & Li, J. (2020). Deep Learning for Effective Refugee Tent - Extraction Near Syria–Jordan Border. *IEEE Geoscience and Remote Sensing Letters*.
- Marx, A., & Goward, S. (2013). Remote sensing in human rights and international humanitarian law monitoring: Concepts and methods. *Geographical Review*, 103(1), 100–111. <https://doi.org/10.1111/j.1931-0846.2013.00188.x>
- Marx, A., Windisch, R., & Kim, J. S. (2019). Detecting village burnings with high-cadence smallsats: A case-study in the Rakhine State of Myanmar. *Remote Sensing Applications: Society and Environment*, 14(February), 119–125. <https://doi.org/10.1016/j.rsase.2019.02.008>
- Maystadt, J. F., Mueller, V., Van Den Hoek, J., & Van Weezel, S. (2020). Vegetation changes attributable to refugees in Africa coincide with agricultural deforestation. *Environmental Research Letters*, 15(4). <https://doi.org/10.1088/1748-9326/ab6d7c>
- Quinn, J. A., Nyhan, M. M., Navarro, C., Coluccia, D., Bromley, L., & Luengo-Oroz, M. (2018). Humanitarian applications of machine learning with remote-sensing data: Review and case study in refugee settlement mapping. *Philosophical Transactions of the Royal Society A: Mathematical, Physical and Engineering Sciences*, 376(2128). <https://doi.org/10.1098/rsta.2017.0363>
- Rashid, K. J., Hoque, M. A., Esha, T. A., Rahman, M. A., & Paul, A. (2021). Spatiotemporal changes of vegetation and land surface temperature in the refugee camps and its surrounding areas of Bangladesh after the Rohingya influx from Myanmar. *Environment, Development and Sustainability*, 23(3), 3562–3577. <https://doi.org/10.1007/s10668-020-00733-x>
- Ren, C. X., Calef, M. T., Durieux, A. M. S., Ziemann, A., & Theiler, J. (2020). On the detectability of conflict: A remote sensing study of the Rohingya conflict. *ArXiv*, 1–4.
- Rossi, M., Rembold, F., Bolognesi, M., Nori, M., Mureithi, S., & Nyberg, G. (2019). Mapping land

- enclosures and vegetation cover changes in the surroundings of Kenya's Dadaab refugee camps with very high resolution satellite imagery. *Land Degradation and Development*, 30(3), 253–265. <https://doi.org/10.1002/ldr.3212>
- Sekertekin, A., Marangoz, A. M., Akcin, H., & Faculty, E. (2017). Pixel-based classification analysis of land use land cover using Sentinel-2 and Landsat-8 data, *XLII*(October), 14–15.
- Shatnawi, N., & Abu Qdais, H. (2019). Mapping urban land surface temperature using remote sensing techniques and artificial neural network modelling. *International Journal of Remote Sensing*, 40(10), 3968–3983. <https://doi.org/10.1080/01431161.2018.1557792>
- Sprohnele, K., Fuchs, E. M., & Aravena Pelizari, P. (2017). Object-Based Analysis and Fusion of Optical and SAR Satellite Data for Dwelling Detection in Refugee Camps. *IEEE Journal of Selected Topics in Applied Earth Observations and Remote Sensing*, 10(5), 1780–1791. <https://doi.org/10.1109/JSTARS.2017.2664982>
- Spröhnle, K., Kranz, O., Schoepfer, E., Moeller, M., & Voigt, S. (2016). Earth observation-based multi-scale impact assessment of internally displaced person (IDP) camps on wood resources in Zalingei, Darfur. *Geocarto International*, 31(5), 575–595. <https://doi.org/10.1080/10106049.2015.1062053>
- Tiede, D., Krafft, P., Füreder, P., & Lang, S. (2017). Stratified template matching to support refugee camp analysis in OBIA workflows. *Remote Sensing*, 9(4). <https://doi.org/10.3390/rs9040326>
- Tomaszewski, B., Tibbets, S., Hamad, Y., & Al-Najdawi, N. (2016). Infrastructure evolution analysis via remote sensing in an urban refugee camp - Evidence from Za'atari. *Procedia Engineering*, 159(June), 118–123. <https://doi.org/10.1016/j.proeng.2016.08.134>
- Trinder, J. C. (2020). Editorial for special issue “Applications of Synthetic aperture radar (SAR) for land cover analysis.” *Remote Sensing*, 12(15). <https://doi.org/10.3390/RS12152428>
- Voigt, S., Schoepfer, E., Fourie, C., & Mager, A. (2014). Towards semi-automated satellite mapping for humanitarian situational awareness. *Proceedings of the 4th IEEE Global Humanitarian Technology Conference, GHTC 2014*, 412–416. <https://doi.org/10.1109/GHTC.2014.6970315>
- Wendt, L., Lang, S., & Rogenhofer, E. (2017). Monitoring of Refugee and Camps for Internally Displaced Persons Using Sentinel-2 Imagery – A Feasibility Study. *GI_Forum*, 1(1), 172–182. https://doi.org/10.1553/giscience2017_01_s172
- Witmer, F. D. W. (2015). Remote sensing of violent conflict: eyes from above. *International Journal of Remote Sensing*, 36(9), 2326–2352. <https://doi.org/10.1080/01431161.2015.1035412>